POLITECNICO DI MILANO

Facoltà di Ingegneria Industriale

Dipartimento di Energia

Corso di Dottorato in Scienze e Tecnologie Energetiche e Nucleari

An Innovative Approach for the Techno-Economic Optimization of Organic Rankine Cycles

Supervisor: Prof. Ennio Macchi

Co-Supervisor: Ing. Matteo Carmelo Romano

Ing. Paola Bombarda

Tutor: Prof. Stefano Campanari

Coordinator: Prof. Carlo Enrico Bottani

PhD candidate

Marco Astolfi

XXVI ciclo

To my relatives and friends,

because life is outside the lab

"Do not forget that every people deserves the regime it is willing to endure"

White Rose Society

Index

List of figures

List of tables

Acknowledgements and apologies

Thanks to Professor Macchi to have been always present, for his fundamental guidance and his help during these three years of Ph.D. Because he always already knows the result I should obtain.

Furthermore I would like to express my apologies to all the colleagues I have bothered in these years and, in particular, in these last months. You were always willing to give me a suggestion in the corridor and you have wasted hours talking about my boring stuff. A special thanks to Matteo, Paola e Antonio.

Thanks to Professor Ghoniem and Progetto Rocca for the possibility to spend a semester in MIT: it was an awesome period of scientific research and personal growth.

A final thanks to the colleagues of office 1.13, the "BdC", to the ones are just arrived and to the ones have been already escape abroad, because a whole day in a room with you is a way lighter.

Notes

As a general note some parts of the text are the result of the arrangement of previous works done by the author in collaboration with other colleagues of Gecos group of Energy Department of Politecnico di Milano. In particular Chapter 3.2 (Applications) is partially based on a non-disclosable internal report and Section 9.1 (Hot geothermal brines) on a couple of publications on the topic [1; 2]. Results presented in Section 6.1.6 (Radial outflow turbines) and in Section 9.2 (Use of mixtures for Biomass plants) are obtained with a methodology already presented in international conferences oral presentations [3; 4; 5] while the approach for the study turbine efficiency has been already presented [6].

For any further information, please contact the author at marco.astolfi@polimi.it

Summary

In the last twenty years the higher attention about climate change, global warming and externalities due to environment contamination and pollution have strongly encouraged the use of green technologies in power production field. ORCs (Organic Rankine Cycles) allow reducing the rate of consumption of fossil fuels and the emission of carbon dioxide by means of a wider exploitation of renewable energy resources like geothermal and solar energy. Furthermore ORCs are a reliable solution to increase the energy efficiency of any industrial plant where waste heat can be recovered for power production instead to be released to the environment. Thanks to their flexibility, they will surely play a relevant role in the world energetic scenario in future years.

ORCs are based on the idea that the working fluid and the power cycle configuration should be selected according to the thermal level of the energy source, to the available thermal power and to the constraints related to key components like the turbine. In particular ORC are extremely attractive in all those application where the use of water as working fluid entails difficulties in components sizing leading to lower plant efficiencies and a less competitive LCOE (Levelized Cost of Electricity). Typical examples are application characterized by a small available thermal power or by low maximum temperatures sources. Despite their great potential, ORCs have been found a large market only in few fields, namely in biomass combustion CHP (Combined Heat and Power) plants and for the exploitation of hot geothermal brines, but their diffusion is still limited in many other applications and the potential upside of this technology is still large. The widespread use of ORC technology in new markets is strictly related to the availability of efficient components and numerical tools for the selection of the best combination of working fluid and plant layout.

The aim of this thesis is to propose an innovative and comprehensive approach for the study of ORCs, their design and their optimization. A software named ORCO (ORC Optimization) has been implemented to reach the over mentioned goal.

The approach proposed in this thesis is innovative from different point of view because it tries to overcome most of the limits highlighted in the methodologies present in literature. Limiting the study to single stream heat sources, the plant with the minimum LCOE is identify by means of the exhaustive investigation of different combinations of working fluids and cycle configurations. Each solution is fully optimized by a suitable algorithm.

In order to obtain a reliable result, many different aspects are taken into account as briefly summarized below:

- *Working fluids thermodynamic properties:* it is crucial to use suitable equations of state for the calculation of physical and thermodynamic properties in order to increase the accuracy and to guarantee a reliable estimation of component sizing and performances. ORCO is integrated with Refprop 9.1 which uses a state-of-the-art database for pure fluids. In addition, it allows defining several UD (User Defined) mixtures but accuracy has to be previously checked comparing the numerical results with experimental VLE (Vapor Liquid Equilibrium) data from reference. A strong reduction of computational time and a higher stability of calculations in two phase region have been achieved thanks to improvements on program routines.
- *Cycle configuration*: several different plant layouts can be investigated, each one presenting different advantages and drawbacks depending on the thermal level of the heat source and the working fluid. With ORCO it is possible to investigate subcritical, supercritical, two pressure levels cycles and flash triangular plants. Any other cycle configuration can be added thanks to the modular structure of the code.
- *Expander efficiency*: the expander is the key component for any ORC system, for big power plants usually axial-flow turbines are adopted while for small power output, positive displacement devices are suggested. In ORCs it is crucial to link the actual efficiency of the expander to the thermodynamic properties of the fluid and to the cycle layout. For axial flow turbines an extensive numerical activity has been carried out optimizing several hundred turbines and comparing the results on the base of similarity theory. Efficiency correlations are proposed for single stage, two stage and three stage turbines at optimized rotational speed in wide ranges of volume ratio and machine radial dimension. For screw volumetric expanders a correlation of efficiency has been derived by analysing maps of performances provided by producers.
- *Cost correlations*: an extensive bibliographic research has been carried out with the aim of defining a suitable cost correlation for each component commonly adopted in ORC field. A detailed analysis is performed for Shell&Tube heat exchangers and axial flow turbines since they are the most expensive components for ORC. In particular the cost correlation for turbines is quite innovative and can be used to estimate the cost of machines working with organic fluids and so characterized by a limited number of stages and high stage volume ratios and steam turbines where usually a higher number of stages is adopted.

Different analyses have been successfully carried out with the proposed approach, investigating some of the most interesting ORC applications. A detailed study is proposed for geothermal energy exploitation where supercritical, subcritical and two pressure levels cycles are compared. Two different analyses are considered: the first one with the aim of maximizing the power production while the second one oriented to the minimization of overall LCOE. The most promising solutions are highlighted leading to the definition of criteria for the pre-selection of suitable working fluids and cycle layouts. In particular the results underline the highest performances attainable with supercritical cycles and two pressure levels cycles compared to the subcritical ones. From a techno-economic point of view, instead, all the cycle configurations when properly optimized, reach a comparable LCOE for a relatively small number of fluids suggesting general rules for the selection of working fluid on the basis of reduced parameters.

Another study has been performed comparing ORC and steam Rankine cycle in waste heat recovery application from big cement production plants; a field characterized by a relatively high available thermal power and a high temperature of the hot source. These applications are part of the so called “grey zone” where it is not easy to define if organic fluids can actually compete against water which shows higher film transfer coefficients, and so less expensive heat exchangers, but a larger turbine. Finally two studies are carried out investigating (i) the potential of mixtures for biomass CHP plants where the temperature glide in phase transition can be advantageous since allow increasing the power output and (ii) the use of volumetric screw expanders for small size applications.

A comprehensive methodology for the analysis of ORCs is proposed and a software, named ORCO, is realized in order to face all the difficulties related to the design and the optimization of ORCs. The numerous innovative aspects implemented into the code allow performing broad spectrum analysis by considering a reliable efficiency for key components and suitable economic evaluations. This approach has been tested on different test cases proving the affordability of the systematic procedure implemented. From these studies interesting conclusions about the general criteria of selection for both working fluid and cycle layout are highlighted.

“I have only made this letter longer because

I have not had the time to make it shorter"

Blaise Pascal

“Procrastinators: leaders of tomorrow”

Brett Steelman

1 Introduction

The increasing attention to pollutants and greenhouse gases emission from the power generation sector and the concerns about fossil fuels supply and price have been leading to a massive growth of those technologies that can produce electric energy from renewable sources and waste heat recovery. Nowadays, favorable feed-in tariffs and other financial incentives make competitive the exploitation of renewable sources and low grade heat for power production in many countries. For this reason, renewable sources and energy efficiency have been receiving an increasing interest in the power generation sector. In this context, the exploitation of heat from a wide variety of sources, like hot geothermal brines, biomass, sun and exhaust gases from engines and industrial processes is certainly one of the most promising options.

While steam cycles will probably remain the only competitive technology for large scale heat recovery and external combustion cycles for power generation, their application in small scale units and for low grade heat utilization, typical of many renewable sources, has a number of drawbacks. In these applications, the use of organic working fluids in Rankine cycles can be preferable vs steam for a number of reasons:

- A favorable "shape" of the thermodynamic cycle, allowing for high cycle and heat recovery efficiencies, achievable by simple cycle layouts (no vapor superheating, no reheating, no multiple regenerative bleedings from the turbine) [7]
- Reasonable volume flow rates and low enthalpy drops in the turbine. These points allow for a favorable turbine design, resulting in high isentropic efficiencies with a limited number of stages (even a single one), a reasonable size and hence competitive manufacturing costs [7]
- Favorable operating conditions for the turbine, with low mechanical stresses due to the low peripheral speeds, no blade erosion issues due to the dry expansion (no droplets formation during fluid expansion even without superheating).
- Possibility of adopting lower maximum pressure and cost of the high pressure components in case of medium-high temperature heat sources.
- Possibility of selecting positive gauge condensing pressure, limiting the size of the low pressure components (condenser, turbine discharge and low pressure vapor piping) and avoiding air in-leakages.

For all these reasons, Organic Rankine Cycles are experiencing a great commercial success and an increased interest in the R&D activities for the optimization of new ORC cycles and the related components [8].

A number of scientific studies has been published relatively recently on the selection of working fluids and on the optimization of the corresponding cycle parameters for a number of applications, namely waste heat recovery [9; 10; 11; 12], biomass combustion [13], solar heat [14; 15; 16], geothermal sources [17; 18; 19; 20; 21; 22; 23]and geothermal-solar hybrid concepts [24]. Advanced cycle configurations, such as supercritical cycles [22; 23; 19; 25; 20; 26] and multi-level cycles [23; 27], the use of mixtures [28; 29] and predictive theoretical methods to define the optimal working fluids [30] are also being explored.

It is evident that dedicated optimization analyses are required for each specific application, due to the wide range of temperatures (~70-350°C) and sizes (from few kW_{el} to tens of MW_{el}) of the potential heat source. In addition, the increased restrictions in the use of fluids with high GWP and ODP and safety issues (flammability and toxicity) make it important to investigate the performance of new environmental friendly and low risk fluids. All these factors justify the abundant literature recently produced on this topic.

However the success, the developing and the extension of this technology to other fields require tools suitable for the design, the optimization and the selection of the best combination of working fluid and cycle configuration. The aim of this work is to bridge the gap in knowledge and provide a reliable strategy for the techno-economic optimization of ORC power systems, based on validated cost and performance correlations for each component.

“If we knew what we were doing,

it wouldn't be called research,

would it?”

Albert Einstein

2 Design of ORCs and their optimization

ORC (Organic Rankine Cycle) is a technology based on the use of a suitable organic compound as working fluid in a simple Rankine cycle. In this section an overview on ORCs design criteria and optimization is first presented, after the available commercial software are listed pointing out the attention on their peculiarities and their limits, finally the proposed methodology is presented. In the next chapters peculiarities of ORC technology are presented together with all the assumptions and the calculation at the basis of this work; however the main characteristics of ORC are here briefly summarized in order to give to the reader all the basic information for a better the understanding of this section:

- ORCs have a good flexibility and are the most suitable solution for the exploitation of many different energy sources. Most of the information about the application fields of ORC are reported in Chapter 3 (ORC field)
- ORCs use an appropriate organic fluid as working fluid into the cycle. Organic fluids appreciably differ one from each other in both thermodynamic and physical properties. Thermodynamic properties of organic fluids and the main differences vs water are discussed in Chapter 4 (Organic fluids and their properties)
- ORCs can be designed in different cycle configurations. Some of them are widely used while other ones are innovative or oriented to very specific applications. Cycle configuration are listed and described in Chapter 5 (Thermodynamic cycle configurations).
- Some components used in ORCs are different from the same developed for common steam cycles. In particular expanders are the key components in ORC technology and their design is greatly affected by working fluid properties and cycle parameters. A detailed study on axial turbines and screw expanders is object of Chapter 6 (Components).

Due to their peculiarities ORCs design and their techno-economic optimization are not trivial and they require a good knowledge of organic fluids thermodynamic properties and component design criteria.

2.1 ORC design steps

ORCs are a widely studied technology. Many different research centres and universities are oriented to the design, the optimization and the dynamic simulation of this kind of systems. Many of these institutions are also involved in experimental campaigns in order to test new devices, new working fluids or new cycle configurations. Regarding the numerical analysis of an ORC several steps are required in order to select the optimal working fluid and the best cycle configuration taking into account, not only nominal performance indexes, but also economic aspects, off-design efficiency and the dynamic behaviour of the plant. These steps have to be faced progressively and wrong assumptions in the first ones compromise the achievement of a good result at the end of the process. Last stages can contribute only partially to final design and are mainly oriented to the detailed analysis of each component, the off-design performances and the dynamic analysis of the system. A schematic view of the design process for a generic ORC is reported in Figure 2.1: four different stages can be highlighted: (i) analysis of the problem, (ii) working fluid and cycle configuration selection, (iii) system optimization and (iv) off-design analysis.

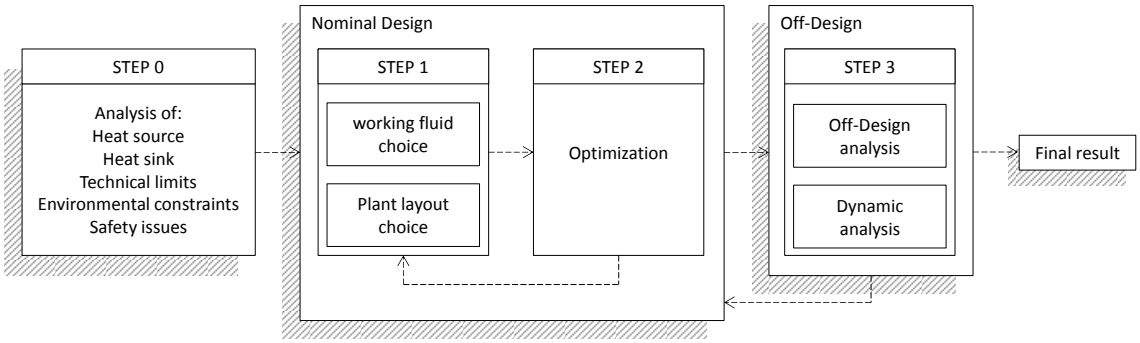

Figure 2.1 - Steps required for design and optimization of ORCs from the analysis of the problem to the definition of the optimal combination of working fluid and cycle configuration.

2.1.1 Problem analysis

Main difficulty in ORC design is the huge number of possible variables combinations: the number of available working fluids, even considering only pure fluids and not mixtures, is greater than 50 and the number of basic cycle layouts is not negligible too. Exhaustive analysis on these two parameters can be extremely time consuming and a good pre-design analysis is required with the aim of reducing the domain of the possible solutions. In this stage the heat source and heat sink characteristics, the size of the plant and the expected performances should be taken in to account, together with all the other technical limits, in order to exclude some working fluids, some cycle configuration or to fix some design

parameters in order to reduce the computational time required by the optimization procedure. For instance, maximum cycle pressure or the necessity to avoid vacuum into the condenser can affect the choice of cycle configuration limiting the investigation to just some plant layouts or some working fluids. In other applications, like the heat recovery from engine exhaust gasses in automotive field, a light plant and small overall occupied volume are required entailing simple plants layouts with a limited number of components. Remote applications, like small solar plants in rural context and WHR (Waste Heat Recovery) from pumping stations along pipelines, need instead simplicity, reliability and low maintenance cost. At the end of this stage a number of promising working fluids and plant layouts for the exploitation of a given heat source are pre-selected. The research of their optimal combination is faced in the next stage.

2.1.2 Working fluid and cycle configuration choice

The most important stage is definitely the correct choice of both working fluid and cycle configuration. Making the wrong choice in working fluid selection entails a poor cycle performance compared to the maximum attainable one with a more suitable fluid. In fluid selection not only thermodynamic properties should be considered because even the cost, the environmental impact and the safety issues related to the use of a certain fluid have to be taken into account. In the same order of magnitude is the choice of cycle configuration: some plant layouts are intrinsically more suitable for some applications while not for other ones. The main characteristics of the heat source, like the maximum temperature and the available temperature variation, have a strong influence on the selection of the working fluid, the cycle layout and the choice of the components to be used. For example the supercritical cycles are more suitable for the exploitation of a variable temperature heat source with a considerable temperature drop, while the subcritical saturated recuperative ones are usually the optimal solution when the hot stream cannot be excessively cooled down. At this stage different combinations of working fluid and plant layout are usually investigated with a brute-force search.

2.1.3 System optimization

For each combination of working fluid and plant layout, an optimization of the plant in nominal condition should be performed in order to define the best ORC system according to a certain objective function. This is the third step in ORCs study and, as the second one, it is crucial to compare different solutions and different assumptions. For a generic system several cycle parameters have to be defined and most of them should be optimize with the aim of maximizing or minimizing a selected parameter. Objective function varies

depending on the application and depending on the plant requirements. In particular two kinds of optimization are usually performed:

- *Thermodynamic optimization*: it is performed with the goal to maximize the power production. The cycle efficiency is maximized and reliable limits in pinch points temperature differences in heat exchangers should be assumed.
- *Techno-economic optimization*: the goal is to minimize the LCOE (Levelized Cost of Electricity) or the specific cost of the plant calculated as the ratio between the total cost and the nominal power production. In this optimization a larger number of design variables is usually considered with a simplified design of key components.

The design variables of the system are, for example, the evaporation and the condensation temperatures, the temperature increases in superheating and pinch point temperature differences in the heat exchangers. Each one of them has a different effect and weight on the final solution but in some cases some of them can be assumed fixed because their effect on the objective function is univocal. An example is a purely thermodynamic analysis of an ORC system where it is not necessary to optimize the pinch point temperature differences in the heat exchangers: in fact decreasing the pinch point temperature differences always allows the reduction of the entropy production in heat transfer process with a positive effect on net power production. Optimizing these variables in a thermodynamic optimization involves pushing them to the lower bound leading to extreme heat exchanger surfaces and a less reliable solution. In a techno-economic optimization instead variation of the pinch point temperature differences entails two contrasting effects on the LCOE and the optimal value for these variables is the result of a trade-off between an increasing of power production and a greater equipment cost caused by larger heat transfer surfaces.

Once the number and type of variables is selected it is crucial to set appropriate lower and upper bounds for each one and possibly some linear constraints between them with the aim to help the optimization algorithm in finding the solution in a well-defined region. Final step consists in the correct choice of the optimization strategy and very different results can be obtained using algorithms that are not suitable to solve the given problem. Some more details about the definition of the optimization algorithm and further details related to optimization algorithms and their features are described in section 8.2.3 (Optimization). Finally it is important to underline that the optimization stage sometimes requires an internal loop because some variables are pushed to a linear bound which can be relaxed.

The exhaustive approach is the strategy commonly used in most of the publications but in some papers other methodologies are proposed even if not directly applied to ORC systems. With the synthesis optimization [31] the plant layout and so the number of components and the connection between them are free variables for the optimization routine: the streams are handled using binary variables which exclude automatically some components or change for example the order of the heat exchangers coupled with the heat source. This type of approach is extremely flexible and general but it entails a more challenging optimization problem which is intrinsically harder to solve because the objective function presents a relevant number of discontinuities and local minimums. Other studies [32; 33] consider the fluid as a variable in the problem: the idea is to optimize the fluid selection and the plant at the same time thus reducing the number of simulations required by the study of a certain problem. Main limit of this strategy consists in working fluid characterization: multi-parameters equations of state cannot be used due to the large number of required additional variables and usually simpler cubic or PC-SAFT equations of state are adopted with a strong reduction in solution accuracy. Furthermore the optimized working fluid might be a non-existing fluid with critical properties similar but not equal to any other commercial fluid. In this case two solutions are possible: (i) selecting the commercial fluid closer to the optimal one and to perform again the system optimization, or (ii) to synthetize the desired fluid. This methodology is demonstrated in [34] but it entails uncertain costs which are surely higher than the purchase of a commercial fluid.

Last consideration is about the number of variables that can be considered. Thermodynamic optimization is relatively easy with usually a reduced number of variables, while a techno-economic optimization entails a larger problem because all the heat exchanger surfaces are optimized. Most of the studies, and even the present work, consider pressure drops fixed and reasonable values for heat transfer coefficients are assumed, while other publications perform the design of every heat exchanger directly with the optimization routine [35]. Pseudo 1D models like the Bell Delaware method [36], [37] for S&T (Shell and tubes) heat exchangers can be used and variables like velocities of streams, baffles and tubes spacing, tube diameter and baffle cut are controlled by the optimization routine allowing the calculation of pressure drops, heat transfer coefficients and eventually a more reliable estimation of the heat exchanger surface and cost. This approach is interesting since in theory it allows to achieve the global optimum for a selected problem without assuming or fixing variables which can affect the final solution but, on the other hand, it entails a high uncertainty because of the size and the complexity of the problem. The number of variables is large, up to 20 or 30 variables, with really different weights on the final solution: a really robust and well

calibrated optimization algorithm is required with difficulties in checking the reliability of the final solution obtained.

A summary of the most relevant publications about ORC thermodynamic and techno-economic optimization are reported in Table 2.1, Table 2.2 and in Table 2.3 respectively.

2.1.4 Off-design and dynamic simulation

The fourth stage is the study of the off-design performances and the dynamic analysis of the whole system. For sure this stage is fundamental to understand the real potential of an ORC system and off-design analysis is necessary in order to calculate realist values for the average seasonal efficiency of the system and the total energy production for one year or one cycle of operation. However this step is not always required: some applications like geothermal energy and waste heat recovery (WHR) from industrial process are characterized by an almost constant operation throughout the year. Off-design operations for these systems are limited to daily start-up and shut- down and small fluctuations around the nominal design point and generally a deep analysis of off-design performances is not required. For other applications, instead, like the exploitation of solar energy in plants without storage or automotive ORC for the heat recovery from flue gases, the evaluation of the off-design performances for each component is a topic of big interest. The governing equation for heat exchangers are well known while the main uncertainty is related to the definition of off-design curve for the turbine performance because this information is owned by few companies in the world and data are rarely conveyed.

Reference	Heat source	Q_{in} or W_{el}	Types of cycles	Considered fluids	Machines efficiencies	Fixed variables	Opt. var.	Optimization function	Component sizing	Optimal cycles
Invernizzi, Bombarda (1997) [17]	Geothermal brine @ 100-300°C	-	Sub-SA rec/no-rec	R11, R114, R245ca, R245fa, R236fa, R134a, HFE-245fa, n-butane, n-pentane, n-perfluoro-pentane	$\eta_{is,turb}$=75% $\eta_{wf,pump}$=50%	$\Delta T_{pp,PHE}$=20°C ΔT_{sh}=10°C $\Delta T_{pp,rec}$=20°C T_{cond}=40°C Δp_i=0	p_{eva}	Plant exergy efficiency	-	-
Invernizzi et al. (2007) [9]	WHR: MGT flue gas @ 250-350°C	-	Sub-SA rec	HFC-43-10mee, HCFC-123, n-Pentane, CFC-113, 2-2-Dimethylbutane, 2-3-Dimethylbutane, n-Hexane, Hexafluorobenzene, MM, Pentafluorobenzene, n-Heptane, c-Hexane, MDM, n-Octane, D4, MD2M	$\eta_{is,turb}$ =75% $\eta_{wf,\ pump}$ =60%	ΔT_{ml}=30°C $\Delta T_{pp,rec}$=20°C T_{cond}=30°C Δp_i=0	T_{eva}	Net power	Considerations on turbine design for power outputs 25-100 kW_{el}	-
Tchanche, Papadakis, al. (2009) [14]	Solar: water @ 75-115°C as HTF	2 kW_{el}	Sub-SA no-rec	RC318, R114, R113, R12, R123, R134a, R141b, R152a, R32, R407C, R500, Ethanol, Methanol, PropaneIsobutane, n-butane, n-pentane, Cyclohexane, NH3, water,	$\eta_{is,turb}$ =70% $\eta_{wf,pump}$ =80% η_{mec-el}=63%	$\Delta T_{ap,PHE}$=15°C $\Delta T_{pp,PHE}$=6°C T_{cond}=35°C Δp_i=0	-	-	Considerations on turbine outlet volume flow rate, volume flow ratio, and cycle pressures	T_{HTF}=90°C and T_{eva}=75°C: <u>n-butane</u> [c]: η_{cycle}=4.24% η_{II}=24.8%
Dai et al. (2009) [10]	WHR: gas @145°C	1100-1400 kW_{th} (15.95 kg/s)	Sub-SA rec/no-rec	NH_3, butane, isobutane, R11, R123, R141B, R236EA, R245CA, R113, water	$\eta_{is,turb}$ =85% $\eta_{wf,pump}$=60%	$\Delta T_{pp,PHE}$=8°C $\Delta T_{pp,rec}$=5°C T_{cond}=25°C Δp_i=0	p_{eva} $T_{in,turb}$	Plant exergy efficiency	-	<u>R236ea</u>: T_{eva}=87.7°C η_{cycle}=11.53% η_{plant}=7.88% [a] η_{II}=35.43% <u>iso-butane</u>: T_{eva}=87.1°C η_{cycle}=11.52% η_{plant}=7.79% [a] η_{II}=35.05%
Lakew, Bolland (2010) [11]	WHR: air @ 80-200°C	6-18 MW_{th} (100 kg/s)	Sub-SA no-rec	R134a, R123, R245fa, R227ea, n-pentane, Propane	$\eta_{is,turb}$ =80% $\eta_{wf,pump}$=80% η_{mec-el}=90%	$\Delta T_{pp,PHE}$=10°C $\Delta T_{pp,cond}$=5°C T_{cond}=20°C Δp_i=0	p_{eva}	Net power	Turbine (SP, single stage turbine), total HE area	T_{ha}=80-160°C: <u>R227ea</u> T_{ha}=200°C: <u>R245fa</u>

Table 2.1 - Most relevant publications on ORC thermodynamic optimization Table 1/2

Reference	Heat source	Q_{in} or W_{el}	Types of cycles	Considered fluids	Machines efficiencies	Fixed variables	Opt. var.	Optimization function	Component sizing	Optimal cycles
Zhang, Jiang (2012) [22]	Geothermal brine @ 100-200°C	~310 kW_{th} 730 kW_{th} (1 kg/s)	Sub-SA/Sup no-rec	R134a, R245fa, isobutene, isopentane	$\eta_{is,turb}$ =85% $\eta_{wf,pump}$=85%	$\Delta T_{pp,PHE}$=4°C ΔT_{cond}=35°C T_{ca}=26°C Δp_i=0	T_{eva}	Plant exergy efficiency	-	T_{geo}=100°C: R134a (T_{eva}=68°C) T_{geo}=150°C: R134a (Sup) T_{geo}=200°C: R245fa (Sup)
Walraven et al. (2012) [23]	Geothermal brine @ 100-150°C	~310 kWth 460 kWth (1 kg/s)	Sub/Sup rec/no-rec Bleed/noBleed 1Pr. Lev. vs multi Pr..Lev.	R12, R22, R41, R32, R115, R124, R125, R134a, R142b, R152a, R218, R227ea, R236ea, R236fa, R245fa, R1234yf, R1234ze, RC318, C4F10, C5F12, CF3I, SF6, Ethane, Propane, iso-butane, Propylene, DME, CO2, N2O, others.	$\eta_{is,turb}$ =85% $\eta_{wf,pump}$=80%	$\Delta T_{pp,PHE}$=5°C ΔT_{cond}=25°C Δpi=0	$T_{in,turb}$ p_{max}	Plant exergy efficiency	-	T_{geo}=125°C, no $T_{lim,geo}$: R227ea Sup, no-rec η_{II}~55% T_{geo}=125°C, $T_{lim,geo}$=75°C: R1234yf Sup, rec η_{II}~41%
Schuster et al. (2010) [38]	Generic source @ 210°C	-	Sub-SA/Sup rec/no-rec	water, R134a, R227ea, R152a, RC318, R236fa, R245fa, isobutene, isopentane, isohexane, cyclohexane, R365mfc	$\eta_{is,turb}$ =80% $\eta_{wf,pump}$=85%	p_{max}=1.03*p_{crit} (Sup cases) $\Delta T_{pp,PHE}$=10°C ΔT_{SH}=2°C $\Delta T_{pp,rec}$=10°C T_{cond}=20°C Δp_i=0	Sub: T_{eva} Sup: $T_{in,turb}$	Net plant efficiency	Heat exchangers area	Sup: R365mfc & iso-pentane: T_{max}≈180°C η_{plant} ≈14% Sub: R245fa & iso-butene: T_{eva}≈140°C η_{plant}≈13.2%
Quoilin, Orosz et al. (2011) [16]	Solar: with HTF @ ~150°C	~60 kW_{th}	Sub-SA rec	n-pentane, SES36, R245fa, R134a	$\eta_{scroll-exp}$: calc $\eta_{wf,pump}$=70% $\eta_{HTF,pump}$=70%	ΔT_{SH}=10°C $\Delta T_{pp,PHE}$=8°C $\Delta T_{pp,rec}$=8°C $\Delta T_{pp,cond}$=8°C $\Delta T_{sc,cond}$=5°C Δp_{HEs}=7.5 kPa	T_{eva} ΔT_{HTF}	Net plant efficiency,	Scroll expander (given geometry), plate PHE area, recuperator area, condenser area	SES36: T_{eva}=169°C η_{cycle} =13.1% η_{plant} =7.9%[b] n-pentane: T_{eva}=189°C η_{cycle}=11.9% η_{plant}=7.0%[b]

Table 2.2 - Most relevant publications on ORC thermodynamic optimization Table 2/2

Reference	Heat source	Types of cycles	Machines efficiencies	Fixed variables	Optimization variables	Optimization function	Component sizing	Optimal cycles
Hettiarachchi, Golubovic, al. (2007) [18]	Geothermal brine @ 70-90°C	Sub-SA no-rec	$\eta_{is,turb}$ =85% $\eta_{wf,\ pump}$=75% η_{mec-el}=96% $\eta_{cw,pump}$=80%	T_{cw}=30°C Δp_i=calc	T_{eva} T_{cond} u_{geo} u_{cw}	Specific heat exchange area: m^2/kW	Heat exchangers area	<u>NH_3</u>: T_{eva}=76.9°C T_{cond}=43.0°C η_{cycle}=8.9% η_{plant}=0.8% [a] α=0.34 m^2/kW
Quoilin, Declaye et al. (2011) [12]	WHR: gas @ 180°C with HTF.	Sub-SA no-rec	$\eta_{scroll-exp}$: calc $\eta_{wf,\ pump}$ =60% $\eta_{HTF,pump}$=60% η_{mec-el}=70%	$\Delta T_{pp,PHE}$=10°C ΔT_{sh}=5°C $\Delta T_{pp,cond}$=10°C $\Delta T_{sc,cond}$=5°C T_{cw}=15°C m_{cw}=0.5 kg/s Δp_{eva}=10 kPa Δp_{cond}=20 kPa	T_{eva}	Net power	Scroll expander (given geometry), plate PHE area, condenser area	<u>R245fa</u>: T_{eva}=113.5°C η_{cycle} =7.78% η_{plant} =5.13%
				ΔT_{sh}=5°C $\Delta T_{sc,cond}$=5°C T_{cw}=15°C m_{cw}=0.5 kg/s	T_{eva} $\Delta T_{pp,PHE}$ $\Delta T_{pp,cond}$ Δp_{eva} Δp_{cond}	Specific cost: €/kW		<u>R123</u>: T_{eva}=111.8°C η_{cycle} =8.41% η_{plant} =5.00% <u>n-butane</u>: T_{eva}=133.2°C $\Delta T_{pp,PHE}$ = 7.5°C η_{plant}=4.47% Cs=2136 €/kW <u>n-pentane</u>: T_{eva}=139.9°C $\Delta T_{pp,PHE}$ = 4.0°C η_{plant}=3.88% Cs=2505 €/kW
Shengjun et al., (2011) [20]	Geothermal brine @ 90°C	Sub-SA/Sup no-rec	$\eta_{is,turb}$ =80% $\eta_{wf,pump}$ =75% η_{mec-el}=96%	$\Delta T_{pp,PHE}$=5°C $\Delta T_{pp,cond}$=5°C T_{cw}=20°C Δp_i=10 kPa	Sub: T_{eva}, p_{cond}	Specific heat exchange area (α): m^2/kW	Heat exchangers area	<u>R152a</u>: T_{eva}=74°C T_{cond}=27.9°C α=1.64 m^2/kW
					Sup: $T_{in,turb}$ p_{max}, p_{cond}	COE (only heat exchangers cost, function of operating pressure, considered)		<u>R152a</u>: T_{eva}=60°C T_{cond}=27.9°C COE=53 €/MWh

Table 2.3 - Most relevant publications on ORC techno-economic optimization

2.2 Software for ORC analysis and optimization

For off-design and dynamic simulations Modelica software [39] with Dymola environment [40] is the most used tool and it is commonly adopted in power system field thanks to the work of Casella [41] which provides a detailed component library, including heat exchangers and turbines, suitable for ORC power systems.

For both the first and the second steps there aren't software or commercial codes that allow performing optimization of several cycle configurations in an easy way, considering a huge number of working fluids and with a detailed description of the key components. However the software that are available on the market and which can be used for the over mentioned analysis are:

- Aspen Plus [42]: Aspen Plus is a software for the modelling of both chemical processes and power systems. The main advantage of Aspen is the possibility to use a large variety of working fluids with a good accuracy. Aspen Plus fluids databank is definitely the most advanced one among commercial software and it allows selecting several different Equations of State (EoS) for the calculation of fluid thermodynamic properties. Some of them are relatively simple, like Peng-Robinson or Redelich-Kwong, while others ones are extremely advanced with the possibility to describe the thermodynamic properties with a really good accuracy on experimental data. In addition Aspen Plus implements several mixing rules methodology for the estimation of the behaviour of blends formed by two or more components ensuring the possibility to perform reliable design of ORC working with mixtures. Finally it is possible to calibrate ad hoc EoS for fluid or mixtures if experiential data are available. One of the drawbacks of this software is the difficulty in creating User Defined Components (UDC). For instance, turbine can be described just with a fixed isentropic efficiency and it is not possible to link its performances to fluid properties and other cycle parameters. Finally it is not possible to perform an internal optimization and Aspen has to be connected with an external optimization algorithm leading to a longer computational time due to the communication between the two softwares. Another limit regards the off-design analysis that is pretty challenging requiring the definition of all the governing equations and the fixed parameters of the system. Last, the economic evaluation of the plant has to be performed in another environment because no information about component costs is already implemented in the software.
- ThermoFlex [43]: The main advantage of ThermoFlex is the possibility to easily perform off-design simulations and the availability of economics databanks.

Unfortunately the software lacks in detail for all the components which don't use water as working fluid. This is due to the core business of ThermoFlow company which is mainly oriented to common power systems with a focus in steam Rankine cycle and gas turbine technologies. ORC can be modelled but it's not possible to evaluate a realistic efficiency for the turbine or the detailed design of the heat exchangers. Another limit of ThermoFlex is the small number of available fluids: the software can use water and some other compounds of interest for chemical and industrial systems but the quality of EoS used for the other working fluids is not sufficient for an accurate analysis of ORC technology. The possibility to link ThermoFlex with Refprop helps to cover this limit but not all the Refprop fluids can be used, EoS are not always updated to the new version and the code gets really slow with a strong increase of computational time. Besides these issues ThermoFlex allows performing simple optimizations varying a limited number of parameters but previous simulation performed by the Gecos Group of Politecnico di Milano on solar power systems [44] have been demonstrated the low accuracy of the implemented optimization algorithms. Finally UDCs are difficult to customize and a very little support by ThermoFlow was given in past works with this program.

- GS: is an *in house* software used by Energy Department of Politecnico di Milano for the simulation of power systems. The code is written in Fortran and it allows the definition of every cycle layout with a number of available components which largely exceeds the requirement of ORC systems. Some components like the turbine are described in detail and performances are calibrated on experimental data and correlation from literature. The main limit is represented by the possibility to use only water and mixtures of gases as working fluids. For water accurate EoS are implemented while for gaseous streams a function of specific heat as a function of temperature is generally adopted. A personal communication with the developers of the code has highlighted difficulties in the integration of GS with Refprop database which requires a strong modification in some fundamental routines and a longer computational time.

The last difficulty common to all these codes is related to their instability when integrated with an optimization algorithm. The lower and upper bounds for each variable are usually set in order to investigate a wide region of possible solutions, this fact entails that some combinations result in a non-feasible designs. The code should be able to recognize if conflicts between the imposed variables are present and to make opportune changes according to the absolute and relative limits. Discrepancies between the inputs and the changed values are then usually accounted with penalty factors with the aim of excluding

these solutions. The listed codes are not ready to handle conflicts, which usually result in the crashing of the code or in the impossibility to control the obtained result. In Table 2.4 a brief summary of available software characteristics is reported.

	Aspen Plus	ThermoFlex	GS
Pure fluid availability	(+)	(~)	(–)
Mixtures availability	(+)	(–)	(–)
Component description	(–)	(–)	(+)
Economics data	(–)	(+)	(–)
Optimization	(–)	(–)	(–)
Off-design	(~)	(+)	(–)

Table 2.4 - Summary of the main features and limits of the commercial codes that can be used in ORC design and optimization. Symbols (+), (~) and (–) mean respectively a good, an average and a poor performance.

2.3 The proposed methodology

In order overcome the limits of the described software it has been decided to develop a new code named ORCO (Organic Rankine Cycle Optimization) able to satisfy all the features required by the design and optimization of ORC systems. The code is written in Matlab [45] and it consists in several scripts and functions for the definition of the cycle, the initialization of the optimization algorithm, the iterative solution of the thermodynamic cycle, the results calculation plus some routines for the results analysis, the consistency check and the chart displaying. With the aim of reducing the computational time the code is suitable for parallel computing and all the internal iterative procedures are written by the author in order to have a more stable and faster code. In further chapters the main characteristics of ORC power systems are described and the main features of the developed code are presented pointing out the attention on the innovative aspects and the details that make this code extremely reliable for the design and the technical-economic optimization of ORC.

"The dictators don't like

relaxed people

and green energy"

Angelo Cippa

3 ORC field

Organic Rankine Cycle is a technology suitable for the thermodynamic conversion of heat into power of many non-conventional energy sources, since it can exploit conveniently heat sources in a wide range of temperature and available thermal power inputs. In particular ORCs can be easily coupled with renewable energy sources and they are used in all those applications where conventional steam Rankine cycle entails a number of technical difficulties which lead to a limited efficiency. The fields of application of ORC and steam cycle are represented in Figure 3.1 while the different sub fields are approximately representative of the different applications where ORCs can be used.

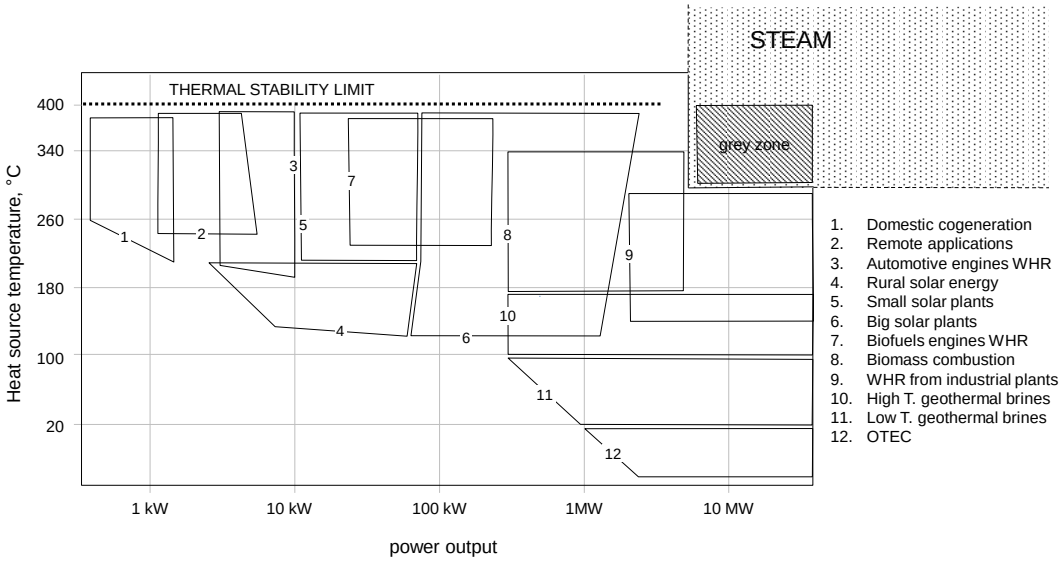

Figure 3.1 - Graphical representation of ORC field in power output-heat source temperature axes. The dotted area in the top-right corner defines common steam Rankine cycle field while the rest of the chart is divided in different ORC applications. The "grey zone" in the top right corner defines a range of applications where ORCs might be competitive against steam Rankine cycles – rearranged form [46]

The chart is limited to heat source temperatures and output powers typical for ORC systems while for higher power outputs and temperatures the power production sector is dominated by steam Rankine cycles as represented in the top right corner. Water is definitely the most used working fluid in power generation field thanks to its excellent physical and thermodynamic properties. The high latent heat in evaporation, the high film transfer coefficients, the high thermal stability and a low cost make this fluid the most suitable one for large power plants and steam water cycles are commonly used for the direct exploitation of fossil fuels combustion like coal, oil or natural gas and are widely used as bottom cycle in combined cycle power plants. Steam cycles can reach a really

high efficiency thanks to decades of technical improvements, full optimization of the key components and a deep knowledge of all the phenomena occurring in the thermodynamic cycle. However the use of water as working fluid, for small available thermal power inputs and/or low maximum temperatures of the heat source, entails a number of difficulties which mainly affect component design and cycle performances. For instance, for small-size plants, namely power outputs below 5 MW_{el}, and medium high heat source temperatures, the mass flow rate at turbine inlet is dramatically low. This is due to the large enthalpy of vaporization of water which involves technical issues in the design of the turbine first stage which usually requires a strong partial admission. On the other hand, for medium-large power outputs but low temperatures, namely below 200°C, the use of water as working fluid entails really low evaporating temperatures with a two phase flow expansion. Since most of the heat is introduced in phase transition the maximum attainable cycle efficiency is limited and issues related to blade erosion have to be considered.

The rest of the diagram in Figure 3.1 is occupied by ORC field where the correct selection of a suitable working fluid allows overcoming the over mentioned difficulties. Most relevant applications are described in next sections while the technical advantages related to the thermodynamic properties of organic fluids are discussed in Section 4.2.5 (Effects on component design and cycle configuration). The upper limit to ORC technology is represented by the thermal stability limit, above this temperature the organic fluid starts to decompose changing in both physical and thermodynamic properties. More information about organic fluids stability at high temperature can be found in section 4.2 (Thermal stability).

3.1 Market Companies

ORC market is relatively small compared to other power generation technologies like steam cycle or gas turbines, and it is characterized by a great variability in terms of plant sizes and plant specifications. As already stated, different plant layouts and different working fluids can be used to exploit a given heat source which can vary from case to case in a large range of available thermal powers and maximum heat source temperatures. Differently from steam power cycle, gas turbines and combined cycle technology, ORC market does not allow the standardization of the technical solutions and generally any plant is customized on the requirements of the client and on the available heat source. Furthermore this sector requires very specific expertise for the design of components working with organic fluids like the turbine. As result of this, only few companies have been establish on the market, two companies in particular ORMAT and Turboden are the

market leaders in geothermal and biomass energy sector respectively, while besides them a notably number of emerging companies are gaining their respectability on the market offering advanced and non-conventional solutions. Among them Exergy is surely the most promising one thanks to a really smart turbine design and the use of supercritical cycles with perfluorinated fluids, while other ones, like Electra-therm and Tri-O-Gen, are oriented to small ORCs for WHR applications. Finally it is important to underline the difference between companies, like those just mentioned, which are able to design the whole plant in detail, optimizing and manufacturing the turbine by themselves and those engineering companies which work as EPC contractor projecting ORC systems but transferring outside the turbine design and the component production.

Five successful companies can be listed in the first group:

- *Ormat* [47] is the most prominent company in ORC field. It is focused on geothermal application, waste heat recovery from industrial plants and remote applications. Ormat has an installed power which is higher than the sum of all the other ORC companies on the market.
- *Turboden* [48] is an Italian Company owned by Mitsubishi, specialized in the design of small multistage axial flow turbines for ORCs. It is the marked leader for biomass application especially in Europe where it has been realized more than 250 plants in the last thirty years. In geothermal field they own a relevant share of the European installed power.
- *Exergy* [49] is an emerging Italian company which offers advanced supercritical cycles with radial outflow turbines. In the last years they have applied their concept to different applications in WHR and geothermal energy fields. In addition they work as EPC contractors for large geothermal power plants in Turkey.
- *ElectraTherm* [50] is a small American company oriented to the development of small 30-60 kW_{el} WHR generators based on a screw volumetric expanders. They have the technical support of prominent scientist in the design and optimization of these devices and a pilot plant (100 kW_{el}) is now under operation in Nevada.
- Tri-O-Gen [51] offers a small scale ORC unit working with toluene. Their 160 kW_{el} module is extremely flexible and it can be integrated with any hot liquid or gaseous stream. A radial inflow turbine with a really advanced design is the core of their technology. Their module is installed in more than 20 industrial plants coupled with biomass or WHR applications.

Companies which work as EPC contractors in ORC field are:

- *TAS Energy* [52] is an American engineering company oriented to different markets. They built several binary geothermal power plants in USA and Turkey and their share is approximately the 10% of the global ORC market.
- *Adoratec* [53] is a German company which installed, in the past years, several small-medium size biomass ORCs around Europe. It has been recently acquired by Maxxtec [54].
- GMK [55] is a company focused on German market. They offer ORCs for biomass application, WHR from ICE and other industrial facilities and they own a small geothermal plant.

Beside these companies there are several other ORC turbine and expander producers which don't offer the whole plant engineering:

- *Atlas Copco* [56] is one of the most prominent company in this field and they provide expanders to most of the ORC EPC contractors. Atlas Copco is the market leader for radial inflow turbines, from really small size up to tens of MW of shaft power. In addition it is one of the first producers of scroll and screw compressors which can be used as expanders in ORC systems.
- *Cryostar* [57] is a French company which develops ORC turbines mainly for the European market.
- *Calnetix GE* [58] is a company recently bought by General Electric which produces high speed small size radial inflow turbines with magnetic bearings
- *Infinity turbine* [59] is an American company which produces expanders of different sizes for the ORC market. Screw models are offered for sizes from 1 to 10 kW_{el} while for higher shaft powers namely 30, 85 and 250 kW_{el} centripetal turbines are designed.

Several other companies are present on the market like Verdicorp [60], a spin-off of Danfoss which is testing oil-free high-speed centripetal turbines with magnetic bearings for small size ORCs (30-45-60-75 kW_{el}) and Durr [61] which proposes four modules (70, 120, 300 and 500kWel) for high temperatures applications (300°C) in both pure electric and CHP configurations and four modules for low temperature heat sources (90-150°C). Cogen [62], Eneftech [63] and Flow Energy [64] are instead oriented to civil and domestic CHP applications and WHR from automotive engines but their models are still under testing and they are not available on the market.

3.2 Applications

ORCs cover a large range of applications: from really small civil cogeneration units up to large waste heat recovery from industrial processes like cement, steel or glass production. ORC systems can be coupled with fossil fuels in remote or civil applications or with renewable energy sources like solar and geothermal energy. In the next sections a brief overview of the different applications where ORC are used, or they might be used, is reported with reference to experimental activities and operative plants for each field [65].

3.2.1 Biomass conversion

Biomass is an important energy source which allows power production with a limited emission of carbon dioxide into the atmosphere. Three main systems can be used for the utilization of biomass as primary energy source for power generation, namely (i) combustion, (ii) gasification and (iii) anaerobic digestion. Combustion and gasification are thermal processes based on the complete or on the partial oxidation of biomass to produce directly thermal power or a CO-H_2-CH_4 based syngas fuel. On the other hand, anaerobic digestion is a biochemical process which also produces a fuel gas which can be used for power generation.

Biomass combustion is usually directly coupled with a cogenerative ORC plant in medium-small scale CHP (Combined Heat and Power) systems and it is one of the fields of major success for ORCs. Biomass combustion power plants are available on the market in a range of power output between 200-6500 kW and they are a common technology in central and north Europe where this sector has been grown considerably in the last decades thanks to a relatively cheap biomass availability and feed-in tariff mechanism promoted by governments with the aim of reducing carbon dioxide emission. Biomass boilers usually operate with synthetic oil as HTF (Heat Transfer Fluid) instead of a direct heat transfer to the working fluid. This last arrangement would allow achieving a higher efficiency but, because of the higher pressures inside of the combustion chamber, it requires the presence of a patented operator on the plant with a relevant increase of operation costs. Using a HTF, on the other hand, entails low pressure of the oil circuit and specific expertise are needed just during regular maintenance. Commonly used HTF are synthetic oils like Dowtherm A and Therminol VP-1 which can generally reach a maximum operating temperature around 300-350°C leading to net electric efficiencies values in the range of 18-21% in CHP configuration. Some studies are instead focused on the use of molten salts as HTF with the purpose to reach a higher efficiency [66] but no experimental plant has been tested so far. The capability of ORCs of adapting easily to load variations, maintaining high electric efficiencies at part load is therefore appreciable,

since it allows following the heat demand, keeping high performance. Generally high complexity fluids are used like hydrocarbons (toluene or hexane), fluorinated fluids or light siloxanes with a subcritical saturated recuperative plant configuration. This combination of working fluid and cycle layout leads to really high expansion volume ratios when the condensation is made with ambient air or water from a river or from a cooling tower. The high volume ratio for each stage entails detrimental effects on turbine efficiency (see Section 6.1(Axial flow turbines) for more details) but, despite this effects, the cycle efficiency in pure power generation can be increased up to 25% [67]. However the design in pure electric production is pretty unusual and biomass plants are usually operated in CHP configuration, connected to a district heating network thus limiting volume flow variations in expansion and entailing an easier design of the turbine.

Market leader for this application is Turboden which has installed so far more than 200 biomass combustion ORCs in Germany, Austria and Italy. All of them are controlled in remote and the plants start-up, the shut-downs and the regulation don't require skilled operators directly on the plant. Another company oriented to this sector is Tri-O-Gen which has installed lately some of their package in different sawmills in Europe.

The other two ways to exploit the biomass for power production are rarely coupled directly with an ORC. Both gasification and anaerobic digestion produce a syngas which is generally use to feed an internal combustion engine (ICE) for power production [68]. ORCs are possibly adopted to recover the heat from the hot streams coming from the engine cooling circuits and from the exhaust gases released by the motor. Anaerobic digestion is widely adopted in many regions and it is mainly connected to agricultural activities for sugar and corn production. Examples of WHR ORC from endothermic engines are already available on the market and are offered by Exergy and by Tri-O-Gen. Biomass gasification entails instead several difficulties related to the high content of humidity, ashes and corrosive compounds which can damage the metal materials or plug the gasification unit. The synthetic fuel gas, mainly composed of CO, H_2, CH_4 and CO_2, has to be cleaned before being fed to an internal combustion engine for electricity production with additional operative costs [69; 70; 71].

A graphical view of the European distribution of ORC coupled with biomass burners is reported in Figure 3.2

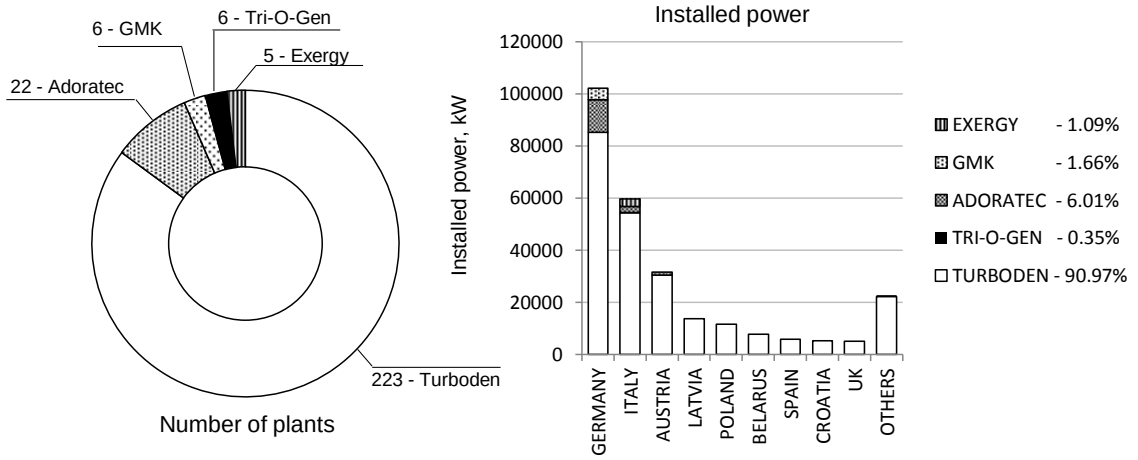

Figure 3.2 - European distribution of biomass ORC divided by number of installation and installed power

3.3 Hot geothermal brines

Geothermal heat sources are characterized by a wide range of temperatures (roughly from 60°C to 300°C) and large available thermal powers (up to hundreds of MW_{th}). Temperature, pressure and composition of the geothermal fluid are extremely site dependent and big differences can be highlighted even among wells in the same geographical area. The deepness of the reservoir, the kind of rocks surrounding it and the presence of marked thermal anomalies are key factors for the selection of the best plant layout for the exploitation of a given geothermal source.

ORCs are used mainly for the exploitation of liquid hot geothermal brines in a pure binary cycle plant layout: the geothermal fluid is pumped from the reservoir to the surface with a submerged pump, it is cooled down releasing heat to the ORC and it is eventually reinjected to the reservoir in order to limit the well depletion. Main concerns about this technology are related to the composition of the hot brine: usually big amounts of salts are dissolved in the water causing fouling deposition on the heat exchanger surfaces thus limiting the global heat transfer coefficients and entailing additional maintenance costs for the chemical or the mechanical cleaning of the inner tubes surfaces. Moreover corrosive compounds like H_2S are usually present entailing special materials and a more expensive equipment. Finally, if the geothermal brine contains a large amount of incondensable gases, the thermodynamic properties of the geothermal fluid can be noticeably different than pressurized water. Usually the two phases are separated and both the vapor and the liquid streams are sent to the ORC unit. The vapor stream is condensed but, since it contains a huge fraction of incondensable gases the process is not isothermal involving more difficulties in the design of the PHE.

ORCs are nowadays proposed even for two phase or superheated vapor geothermal fluids because of the higher attention to global warming effect. In the past the vapor stream was simply expanded by a steam turbine and the discharged fluid was generally released to the environment. Nowadays this plant layout is not allowed anymore because of the high content of carbon dioxide, H_2S and other compounds with a relevant impact on greenhouse effect. The general trend is to adopt zero-emission geothermal plants where the whole fluid extracted is reinjected to the reservoir. This practice limits the depletion of the geothermal well, reducing the temperature decay and it guarantees a higher power production during the plant life. Depending on the quality of the geothermal fluid, its temperature, pressure and content of incondensable gases different plant layouts can be adopted but basically ORCs can be used to recover heat from the both the liquid and the gaseous stream discharged by the steam turbine as reported in Figure 3.3. These solutions are named "mixed cycles" or "combined cycles" [72].

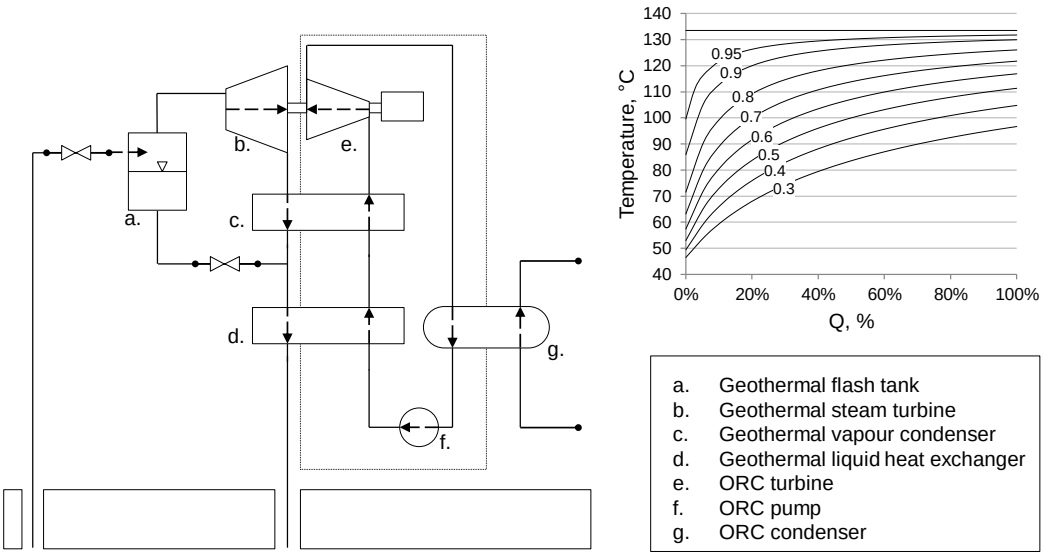

Figure 3.3 - Scheme of a geothermal binary plant exploiting a two phase flow geothermal fluid and temperature variation in a T-Q diagram for vapour condensation in presence of non-condensable gases at 3 bar.

In geothermal field usually subcritical saturated cycles are adopted using linear or branched hydrocarbons like butane or pentane or refrigerant fluids as R245fa. Supercritical cycles are adopted as well generally using refrigerants. For instance, TAS Energy, which owns the 15% of the installed world power, is specialized in supercritical cycles, while in Italy can be highlighted the experimental activity on a 500 kW_{el} supercritical cycle with R134a carried out by Enel Green Power, Turboden and Politecnico di Milano.

Geothermal ORCs are characterized by a relatively high specific investment costs, related to the relevant exploration and drilling costs (more than 50% of plant cost) and the

relatively low cycle efficiencies (7-15%). The market have been oriented so far to large power plants from 10 to 100 MW_{el} even if in the last years more attention have been reserved to small medium size power plant (2-5MW_{el}) and low temperature geothermal brines (100-120°C). In Figure 3.4 the world distribution of the binary geothermal power plants is reported.

A last field of possible application are the EGS (Enhanced Geothermal System) which are deep, dry and high temperature rocks which can be fractured by the injection of pressurized water in order enhance the system permeability and to create a system of cavity which behaves like a large surface heat exchanger. An ORC binary plant can be used to exploit these resources [73; 74].

3.3.1 Waste heat recovery

In many industrial processes, large amount of heat are available like hot gaseous or liquid streams. They were generally wasted and heat was released to the environment. Energy efficiency policies, the higher cost of both the electrical energy and the fuels have lead many industrial sectors to pay more attention to the energy recovery from available hot streams with the aim of reducing the overall plant power consumption. Many of these industrial applications are characterized by large available thermal power (tens of MW_{th}) and high temperatures (300-400°C); in this range ORCs have to compete with small steam Rankine cycles which are commonly proposed for these applications. Steam cycles can take advantage from a lower heat exchanger cost, thanks to the higher heat transfer coefficients, while usually the turbine requires a larger number of stages and it is more expensive. From a techno-economical point of view it is not clear which technology presents the lower LCOE and applications are commonly labeled as “grey zone”.

Cement plants are an example of industrial processes suitable for the application of ORCs and some commercial installation are currently under operation. In cement plants, heat is released as hot exhaust combustion gases and hot air from clinker cooling. Approximately 26% of the total heat input is lost [75; 76] and the available thermal power ranges between 5 and 100 MW_{th}, depending on the size and the efficiency of the plant with temperatures in a range between 200 and 400°C. Examples of this kind of installations are the Turboden plants in Marocco (owned by Italcementi) and in Romania (owned by Holcim) producing 2 MW_{el} and 4 MW_{el} respectively and the Ormat plants in India (owned by A.P. Cement) and Germany (owned by Heidelberger Zement) producing 4.8 MW_{el} and 1.5 MW_{el} respectively. Several papers have been published lately investigating the potential of ORC for this application [75; 77].

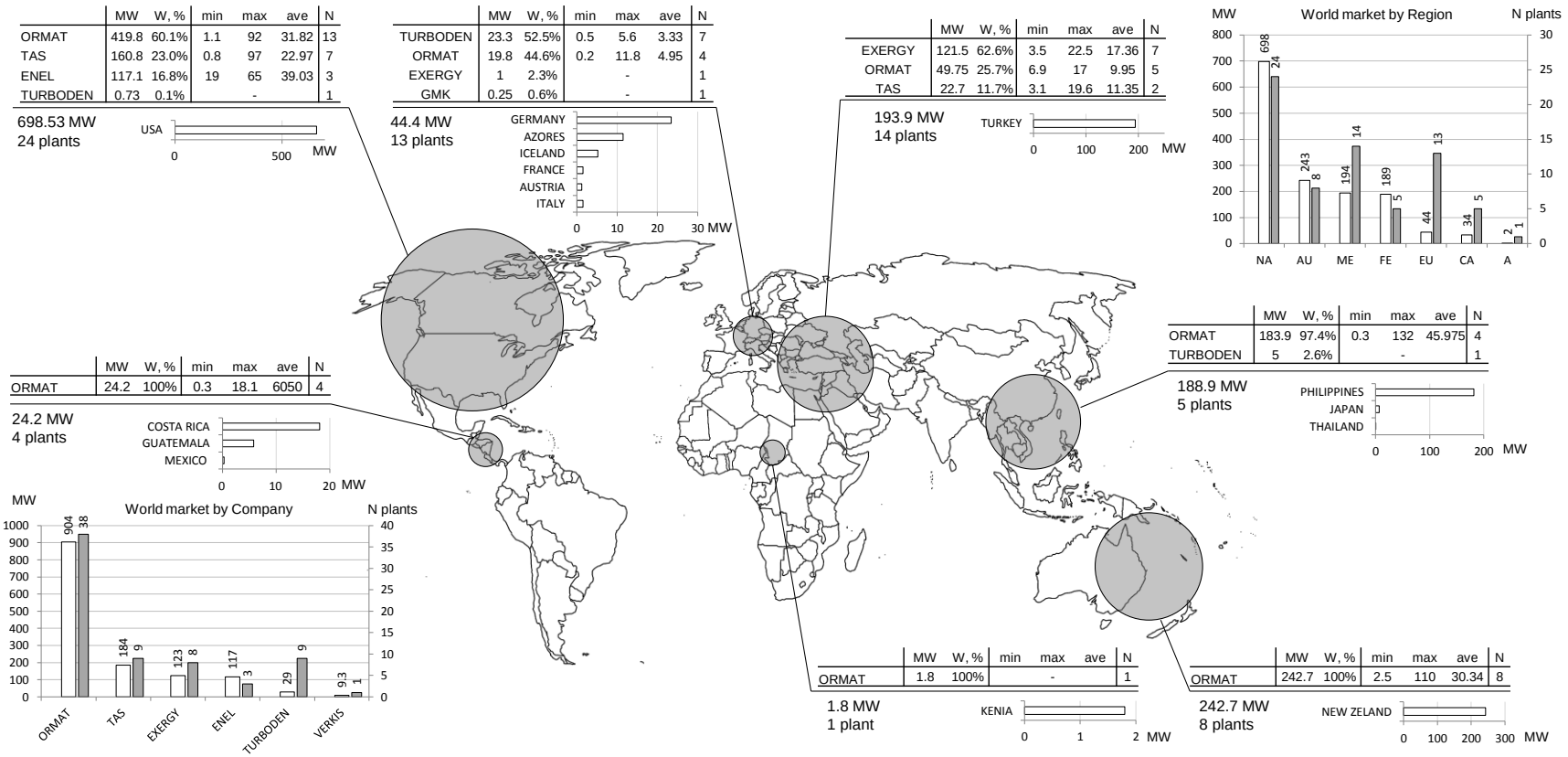

Figure 3.4 - Use of ORC geothermal binary plants installed in the world.

Iron and steel industry is another important candidate for the application of ORCs. Two main sources of waste heat are present. The first one is the exhaust combustion gas from pre-heating furnaces of rolling mills. This gas results from natural gas combustion and it is hence quite clean. Heat is normally available after the air preheater at temperatures around 300°C, with thermal powers in the order of 2.5-4.0 MW_{th} [78]. Heat might be exploited at higher temperatures, thus leading to potentially higher ORC efficiencies, if the heat exchanger of the heat transfer fluid is placed before the air preheater at the furnace outlet (700-800°C). Another important application in the iron and steel industry is heat recovery from electric arc furnaces [79]. In this application the high dust content in the flue gas and the variations of temperature and flow rate make the heat recovery process more complex entailing relevant off-design operation for the ORC. In addition, the high temperatures of the heat available (in principle even higher than 1000°C) and the high power (tens of MW_{th}) make steam cycles more appropriate for these applications. However, plant owners may be interest to ORC for their simplicity and their competitive off-design performances.

Glass industry is another sector of possible application of ORC technology. Heat can be recovered at temperatures of 400-600°C, down to about 200°C. This source is characterized by stable temperature profile and a constant mass flow rate of the exhaust gases.

Last important applications are related to the recovery of the heat from internal combustion engines (ICE), small gas turbines and high temperature fuel cells. The integration with ICE is a common commercial practice to improve the system overall efficiency and almost all the ORC producers offer this solution in their catalogues. With this solution it is possible to increase the power output up to 3% if the heat is recovered simply from the water jacket and up to 10% if the heat of the high temperature flue gas is exploited. A particular success of this application has been observed recently on biogas-fired engines, as already described previously in the dedicated section. An interesting package is the PowerBox 125 commercialized by Exergy and Ingeco [80]: the whole ORC is realized on a skid which can be installed and connected to the plant in a single day. It is based on a R245fa saturated cycle using an high speed (around 20000-25000 RPM) turbine produced by Calnetix GE with magnetic bearings and direct connection with a fast generator. Frequency is reported to the grid one by means of a power electronics group.

A similar application is proposed for the recovery of the heat from small-size gas turbines flue gases, which are too small for a conventional bottoming heat recovery steam cycle. The impact of the application of an ORC coupled with a gas turbines with power outputs

in the 4-35 MW_{el} range is investigated in literature with a possible increase of power output around 20-35%. A study of the Politecnico di Milano, also analyzed the possibility of applying ORCs on even smaller machines, like a 100 kW_{el} microturbine [9]. In this study, an additional power output of 45 kW_{el} has been estimated, with an overall estimated cost of the entire system of about 4000 €/kW_{el}.

Another application is WHR from fuel cells where large amount of heat is available at different temperatures according to the fuel cell type: the overall performance can be increased of more than 5% with PEM (Proton Exchange Membranes) [81; 82] while other studies investigate the matching with high temperature fuel cells like SOFC (Solid Oxide) and Molten Carbonate fuel cells [83; 84].

A schematic view of the use of ORCs for WHR application is reported in Figure 3.5.

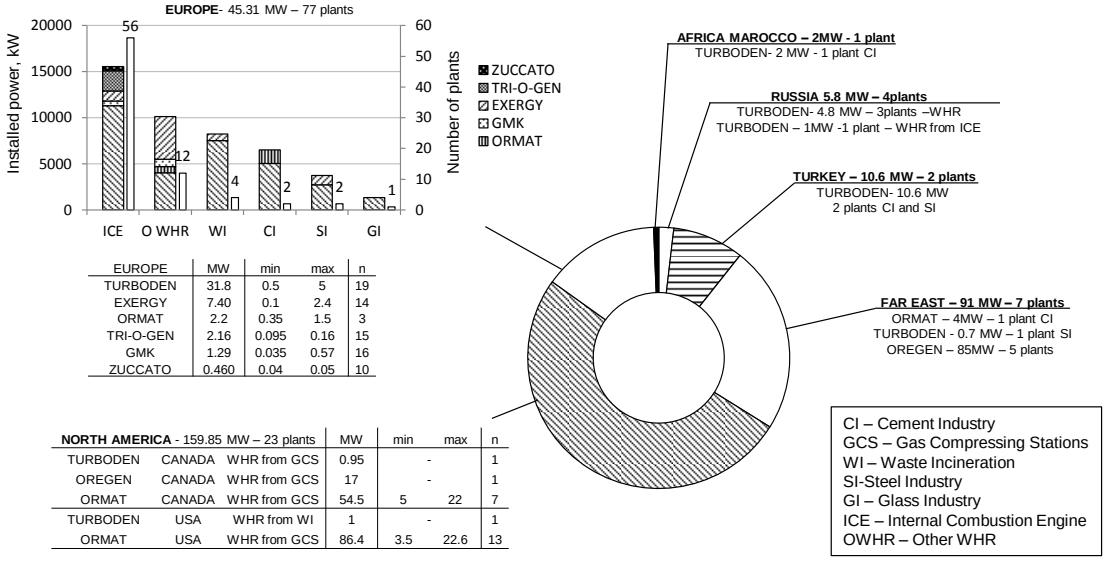

EUROPE	MW	min	max	n
TURBODEN	31.8	0.5	5	19
EXERGY	7.40	0.1	2.4	14
ORMAT	2.2	0.35	1.5	3
TRI-O-GEN	2.16	0.095	0.16	15
GMK	1.29	0.035	0.57	16
ZUCCATO	0.460	0.04	0.05	10

NORTH AMERICA - 159.85 MW – 23 plants			MW	min	max	n
TURBODEN	CANADA	WHR from GCS	0.95	-		1
OREGEN	CANADA	WHR from GCS	17	-		1
ORMAT	CANADA	WHR from GCS	54.5	5	22	7
TURBODEN	USA	WHR from WI	1	-		1
ORMAT	USA	WHR from GCS	86.4	3.5	22.6	13

Figure 3.5 - ORC WHR world market divided by countries and producers

3.3.2 Solar power application

Concentrating solar power is a proven technology, which can be used in combination with ORC cycles in small scale installations. This technology exploits the solar radiation to heat up an opportune HTF, generally a synthetic oil or a molten salt, in the solar collectors. The hot fluid eventually transfers the heat to the working fluid driving the ORC.

In large-scale multi-MW plants, this heat is used in steam water cycle for power production, with average annual overall conversion efficiencies of 14-18% [85; 86]. In these plants, high cost collectors and large thermal storage (7.7h_{eq}) are usually employed,

allowing for high temperatures of the heat transfer fluids, high efficiencies of solar radiation to heat conversion and hence high overall plant efficiencies [87]. In smaller scale installations instead, ORCs become competitive with steam cycles. In these plants, cheaper collectors, suitable for lower maximum temperatures can be used. Two examples of such application are the concentrating 1.2 MW_{el} solar power plant built by ORMAT in Arizona in 2006 and the 5.5 MW_{el} Turboden plant in Kalaeloa Hawaii which is not yet in operation. N-pentane was selected in the first case as working fluid, allowing for cycle efficiency higher than 20%, with an overall solar to electricity efficiency at the design point of 12.1%. Another interesting application of ORCs combined with solar power is the stand-alone configuration in remote areas, for final users not connected with the electric grid. The application of this system was recently proposed by STG International [88; 16] for a rural clinic in Lesotho, utilizing built-in-site parabolic trough collectors, monoethylene glycol as HTF and a R245fa-based ORC with a 3kW_{el} scroll expander.

An interesting use of ORCs with solar power is the direct use of organic fluid into the solar collectors [89]: in this application working fluid is not evaporated in the solar field thus allowing the direct storage in tanks filled by a solid medium as represented in Figure 3.6. Flash triangular cycles or one level cycle with throttled admission in Complete Flashing Cycles are proposed for low temperature and high temperature applications respectively. More details about these cycle configurations are reported in Chapter 5 (Thermodynamic cycle configurations).

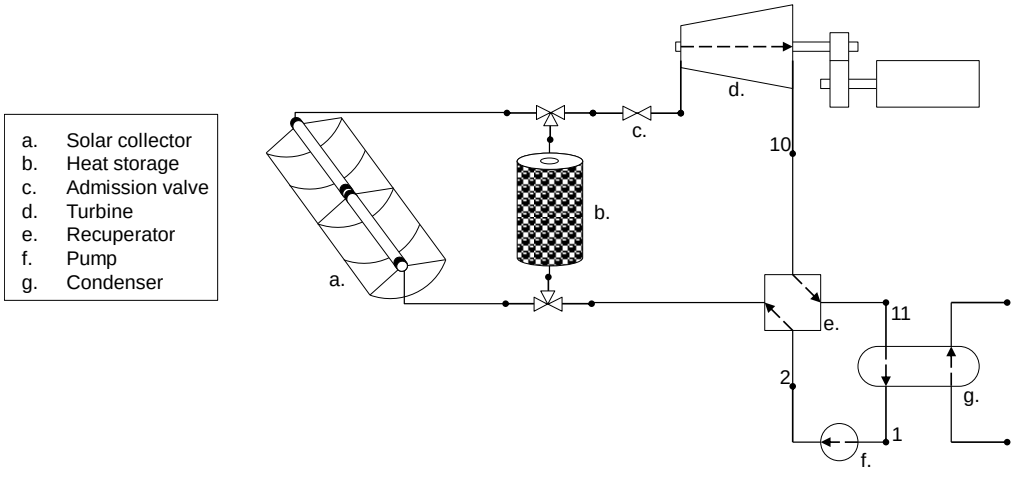

Figure 3.6 - Direct solar power plant layout with direct storage and throttled turbine admission.

Some experimental activities have been carried out investigating the coupling of ORC with linear Fresnel collectors [90], with plane or evacuated collectors [91; 92] and with small compound parabolic collectors [93].

3.3.3 Other applications

Many other applications are proposed for ORCs for very small available thermal powers or very low heat source temperatures. Even if their use is nowadays confined to niche markets, the potential upside of these fields is impressive due to high number of possible installations.

Civil and domestic cogeneration

Domestic burners are today characterized by high thermal efficiencies, often greater than 100% respect to the LHV of the natural gas, thanks to the use of condensing boilers. However large second law losses are related the heat transfer process from the hot gases produced by the natural gas combustion to the hot water for domestic purposes. Small domestic CHP unit are proposed on the market and they are based on a Stirling engine receiving heat from the hot gases and releasing thermal power to the water circuit. Wispergen [94] and Baxi [95] are the market leaders in this field with a relevant number of units in operation around the world. Both models consist in a package with a dimension slightly larger than a common domestic burner which can fit in regular kitchens but they differ in the design of the Stirling engine. Wispergen engine is based on a four pistons wobble joke mechanism while Baxi uses a free piston machine. The units are operated following the thermal load and in nominal condition they can produce 1kW$_{el}$ with an electric efficiency around 9-11%. In this field small ORCs using a volumetric expander are proposed as possible competitors of Stirling units. Few examples of commercial packages offered on the domestic and the civil market are reported in Table 3.1.

	Flow energy	Cogen	Enef tech			
level	commercialized	testing	commercialized			
country	UK	Australia	Switzerland			
Model name	Flow (ex Kingston)	Cogen	Enefcogen ^{PLUS}	Enefcogen ^{GREEN}		
Heat source	Natural gas biofuels	Solar panels hot gases	Any hot stream In (160-200) Out (130-170)	Any hot stream In (140-150) Out (115-130)		
expander	scroll	Protected by patent (no scroll or screw)	scroll	scroll		
W_{th}	7 -18 (add.burner)	8.8	33	80	170	255
W_{el}	1	1	5	10	20	30
η_{tot}	95%	ND	95%	95%		
η_{el}	6.8%	ND	12.5%	10%		
Hot water T, °C	Out (85°C)	NS	In (20-50) Out (30-60)			

Table 3.1 - Commercial models of ORC for domestic and civil CHP applications.

Specific cost is relevant for ORCs as well for Stirling based units (at least around 12500 $/unit) and their diffusion is strictly connected to government subsidies.

WHR from automotive engines

Another field which is gaining more and more attention in the last years is the use of ORC coupled with on-road engines. Truck heavy duty diesel engines release to the environment large amount of heat since the efficiency of these devices generally ranges between 30-35% and the thermal power can be recovered from different streams having different thermal levels. In particular heat is available at low temperature from the CAC[1] (Charge Air Cooler) and from the LT-EGR[2] (Low Temperature Exhaust Gases Recirculation) and at high temperature from the HT-EGR and the EC (Exhaust flue gas Cooler). In Table 3.2 the thermal power available from each stream and the temperature of these sources are reported: the highest temperature is found in the HT-EGR where heat is available at combustion chamber temperature, while the temperature of flue gases is considerably lower because of the presence of the expander and the after treatment unit for the removal of NO_x (SCR or LNT) and particulate (DPF). Heat is available instead at temperature around 150°C from CAC and LT-EGR. In addition, thermal powers are not homogeneously distributed and the amount of heat available at the exhaust cooler greatly exceed the other ones entailing a non trivial configuration of the ORC for the WHR from all the streams.

	HT-EGR	EC	LT-EGR	CAC
Available heat, kW	57	391	21	55
Max Temperature, °C	688	540	250	185
Min temperature, °C	250	120	100	60

Table 3.2 – Thermal power and temperature level of the hot streams available from a 2010 heavy duty diesel engine [96]

One of the most advanced configuration proposed in literature [96] is based on a supercritical cycle with a preheating at low pressure with the LT-EGR and the CAC in parallel and a heat introduction at high pressure with the HT-EGR and the exhaust cooler as shown in Figure 3.7.

[1] In the CAC the air charge is cooled down after the turbo compressor stage in order to increase the performances of the engine.

[2] The EGR allows the recirculation of a fraction of high cooled exhaust gases rate into the combustion chamber with the fresh compressed air. This practice allows delaying the combustion and reducing the NO_x production.

Heat is rejected to the environment in the radiator where a temperature difference with the ambient air of at least 50°C is required. Usually a volumetric expander is proposed since the power output ranges between 3 kW to 50 kW depending on the size of the motor which consist in a power production increase of 20% without additional fuel consumption.

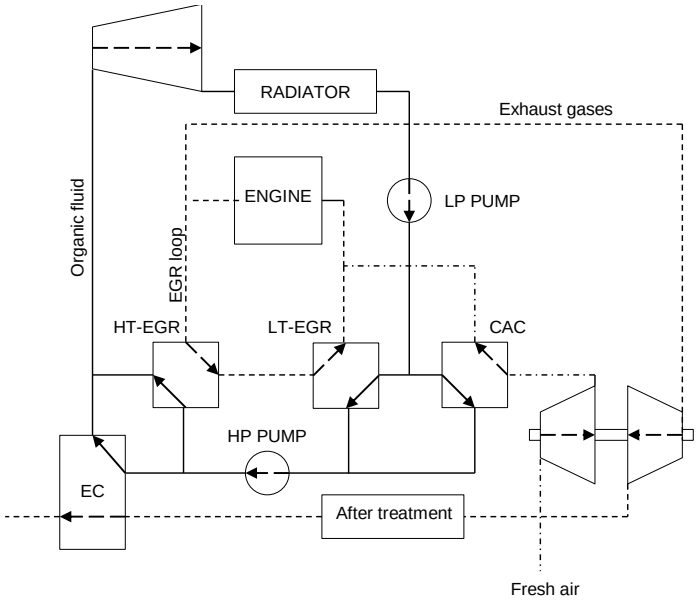

Figure 3.7 - Scheme of the integration of ORC in an automotive turbo diesel engine – rearranged from [96]

Water desalinization

ORC plant could be directly used to drive the pump of a reverse osmosis process, leading to the possibility to produce fresh water in dry areas using sunlight, which is usually abundant in areas where water desalinization is needed. The best combination within solar collector and ORC comes from the use of low concentration parabolic trough or flat plate collectors (e.g. AoSol 1.12X, FPC Vitosol 200F, FPC SchücoSol U.5DG, ETC Vitosol 300), combined with a low temperature ORC [97]. In this way is possible to achieve an overall efficiency (solar to electricity) of the system between 20.6% and 14% using toluene, 18% and 12% with octamethylcyclotetrasiloxane (D4) 17% and 10% with hexamethyldisiloxane (MM) (the efficiency range is obtained from different minimum temperature of the thermodynamic cycle) [98]. All these values show how the desalination process combined with an ORC presents lower specific energy consumption than solar distillation and solar photovoltaic systems separately.

Remote applications

Another important advantage of ORC technology is the possibility of producing small amounts of power in remote installations, like arctic areas or offshore and on shore platforms, where high reliability and the possibility of operation without skilled staff are of primary importance. Leader in this application is Ormat which offers on the market a very compact micro-mini ORC named CCVT (Closed Cycle Vapor Turbogenerator) with a power output ranging from 0.4 kW_{el} to 40 kW_{el} even if the average size installed so far is around few kW_{el}. These devices are extremely reliable, they can be fed with several different fuels and they don't need the presence of operators on site. The CCVT is used in remote areas mainly for pipelines anodic protection or for off-shore platform not connected to the grid. In table the list of Ormat installations is reported in Table 3.3.

Location	Year	Unit size, W	Unit number
Alaska	2010	800	144
Italy	2003	4000	2
UK	2004	4000	1
Netherland	2004	4000	1
Russian Federation	1974	1200	30
	1983	400-2000	270
	1994	1200	220
	1999	2000	38
	2000	1200	80
	2004	2500	8
	2006	1200	4
	2006	800	12
	2007	1200	4
	2007	2000	102
	2010	4000	22
China	2007	600	8
Indonesia	2005	4000	1
	2008	4000	1
Australia	1984	4000	28
TOTAL		1383 kW	976

Table 3.3 - Ormat remote CCVT ORC installations.

OTEC

The last application where ORC can be used is OTEC (Ocean Thermal Energy Conversion) which is based on the fascinating idea to exploit the temperature difference between deep and surface waters in oceans. A thermodynamic cycle working with ammonia or a refrigerant fluid like R134a can be design to work between the warm surface water and the cold deep water and in particular the OTEC technology is attractive where the thermal gradient is relevant within 1000 m depth. A large belt around the equator presents temperature difference higher than 20°C, a value which makes OTEC

technology able to produce power with reasonable efficiencies [99; 100]. Many issues are related to this technology and many attempts were carried out in the last fifty years but no one of them had success mainly because of the failures and damaging of the deep tube. In fact, it is necessary to pump a huge deep water flow rate with flexible pipes which are subjected to relevant stress due to the action of ocean streams and tidal currents. In conclusion this technology is ideally characterized by large power outputs and very small temperature differences and it might greatly contribute to the power production for many countries but its reliability is far to be proved. It represents an application with intrinsic low efficiencies and techno-economic difficulties and so far only few projects have been operated for a short time [101].

3.4 Typical heat source temperature profiles and limits

In ORC field most of the heat sources can be described with a single phase fluid. Hot geothermal brines and synthetic oil from engine cooling circuit, biomass combustion chamber or solar power plants can be assumed as incompressible liquids with a heat capacity value described with a polynomial function of temperature. This latter assumption is valid even for gaseous streams like exhaust gases from ICE or hot gases from industrial processes whose behaviour can be described with an ideal gas model. For all the above mentioned cases a constant value or a linear function of temperature can be assumed to describe the hot source heat capacity without introducing any relevant error. The only case where all this assumption cannot be adopted is a geothermal brine characterized by a two phase stream with a relevant amount of non-condensable gases which is nowadays a niche market in ORC field. The temperature profile of this hot source shows a particular trend which is reported in Figure 3.3 due to the fact that vapour condensation in presence of non-condensable gases entails a progressive reduction of vapour partial pressure thus reducing the temperature. This trend is not easily described by a polynomial curve and the numerical solution of the phase equilibrium is required in several sections of the heat exchanger in order to locate the exact pinch point of the PHE (Primary Heat Exchanger).

Another parameter which affects the final solution and in particular the choice of the best combination of working fluid and plant layout is the heat source minimum temperature. The cooling down of the heat source can be limited by a number of technical reasons which substantially change depending on the type of exploited energy source:

- For geothermal application the limit is related to the precipitation of salts present into the geothermal brine. Independently if the hot water stream is obtained from the flash of the geothermal fluid, from the separation of vapour and incondensable

gasses or by using a submerged pump into the well, the geothermal brine contains a high percentage of salts which can greatly vary from one well to well. These compounds are mainly carbonates, sulphates and nitrates of alkaline metals like sodium and calcium and their composition is strictly related to the kind of rocks surrounding the geothermal reservoir. Depending on chemical species and their concentration there is an operative temperature limit below which salts start precipitating with the formation of fouling on heat exchanger surfaces and entailing a reduction of heat transfer coefficients and an increase of pressure drops. This limit, also called reinjection temperature limit, is pretty difficult to define and its evaluation procedure requires the exact knowledge of the brine composition and the calculation of the chemical species equilibrium for different temperatures. On the basis of Enel experience in geothermal energy exploitation this technical limit is fixed to 70 °C for most of the geothermal plants nowadays in operation in Nevada and Arizona. Another consequence of an excessive cooling down of the geothermal brine is the premature depletion of the reservoir whose temperature is progressively reduced during the plant life time. A cooling down of about 1-2°C per year was reported in operating plants exploiting a geothermal brine with an initial maximum temperature of 150°C involving a reduction of cycle performances in the last year of operation. Last concern about the presence of salts into the geothermal brine is related to the design and operation of primary heat exchangers. In particular the necessity of periodical surface cleaning, in order to remove fouling, involves the location of hot brine inside of the tubes. In this way maintenance of the devices is easier and cheap techniques, as mechanical cleaning using passive cleaning bodies, can be used. This technique consists in conveying bodies made by a matter brushes or scrapers, called pigs, to the tubes. Pigs are pushed by compressed air or pressurized water and they remove incrustations by friction. However the high pressure working fluid is located in the shell side in contrast with common design principles and the resulting heat exchanger requires a thicker vessel and it is more expensive, but the operation and maintenance costs are strongly reduced with an increase of plant reliability.

- In heat recovery applications hot gasses are usually obtained from combustion processes or from the cooling of hot devices like endothermic engines. In the first case the lower limit of exploitation of the heat source is related to the minimum temperature allowable at the stack in order to avoid condensation of water which is present in the gases as combustion product. Depending on the fuel used and on the excess of air in combustion this temperature can vary in a range of 100-180°C where the higher value is referred to low C/H ratio fuels. In the case of biomass

combustion hot gases usually do not release heat directly to the working fluid and generally a HTF is used in loop circulation between the biomass boiler and the ORC. In this latter case the lower temperature limit is set according to the specifications of pollutants removal units placed after the heat recovery and the requirements of air pre-heating. If the hot stream is a hot liquid or a clean and non humid gas it can be cooled down to ambient temperature without any drawbacks and the lower limit is set by a techno-economic optimization of the whole system.

- In solar thermal power plants the lower temperature limit of the heat source is mainly related to physical properties of the heat transfer fluid, usually a synthetic oil, which flows into the collector of the solar field. From a general point of view reducing the temperature of the HTF at solar field inlet allows achieving two main effects for a constant heat input to the ORC.
    - The solar collectors work with a lower average tube wall temperature limiting the heat losses to the ambient. The thermal efficiency of the solar field is higher guaranteeing a better exploitation of solar energy and thus reducing the area of solar collectors.
    - Furthermore the HTF temperature change is larger and the mass flow rate required is smaller with a completely different design of the solar field where a smaller number of longer loops is required. However the decreasing of pressure drops in the piping and in the headers is usually lower than the corresponding increase in the solar collectors leading to higher pressure drops which might cause an higher solar field pump consumption. This is due to both the modular architecture of solar collectors and the physical properties of synthetic oil. At temperature below 50 °C synthetic oils commonly used in solar plants show a rapid increase of viscosity which contributes to the increase of specific pressure drops.

  The selection of the optimal temperature limit for an indirect solar power plant is the result of a trade of between the increase of solar collector efficiency, the oil mass flow reduction and the pressure drops increase which results in a smaller solar collector area but likely in a larger auxiliaries power consumption.

“If it can't be expressed in figures,

it is not science; it is opinion.”

Lazarus Long

4 Organic fluids and their properties

The key idea of ORC technology is to select the most suitable working fluid according to the temperature level of the heat source and the available thermal power input. Several studies have been carried out with the aim of selecting the best working fluid for a given heat source but just few of them face the problem with a general approach allowing to define criteria, rules or a methodology for working fluid selection process. The main limit of most of the studies is a non-clear pre-selection of working fluids candidates which leads to comparisons between solutions which are far to be optimized from this point of view. In addition, in many papers, results are compared with a poor detail and the effects on components design and sizing are usually not taken in to account. However, some publications [12; 18; 20] present a clear methodology considering different fluids and the effects of fluid choice on equipment performance and cost. To perform the correct evaluation of both ORCs performance and cost it is crucial to use (i) state of the art equations of state for the calculation of fluid thermodynamic properties and (ii) reliable routines to link the component design and efficiency to the fluid characteristics. In this section, organic working fluids are presented first on the basis of their chemical classification and their environmental impact and safety issues. After, a comparison among the possible working fluids for ORCs is presented in terms of specific properties and the effects of the working fluid selection on the cycle configuration or on the components design are addressed. Finally, some information and some recommendations regarding the effect of using different working fluids on component sizing is presented.

4.1 Environmental impact

In ORCs the working fluid is usually confined and it is not vented to the atmosphere, excepted in case of failure of some components and the consequent fluid leakage. However, accidents are always possible and a minimum amount of fluid is always released even in normal operation. Therefore, the use of fluid with a low environmental impact is preferable. Environmental impact can be described by two indexes namely the ODP (Ozone Depletion Potential) and the GWP (Global Warming Potential).

Ozone Depletion Potential

The ozone layer is a portion of the stratosphere, between 20 and 30 km from the earth surfaces where the concentration of ozone O_3 is higher. The Ozone layer absorbs most of

the Sun's UV (Ultra Violet) radiation (97%-99%) which otherwise can damage the life organisms on the earth, an example is the cancer onsets for the human beings due to skin absorption of UV rays. The ozone layer is constantly depleted by chemical compounds released by anthropologic activities which have caused the reduction of the layer thickness and a reduction of ozone concentration evaluated in 4% per decade [102] with a consequent hazard for the whole ecosystem. These compounds are free radical catalysts like nitric oxide (NO), nitrous oxide (N_2O) and atomic chlorine (Cl) and bromine (Br). The emission of these chemical species is strictly related to industrial activities and in particular the release of halogen atoms is exclusively due to the use of man-made organ-halogen compounds like CFC (chloro fluoro carbons), HCFC (Hydrochlorofluoro carbons) and bromofluorocarbons which were widely used in the 70s and 80s as refrigerant fluids, propellants for aerosol and solvents. A single radical of these species can activate a sequence of reactions which can destroy more than 100000 molecules of ozone. The damaging potential of a chemical compound is defined by means of the ODP index which represents the overall potential of a compound respect to a molecule of chlorofluoro carbon whose ODP is equal to unit by definition. Compounds containing Br atoms are more stable entailing a higher ODP while, if hydrogen atoms are present, the molecule tends to decompose easily leading to a lower ODP index. If no atoms of Br or Cl are present, the ODP is null [103].

The use of these compounds is regulated by a series of normatives which, starting from the Montreal Protocol 1987, have progressively reduced the use of halogenated molecules which have been banned since 1996 in most of the developed countries.

Chemical class	ODP	group
CFC	1	Group I,III section 602 of the CAA
BrFC	3-16	Group II section 602 of the CAA
HCFC/HBrFC	0.002-2.2 (depending on the H/Cl, H/Br ratios)	Group V-VI-VII-VIII accelerated phaseout final rule

Table 4.1 - ODP index for different chemical compounds and their classification in the international normative

Global Warming Potential

Global warming potential index is a quantity which expresses the impact of a single molecule of a certain compound compared to the CO_2 molecule in term of greenhouse effect. Greenhouse effect is a phenomenon which interests the atmosphere of our planet and it is recognized as the main reason of the increase of the atmosphere temperature in the last decades. Solar radiation penetrates the atmosphere and it is absorbed by the earth surface. A certain amount of energy is re-emitted with a wavelength typical of infra-red

radiation. This radiation in normal condition is dissipated toward the space while in presence of chemical compounds in the air it is absorbed and re-emitted again toward the Earth surface. This effect is leading to an uncontrolled temperature increase of the atmosphere, entailing a high desertification rate in many regions and melting of poles ice with a consequent rising of sea levels. From Kyoto protocol in 1997, which entered in legal effect in 2005, many countries have been started to put the global warming effect at the centre of their environmental policy. Unfortunately, the whole project is far to be incisive because (i) no monetary penalty are considered for countries which don't respect the protocol, (ii) the participation is voluntary and nations like USA, and Canada did not ratified the protocol or they have decide to renounce to the further agreements and (iii) many countries like China and India are considered developing countries and they do not have any binding targets. As a result, despite the increase of renewable energy sources, a higher efficiency of industrial processes and the use of more eco-compatible automotive solutions, the concentration of carbon dioxide into the atmosphere have been constantly increased in the last ten years.

Most of the organic fluids used in ORCs have a high GWP: in particular fluorinated compounds which are used as fluids in refrigeration and automotive air conditioning show GWP index which can exceed 2000, with consequent issues concerning their release into the environment at the end of devices life. Refrigerant fluids are not yet banned from these applications but many chemical companies like Honeywell [104] have invested great efforts in producing low GWP drop-in fluids for refrigerant R134a like R1234yf.

4.2 Safety concerns

The flammability and the toxicity of the working fluid entail safety issues and additional hazard protections which can increase the overall plant cost. Different safety standards have been defined by different institutions for the classification of the flammability and the health hazard of chemical compounds but, due to the different scale and quantities taken as reference, the comparison among them is not easy. In this chapter the NFPA (National Fire Protection Association) standard 704 "Standard system for the identification of the Hazards of Materials for Emergency Response" is adopted. Four categories are considered forming the so called "fire diamond": health hazard (blue), flammability (red), Reactivity (yellow) and white containing special notes for particular hazards. Each category is rated from 0 to 4 corresponding respectively to no hazard and severe risk according to definition in Table 4.2.

	Health (blue)	Flammability (red)	Reactivity (yellow)
0	Material that on exposure under fire conditions would offer no hazard beyond that of ordinary combustible material.	Material will not burn. (if combustion does not occur in air at 816°C for an exposure period of 5 minutes)	Material that in itself is normally stable, even under fire exposure conditions, and is not reactive with water.
1	Material that on exposure would cause irritation but only minor residual injury.	Material must be pre-heated before ignition can occur.Flash point >93°C	Material that in itself is normally stable, but which can become unstable at elevated temperatures and pressures
2	Material that on intense or continued but not chronic exposure could cause temporary incapacitation or possible residual injury.	Material must be moderately heated or exposed to relatively high ambient temperature before ignition can occur. 38<Flash point <93	Material that readily undergoes violent chemical change at elevated temperatures and pressures or which reacts violently with water or which may form explosive mixtures with water.
3	Material that on short exposure could cause serious temporary or residual injury.	Liquids and solids which can be ignited at ambient conditions 23<Flash point <38	Material that in itself is capable of detonation or explosive decomposition or reaction but requires a strong initiating source or which must be heated under confinement before initiation or which reacts explosively with water.
4	Material that on very short exposure could cause death or major residual injury	Materials that will rapidly or completely vaporize at atmospheric pressure and normal ambient temperature, or that are readily dispersed in air and that will burn readily. Flash point <23°C	Material that in itself is readily capable of detonation or of explosive decomposition or reaction at normal temperatures and pressures.

Table 4.2 – NPFA standard 704 for hazard classification of chemical compounds

Thermal stability

Organic fluids exposed to high temperature tend to decompose entailing a maximum temperature limit in ORC field as represented by the dotted line in Figure 3.1. Hydrocarbons and halogenated compounds with a molecule backbone chain formed by carbon atoms are subject to cracking processes at temperature higher than their critical point. Cracking and pyrolysis of the molecule forms residual molecules and solid particles, with a consequent increase of the fouling resistance on heat exchanger surfaces, damage of turbine blade surfaces and a notable change of the fluid thermodynamic properties.

Chemical stability limit for most of the fluids used in ORCs is set around 400°C even if for low boiling temperature fluids a lower limit is considered. The threshold of thermal stability is evaluated by experimental activities where the saturation pressure of fluid is measured after a permanence of 5 to 50 hours at high temperatures and comparing the obtained values with the nominal ones. The departure from nominal data is evaluated during and after the exposure at high temperatures because for some fluids the degradation starts during the cooling process. Different campaigns are usually performed for different temperatures and different time of permanence at high temperature [105]. A difference of 1% respect to nominal data after a permanence of 50 h is assumed as the threshold for the definition of the temperature stability limit.

4.1 Chemical classification

By definition an organic compound is a molecule containing carbon atoms but usually the label “organic fluid” is used to define all the fluids different from water. Some examples are present in literature: for instance $TiCl_4$ biomass combustion power plant [66] and all the publication focused on ammonia Kalina cycle. However, even limiting the classification to organic compounds, the variety of available working fluids is very wide, including very different molecules, from light and simple molecules like CO_2 and CH_4 up to complex fluorinated hydrocarbons and siloxanes.

Hydrocarbons

Hydrocarbons are molecules made exclusively by carbon and hydrogen atoms: the basic molecule is methane (CH_4) while more complex hydrocarbons are obtained by combination of CH_x unit where x can vary from 0 to 3 depending on the type of chemical

bounds and the molecule configuration. Hydrocarbons can be divided in several others subgroups on the basis of:

- *C-C bounds type*: a couple of adjacent carbon atoms can be bounded with single, double or triple bound depending on the number of electrons shared by each atom. If all the carbon atoms are connected by single bounds the molecule is an alkane while if at least one double or triple bound is present, the molecule is an alkene or an alkyne respectively.
- *Molecule spatial configuration*: a single carbon atom bounded with four single bounds to four other atoms of the same type, like CH_4 or CF_4 for instance, is characterized by a tetrahedral spatial configuration which minimizes the molecule energy maximizing the angles between bounds (109.5°). If different atoms are substituted to the central atom or the atoms are connected by double or triple bounds the tetrahedral configuration is distorted because of the different atomic radius of bounded atoms or radicals and their different electro negativity. Hydrocarbons can be classified in three main groups: linear, branched and cyclic molecules.

Thermodynamic properties of alkanes with the same number of atoms are not really affected either by bound type or molecule spatial configuration.

In ORCs, hydrocarbons are commonly used in many different applications: relatively light linear and branched hydrocarbons like iso-butane, n-butane are suitable fluids in subcritical saturated cycles for the exploitation of low temperature geothermal brines, while more complex fluids like hexane and toluene are employed in CHP biomass combustion power plant.

In ORCO, 23 hydrocarbons are considered: they are reported in Table 4.3 with their critical properties, the minimum temperature, the maximum temperature and pressure, the NFPA 704 hazard codes and the GWP.

Fluorinated hydrocarbons

They are formed by a backbone chain of carbon atoms with fluorine atoms substituted instead of hydrogen ones. If no hydrogen atom is present the molecule is labeled perfluoro carbon. Fluorinated molecules can be spatially arranged in linear, branched or cyclic configuration. Their molecular complexity is comparable to hydrocarbons having the same number of atoms but their molecular weight is higher due to the presence of fluorine atom, entailing different thermodynamic properties. The lightest fluids of this category are commonly used in the air conditioning and refrigeration field as pure fluid or

in mixture, but they are recommended even for low temperature ORC power systems. High temperature fluorocarbons are proposed for WHR from industrial processes and biomass combustion application. The main advantage in using hydrofluorocarbons and perfluorocarbons is the limited safety issues and the less expensive hazard protection required since most of these fluids are neither toxic nor flammable. On the other hand they are usually more expensive than other organic fluids but price greatly varies depending on the fluid type and the application.

Siloxanes

Siloxanes are long and complex molecules formed by a long chain or a large ring of Silicon and Oxygen atoms connected by single bounds. These molecules are chemically similar to silicones and thus they are extremely stable even at high temperatures. In addition most of them are chemically inert and they are not either flammable or toxic (except for MM). Siloxanes are used in biomass applications and are suggested for high temperature concentrating solar power plants with working fluid circulating directly in the solar collectors and throttled turbine admission.

Other organic fluids

Other organic compounds are alcohols and ketones where a –OH group or a =O atom is connected to a carbon atom. They are generally characterized by a relatively low molecular mass compared to high complexity organic fluids but the possibility to create hydrogen bounds leads to high critical temperatures.

	fluid	chemical formula	Tcrit, °C	pcrit, bar	Tmin, °C	Tmax, °C	pmax, bar	H	F	I	GWP
Linear alkanes	propane	CH_3-CH_2-CH_3	96.7	42.5	-188	376.9	10000	1	4	0	
	iso-butane	$(CH_3)_2$-CH-CH_3	135	36.3	-159	301.9	350	1	4	0	
	butane	CH_2-$(CH_2)_2$-CH_2	152	38	-138	301.9	690	1	4	0	
	neo-pentane	$(CH_3)_3$-C-CH_3	161	32	-16.6	276.9	2000	1	4	0	
	iso-pentane	$(CH_3)_2$-CH-CH_2-CH_3	187	33.8	-161	226.9	10000	1	4	0	
	pentane	CH_2-$(CH_2)_3$-CH_2	197	33.7	-130	326.9	1000	1	4	0	
	iso-hexane	$(CH_3)_2$-CH-$(CH_2)_2$-CH_3	225	30.4	-154	276.9	10000	2	3	0	
	hexane	CH_2-$(CH_2)_4$-CH_2	235	30.3	-95.3	326.9	1000	2	4	0	
	heptane	CH_2-$(CH_2)_5$-CH_2	267	27.4	-90.6	326.9	1000	1	3	0	3-6
	octane	CH_2-$(CH_2)_6$-CH_2	296	25	-56.8	326.9	1000	1	3	0	
	nonane	CH_2-$(CH_2)_7$-CH_2	321	22.8	-53.5	326.9	8000	1	3	0	
	decane	CH_2-$(CH_2)_8$-CH_2	345	21	-29.7	401.9	8000	1	2	0	
	dodecane	CH_2-$(CH_2)_{10}$-CH_2	385	18.2	-9.55	426.9	7000	1	2	0	
Cyclo alkanes	cyclo-pentane	cycle $(CH_2)_5$	239	45.7	-93.4	326.9	2000	1	3	0	
	cyclo-hexane	cycle $(CH_2)_6$	280	40.8	6.32	426.9	800	1	3	0	
	methyl-cyclo-hexane	cycle $(CH_2)_6$-CH_3	299	34.7	-126	326.9	5000	1	3	0	
	n-propyl-cyclo-hexane	cycle $(CH_2)_6$-CH-$(CH_3)_2$	358	28.6	-95	376.9	500	1	3	0	
Aliene and alkynes	1-butene	CH_2=C-$(CH_3)_2$	145	40.1	-141	276.9	500	1	4	0	
	2-methyl-1-propene	CH≡C-CH_2-CH_3	146	40.1	-185	251.9	700	1	4	0	
	trans-2-butene	CH_3-CH=CH-CH_3	155	40.3	-106	251.9	500	1	4	0	
	cis-2-butene	CH_3-CH=CH-CH_3	163	42.3	-139	251.9	500	1	4	0	
	benzene	cycle =(CH)-	289	49.1	5.55	476.9	5000	2	3	0	
	methyl-benzene	cycle =(CH)-CH_3	319	41.3	-95.2	426.9	5000	2	3	0	
Alcohols and ketons	dimethyl ether	CH_3-O-CH_3	127	53.4	131.7	525	400	1	4	1	
	acetone	$(CH_3)_2$-C=O	235	47	178.5	550	7000	1	3	0	
	methanol	CH_3-OH	240	82.2	175.6	620	8000	1	3	0	
	ethanol	CH_3-CH_2-OH	242	62.7	250	650	2800	1	3	0	

Table 4.3 - Working fluids available in Refprop which are considered in this study and ORCO software: H, F, I refer to NFPA 704 standard - Table 1/2

	fluid	chemical formula	Tcrit, °C	pcrit, bar	Tmin, °C	Tmax, °C	pmax, bar	H	F	I	GWP
Refrigerant fluids	R125	CF_3-CHF_2	66	36.2	172.5	500	600	1	0	0	3500
	R218 (perfluoro propane)	CF_3-CF_2-CF_3	71.9	26.4	125.5	440	200	1	0	0	8830
	R143a	CF_3-CH_3	72.7	37.6	161.3	650	1000	1	4	0	4470
	R32	CH_2F_2	78.1	57.8	136.3	435	700	1	4	1	675
	R1234yf	CH_2=CH-CF_3	94.7	33.8	220	410	300	1	4	0	4
	R134a	CF_3-CH_2F	101	40.6	169.9	455	700	1	0	1	1430
	R227ea	CF_3-CH_2F-CF_3	102	29.3	146.4	475	600	1	0	1	3220
	R161	CFH_2-CH_3	102	50.1	130	400	500	1	4	0	12
	R1234ze	CHF=CH-CF_3	109	36.3	168.6	420	200	1	4	0	
	perfluoro butane	CF_3-$(CF_2)_2$-CF_3	113	23.2	189	500	300	1	0	0	
	R152a	CHF_2-CH_3	113	45.2	154.6	500	600	1	4	1	124
	perfluoro cycle propane	cycle -(CF_2)-	115	27.8	233.4	623	600	2	0	0	10300
	R236fa	CF_3-CH_2-CF_3	125	32	179.5	500	400	1	0	0	9810
	R236ea	CF_3-CF_2-CHF_2	139	34.2	242	500	600	1	0	0	9810
	R245fa	CF_3-CH_2-CHF_2	154	36.5	171.1	440	2000	2	1	0	1030
	R365mfc	CF_3-CH_2-CH_2-CHF_2	187	32.7	239	500	350	0	4	1	794
siloxanes	MM	$C_6H_{18}OSi_2$	246	19.4	273	673	300	1	4	0	
	MDM	$C_8H_{24}O_2Si_3$	291	14.2	187.2	673	300	1	3	1	
	D4	$C_8H_{24}O_4Si_4$	313	13.3	300	673	300	1	2	0	
	MD2M	$C_{10}H_{30}O_3Si_4$	326	12.3	205.2	673	300	1	2	1	
	D5	$C_{10}H_{30}O_5Si_5$	346	11.6	300	673	300	1	2	0	
	MD3M	$C_{12}H_{36}O_4Si_5$	355	9.45	192	673	300	1	1	0	
	D6	$C_{12}H_{36}O_6Si_6$	373	9.61	270.2	673	300	1	2	0	
	MD4M	$C_{14}H_{42}O_5Si_6$	380	8.77	300	673	300	1	1	0	
	ammonia	NH_3	132	221	-77.7	426.9	10000	3	1	0	
	water	H_2O	374	113	0.01	1727	10000	0	0	0	

Table 4.4 - Working fluids available in Refprop which are considered in this study and ORCO software: H, F, I refer to NFPA 704 standard - Table 2/2

4.2 Thermodynamic properties of organic fluids

As mentioned in the previous section, organic fluids are usually characterized by long, heavy and complex molecules. These peculiarities entail thermodynamic properties which are very different from water. In particular, some properties are affected by molecular complexity while other ones by fluid molecular mass [7]. In ORC field it is crucial to understand the independent effects of these two parameters on fluid properties and eventually on cycle configuration and components design. It is important to underline that in the same chemical group molecular complexity is strictly connected to molecular mass. For instance, for linear hydrocarbons an increase of molecular complexity, obtained by adding -(CH_2)- units, always leads to a heavier molecule. The same is true for fluorinated fluids. However, from a general point of view, considering the effects of these two quantities equivalent is not possible, especially if fluids from different chemical groups are compared.

In this section, a brief summary of the equations used to describe ideal fluids are reported together with some calculations applied to real fluids. Similarities and differences are highlighted with a focus on those properties which mainly affect turbine design and the configuration of the thermodynamic cycle. Only pure fluids are here considered and some notes about the use of mixtures are reported in section 4.2.6 (Use of mixtures vs pure fluids).

An ideal gas is a fluid which matches the following assumptions:

- Molecules are described by points, they do not have a finite volume and their mass is lumped into the barycenter. They can be assumed as very small hard spheres.
- No dissipative phenomena occur during motion and during collisions, thus frictionless movement and perfectly elastic physical interactions are assumed.
- There are no repulsive or attracting forces between the molecules or between the molecules and the environment.

These hypotheses are verified for every fluid at very low pressure and high temperature: a thermodynamic state where molecules are far from each others, collisions occur with a small probability and molecules are moving fast without interference in their trajectories. In ORCs the hypothesis of ideal gas is never verified because usually saturated cycles or supercritical cycles with expansion close to the saturation line are used. Fluid thermodynamic behavior greatly differs from the ideal one because real gas effects affect notably the volumetric and some thermodynamic properties of the working fluid.

Reliable equations of state are required in order to estimate with good accuracy the thermodynamic properties of organic fluids in a wide range of temperatures and pressures (in particular near the saturated vapor condition and above the critical point) and to correctly evaluate the performances and the dimension of key components like the turbine. In this work, Refprop 9.1 [106] is used because it implements state of the art equation of state as better explained in section 8.2.1 (Case definition) and it is definitely the most suitable database for fluid thermodynamic properties estimation. In Refprop more than 50 pure organic fluids are available without considering chlorinated compounds which are not usable anymore because of their high ODP. The complete list of the pure fluids that can be used in ORCO is reported in Table 4.3 and Table 4.4 together with their critical parameters. In this chapter, the available working fluids are divided in the previously defined chemical classes with the aim of underlining general considerations about real fluids behavior. If not otherwise stated, the reference condition for the calculation of real fluids thermodynamic properties is the same for all the considered fluids. Since most of the ORC thermodynamic cycles are based on a subcritical cycle with a small superheating and because the turbine is the component which is mainly affected by real gas effects, the reference condition is calculated by imposing an evaporation temperature intermediate between ambient temperature and the critical one according to eq. 4.1.

$$T_{ref}^{eva} = T_{cond} + 0.7\,(T_{crit} - T_{cond}) \qquad \text{eq. 4.1}$$

A superheating equal to 10°C is considered.

4.2.1 Compressibility factor

Compressibility factor Z is a useful parameter to understand if a fluid, in a certain condition is close to an ideal gas behavior and the ideal gas law can be used to describe it. Z is equal to the ratio between the real density of the fluid and the ideal gas one calculated in the same condition of pressure and temperature according to eq. 4.2.

$$Z = \frac{p}{T\frac{R}{MM}\rho} \qquad \text{eq. 4.2}$$

The corresponding state principle states that all the fluids show the same volumetric behavior as function of reduced temperature and pressure and so a conclusion obtained for a fluid can be, with a reasonable accuracy, extended to other compounds. In Figure

4.1 the contour map of Z factor for R134 fluid is reported. It is possible to notice how an almost ideal gas behavior is found only at very low pressures, in a region compatible with turbine outlet condition while at turbine inlet, for pressure close to the critical point, Z values between 0.6 and 0.9 are obtained even with a considerable superheating.

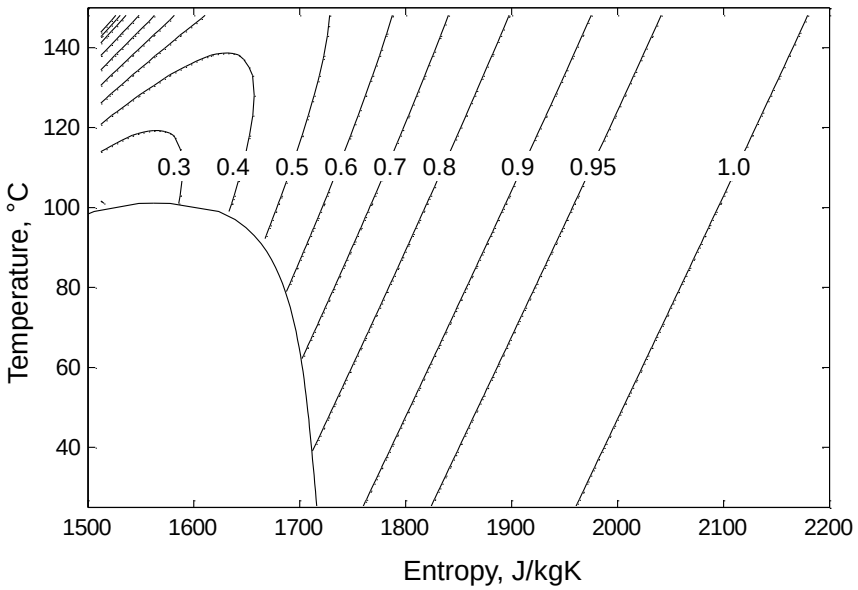

Figure 4.1 - Compressibility factor close to the saturation line and above the critical point for R134a

Variations of compressibility factor along the expansion greatly affects the turbine design since the larger volume flow ratio entails a more challenging design of turbine stages having big flaring angles and smaller blades at the first row.

4.2.2 Properties affected by molecular complexity

Some thermodynamic properties are mainly influenced by molecular complexity; in this section a brief overview of their calculation for ideal gases and a comparison with real fluid values calculated at the reference point is proposed.

Molar heat capacities

Molar heat capacity at constant volume is defined by eq. 4.3 and its value can be calculated by the sum of the contributions of the excited degrees of freedom of the molecule (n_{DoF}). According to the kinetic theory of gases the contribution of a single degree of freedom is equal to 1/2 R.

$$Cv_{molar} = \left(\frac{\partial u}{\partial T}\right)_V = \frac{1}{2} R\, n_{DoF} \qquad \text{eq. 4.3}$$

Where R is the gas constant equal to 8.314 kJ/kmolK.

Degrees of freedom are divided in translational, rotational and vibrational and the number of each of them strictly depends on the molecule structure.

- *Mono-atomic molecules*: the only mechanism which allows the molecule to absorb energy is to increase the kinetic energy along the three spatial directions *x*, *y* and *z*. The corresponding n_{DoF} is equal to 3[3].
- *Bi-atomic* and *tri-atomic linear molecules*: in addition to the three translational degrees of freedom bi-atomic molecules can absorb energy by rotation around the two axis perpendicular to the direction defined by the bound between the two atoms[4]. In addition to translational and rotational degrees of freedom, molecules with more than one atom can store energy by vibration thus changing the distance between the atoms. This latter effect is function of the temperature and its contribution can be calculated as the sum of the vibrational energies corresponding to molecules natural frequencies. n_{DoF} is equal to 5 without considering vibration contribution.
- *Poly-atomic molecules*: for molecules with more than two atoms even the rotation around molecule axis is considered because usually the presence of substituted atoms or radicals increases the corresponding momentum of inertia. Furthermore the high number of natural frequencies entails a strong dependency of heat capacity on the temperature as reported in Figure 4.2.

[3] At really high temperatures phenomena like ionization or electronic excitation contribute to absorb energy but, referring to ORC technology, these effects are certainly negligible because usually maximum temperatures are limited by the thermal stability limit of the fluid.

[4] The rotation around the axis of the molecule passing through the barycentre of the two atoms is possible but the corresponding momentum of inertia is extremely small and its contribution can be considered negligible.

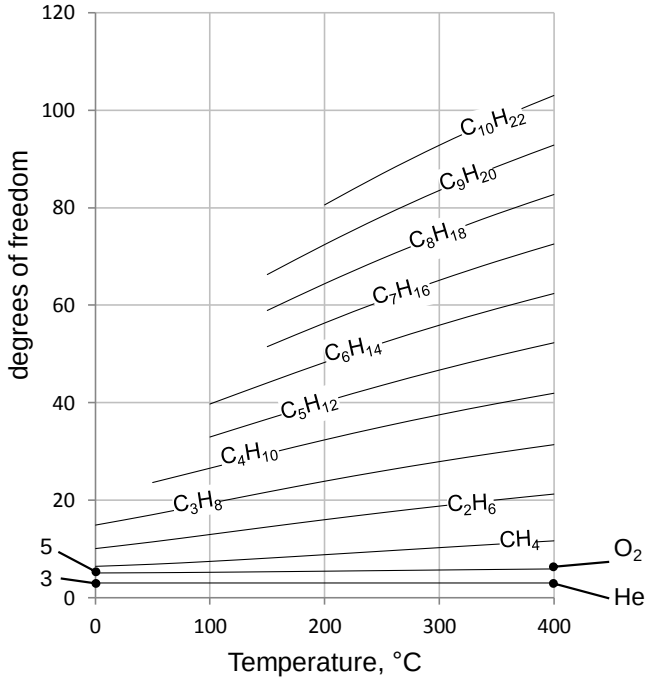

Figure 4.2 – Degrees of freedom of different compounds computed from the value of Cv_{molar}. Data are calculated with Refprop 9.1 for helium, oxygen and linear hydrocarbons series from methane to decane.

According to the ideal gas analysis for helium the n_{DoF} is equal to 3 and constant for all the temperatures while for oxygen it is 5 at low temperatures and it reaches a value around 7 at 400°C thanks to the small contribution of vibrational energies typical of a bi-atomic molecule. For the others fluids, the numbers of degrees of freedom is notably higher than 6 (3 translational plus 3 rotational) and it strongly increases with the number of atoms in the molecule and so the number of natural frequencies. In particular for complex fluids the share of vibrational energies can be 10 times more than the sum of translational and rotational degrees of freedom. As a general rule the number of degrees of freedom for a polyatomic molecule is approximately equal to three times the number of atoms.

Molar heat capacity at constant pressure is defined by eq. 4.4 and, for ideal gases, it can be calculated from constant volume heat capacity by eq. 4.5.

$$Cp_{molar} = \left(\frac{\partial h}{\partial T}\right)_p \qquad \text{eq. 4.4}$$

$$Cp_{molar} = Cv_{molar} + R \qquad \text{eq. 4.5}$$

In Figure 4.3.a the trend of Cp_{molar} against the number of atoms in the molecule is represented for different classes of fluids. All the data are aligned on the same line and molecular mass, bounds type and molecule spatial configuration have a little effect on this property compared to the number of atoms and to molecular complexity.

Heat capacity ratio γ

From the value of molar heat capacities, it is possible to calculate the value of the γ coefficient which is a fundamental parameter for the evaluation of the thermodynamic properties of ideal gases along an isentropic expansion. This quantity is greatly influenced by molecular complexity because it is the ratio between isobaric and isochoric heat capacities and it can be calculated by eq. 4.6.

$$\gamma = \frac{Cp_{molar}}{Cv_{molar}} = 1 + \frac{R}{n_{DoF}} \qquad \text{eq. 4.6}$$

For high complexity fluids with a large degrees of freedom, the value of γ tends to unit as represented in Figure 4.3.b. It is possible to note that γ is always a decreasing function respect to the number of atoms and all the data are ordered almost on the same trend independently of the chemical group, the molecule configuration and the molar mass of the molecule.

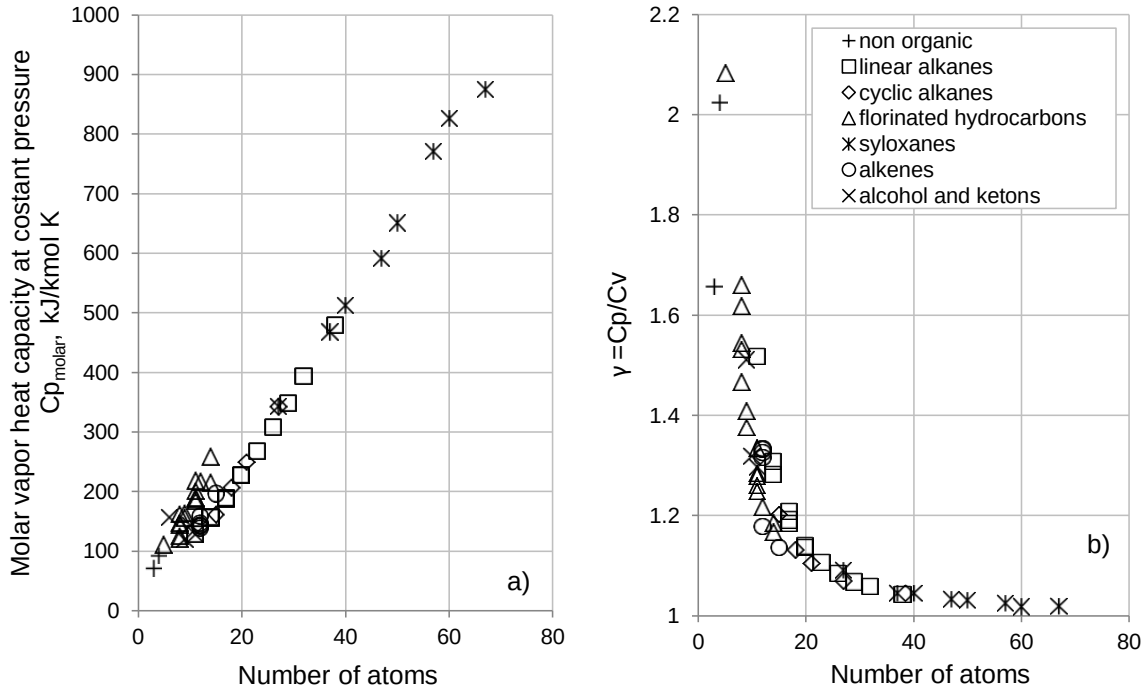

Figure 4.3 - Trends of Cp_{molar} (a) and heat capacity ratio (b) against molecule number of atoms.

Cv_{molar}, Cp_{molar} and γ values for mono-atomic, bi-atomic and poly-atomic molecules are reported in Table 4.5.

	n_{DoF}			Cv_{molar}	Cp_{molar}	γ
	translational	rotational	vibrational			
Mono-atomic	3	-	-	$3/2\,R$	$5/2\,R$	$1.\overline{6}$
Bi-atomic	3	2	1	$\sim 3R$	$\sim 4R$	$\sim 1.\overline{3}$
Linear	3	2	$\sim 3n-5$	$\sim 3nR$	$\sim (3n+1)R$	$\frac{3n+1}{3n} \to 1$
Poly-atomic	3	3	$\sim 3n-6$			

Table 4.5 - Summary of ideal gases heat capacity

However, γ is equal to the heat capacity ratio only with ideal gases, while for real gases three different isentropic expansion coefficients should be calculated by equations from eq. 4.7 to eq. 4.9 [107].

$$pv^{\gamma_{pv}} = const \qquad \text{eq. 4.7}$$

$$Tv^{(\gamma_{Tv}-1)} = const \qquad \text{eq. 4.8}$$

$$p^{(1-\gamma_{pT})}T^{\gamma_{pT}} = const \qquad \text{eq. 4.9}$$

A comparison between the values of the two isentropic expansion coefficients and the value of the ideal Cp/Cv is reported in Figure 4.4. It is important to notice that for real gases the use of the ideal heat capacity ratio leads to large errors in the evaluation of expansion process form a volumetric point of view, underling once again that the use of a suitable equation of state is of primary importance to achieve reliable results.

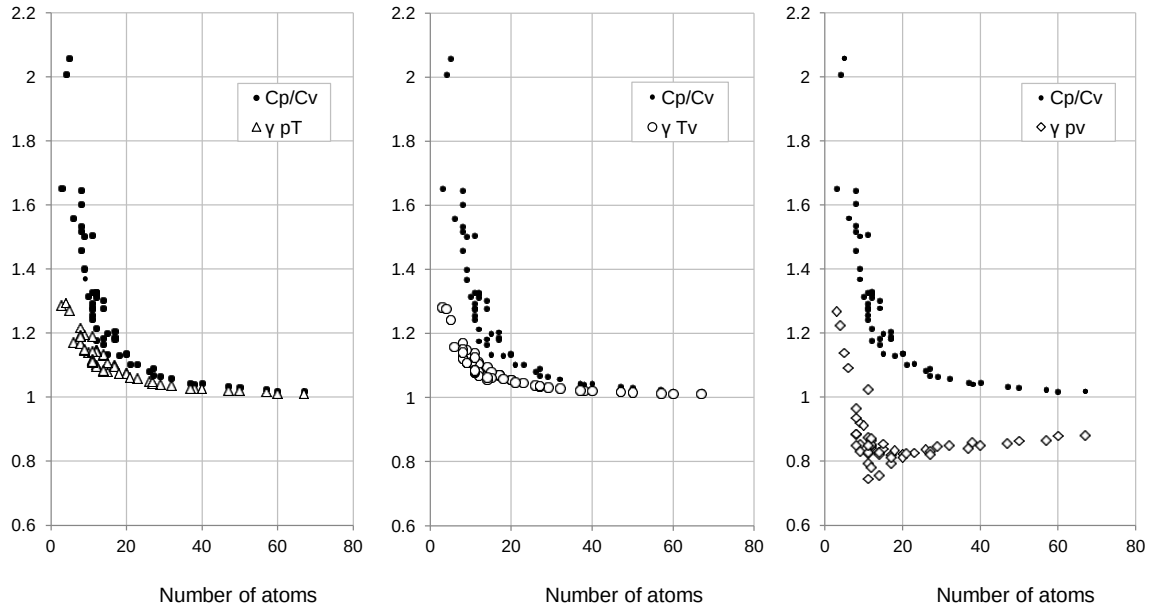

Figure 4.4 - Real isentropic expansion coefficients compared with the ideal gas heat capacity ratio

Andrew curve

Other considerations can be done about the value of liquid heat capacity respect to the vapor one: both of them are increasing functions of the molecular complexity but for high complexity fluids the two values get closer affecting the shape of the Andrew saturation line. As demonstrated in literature [9], the higher the value of vapor heat capacity compared to the liquid one, the steeper the saturated vapor side of the Andrew curve. In Figure 4.5.a the trend of the ratio between the liquid and the vapor heat capacities is reported against the number of atoms. It is possible to notice that this parameter is around 0.8 for light fluids, like water, and it approaches values closer to 0.9 for high complexity fluids. An index for fluid complexity proposed in literature is σ which is defined as the slope of the vapor saturation line according to eq. 4.10[5].

$$\sigma = \frac{T_{crit}}{R}\left(\frac{dT}{ds}\right)_{T_{ref}^{eva}} \qquad \text{eq. 4.10}$$

[5] The equation reported in [9] the temperature to be used is equal to a reduced temperature of 0.7. Nevertheless using this definition entails that for low critical temperature fluids a $T_{red-0.7}$ below ambient temperature. For example for R134a (Tcrit~101°C) the reference temperature is -11,2°C which is a value not really interesting for common ORC systems.

Calculated values of σ and saturation lines for different fluids in reduced quantities are shown in Figure 4.5.b and Figure 4.5.c respectively.

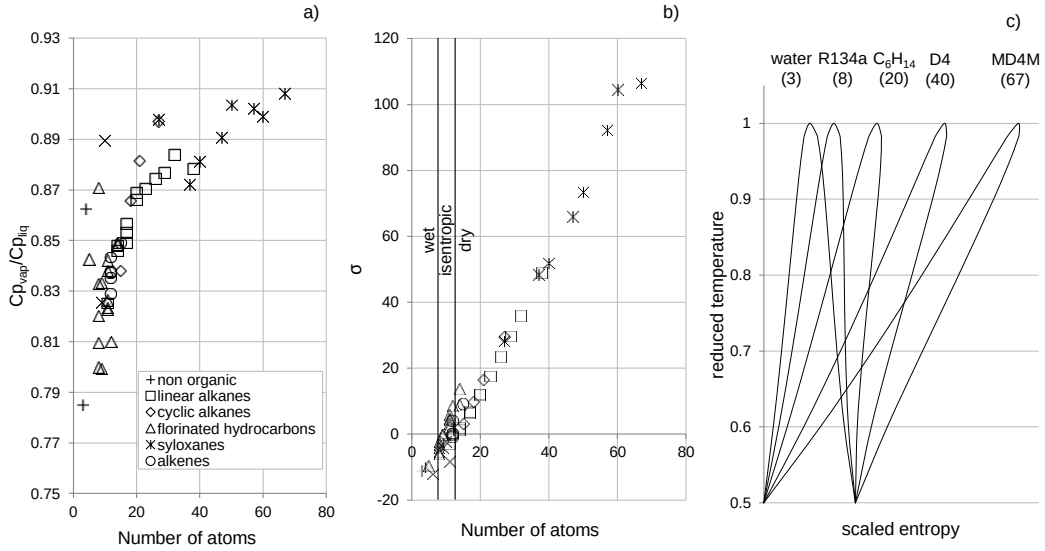

Figure 4.5 – ratio between liquid and vapour heat capacities (a), *σ* values against molecule number of atoms (b) and shape of Andrews saturation lines for fluids having a different number of atoms reported in brackets (c)

Observing the shape of the saturation lines it is possible to classify the organic fluids in three different categories:

- *Wet fluids* are characterized by simple molecules and a negative slope of the saturation line and *σ* values below -4. These fluids can be used only in supercritical or superheated cycles if a two-phase flow expansion is not allowed. Part of this group are light linear hydrocarbons like methane and ethane, refrigerant fluids like R161, R152a, R143a and R32 and other hydrocarbons like methanol and ethanol. Water and ammonia are also wet fluids.
- *Isentropic fluid*s have a limited number of atoms and *σ* values in the range between -4 and 4. The saturated vapor line is almost vertical in a large range of temperatures. It is possible to design the cycle in a subcritical saturated configuration with the expansion in the superheated vapor region because of the non-ideality of the turbine. Hydrocarbons with a number of carbon atoms between 3 and 4 (propane and butane based fluids) can be considered isentropic fluids. Other compounds are fluorinated molecules like R134a, R1234ze, R236fa, R125 and R1234yf.
- *Dry fluids* are characterized by values of *σ* greater than 4 and a completely overhanging saturation line. Dry expansion is always guaranteed for turbine inlet in saturated vapor condition. Part of this group are all the hydrocarbons with more than 4 carbon atoms, several fluorinated fluids and all the siloxanes.

Critical volume and pressure ratios

An isentropic expansion through a nozzle with an imposed pressure ratio equal to the critical one results in sonic velocity at blade exit. The same phenomena occurs in stator and rotor blades when a pressure ratio higher than the critical one is imposed. The presence of shock waves and other phenomena strictly related to flows with Mach numbers greater than unit are crucial information for turbine designers because they lead to a completely different optimal blade profiles with the adoption of converging diverging nozzle. If the degree of reaction of a turbine stage is around 0.5, it means that the isentropic enthalpy drop is almost equally divided between stator and rotor. The volume ratio is not equally divided, but for ideal gases the two quantities are very close, thus imposing a stage pressure or volume ratio greater than twice the corresponding critical value, leading to the possibility of supersonic flows in both stator and rotor blades. Critical volume and pressure ratio can be calculated for an ideal fluid by eq. 4.11 and eq. 4.12, by imposing the conservation of energy between inlet and outlet section of the nozzle and a sonic isentropic outlet velocity respectively.

$$\beta_{crit} = \left(\frac{2}{\gamma+1}\right)^{\frac{\gamma}{\gamma-1}} \qquad \text{eq. 4.11}$$

$$Vr_{crit} = \left(\frac{2}{\gamma+1}\right)^{\frac{1}{\gamma-1}} = {\beta_{crit}}^{1/\gamma} \qquad \text{eq. 4.12}$$

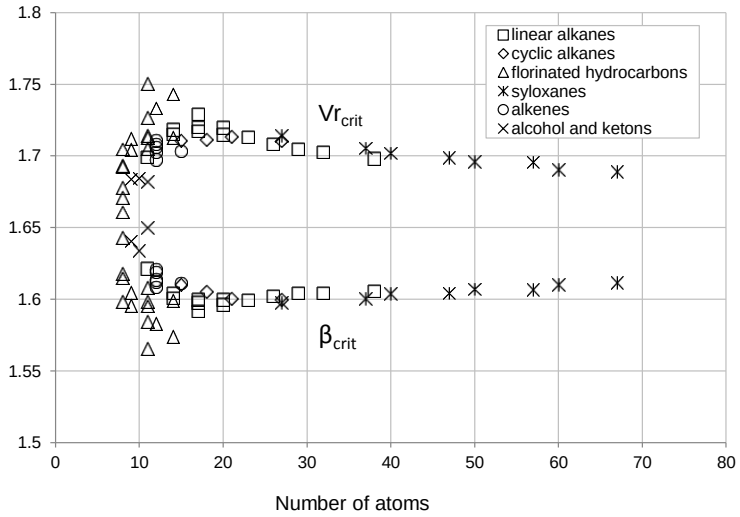

Figure 4.6 - Trends of β_{crit} (lower half of the figure) and Vr_{crit} (upper half) for several real fluids divided by chemical class.

The trends of both the critical pressure and the critical volume ratios are reported in Figure 4.6 for real fluids. Among the possible working fluids, critical volume and pressure ratios vary in a small range allowing the definition of limits independently of fluid molecular complexity.

Isentropic temperature drop along expansion

Another quantity that is strongly influenced by molecule complexity is the isentropic temperature drop in expansion for a given pressure ratio. The ideal value can be evaluated with eq. 4.13 and the trend for the corresponding real values is reported in Figure 4.7

$$\Delta T_{is} = T_{in}\left(1 - \beta^{(\gamma-1)/\gamma}\right) \qquad \text{eq. 4.13}$$

High complexity fluids show a small isentropic temperature drop along expansion compared to simpler molecules. This peculiarity affects the plant layout of ORCs, where usually a recuperator is adopted in order to recover the heat from the hot stream discharged by the turbine heating up the compressed liquid pressurized from the pump.

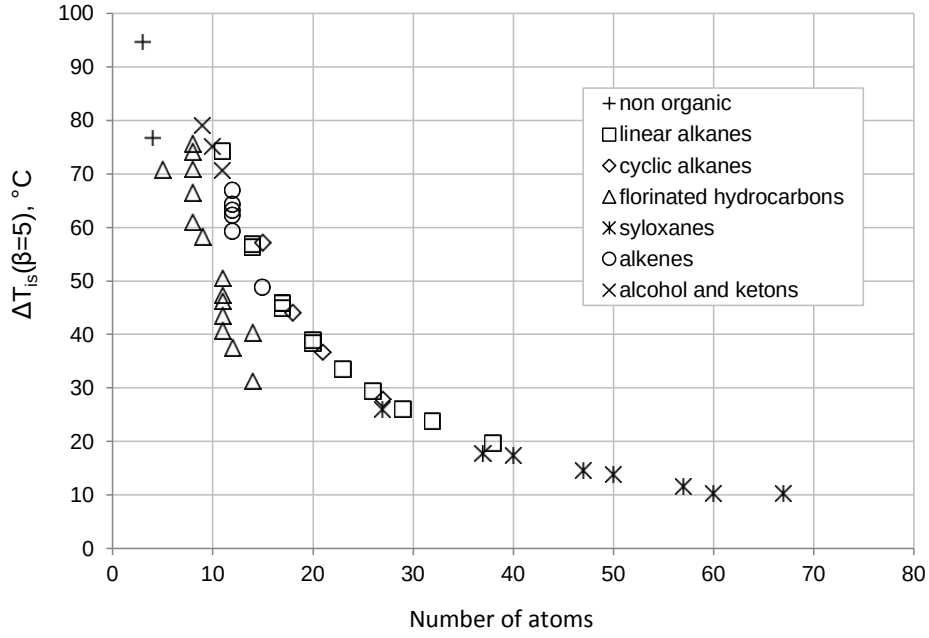

Figure 4.7 - trend of isentropic temperature drop along expansion for a fixed pressure ratio of 5, for different real fluids divided by chemical class

4.2.3 Properties affected by molar mass

Some other properties, instead, are more affected by the fluid molar mass.

Speed of sound

The value of the speed of sound is a quantity of great interest in turbine design process because, for supersonic flows, a completely different shape of blades is required with the adoption of converging-diverging nozzles. For ideal gases, the Speed of Sound can be calculated with eq. 4.14 so its value depends on both molecular complexity (γ) and molecular mass. The effect of complexity is much lower than the molecular weight as can be deduced from data reported in Figure 4.8.a if fluids in a large range of MM are considered.

$$SoS = \sqrt{\frac{R}{MM}\gamma T} \qquad \text{eq. 4.14}$$

It is possible to observe that speed of sound is slightly affected by molecular complexity and it is strongly influenced by molecular mass. The value of the speed of sound for real fluids calculated with Refprop is reported in Figure 4.8.b confirming the results achieved with an ideal fluid.

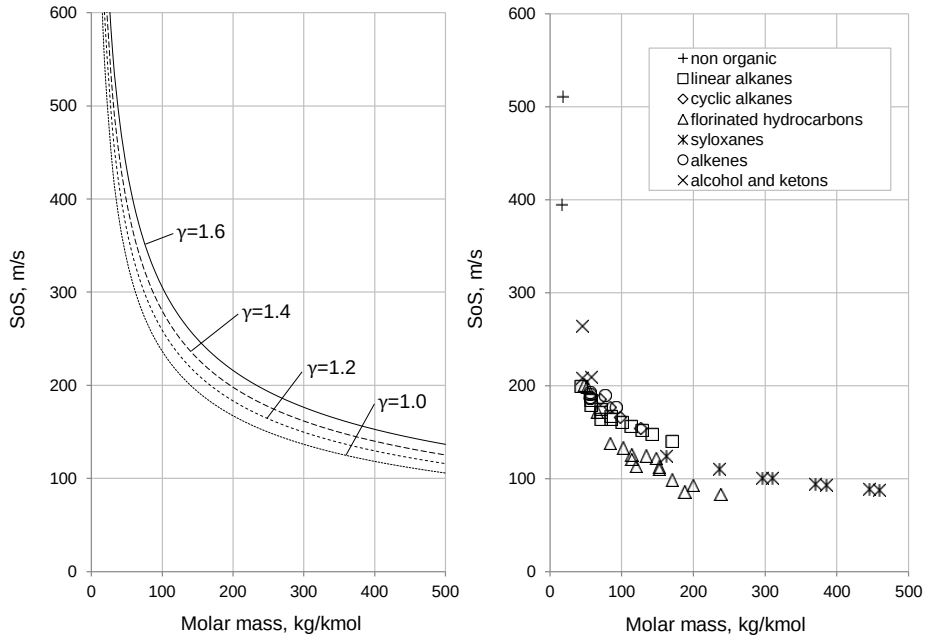

Figure 4.8 - Speed of sound calculated for ideal gases (a) in a range of molar mass (20-500) and molecular complexity γ (1-1.667), and real values for different fluids (b)

Isentropic enthalpy drop along expansion

The last quantity that is affected by the molar mass is the isentropic enthalpy drop along expansion. For an ideal gas it is calculated with eq. 4.15 while results for real gases are presented in Figure 4.9.

$$\Delta h_{is} = Cp_{mass}\Delta T = \frac{R}{MM}\frac{\gamma}{\gamma - 1}T_{in}\left(1 - \beta^{(\gamma-1)/\gamma}\right) \qquad \text{eq. 4.15}$$

It is possible to notice that the enthalpy drop for a fixed pressure ratio is strongly reduced for heavy fluids leading to a smaller load on turbine stages and a turbine which can be designed with a limited number of stages.

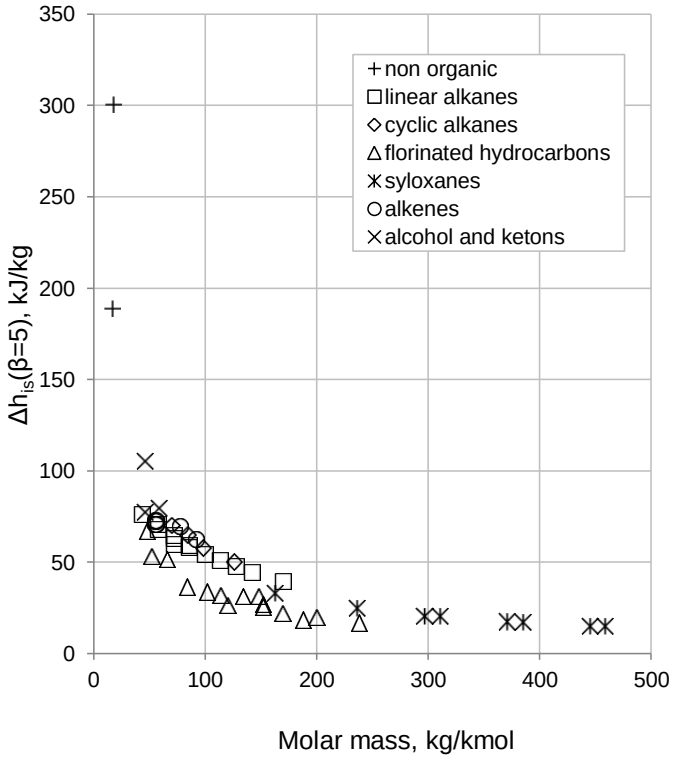

Figure 4.9 - Isentropic enthalpy drop for a fixed pressure ratio

4.2.4 Quantities affected by the critical properties

Critical temperature and critical pressure have a direct influence on cycle operating pressures, pressure ratio of both pump and turbine and sizing of key components like the turbine, the recuperator and the condenser. Critical properties are affected by fluid chemical structure namely by the type and the number of atoms, the bounds between them and the spatial configuration. The knowledge of these properties is of crucial

importance if an equation of state is not available for a selected fluid. Simply knowing the values of critical temperature, pressure and density and the value of the acentric factor ω of the molecule[6] all the other thermodynamic quantities can be roughly retrieved applying the corresponding state principle. Critical temperature and pressure are reported in Figure 4.10 and it is possible to note that a common trend of these variables as function of molecular weight or molecular complexity cannot be identified (in the figure, only data against the number of atoms are reported). An overall conclusion is that for fluids of the same class, like linear hydrocarbons or siloxanes, an increase of molar mass and complexity leads to higher critical temperatures and lower critical pressures. However, the critical properties are strongly affected by interaction forces between molecules. For instance water, although being a light and simple fluid, shows a very high critical temperature, comparable with long chain hydrocarbon or complex siloxanes.

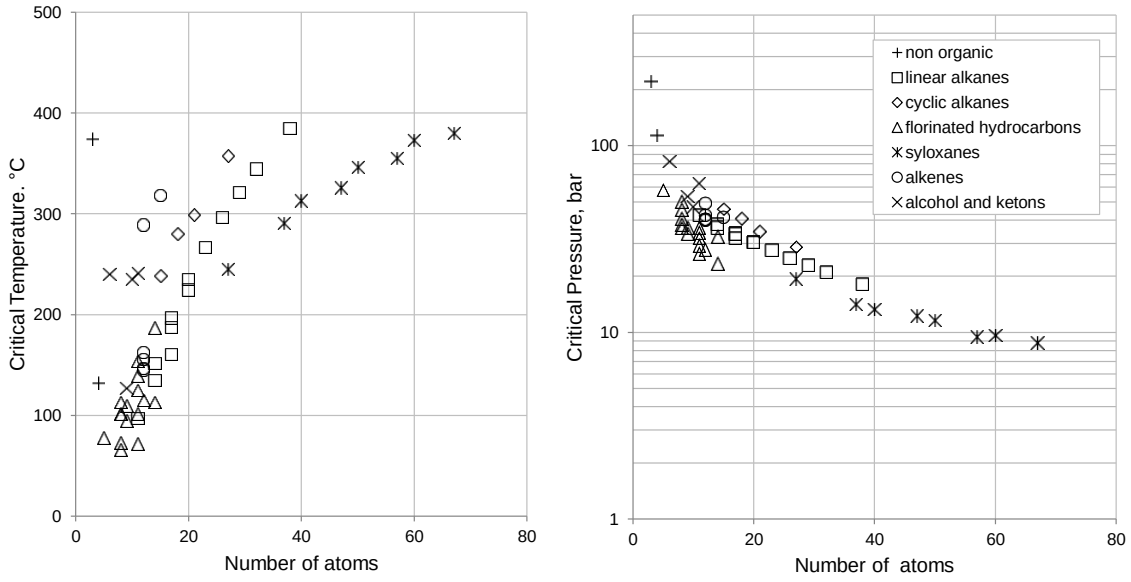

Figure 4.10 - Trend of critical temperature and pressure against number of atoms

Several methods for the prediction of these properties are proposed in literature and are mainly based on group contribution theory. Among them, the most suitable are the Joback, the Costantious&Gani and the Wilson&Jasperson method. For all the different chemical groups which can form a molecule, a coefficient is calibrated for each property of interest regressing experimental data. Property value is then obtained by summing the contributions of each functional group in the molecule. However, these methods allow

[6] The acentric factor is a parameter introduced by Pitzer K. in 1955 to account the non-sphericity of molecules. It is calculated from the reduced saturation pressure at reduced temperature equal to 0.7.

only rough estimations of critical properties and they should be used only if no other indication about these quantities is available. Fortunately, in most of the applications, the critical properties of the investigated working fluids are known and accurate EoS are available. Here it is interesting focus on the effects that these properties have on the optimal cycle layout and the components design.

In particular, for a fixed condensing temperature, using fluids with high critical temperatures leads to a very low condensing pressure which can become and issues for very complex and heavy organic fluids. The trend of condensing pressure against critical temperature is reported in Figure 4.11 for a temperature of 40°C. It is possible to notice that for fluids with critical temperatures higher than 200°C the condensing pressure is higher than the ambient one. In this case there are no difficulties related to the presence of incondensable gases which leaks from the environment into the condenser and no vacuum pump is needed to remove these gases which would gradually increase the condensing pressure with a penalization of cycle efficiency.

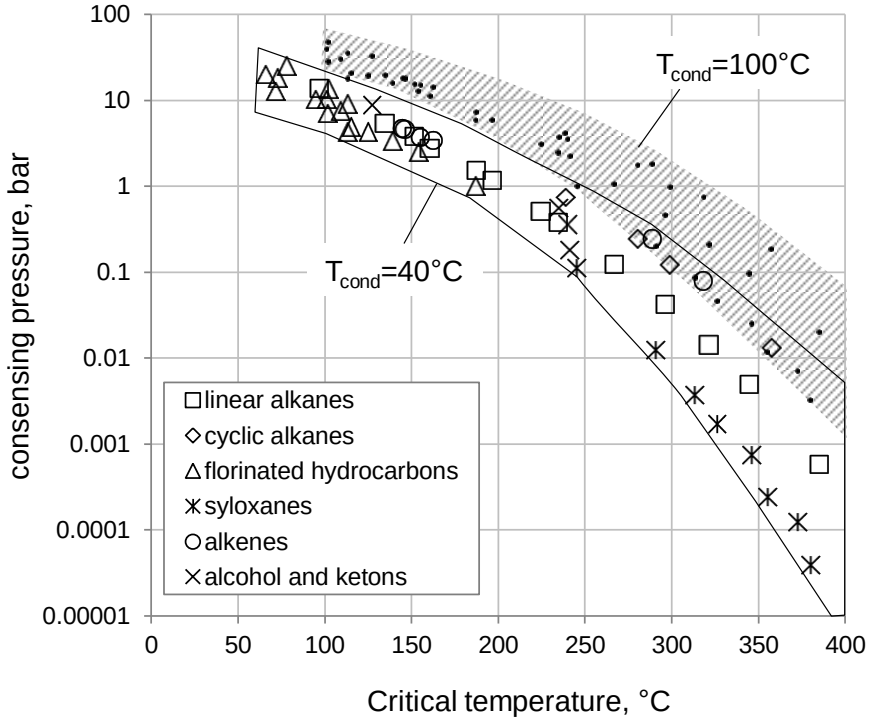

Figure 4.11 - Condensing pressure for different fluid with a condensing temperature of 40°C (markers) and 100°C (dots) representative of pure power production plants and CHP plants respectively

Other two quantities which are affected by the critical temperature are the isentropic volume ratio in expansion and the volume flow rate at turbine discharge. An ideal non-recuperative subcritical saturated cycle is assumed working between 90°C and 25°C.

Different working fluids are available and a fixed available power input equal to 10 MW is considered. Mass flow rate does not show any particular trend against critical properties while volume flow rates have an exponential trend at both turbine inlet and isentropic outlet conditions but difference in slope entails a larger volume ratio for high temperature fluids as reported in Figure 4.12.

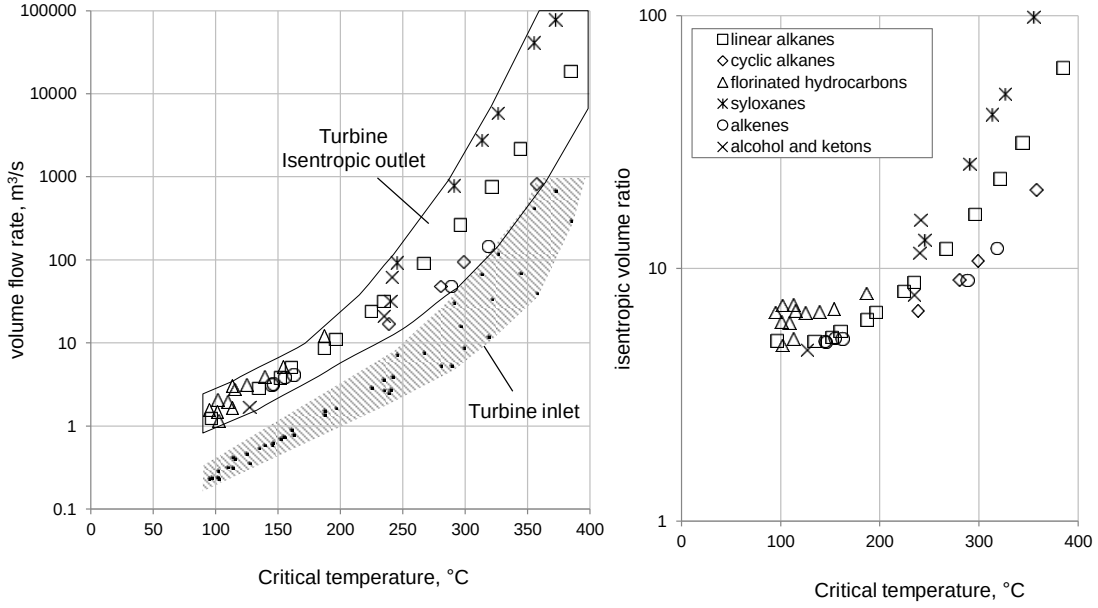

Figure 4.12 - Volume flow rate against critical temperature (a) and isentropic volume ratio (b) for a cycle working between 90°C and 25°C.

4.2.5 Effects on component design and cycle configuration

In conclusion both the complexity and the molar mass greatly affect many fluid properties and quantities which have a strong impact on component design criteria and plant layout. The effect of complexity and molar mass can be isolated, even if in real fluids there are cross effects:

- Molecular complexity is mainly influenced by the number of atoms in the molecule even if the atoms type, the molar weight and the molecule spatial configuration have a small influence on the σ value.
- By increasing the number of atoms in a molecule, it is possible to summarize that:
  - Values of the molar heat capacity at constant pressure and at constant volume get similar and γ value tents to unit
  - The ratio between vapor and liquid heat capacities increase leading to a slope of the saturated vapor line similar to the liquid side. The Andrew curve becomes overhanging and the corresponding σ value gets positive.

Overhanging Andrew curves allow a dry expansion from saturated vapor condition without problems related to blade erosion typical of simpler fluid like water or ammonia. In these cases, it is possible to arrange the plant layout as a subcritical saturated cycle.

- Critical volume ratio and critical pressure ratio are not really affected by molecular complexity and so the criterion in defining the maximum allowable volume ratio per stage is fluid independent. In order to limit supersonic flows in both stator and rotor rows the maximum value of volume ratio should not exceed twice of the critical one. This is one of the constraints that are commonly used for organic fluids in order to define turbine number of stages. This limit is not present for light molecules, like water, where a limit on the maximum load is considered.
- Isentropic temperature drop for a given beta is smaller for complex fluids. Higher temperatures at turbine outlet are obtained and usually a recuperator is advantageous because it reduces the entropy generation in the heat introduction process and the condenser duty.

- Heavy molecules are instead characterized by:
  - A lower speed of sounds and so Mach numbers greater than unit and supersonic velocities. Blade profile design is more challenging and usually stage efficiency is limited by high profile losses.
  - Lower enthalpy drops along expansion with the possibility to design turbine stages with a small load coefficient even working at low peripheral speeds leading to limited mechanical stresses. As a final result, ORC turbines have a limited number of stages and in some application it is possible to exploit the whole enthalpy drop in a single-high velocity stage.
- Selecting a working fluid with an opportune critical temperature:
  - It is possible to set the condensing pressure above the ambient one thus solving all the difficulties related to air leakage in the power cycle and the use of vacuum pump for the extraction of incondensable gasses. The pump consumption increases according to the higher evaporation pressure. In CHP applications the higher condensing temperatures allow using more complex organic fluids.
  - It is possible to limit the volume flow rate at turbine discharge, limiting the size and the cost of the turbine, the recuperator and the condenser: low critical temperature fluids should be used for high power outputs. On the other hand, in small power applications difficulties are related to the design of the first stage, which results in very small blade heights and a

limited efficiency. With the use of a higher critical temperature fluid, it is possible to increase the volume flow rate at turbine inlet with an easier design of the turbine or the adoption of total admission instead of partial admission.

- It is possible to limit the isentropic volume ratio and so the number of stages required by the expansion. Otherwise it is possible to achieve higher efficiency using the same number of stages.

4.2.6 Use of mixtures vs pure fluids

The use of mixtures of fluids is proposed for ORC systems in some papers [108; 109; 110] where the thermodynamic behavior of fluid blends is investigated and the potential advantages of their use are presented. In some applications, using a mixture of fluids instead of a pure fluid as working medium in a thermodynamic cycle allows reaching a higher efficiency and a higher power production thanks to the minimization of irreversible process connected to heat transfer process. The main effect in using mixtures is represented by a phase transition process which is isobaric but not isothermal. A certain increment in temperature is obtained during evaporation while the temperature decreases in condensation. This peculiarity allows reducing the temperature difference in both the PHE and the condenser thus reducing the second law losses in these components with an overall increase of net power production. The non-isothermal phase transition can be explained considering an isobaric Vapor Liquid Equilibrium diagram for a general mixture where a low boiling temperature fluid A is mixed with a high boiling temperature fluid B[7] as reported in Figure 4.13. For a mixture of A+B the dew line and the bubble line can be represented in an isobaric diagram reporting the molar concentration of B component on x axes. The bubble line represents the locus of temperatures at which the first bubble of fluid is formed while the dew point is determined by the formation of the first drop. The values of T_{dew} and T_{bubble} are the same at the two extremities namely for pure A or pure B component, in the rest of the VLE diagram instead the two temperature are different and the gap between them represents the temperature glide during phase transition[8].

[7] With reference to an isobaric VLE diagram the high boiling temperature fluid is the compound with the higher saturation temperature thus the fluid which is less volatile. For isothermal VLE, the more volatile fluid shows the higher saturation pressure.

[8] An exception is the presence of an azeotropic point which entails no differences in composition between the vapor phase and the liquid phase. These points are not very interesting in ORC field since they behave like a pure fluid.

Let's consider to heat up a mixture corresponding to a composition $A_{(1-x)}B_x$ from a temperature lower than the corresponding bubble temperature $T_{b,x}$. As long as the temperature is lower than $T_{b,x}$ the composition of the mixture is unchanged but, when the boiling temperature is reached the first bubble of vapor is formed with a composition $A_{(1-x1)}B_{x1}$. The vapor phase is always more concentrated in the more volatile component, thus the remaining liquid results enriched in the high boiling temperature compound and its composition moves on the boiling line toward higher concentration of B. The vapor composition respect to the liquid one can be determined by imposing the same temperature on the two saturation lines. The process goes ahead until the last drop of liquid with composition $A_{(1-x2)}B_{x2}$. is evaporated. The vapor phase now has the same composition of the initial liquid mixture and any further temperature increment happens in superheated vapor phase. The same consideration is valid for the condensation process.

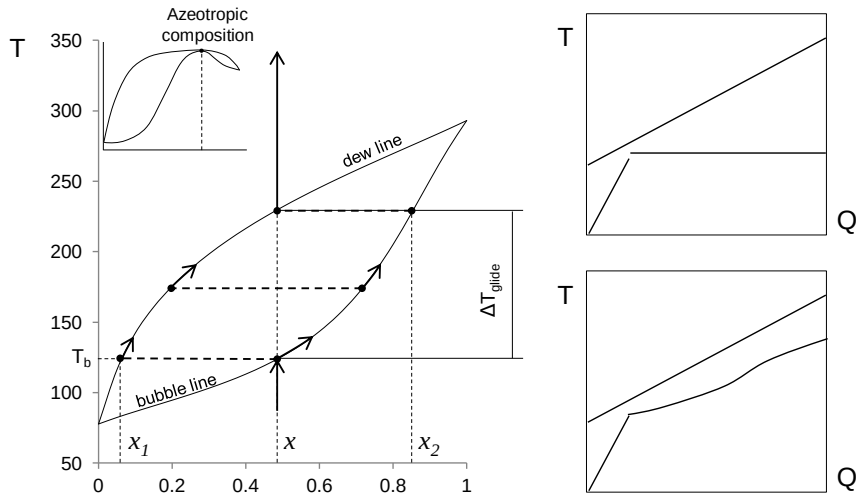

Figure 4.13 - VLE diagram for a binary mixture and TQ diagrams for pure fluid and mixture

The temperature glide during phase transition depends on the nature of the fluids and on the composition: high temperature glides can be obtained for mixture of fluids having noticeably different critical temperatures or fluids of different chemical classes. The huge number of fluid combinations and the mixture composition are additional variables for the optimization process, making the problem more and more difficult to be solved: in particular the number of mixtures which can be potentially used is impressive since among hydrocarbons and refrigerant fluids no relevant miscibility limits are highlighted and it is not numerically feasible to approach the solution with an exhaustive methodology. A pre-selection among the available mixtures is always required checking miscibility, verifying the trends of VLE data in the range of temperature of interest and

finding information about the chemical stability of the blend. An example is reported in Section 9.2 (Use of mixtures for Biomass plants).

Despite the advantages achievable with mixtures, their use as working fluids in binary ORCs is still extremely limited because of a number of difficulties which make these solutions less practical and affordable than using a pure fluid. The two main issues to be faced are due to (i) fluid composition changes and (ii) limitation of film transfer coefficients.

- *Composition change*: if a leakage of fluid occurs, the vapor which is vented to the environment, has a different composition than the nominal one and so a differential refill is required in order to restore the original composition. This requires additional cost for the fluid analysis, a more expensive fluid storage area and possible malfunctioning if the leakage is not rapidly revealed.
- *Reduction of heat transfer coefficient*: the film transfer coefficients are lower in phase transition for mixtures than for pure fluids [111; 112]. By using mixtures, it is possible to reduce the ΔT_{mln} in the heat exchangers thus increasing the UA parameter respect to an isothermobaric process. In addition, the overall heat transfer coefficient U is smaller leading to a more marked increase of the heat exchanger surface. From previous works, a reduction of U close to -30% was obtained for a toluene-methanol mixture using Aspen software and Huron Vidal mixing rules. However for any new mixture a detailed bibliographic review is required. Unfortunately, there is a very little availability of experimental data on transport properties, which entails relevant difficulties in a reliable estimation of heat exchangers cost.

“If it's not worth doing it,

it's not worth doing it well”

Daniel Kleppner

5 Thermodynamic cycle configurations

As already mentioned in section 3.2 (Applications) Organic Rankine cycles are a technology suitable for the exploitation of many different energy sources in the range of medium-low temperatures or for micro-small power outputs. In both fields the efficiency is limited: in the first case because of the low efficiency of the ideal Carnot or Lorentz cycle, and, in the second case, because of the limited efficiency of some key components, like the turbine which is affected by miniaturization of blades at the first stage. Since the achievable performances are limited, it is not interesting to adopt complex plant layouts and usually maximum two pressure levels cycles are proposed on the market. Another reason is related to the thermodynamic properties of working fluids used in ORC. As already stated in Section 4.2.5 (Effects on component design and cycle configuration) complex fluids entail a small temperature drop along expansion, with temperature at turbine discharge extremely high compared to those attainable with a simpler fluid like water or ammonia. Recuperative cycles are usually adopted in these cases with a relevant efficiency increase especially if the cooling down of the heat source is limited by some technical reasons (see section 3.4 for further details). Regenerative bleedings are never suggested neither for simpler molecules. The highest value of power output for a single turbine in ORC is below 15 MW_{el} leading to volume flow rates which are never so large to require a cross over and case splitting in two or more turbine groups. Another aspect of interest, in using organic fluids, is the possibility to set up thermodynamic cycles with condensing pressure higher than the ambient one. Deaerator, in these cases, is not necessary and usually it cannot be used in any case: organic working fluids cannot be vented to the environment because of their high GWP or because of safety reasons related to their flammability or toxicity. If the condensing pressure is below the ambient one a vacuum pump is used followed by a treatment unit for the extracted gases formed by activated carbon filters. In conclusion, ORCs compared to other power systems have an intrinsically simpler plant layout characterized by a limited number of components, an easy operation and a great flexibility in off-design condition thanks to a small thermal inertia.

In next sections a brief overview of the cycle configurations that are implemented in ORCO is presented, together with a review about the publications, the experimental activities and the commercial plants for each proposed solution. Cycle configurations can be divided in three main groups: (i) single pressure level cycle, (ii) two pressure levels cycle and (iii) triangular or two phase flow expansion cycles. All the plant schemes

reported in this chapter are referred to the exploitation of geothermal brines but the same description of the thermodynamic cycles is valid for any other application.

5.1 Ideal thermodynamic cycle

Before introducing the different thermodynamic cycles used in ORC field it is necessary to briefly present the ideal cycles that can be considered as the reference case for the exploitation of a variable temperature heat source. Two ideal cycles can be used for this purpose. The first one is a Carnot cycle, whose maximum temperature has to be optimized according to both maximum and minimum temperatures of the heat source and the temperature of the cold sink. The second one is a Lorentz cycle also called triangular or trapezoidal cycle. In this section the thermodynamic efficiencies of the two ideal cycles are compared underling the reasons why the Carnot cycle is not the appropriate reference thermodynamic cycle for binary ORC exploiting variable temperature heat sources [113].

Thermodynamic background

Any ideal thermodynamic cycle can be described with a sequence of reversible transformations: every process follows the relation between work, heat and internal energy reported in eq. 5.1 where the heat is considered positive when introduced in the system and work is positive when extracted. The corresponding entropy variation can be calculated with eq. 5.2.

$$dU = dQ - dW \qquad \text{eq. 5.1}$$

$$\Delta S = \int_1^2 \frac{\delta Q}{T} \qquad \text{eq. 5.2}$$

As stated by the Clausius theorem, also called Clausius inequality (eq. 5.3), the final entropy variation for a cyclic reversible system is null and processes characterized by an entropy reduction are required in order to balance those transformations characterized by an entropy increase like heat introduction. As result it is not possible to exploit a given thermal power with efficiency equal to unit since a certain amount of heat has to be always released to the environment.

$$\oint \frac{\delta Q}{T} \leq 0 \qquad \text{eq. 5.3}$$

The power output from an ideal system undergoing a cyclic process can be computed by eq. 5.4 where the integral of the dU is equal to zero because the two extremes of integration are equal.

$$W = \oint pdV = \oint (dQ - dU) = \oint TdS - \oint dU \rightarrow$$
$$W = \oint TdS = \oint dQ \qquad \text{eq. 5.4}$$

The work of ideal cycles is thus equal to the area of the cycle in the T-s diagram or otherwise it is equal to the sum of the thermal power exchanged by the system with the heat source and the environment.

Carnot cycle

In figure Figure 5.1 the Carnot cycle working between T_0 and T_c is represented in both T-S and p-V diagrams. The Carnot cycle when acting as an engine consists in four processes:

a. An isentropic compression: the process is reversible and adiabatic, no heat is exchanged and the work introduced is equal to internal energy variation;
b. An isothermal transformation: heat is introduced and the same amount of work is extracted from the system. Internal energy does not change since the process is isothermal;
c. An isentropic expansion: similar to process a. but where work is extracted;
d. An isothermal transformation: where heat is released to the cold sink and work is introduced.

The two isothermal processes involve the same entropy variation but the corresponding heat fluxes exchanged are different since they two transformations are performed at different temperatures. The difference between the heat introduced into the system at temperature T_c and the heat released to the cold sink at T_0 is equal to the power output of the Carnot cycle. The corresponding efficiency of an ideal Carnot cycle is finally computed by eq. 5.5

$$\eta_c = \frac{W}{Q_b} = \frac{Q_b + Q_d}{Q_b} = 1 - \frac{Q_d}{Q_b} = 1 + \frac{T_0 \Delta S_{4\rightarrow 1}}{T_c \Delta S_{2\rightarrow 3}} = 1 - \frac{T_0}{T_c} \qquad \text{eq. 5.5}$$

Where T_0 is the cold sink temperature and T_c is the maximum temperature of Carnot cycle.

As already mentioned in section 3.4 (Typical heat source temperature profiles and limits) a constant heat capacity heat source C_{HS} can be assumed and its exploitation between T_{max} and T_{min} by using a Carnot cycle is represented in Figure 5.1. The corresponding system efficiency can be calculated with eq. 5.6

$$\eta_c^* = \frac{W}{Q_{max}} = \frac{Q_{in}\eta_c}{Q_{max}} = \frac{C_{HS}(T_{max} - T_c)\left(1 - \frac{T_0}{T_c}\right)}{C_{HS}(T_{max} - T_{min})} \qquad \text{eq. 5.6}$$

Where Q_{in} is the introduced thermal power and Q_{max} the maximum available thermal power exploitable cooling the heat source down to T_{min}.

Deriving the system efficiency respect to T_c and setting equal to zero the resulting equation it is possible to find the value of Carnot cycle temperature $T_{c,opt}$ which maximize η_c^*.

$$\frac{\partial \eta_c^*}{\partial T_c} = 0 \;\rightarrow\; T_{c,opt} = \sqrt{T_{max}T_0} \qquad \text{eq. 5.7}$$

$T_{c,opt}$ is not affected by T_{min} value and the optimal Carnot cycle temperature is constant as long as the value of T_{min} is below the value of $\sqrt{T_{max}T_0}$. On the other hand, if the minimum heat source temperature is higher, the value of $T_{c,opt}$ is equal to T_{min} according to eq. 5.8.

$$T_{c,opt} = max\left\{\sqrt{T_{max}T_0}, T_{min}\right\} \qquad \text{eq. 5.8}$$

Obviously a Carnot cycle, even if optimized, entails two irreversible processes, namely the heat introduction and the cooling of the heat source down to its minimum temperature. The trend of system efficiency against T_{min} is reported in Figure 5.2 and compared with the Lorentz cycle.

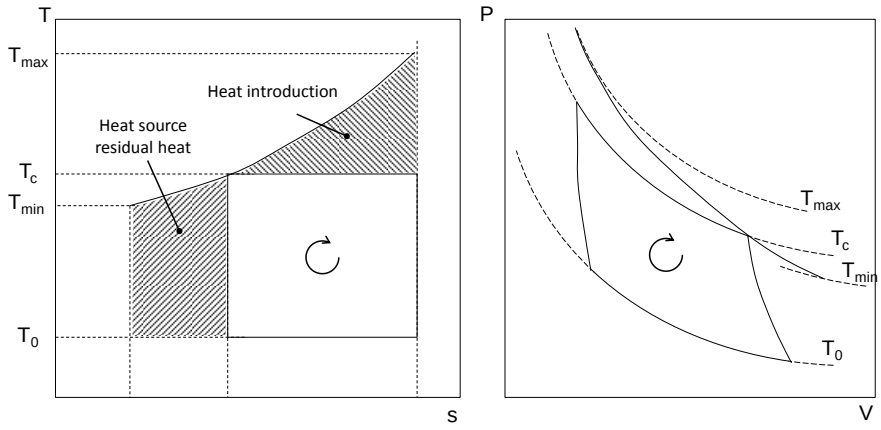

Figure 5.1 - Carnot Cycle in T-s and pV axes. The shaded areas are representative of the energy losses in heat introduction process and for the non-total exploitation of the energy source

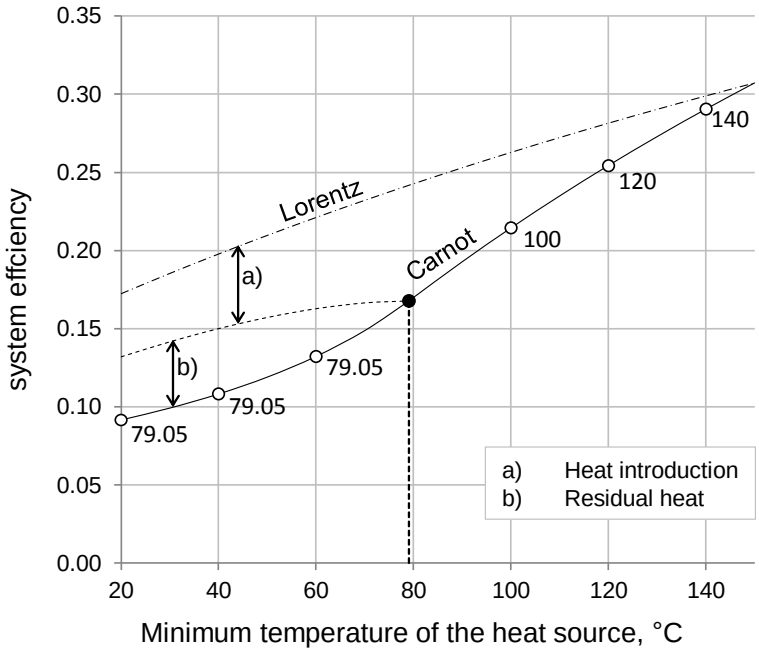

Figure 5.2 - Comparison between Lorentz cycle efficiency and Optimized Carnot cycle efficiency. Markers on Carnot line represent the value of optimal maximum temperature.

Lorentz cycle

In the Lorentz ideal cycle, differently from the Carnot cycle, the heat introduction is performed by a variable temperature reversible process without temperature differences between the heat source and the working fluid. The entropy increase in the heat introduction process can be calculated by eq. 5.9, where a constant heat capacity is assumed for the heat source, leading to a linear relationship between the temperature and the exchanged thermal power.

$$\Delta S_{2\to3} = \int_0^{Q_b} \frac{dQ}{T} = \int_0^{Q_b} \frac{dQ}{T_{min} + Q/C_{HS}} = C_{HS} \ln\left(\frac{T_{max}}{T_{min}}\right) \qquad \text{eq. 5.9}$$

Heat rejected and cycle efficiency are calculated with eq. 5.10 and eq. 5.11.

$$\Delta S_{2\to3} = -\Delta S_{4\to1} = \int_0^{Q_d} \frac{dQ}{T} \;\to\; Q_d = -T_0 C_{HS} \ln\left(\frac{T_{max}}{T_{min}}\right) \qquad \text{eq. 5.10}$$

$$\eta_l = \frac{W}{Q_b} = \frac{Q_b + Q_d}{Q_b} = 1 - \frac{T_0 C_{HS} \ln\left(\frac{T_{max}}{T_{min}}\right)}{C_{HS}(T_{max} - T_{min})} = 1 - \frac{T_0}{\frac{(T_{max} - T_{min})}{\ln\left(\frac{T_{max}}{T_{min}}\right)}} \qquad \text{eq. 5.11}$$

It is interesting to note that the equation for the efficiency of a generic trapezoidal Lorentz cycle corresponds to an equivalent Carnot cycle working between ambient temperature T_0 and the mean logarithmic temperature of T_{max} and T_{min}.

In Figure 5.2 the comparison between Carnot and Lorentz efficiencies is reported. Results refer to ideal cycles exploiting a heat source with a maximum temperature equal to 150°C and to an ambient temperature of 20°C. Lorentz cycle efficiency is always higher than Carnot one because this latter one presents two irreversible process namely the heat introduction with finite temperature difference and the cooling of the heat source from T_c to T_{min}. The two trends obviously converge to the same value for minimum temperatures equal to the maximum one. For the Carnot trend, the values of T_c are reported and it is possible to note how they remain constant as long the minimum temperature is below $\sqrt{T_{max} T_0}$.

5.2 One pressure level cycles

It is the simplest plant layout and it has the minimum number of components: a pump, a turbine, a condenser and a Primary Heat Exchanger (PHE). Recuperator is optional and it is used when it is not possible to cool down the heat source due to technical reasons. In Figure 5.3, the basic plant layout for a recuperative one level cycle is presented. Fluid in saturated liquid condition is extracted from the condenser hotwell and its pressure is increased with a pump to the maximum cycle pressure. If a recuperator is present, fluid is heated up by cooling down the hot fluid discharged by the turbine. Working fluid then enters the primary heat exchanger where heat is introduced from the heat source. Depending on the size of the plant the PHE is formed by a single once-through heat exchanger or by different units. In particular, if the cycle is a supercritical one the once-through heat exchanger is the only option conversely, especially for big subcritical power plants, a physical division in economizer, evaporator and possibly superheating is usually adopted. After the turbine control valve, the high pressure and temperature fluid is expanded in a turbine or in a volumetric expander to a pressure slightly higher than the condensation one. Mechanical work is extracted and converted in electric power with the generator connected to the turbine shaft. If the rotational speed of the turbine is different from the grid frequency a gear box is used for high velocity turbines while a generator with a number of pole pairs greater than one is commonly adopted for low speed machines. For very small applications, it is preferable to produce power with a fast generator and use a power electronic unit to adjust the frequency. Expanded fluid flows possibly through the recuperator and it is eventually condensed.

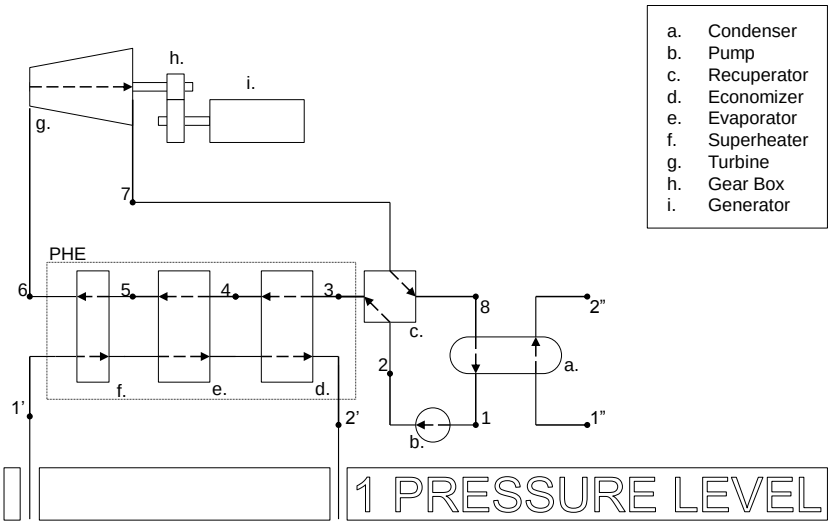

Figure 5.3 - Plant layout for a one pressure level cycle. A once- through PHE is used for supercritical cycles and for subcritical cycles where a division between economizer, evaporator and superheater is not convenient.

Its simplicity and the good attainable efficiencies make this kind of cycles the first option for many different applications, from geothermal to solar energy, from waste heat recovery to biomass combustion. This configuration is divided into two big families based on the same plant layout, but notably different in both maximum efficiency and levelized cost of electricity, namely subcritical and supercritical cycles.

The T-s diagram for both subcritical and supercritical cycles is reported in Figure 5.4, where it is possible to appreciate the reduction of the average temperature difference in the PHE adopting a supercritical configuration and an opportune working fluid.

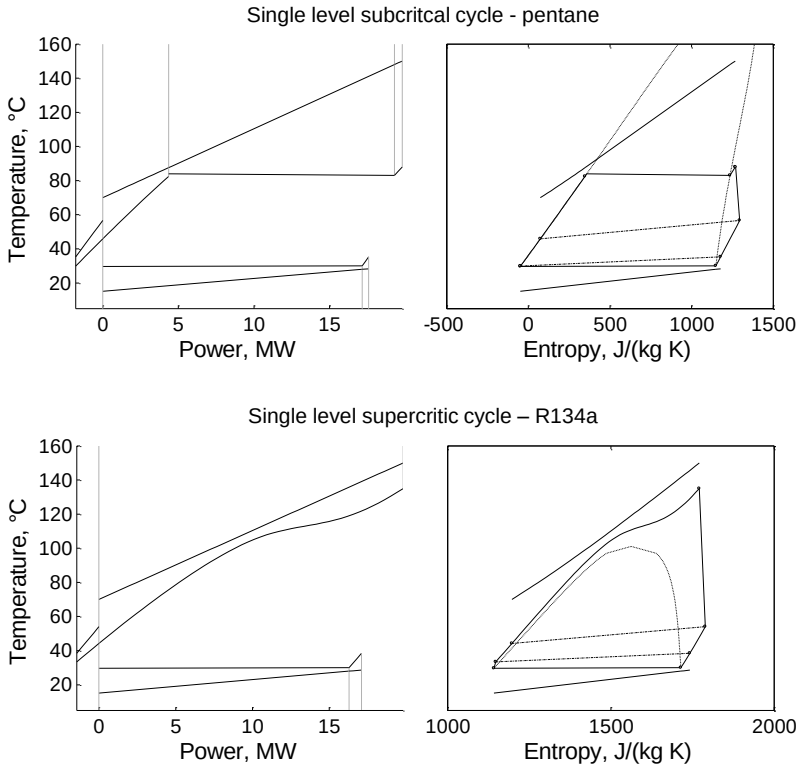

Figure 5.4 - Subcritical and supercritical single level cycles

5.2.1 Subcritical cycles

A subcritical cycle has a maximum pressure that is lower than the critical one. Working fluid passes through an evaporation process that is isothermal if the fluid is a pure compound or it presents the characteristic glide in temperature if a mixture is used. More details about the use of mixtures are discussed in Section 4.2.6 (Use of mixtures vs pure fluids) and numerical results are presented in Section 9.2 (Use of mixtures for Biomass plants). Subcritical cycles are the common solution for geothermal binary plant and for biomass combustion. If a fluid with a critical temperature higher than the heat source inlet

temperature is used superheating is generally detrimental and the saturated cycle is the optimal solution for subcritical single level cycles. A detailed analysis on the effects of superheating and a comparison on the efficiency attainable with saturated cycles are reported in Section 9.1.1 (Two examples of thermodynamic optimization). Otherwise, a low critical temperature fluid can be used if there is the necessity to maintain a condensing pressure higher than the ambient one or if a limitation in both the volumetric flow and the expansion volume ratios is required. In this case superheating is strongly recommended because it allows a higher average temperature of heat introduction and the reduction of entropy production in heat transfer process without limiting the exploitation of the heat source.

5.2.2 Supercritical cycles

A supercritical or transcritical cycle is a cycle with a maximum pressure higher than the critical one. Working fluid is heated up form a subcooled liquid region to superheated vapour with a smooth transition above the critical point. There is no phase change and all the physic and thermodynamic properties vary without discontinuity in the heat introduction process. Supercritical cycles are interesting because they can achieve a higher efficiency compared to the subcritical ones. With a proper selection of the working fluid and of the operational parameters, it is possible to obtain a heating curve that matches well the variable temperature heat source, reducing the overall logarithmic temperature difference and the efficiency losses due to heat introduction with finite temperature differences. Despite this advantage supercritical cycles generally have higher pressures than the subcritical cycles and more expensive devices are required: usually multistage centrifugal pumps are used and their efficiency should be carefully considered because their power consumption can be a relevant share of the gross power production (up to 30%). Furthermore, a higher metal thickness is required for piping and heat exchanger, especially for geothermal application where the working fluid is placed in the shell side. Supercritical cycles are object of a number of publications [22; 23; 19; 25; 20; 26] and they are studied mainly for geothermic application and heat recovery from industrial processes where the glide in temperature of heat source is compatible with the shape of a supercritical transition. Experimental activities have been performed in Livorno by Enel, Turboden and Politecnico di Milano on a 500 kW_{el} supercritical cycle with R134a for geothermal applications [114]. The cycle after one year of experimental activities has been moved near Larderello where it has been working since last year with a real geothermal fluid. The experimental activity has demonstrated the great flexibility of this kind of cycles with a really easy operation and control. Off-design control is performed by varying the speed of revolution of the pump and it has been demonstrated

that the cycle is able to smoothly switch from a supercritical to a subcritical operation according to the heat source maximum temperature and mass flow rate without showing any instability. Another example is the cycle proposed by Exergy [5] which is a 1 MW_{el} high efficiency supercritical cycle for heat recovery or biomass combustion application. Other particular features of this cycle are the innovative design of the expander which is a radial outflow turbine and the working fluid which is used, a perfluorinated hydrocarbon PP1 never used before in ORC field. Some more information about this plant and the radial outflow turbine can be found in Section 6.1.6 (Radial outflow turbines).

5.3 Two pressure levels cycles

This kind of cycle is so far rarely adopted even if it can achieve higher efficiency compared to subcritical one level cycle and performances similar to the supercritical ones. The adoption of two pressures of evaporation allows following better the variable temperature heat source but it requires more expensive equipment: two turbines, two pumps and a more complicated plant layout. Due to this latter reason they are proposed only in particular application where the efficiency of power conversion is extremely important or the fixed cost of heat source greatly overcome the cost of the power block. An example of application where two level cycles might be profitable are deep geothermal reservoir with high exploration and drilling costs and industrial heat recovery in a power production range between 5 and 10 MW_{el} like cement production plants. In this field ORCs have to compete with steam cycles and so reaching a high efficiency is extremely important. An example of the comparison between one level and two pressure level cycle for geothermal application is reported in section 9.1 (Hot geothermal brines).

A two pressure levels cycle in the most general configuration can be superheated on both evaporation levels and it can present a recuperator on both levels. Finally turbines can be arranged in series or in parallel depending on the two temperatures of evaporation and the mass flow ratio between high and low pressure streams. In Figure 5.5 the general layout of a two level cycle is proposed while in Figure 5.6 the T-s diagrams for two cycles differing in turbines arrangement are shown.

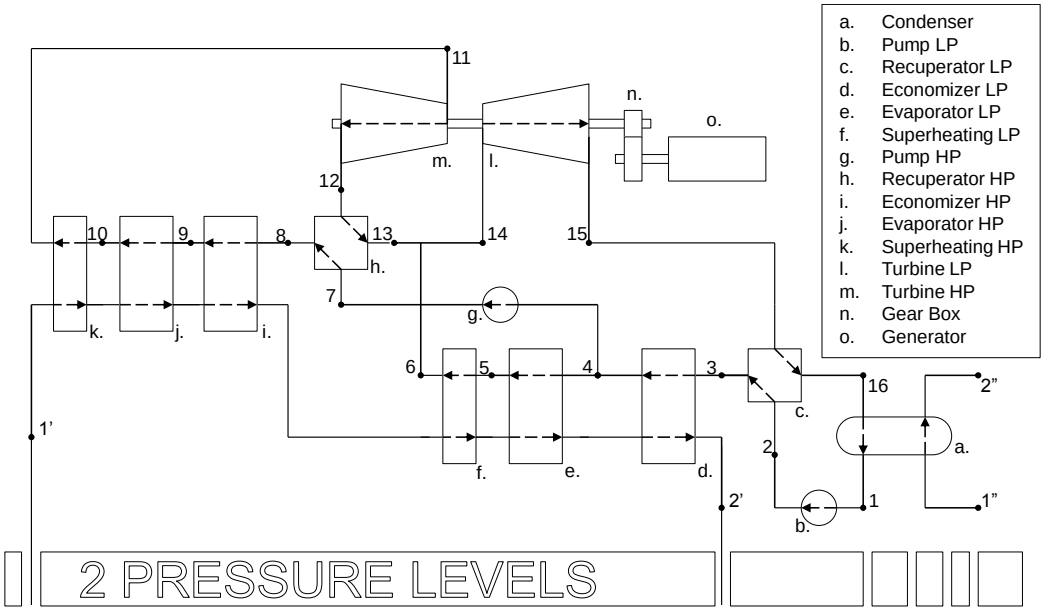

Figure 5.5 - Plant layout scheme for a generic two pressure levels cycle with turbines placed in series

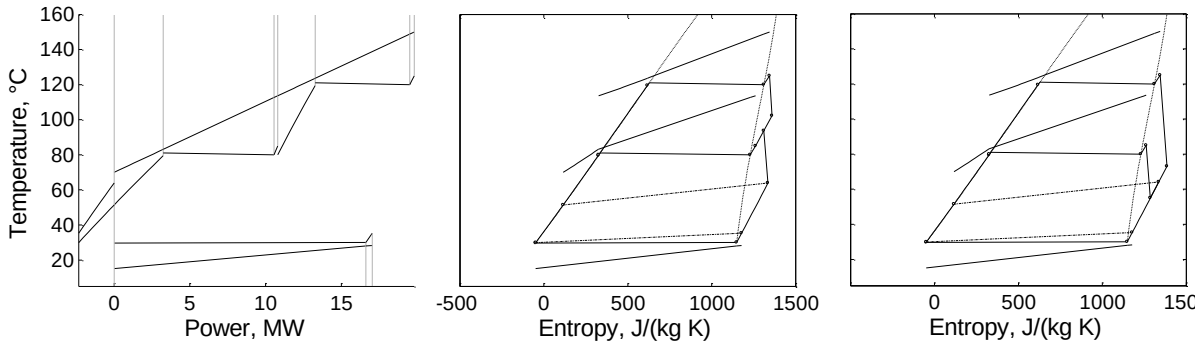

Figure 5.6 - T-Q diagram for a pentane 2 pressure levels cycle for geothermal applications, T-s diagrams with turbines in series and parallel configurations

5.4 Trilateral cycles

Many other cycle configurations are proposed in literature in order to further increase the plant efficiency. These cycles try to reproduce as close as possible the ideal Lorentz cycle. As discussed in section 5.1(Ideal thermodynamic cycle) the maximum efficiency is obtained with ideal turbomachines and both the heat introduction and heat release with zero temperature differences between the working fluid and the sinks. The easiest cycle which is close to an ideal cycle is a triangular cycle with a two phase flow expansion starting from a saturated liquid condition [115; 116]. Heat capacity Cp_{mass} of the working fluid is almost constant because heat is introduced in conditions far from the critical point

thus entailing the possibility to maintain an almost constant temperature difference in the whole PHE. The idea is fascinating but it entails a number of difficulties that are mainly related to the expander design and operation. The expansion in two phase flow starting from a saturated liquid condition involves a series of detrimental effects which affect the efficiency and the reliability of the expander. The first one is the presence of droplets of liquid which cause erosion of metal surface and force to maintain low peripheral speed. Screw compressors operating in expansion mode are the suggested technology for this kind of cycle because they can handle two phase flows without remarkable problems if a correct volume ratio is imposed. More details about their architecture, their operation and the maximum attainable efficiencies are discussed in Section 6.2.3 (Screw devices). The second difficulty is due to the really high volume ratio along the expansion for relatively small temperature drops. Positive displacement devices are characterized by small built in volume ratios (<5) and, using a single device, it is not possible to efficiently reduce the temperature difference into the PHE and match properly the heat source and the working fluid in the heat introduction process. The effect is more marked for high complexity fluid: the Andrews curve is overhanging and moving along an isentropic expansion high vapour quality are rapidly obtained.

With the aim of exploiting heat sources with a relevant temperature variation, the overall expansion is divided in more than one device but screw expanders cannot handle two phase flow at the intake port due to the phase stratification which leads to a non-correct feeding of the device. A proposed solution consists in an almost triangular two pressure levels cycle [117]. Plant layout is reported in Figure 5.7: the working fluid is expanded from a condition close to saturated liquid at the maximum cycle temperature by a high pressure screw expander. A two phase fluid at screw outlet is found with a vapour quality related to fluid complexity and device built in volume ratio. Fluid cannot be directly sent to a low pressure screw expander and a flash stage is required to separate vapour to liquid phase. Vapour stream is expanded from saturated condition to condensing pressure, it flows possibly in a recuperator and it is eventually condensed. Liquid from the condenser hotwell is pumped to a pressure greater than the flash one; it is heated in an economizer and mixed with the liquid coming from the flash stage. The high pressure pump feeds the high pressure economizer where fluid is brought again to saturated liquid condition.

This cycle allows exploiting a variable temperature heat source minimizing the entropy generation in the heat introduction process and thus achieving higher efficiencies. Despite the good potential of this plant layout a number of issues have to be faced and this solution is far from to be available on the market. The first problem is related to two phase flow screw expander, this component is widely studied for HVAC (Heating Ventilation and Air Conditioning) applications to substitute the lamination valve and

increase the COP of the cycle. Experimental activities which have been carried out so far have pointed out technical limits in their use. The other limit is related to the small built in volume ratio of common volumetric expanders and thus the small temperature increase attainable in the high pressure economizer. This detrimental effect can be mitigate using low complexity fluids because of the smaller variation of quality along an isentropic expansion for a given temperature difference. Furthermore, it is crucial to use fluids with a critical temperature close to maximum temperature of the cycle in order to increase the density of the saturated vapour resulting from the flash stage. These constraints entail that flash trilateral cycles are suitable for the exploitation of medium low temperature heat sources using small-medium complexity fluid. The T-Q and the T-s diagram for the flash trilateral cycle are reported in Figure 5.8.

An example of their use for low temperature solar systems is discussed in Section 9.3 (Small direct solar power plants).

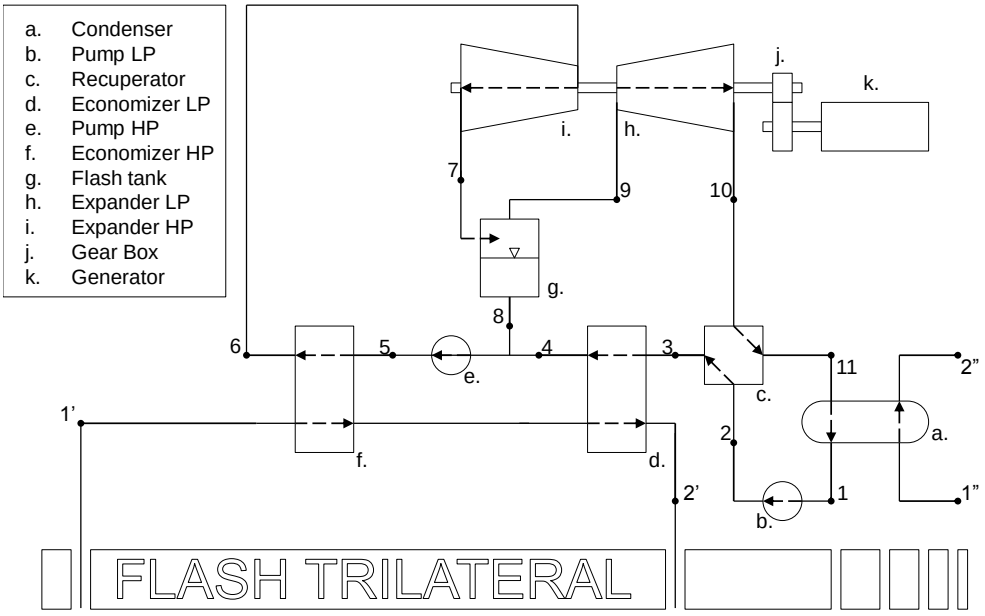

Figure 5.7 - Plant layout scheme of a flash trilateral cycle as proposed by Smith [115]

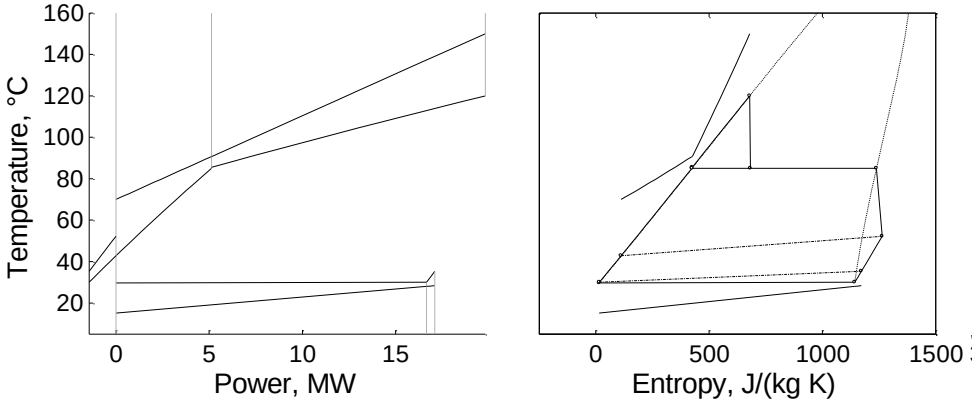

Figure 5.8 - T-Q and T-s diagrams for the flash trilateral cycle

Finally a Complete Flashing Cycle (CFC) is proposed [89] with the aim to approximate a trilateral cycle in high temperature applications like for example solar energy using advanced solar collectors. A throttled admission cycle generally uses a high complexity fluid like a siloxane or a long chain hydrocarbon exploiting the overhanging shape of the Andrews curve. For these fluids lamination from saturated liquid to saturated vapour conditions is almost isentropic and it results in a small temperature and pressure drops. T-s diagram is reported in Figure 5.9: heat is introduced to the fluid in liquid state up to a temperature close to the saturated one where it is throttled crossing the two phase region and reaching a saturated vapour or a slightly superheated vapour condition. Generally, isenthalpic lamination is a strongly irreversible process and it entails a notable entropy generation but for complex fluids, and in particular, crossing the two phase flow region this is not true and there is a huge portion under the saturation line and near the critical point where the trend of isenthalpic lines is almost isentropic.

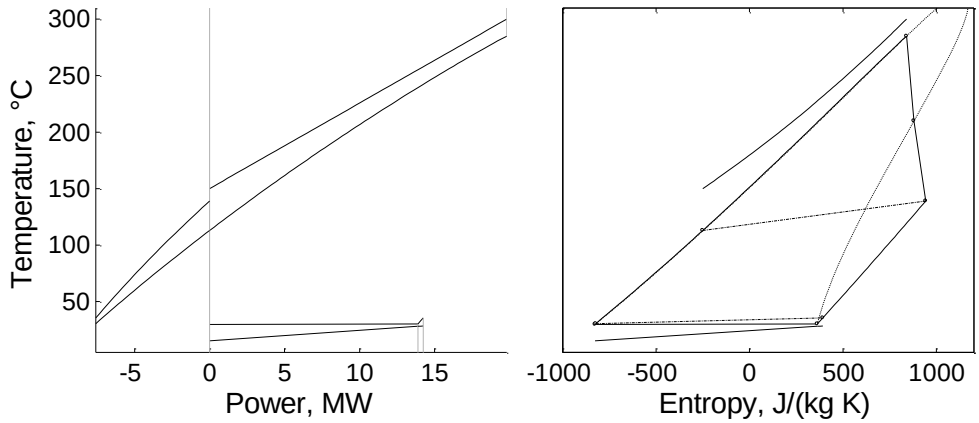

Figure 5.9 - Throttled admission CFC cycle for high temperature applications

The last interesting characteristic of this class of cycles is represented by the possibility to design direct heat storage solar power plants with the working fluid directly into the solar field. The working fluid during the heating process is always liquid and so it can be easily handled in conventional solar collectors because evaporation does not occur and so DSG collectors are not required limiting the issues related to pressure drops, thicker and more expensive collector tubes and additional hazard protections due to the presence of high pressure vapour in the solar field. Furthermore, heat storage can be realized directly with the hot working fluid. The most suitable solution is a solid medium heat storage formed by a vessel filled with rocks or small metal balls [118]: in charging mode, hot fluid enters the heat storage tank from the top, it flows in the gaps between the particles heating the solid medium. In discharging mode the flux is inverted and heat is released to the working fluid. The main advantage of this solution is the reduced amount of fluid compared to the conventional two tanks storage that results extremely expensive because of the high cost of organic fluids. A direct solar-direct heat storage ORC power plant has a simpler system; it does not require oil or molten salt as Heat Transfer Fluid and the HTF-working fluid heat exchanger. A comparison between the common saturated Rankine cycle for medium low concentration parabolic collector and advanced solution using triangular shaped ORC is presented in Section 9.3 (Small direct solar power plants).

"An expert is a person who has made all the mistakes

that can be made in a very narrow field"

Niels Bohr

6 Components

In typical ORC plants, a limited number of components are used, some of them are common devices like multistage centrifugal pumps, Shell&Tubes heat exchangers and air cooled condensers, while others appreciably differ from devices generally used in steam Rankine cycles. In particular, two components, namely the axial turbine and the volumetric expanders, are here discussed in detail because they are the key components in ORC field.

6.1 Axial flow turbines

As already stated in Section 4.2.5 (Effects on component design and cycle configuration), axial turbines allow handling the expansion in limited number of stages and they can achieve high performances in an extend range of applications. The efficiency of an axial turbine is strictly related to the inlet and outlet conditions, to the working fluid used in the thermodynamic cycle and finally to the number of stages and their optimization. As reported in section 4.2 (Thermodynamic properties of organic fluids), organic fluids are characterized by large volume ratios per stage compared to light molecules and a low speed of sound. Both of these peculiarities make the design of a turbine and its stages a quite challenging task which cannot be faced without the support of specific optimization software. On the other hand organic fluids have a small isentropic enthalpy drop compared to lighter fluids and so generally the load on each stage is lower, partially balancing the difficulties previously mentioned. In literature there are some examples of correlation, charts and diagrams that can be used to estimate the efficiency of an axial turbine but usually they lack in accuracy or they don't take into account some variables of interest in ORC field. For instance, a rough estimation of stage efficiency can be performed using Smith diagrams [119] which are based on flow and load coefficients but they don't consider blade geometry and stages specific speed. Better results can be achieved using Baljé and Binsley [120] plots, where efficiency is reported as function of specific speed and specific diameter and they are able to catch the influence of turbine size and the effect of volume flow rate variation for multistage machines. Even this approach is not complete and it cannot provide all the information required by the design of ORC turbines. As already demonstrated by Macchi [7; 121] and Lozza [122], a reliable design of an axial flow turbine should take into account real blade geometries and the effects of Mach numbers greater than unit. These aspects are crucial for organic fluids, where

blades are characterized by a large height variation, large flaring angles and supersonic velocities. In particular in Macchi [7], the effect of volume ratio and specific speed is analysed for different single stages turbines operating with heavy and complex fluids while in Lozza [122] even the number of stages is considered giving a more general description of the problem. Unfortunately, in these studies a fixed size parameter is considered and so no information about the effect of size on the turbine efficiency is available. The purpose of this section is to propose an efficiency correlation for the single stage, the two stage and the three stage axial flow turbines at optimized rotational speed in a wide range of volume ratios and size parameters.

6.1.1 Description of the code Axtur

The design and the optimization of a turbine stage or a multistage turbine is a challenging task. It is a strongly iterative procedure which entails various assumptions and constrains in order to achieve a reliable result and the complexity of the problem cannot be faced without the use of a specific numerical code. All the results presented in the next sections are obtained with Axtur tool which is an *in house* optimization code for axial flow and radial outflow turbines developed by Prof. Macchi and Prof. Lozza of Energy Department of Politecnico di Milano. The code is based on a pseudo 1D approach and both blade channels geometry and velocity triangles are defined at mean diameter for each blade row. Blade heights are hence obtained from continuity equation and the actual blade geometry is considered in efficiency losses calculation. Efficiency for each row is computed using correlations from literature to take into account boundary layer and secondary effects, supersonic flows and flow angle variations. The correlations used into the code are reported in Table 6.1.

effect	reference
Profile and secondary losses	Craig&Cox [123]
Annulus losses	Craig&Cox [123] or Kacker&Okapuu [124]
Partial admission losses	Traupel [125] or Baljè&Binsley [120]
Exit flow angles:	
• Subsonic flow	Ainley&Mathieson [126]
• Supersonic flow with after expansion	Vavra [127]
• Supersonic flow with converging diverging nozzle	Deich [128]

Table 6.1 – Correlations from reference used into Axtur to evaluate efficiency losses and exit flow angles correction

Lately, a user interface in Excel has been implemented by the author in order to easily handle both the input of a selected geometry and the resulting optimization output. Graphics of the velocity triangles, the geometry in the meridional plane and the efficiency loss breakdown for each stage are automatically generated. Finally, Axtur has been linked with Refprop [129] in order to derive reliable values for the pseudo-real fluid parameters required by the code. The code was developed following a pseudo real characterization of the fluid and the dependency between the thermodynamic variables is expressed by means of the definition of four coefficients.

- γ_{pT}: it has the same meaning of γ coefficient for ideal fluid and it is obtained knowing the inlet and outlet condition of the isentropic expansion. One value for each stage is required and it can be calculated with eq. 6.1

$$\gamma_{pT} = \frac{\ln\left(\frac{p_{out}}{p_{in}}\right)}{\ln\left(\frac{p_{out}}{p_{in}}\frac{T_{in}}{T_{out}}\right)} \qquad \text{eq. 6.1}$$

  where p_{out} is the outlet pressure for single stage turbines while for multistage turbines it is initialized dividing the expansion is a number of stages with the same volume ratio.
- γ_{pv}: it gives information about the volumetric behaviour of the fluid as a function of pressure. It is defined by the following equation which respects the same assumption of γ_{pT} for multistage turbines.

$$\gamma_{pT} = \frac{\ln\left(\frac{p_{in}}{p_{out}}\right)}{\ln\left(\frac{\rho_{in}}{\rho_{out}}\right)} \qquad \text{eq. 6.2}$$

- C_x: it is the pseudo mean specific heat capacity for each stage obtained by dividing the stage specific isentropic enthalpy drop for the temperature change.

$$C_x = \frac{\Delta h_{is}}{\Delta T_{is}} \qquad \text{eq. 6.3}$$

- Z: it is the compressibility factor, three values are always required, at inlet, outlet and a properly defined mean pressure respectively.

$$Z = \frac{P}{T\frac{R}{MM}\rho} \qquad \text{eq. 6.4}$$

The values of these parameters must be defined by the user in order to model any desired fluid, otherwise they can be retrieved from Refprop dividing the overall expansion in a number of stages with the same volume ratio. If a very non-homogeneous repartition of the volume ratio is achieved in the final optimized solution, iteration can be helpful to obtain more reliable results. In common cases this expedient is not required and it little affects the final solution. For ideal fluid only γ_{pT} parameter is required.

Axtur, starting from a feasible initial point, is able to perform multivariable constrained optimizations of turbines with a maximum stage number equal to three. Every stage is fully defined by nine parameters: three of them are global variables defining the stage load and the stage type while the other six (three for each row) are representative of characteristic geometrical ratios and they define the blade geometry. These variables can be varied in a range defined by a lower and an upper bound labelled as linear constraints. In addition, nonlinear constraints are considered for other variables of interest and penalty factors are introduced if the upper or the lower bounds are not respected. Penalty weights are assumed equal for all the nonlinear constraints and changing the relative weight of some of them to force the solution in some regions often entails instability of the optimization algorithm and a poor accuracy of the final solution.

The code requires a number of inputs that can be divided in different categories; in Table 6.2 and Table 6.3 all the parameters in input to Axtur tool are briefly described and the notation used is reported in Figure 6.1.

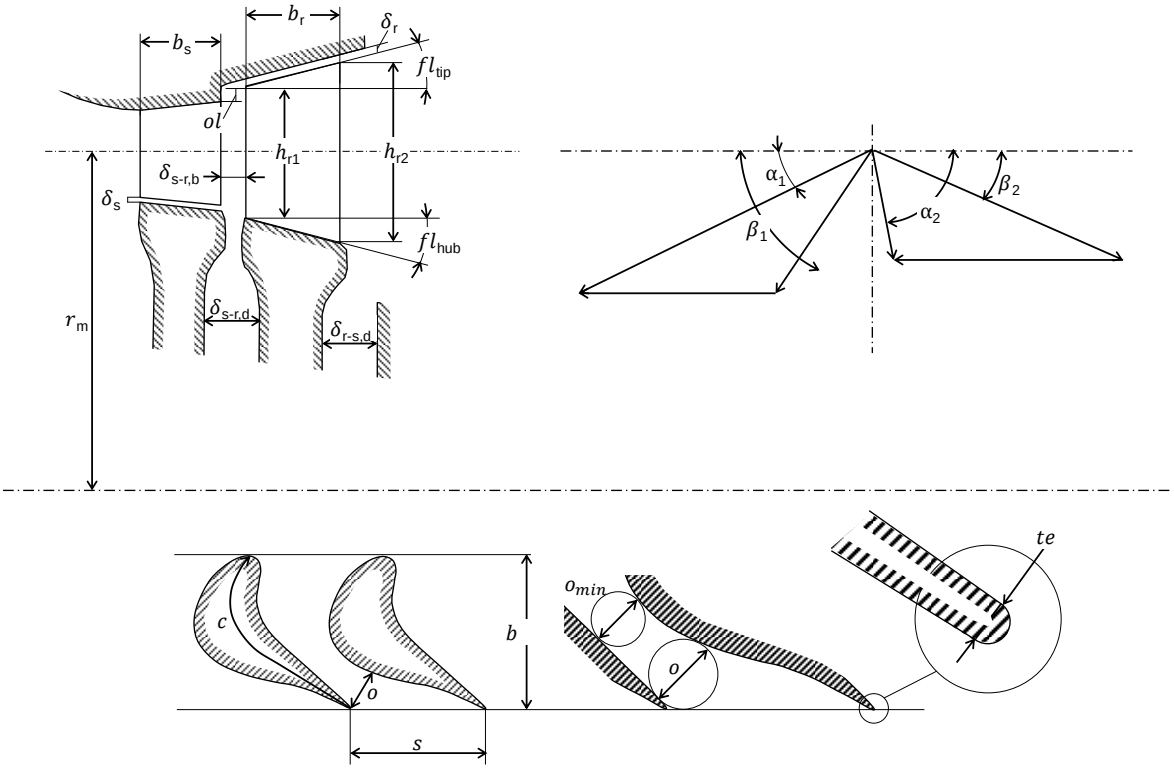

Figure 6.1 - Notation used in Axtur for the blade geometry and the velocity triangles.

Axtur optimizes the total to static efficiency corrected by the fraction of kinetic energy recovered by the diffuser according to eq. 6.5.

$$\eta = \frac{\mathrm{W}}{\Delta h_{T-S} - \phi_{\mathrm{E}} \frac{\mathrm{v}_{2,\mathrm{a}}^2}{2}} \qquad \text{eq. 6.5}$$

Where ϕ_{E} is the efficiency of the diffuser; usually a value of 0.5 is adopted.

The approach is not completely rigorous because the recovery of kinetic energy entails a reduction of the pressure at turbine discharge and so a higher pressure drop and a higher power production while here the effect is accounted subtracting the same term from the denominator. As proved by Macchi [7], the approximation is generally valid and does not affect the quality of the solution, in terms of turbine efficiency.

Input data group	parameters	n		Value	Definition and notes
Thermodynamic	Total inlet pressure	1	UD	bar	This group of parameters completely defines both the inlet and the isentropic outlet conditions
	Total inlet temperature	1	UD	K	
	Static outlet pressure	1	UD	bar	
Fluid properties	m_{fluid}	1	UD	kg/s	mass flow rate
	type of fluid	1	UD	ideal – real	
	γ_{pT}	1xst	UD	-	See eq. 6.1
	γ_{pv}	1xst	UD	-	See eq. 6.2
	C_x	1xst	(real f.)	kJ/kgK	See eq. 6.3
	Z	3	SD (ideal f.)	-	See eq. 6.4
	Δh_{is}	1	SD (ideal f.)	kJ/kg	Isentropic enthalpy drop from total inlet and static outlet pressure
Optimization routine	N_{iter}	1	SV	300000	Maximum number of iterations
	N_{cyc}	1	SV	2	Number of optimization cycles
	w_i	15xst	SV	0.1	Weights for nonlinear constraints
stage Fixed geometrical	δ_d/δ_{s-r}	1	SV	1.25	Ratio between disk clearance and stator-rotor clearance
	$h_{in,s}/h_{out,r}$	1	SV	1.1	Overlapping between outlet rotor blade and stator inlet blade
	roughness	1	SV	2e-6	Absolute roughness of blade surfaces
	blade curvature	1	SV	1e+5	Radius of curvature of blade profile after the throat section
	stator inlet angle	1	SV	90	Absolute direction of the flow at stator inlet
	loss coeff. for $Mach_{w1}>0.8$	1	SV	0.5	Additional loss coefficient for relative Mach number at rotor inlet
	Maximum Mach for post expansion	1	SV	1.4	Maximum value for purely convergent nozzle
Row fixed geometrical	Min t_k (stator-rotor)	2xst	SV	0.1, 0.1	Absolute minimum thickness value of the trailing edge
	Min t_k/o (stator-rotor)	2xst	SV	0.0002, 0.0002	Minimum thickness of the trailing edge relative to throat
	Min δ_{tip} (stator-rotor)	2xst	SV	0, 0.001	Absolute minimum value for the tip clearance
	Min δ_{tip}/r_m (stator-rotor)	1xst	SV	0, 0.002	Minimum blade tip clearance relative to stage mean radius
	r_{rot}/r_{stat}	1xst	SV	1	Variation of mean radius from stage to stage
	δ_{r-s}/h_r	1xst	SV	0.2	Clearance between rotor and stator relative to rotor blade height
	δ_{s-r}/b_s	1xst	SV	0.1	Clearance between stator and rotor relative to stator blade chord

Table 6.2 - input required by Axtur and their meaning. User Defined (UD) inputs are free to be set by the user, System defined (SD) inputs are calculated by Axtur prior to calculation. Suggested Values (SV) for other variables are set on the basis of axial flow turbines technical constraints. Optimization variables are signed by (OPT).

Table 1/2

Stage nonlinear constr.	b (min-max)	2	SV	0.003, 0.100	Minimum and maximum absolute values for blade axial chord
	o (min-max)	2	SV	0.002, 0.100	Minimum and maximum absolute values for blade axial throat
	fl_{hub} (min-max)	2	SV	-30, 0	Minimum and maximum absolute values for hub flaring
	fl_{tip} (min-max)	2	SV	0, 30	Minimum and maximum absolute values for tip flaring
	$h_{out,r}/D_m$ (max)	1	SV	0.2	Maximum ratio between rotor blade height and mean stage diameter
	$h_{out,r}/h_{in,s}$ (max)	1	SV	1.5	Maximum variation of blade height
	$ol_{,s-r}$ (max)	1	SV	0.003	Overlap maximum between stator and rotor blades
	n_{blades} (stator-rotor)	2	SV	100, 100	Maximum number of blades
	$Mach_{max}$ (in-out rotor)	2	SV	1.2, 1.5	Maximum Mach number at inlet and outlet of rotor blades
Stage optimization var.	k_{is}	1xst	OPT	-	Stage isentropic load coefficient
	Degree of reaction - admission	1xst	OPT	-	For total and partial admission stages
	V_r	1xst	OPT	-	Stage volume ratio
Row optimization var.	o/s	2xst	OPT	-	Ratio between throat and blade step
	o/b	2xst	OPT	-	Ratio between throat and blade axial chord
	b/r_m	2xst	OPT	-	Ratio between blade axial chord and stage mean diameter

Table 6.3 - input required by Axtur and their meaning. User Defined (UD) inputs are free to be set by the user, System defined (SD) inputs are calculated by Axtur prior to calculation. Suggested Values (SV) for other variables are set on the basis of axial flow turbines technical constraints. Optimization variables are signed by (OPT).

Table 2/2

The results provided by Axtur consist in all the information about blade geometry in both blade to blade and meridional planes and velocity triangles. Furthermore the breakup of the efficiency losses is given considering the following effects:

- *Profile loss*: it is due to the blade shape and effects related to friction, fluid vane deflection and boundary layer dissipation. This loss mainly depends on blade pitch, blade backbone length, trailing edge thickness and roughness of blade surface. For instance, high deflection blades with small pressure gradients, like in the rotor of an impulse stage, show poor efficiency due to boundary layer detaching. Other examples are blade channels with narrow openings where the share of dissipative boundary layer on the total flow is relevant and turbulent wake caused by a finite trailing edge thickness which modifies the fluid dynamic of exit flow.
- *Secondary losses*: they are caused by secondary flow structures mainly described by passage vortex, horseshoe vortex, trailing edge vortex and corner vortex. These losses are affected by the same parameters which have influence on profile losses plus blade height. Efficiency of small height blades, like high pressure stages without partial admission and direct coupling with generators, is strongly affected by dissipative phenomena which occur in the corners of the blade channel. Higher is the blade and larger is the throat dimension, lower is the share of the flow interested by these phenomena.
- *Annulus losses*: they are due to the passage of fluid in the gap between two blade rows. Fluid flow is deflected when two streams coming from two adjacent channels are mixing together.
- *Leakage losses*: they are caused by the unwanted passage of fluid above blade tip or between stator and rotor blades whose expansion does not contribute to power production. This kind of loss is mainly related to radial clearance, blade length and blade overlap. They are assumed to be null for the first stator blades
- *Disk windage losses*: they are due to velocity gradient in the clearance between stator and rotor disk walls. They are strongly affected by rotational speed and by both absolute disk clearance and disk diameter.
- *Kinetic energy loss*: it is the fraction of kinetic energy of the axial component of discharge velocity which cannot be recovered with the diffuser. Usually it is defined with a coefficient Φ_e smaller than unit.

6.1.2 Similarity rules

As shown in Macchi [121], optimal results coming from different turbines can be compared on the basis of some specific parameters. Furthermore, the results, displayed on specific or relative axes, are useful to determine general trends of efficiency for different turbine stages if they respect similarity rules [130].

According to these rules, the results achieved for a certain turbine stage can be extended to any other case if the two stages respect the following conditions:

1. They have the same specific speed
2. The Reynold number effects are negligible
3. The thermodynamic behaviour of the two fluids is the same, namely the flow is incompressible or fluids with the same pressure ratio and the same heat capacity ratio are considered [121]
4. The geometric similarity is verified: all the geometrical ratios are equal for the two stages.

These laws are substantially valid if the same fluid or fluids with a similar complexity are used. It is important to note that imposing the same pressure ratio for a simple and complex gas results in very different thermodynamic properties along the expansion as reported in Section 4.2 (Thermodynamic properties of organic fluids). Compressibility effects and large volume flow variations affect the design of turbines working with complex fluids entailing a lower efficiency. With the aim to extend the analysis to different fluids point 3 should be modified in:

3. The thermodynamic behaviour of the two fluids is the same, namely the flow is incompressible or fluids with the same isentropic volume ratio are considered.

The approach is not totally rigorous because the Mach numbers can be slightly different if different fluids, with different molecular mass, are used with the same volume ratio. The effect of these differences on the overall efficiency is an order of magnitude lower than other losses and so it can be neglected [121]

In conclusion the parameters suggested as independent variables for a parametric analysis of axial-flows turbine are: the specific speed (Ns), the size parameter (SP) and the volume ratio (V_r) which can be calculated with the following equations:

$$Ns = \frac{RPM}{60}\frac{\mathrm{V}_{out}{}^{0.5}}{\Delta h_{is}{}^{0.75}} \quad \text{eq. 6.6}$$

$$SP = \frac{\mathrm{V}_{out}{}^{0.5}}{\Delta h_{is}{}^{0.25}} \quad \text{eq. 6.7}$$

$$Vr = \frac{\mathrm{V}_{out}}{\mathrm{V}_{in}} \quad \text{eq. 6.8}$$

According to similarity rules and with the over mentioned assumptions, two turbine stages with the same value of Ns, SP and Vr, show a really similar efficiency. The optimizations presented in next sections are realized assuming a complex perfect gas with a γ_{pT} value equal to 1.05 as representative of a generic organic fluid.

6.1.3 Results for single stage turbines

Three parameters are assumed as independent variables in this analysis, namely Ns, SP and Vr, and more than five hundreds of turbines are optimized. It is important to remember that, according to similarity rules, for the same set of independent variables the choice of a different γ_{pT} affects variables like speed of revolution, pressure ratio, temperature and enthalpy drop along the isentropic expansion and mass flow rate but it doesn't have influence on the final optimal solution.

Effect of Ns

The first analysis proposed is the optimization of Ns for a single stage turbine. SP and Vr are assumed constant and equal to 0.4 and 4 respectively. Results are reported in Figure 6.2. In this case, both volume flow rate at turbine exit and isentropic enthalpy drop are fixed and so Ns parameter has a direct effect on both speed of revolution and mean diameter, if a maximum peripheral velocity is defined. A low specific speed entails a larger mean diameter because of the necessity to maintain u velocity above a certain value and to reduce the stage load. Optimized stages in this region have small h/D parameters and they are affected by high leakage and secondary losses. Velocity triangles are representative of impulse stages with an almost axial absolute velocity v_2, thus the kinetic losses are minimized; disk windage loss is noticeable because of the large diameter interested by this dissipation effect. Increasing the rotational speed allows reducing both the secondary and leakage losses thanks to higher blades and a larger h/D

ratio while the profile and the kinetic losses become more and more relevant. Optimal Ns value is equal to 0.15 corresponding to well-proportioned turbine stages and an almost perfect reaction velocity triangle with an axial absolute velocity at turbine outlet. On the other hand, for high Ns values, the rotational speed is higher and the stage mean diameter is strongly reduced leading to high values of h/D parameter. Both the secondary and the leakage losses are minimized but the distorted shape of the velocity triangles entails high values of discharge velocity which cannot be maintained in axial direction. Furthermore the solution for high specific speeds is affected by supercritical flows at rotor inlet where shock waves strongly penalize the profile efficiency. The trade-off between these opposite effects leads to the presence of a maximum in efficiency.

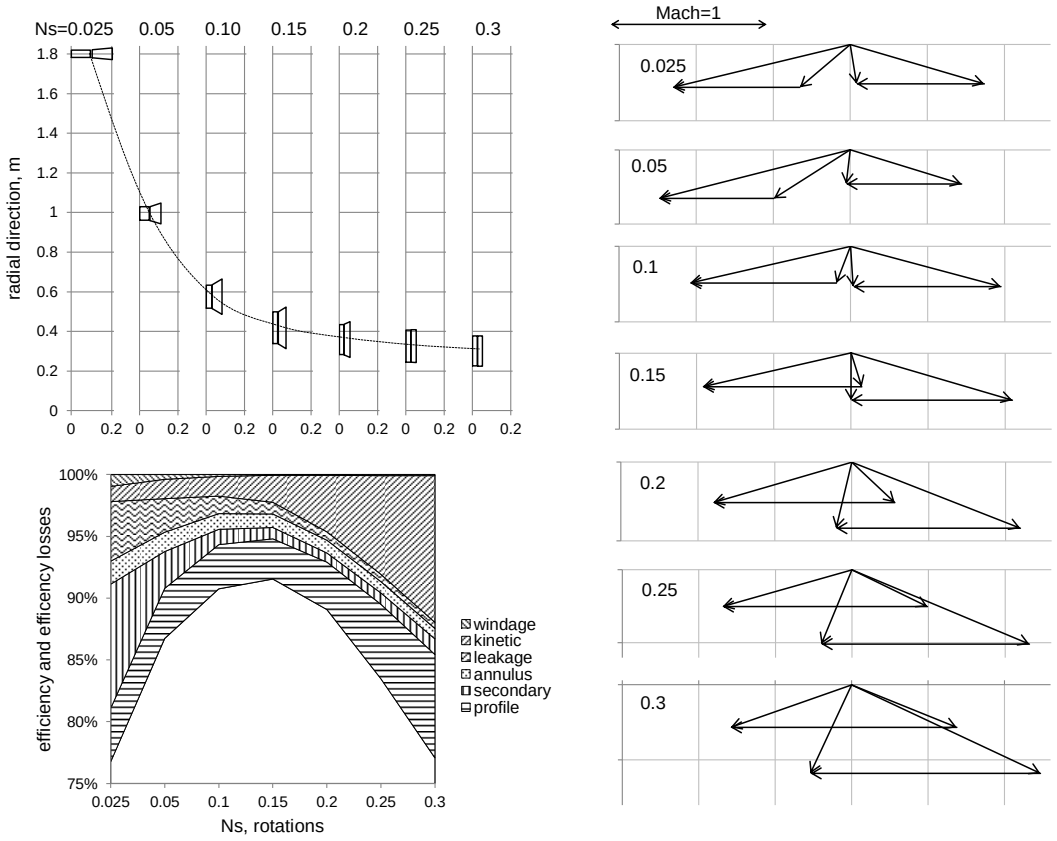

Figure 6.2 - Blade profiles, velocity diagrams and efficiency losses breakup for a single stage turbine with SP=0.04 and Vr=4 for different Ns.

The same procedure can be applied for different combinations of SP and Vr obtaining a series of charts like those reported in Figure 6.4 where the effect of SP, Vr and Ns on stage efficiency are represented. For every couple of SP and Vr, an optimal specific speed

is found as result of the trade-off between opposite effects previously mentioned. The optimal value of Ns varies depending on both the other two parameters.

As a general consideration, there is a huge range in SP and Vr where the optimal specific speed is between 0.1 and 0.15, as already pointed out in Macchi [7]. For high volume ratios and small size parameters, this is not true anymore and optimal Ns decreases for high volume ratios. This is justified by the presence of lower and upper bounds on some geometrical dimensions like minimum blade height and maximum h/D ratio. In these cases, Ns values around 0.1 entail an almost unfeasible design of the blade with a strong increase of secondary losses. In Figure 6.3 the maximum point for every curve are collected and organized in two logarithmic charts against SP and Vr giving a graphical view of the maximum turbine efficiency attainable optimizing the specific speed.

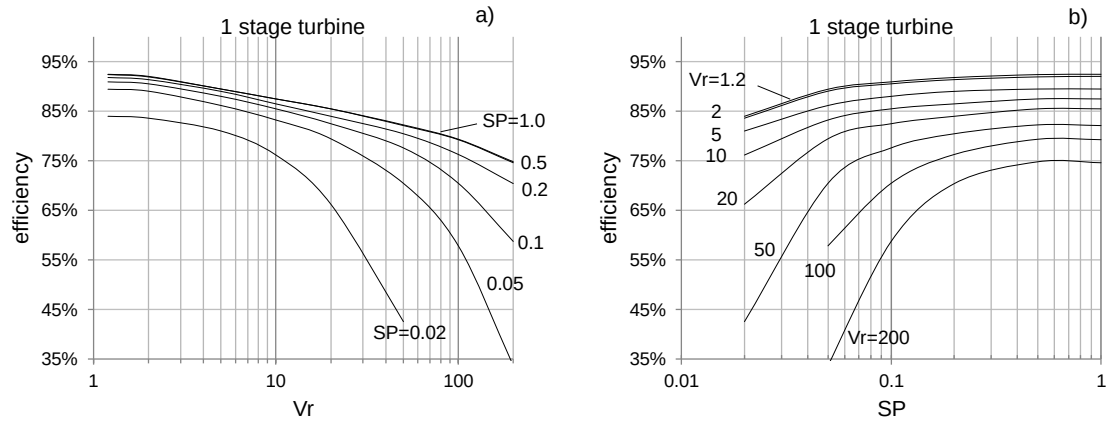

Figure 6.3 - Specific speed optimized results for a single stage turbine. A parametric SP representation against Vr is reported in (a) while the same data organized against SP are proposed in (b).

For a better understanding of the effects occurring in the definition of optimized stage geometry, two parametric analyses are here proposed. The first one is carried out varying Vr for fixed SP equal to 0.05 with the aim of pointing out the attention on the effects of volume flow variation, high loads and supercritical velocities. The other one instead, is performed at fixed Vr =20 for turbine stages having different SP in order to highlight the influence of both turbine size and geometrical constraints on overall efficiency. In Figure 6.7 the directrixes for the two above mentioned analyses are displayed with two dotted lines.

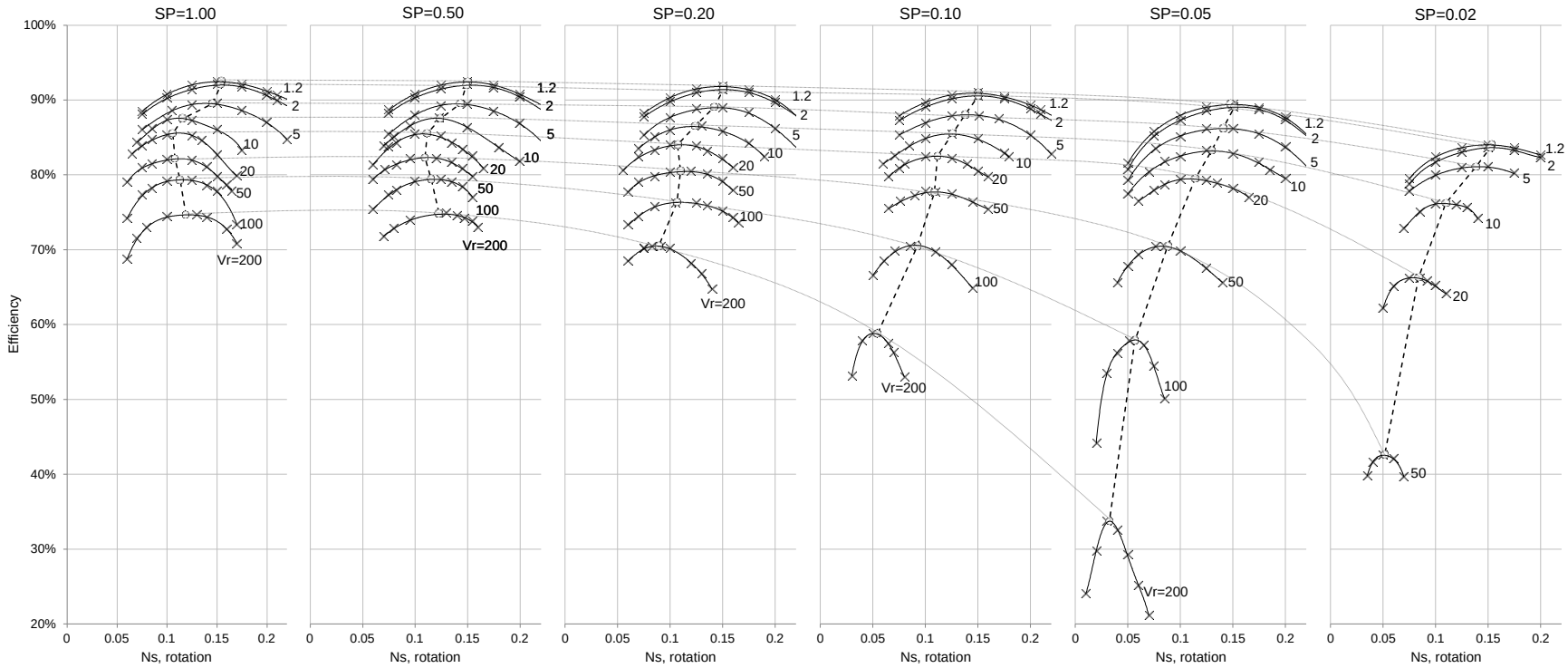

Figure 6.4 - Efficiency trends for 6 different SP (1, 0.5, 0.2, 0.1, 0.05, 0.02) and 8 different Vr (1.2, 2, 5, 10, 20, 50, 100, 200) for various Ns. Dashed lines connect maximum of every line for different Vr and fixed SP. Dotted lines connect maximum of every line for different Vr and fixed SP.

Effect of Vr

Optimized results for single stage turbines, with different Vr and a fixed SP equal to 0.05, are presented in Figure 6.5. The breakdown of efficiency losses shows that the maximum attainable efficiency optimizing Ns is a decreasing function of Vr.

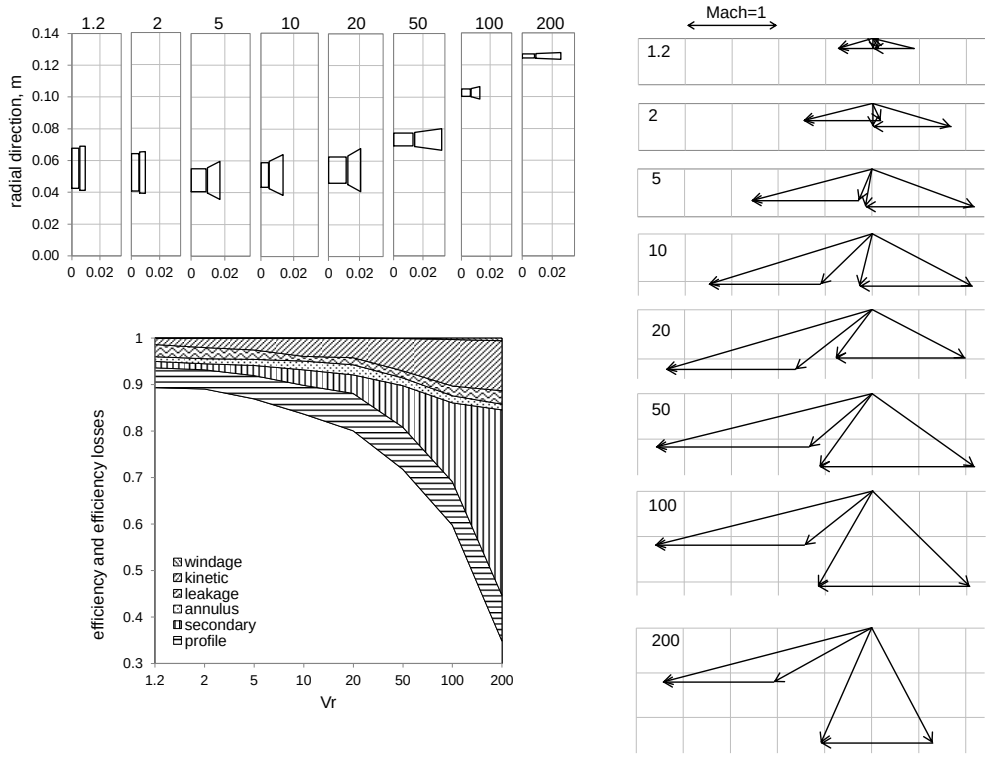

Figure 6.5 - Parametric analysis for different single stage turbines having the same SP=0.05, Volume ratio varies in the range 1.2-200 and the results are obtained at the optimal specific speed

For really low volume ratios, namely values below twice the $Vr_{crit} = 1.64$, velocity triangles are always subsonic, the load is limited and pure reaction stages with high efficiency can be designed. h/D ratio is favourable, no flaring is required and both secondary and profile losses are small. Increasing Vr, velocities with Mach numbers greater than unit are obtained, in particular for v_1 and w_2 vectors, with an increase of profile losses. Converging-diverging stator nozzles are required for Vr above 5, while they are needed at rotor row for values beyond 10. If a Vr greater than 20 is imposed a velocity close to the sonic one is obtained at w_1 vector with problems of shock waves at rotor inlet. Loss coefficients to take into account this effect contribute to penalize the efficiency. Velocity triangles become more and more distorted due to the necessity to handle higher volume flow variations and contextually maintaining a velocity vector v_2 close to the axial direction. Increasing the volume ratio involves a higher isentropic

enthalpy drop and it leads to optimized stages with higher peripheral speed u and larger mean diameter in order to limit the stage load. Solution moves toward impulse stages with really small blade heights and high secondary losses. Disk windage increases due to larger surface interested by the phenomena. In conclusion, adopting Vr higher than 5 for a single stage turbine entails a strong limitation in the attainable efficiency and multistage turbines should be considered in order to contain the load on each stage.

Effect of SP

A similar analysis is realized for different single stage turbines with the same Vr=20 but different SP. Size parameter is varied from 0.02 to 1 which is a value representative of turbines close to the maximum size of normal ORC expanders. All the stages work with the same isentropic enthalpy drop but they notably differ in volumetric flow rate because of the quadratic dependence on the SP. Small size parameters lead to very small volumes flow rates at turbine discharge section with a reduced passage area. Due to geometrical limits on minimum blade height and minimum h/D ratio the mean diameter gets smaller with an increase of rotational speed in order to maintain the optimal value of specific speed. These two effects result in a strong efficiency drop for small turbines with a considerable increase of secondary and leakage losses.

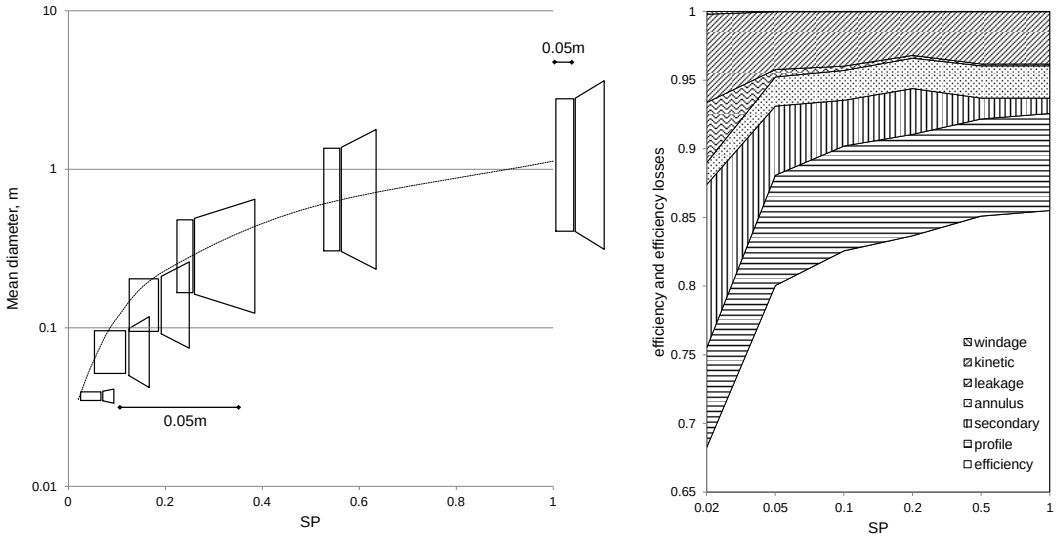

Figure 6.6 - Parametric analysis for different single stage turbines having the same Vr=20, Size Parameter varies in the range 0.02-1 and the results are obtained at the optimal specific speed

Proposed correlation for single stage turbines

Specific speed optimal data reported in Figure 6.3 can be organized in a contour map as reported in Figure 6.7. It is possible to notice that there is a large region in both SP and Vr where very high efficiencies can be achieved. A OLS regression is performed in Gretl [131] selecting the functions of SP and Vr which are more suitable to describe the set of data; some variables are excluded because their omission allows obtaining an higher value of the adjusted R^2 coefficient which finally results equal to 0.997. The proposed correlation for the maximum efficiency of single stage turbines has a functional form reported in eq. 6.9 while the numerical values of the retrieved coefficients can be found in Table 6.4.

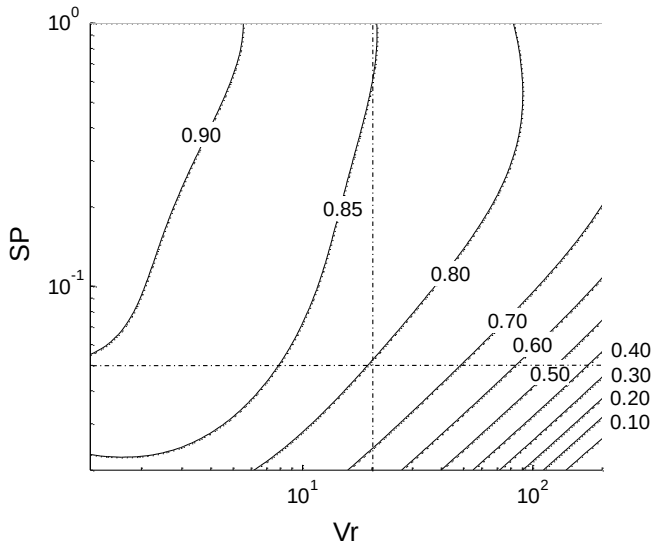

Figure 6.7 - Contour map of efficiency for a single stage turbine, efficiency decreases for high volume ratios, due to the higher load and supersonic flows. Efficiency decreases for low SP due to miniaturized blades, high secondary and leakage losses. Dotted lines are referred to the fixed SP and fixed Vr analysis.

$$\eta = A_0 + \sum_{i=1}^{17} A_i F_i \qquad \text{eq. 6.9}$$

	n	F_i	A_i
	0	const	0.90831500
$f(SP)$	1	SP	-
	2	$\ln(SP)$	-0.05248690
	3	$\ln(SP)^2$	-0.04799080
	4	$\ln(SP)^3$	-0.01710380
	5	$\ln(SP)^4$	-0.00244002
$f(Vr)$	6	Vr	-
	7	$\ln(Vr)$	0.04961780
	8	$\ln(Vr)^2$	-0.04894860
	9	$\ln(Vr)^3$	0.01171650
	10	$\ln(Vr)^4$	-0.00100473
Cross terms	11	$\ln(Vr)\ \ln(SP)$	0.05645970
	12	$\ln(Vr)^2 \ln(SP)$	-0.01859440
	13	$\ln(Vr)\ \ln(SP)^2$	0.01288860
	14	$\ln(Vr)^3 \ln(SP)$	0.00178187
	15	$\ln(Vr)\ \ln(SP)^3$	-
	16	$\ln(Vr)^3 \ln(SP)^2$	-0.00021196
	17	$\ln(Vr)^2 \ln(SP)^3$	0.00078667

Table 6.4 - Regressed coefficients for single stage turbine optimal efficiency correlation

6.1.4 Results for multi stage turbines

In previous section, single stage turbines have been considered, but as pointed out from this analysis, their efficiency is strongly limited for high volume ratios and small size parameters. Multistage turbines are commonly adopted because they can achieve a higher efficiency taking advantage by the repartition of the whole volume flow variation on two or more stages. In this work only two stage and three stage turbines are considered because in most of the applications the advantages in adopting a higher number of stages are limited and these solutions usually lead to a higher cost of electricity. Furthermore, axial turbines are usually overhung with rolling bearing just on one side: this design allows an easy inspection of the turbine during maintenance operation but it limits the number of stages to three because of rotodynamic issues. A rotodynamic analysis performed by Exergy [4; 132] shows that for a number of stages greater than three the natural frequencies of the turbine shaft get closer to 50 (or 60 Hz) with the risk of resonance during normal operation.

The analysis presented in previous section referred to a single stage turbine is repeated for both two stage and three stage machines. The results, obtained optimizing the rotational speed, are presented in terms of Ns, Vr and SP calculated for the overall expansion as

though it is exploited by a single stage. The parametric families of curves are reported in Figure 6.8 for the considered multi stage turbines.

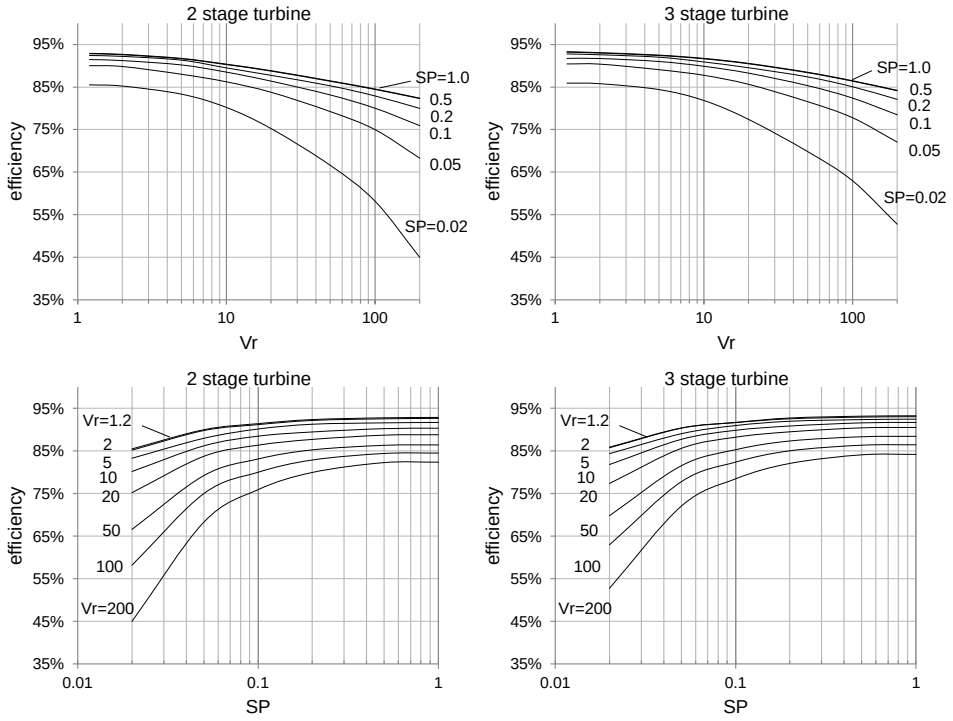

Figure 6.8 - Parametric curves on SP and Vr for two stage and three stage turbines

In Figure 6.9.a a comparison between the maximum efficiencies achievable for a single stage and a two stage turbine is reported while in Figure 6.9.b the increment of efficiency is displayed. Increases of efficiency are not constant over the considered range of SP and Vr, and more relevant increments are obtained for high overall volume ratio and small size parameter. For Vr equal to 5 the efficiency increment is greater than 2 percentage points independently to SP value: an increment that justifies a more expensive device with the adoption of a two stage turbine. Benefits are obviously larger for higher Vr and the efficiency increase reaches value above 10% for medium-small machines and volume ratios greater than 50. Last observation regards the possibility to extend the domain of solution: in particular for a SP lower than 0.02 and Vr of 100 and 200 it is not possible to design a single stage turbine with a reasonable efficiency. The high load on such a small stage and the presence of geometric constrains entail a non-feasible execution of the optimization algorithm with variables values always outside of the efficiency losses correlation limits. This problem is not found for two stage turbines and the whole range of SP and Vr is explored.

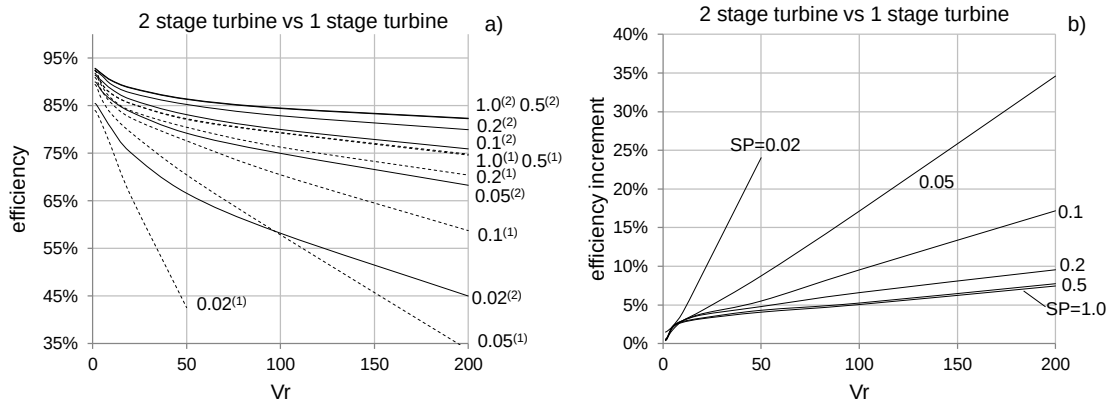

Figure 6.9 - Comparison between attainable efficiency adopting a two stage turbine instead of a single stage turbine (a) and corresponding efficiency increases (b)

Similar consideration can be done comparing two stages and three stage turbines. Results are reported in Figure 6.10.a and Figure 6.10.b. The attainable efficiency increase is lower than in the previous case but, once again, notable advantages are highlighted for high volume ratios and small turbines.

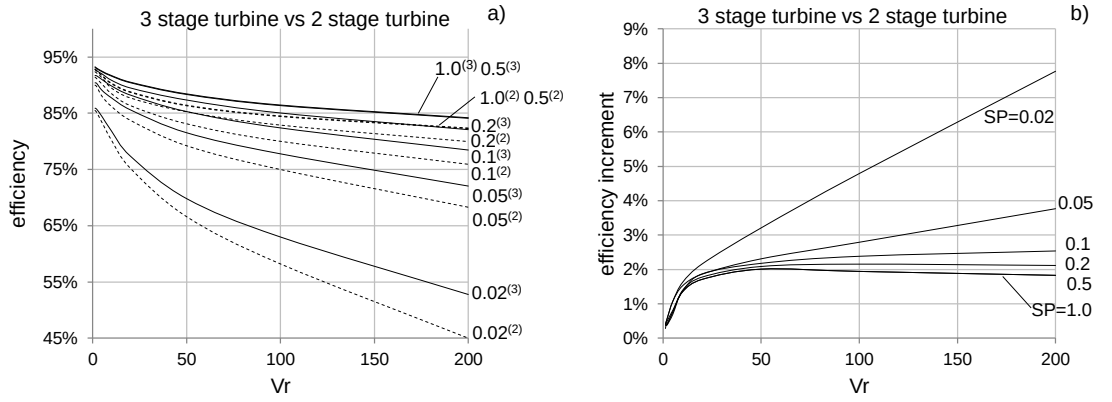

Figure 6.10 - Comparison between attainable efficiency adopting a three stage turbine instead of a two stage turbine (a) and corresponding efficiency increases (b)

A regression of the two data sets is performed in Gretl with the same procedure over mentioned for a single stage turbine. The retrieved coefficients are reported in Table 6.5 with the values of adjusted R^2. Finally, a graphical view of the performance maps is reported in Figure 6.11.

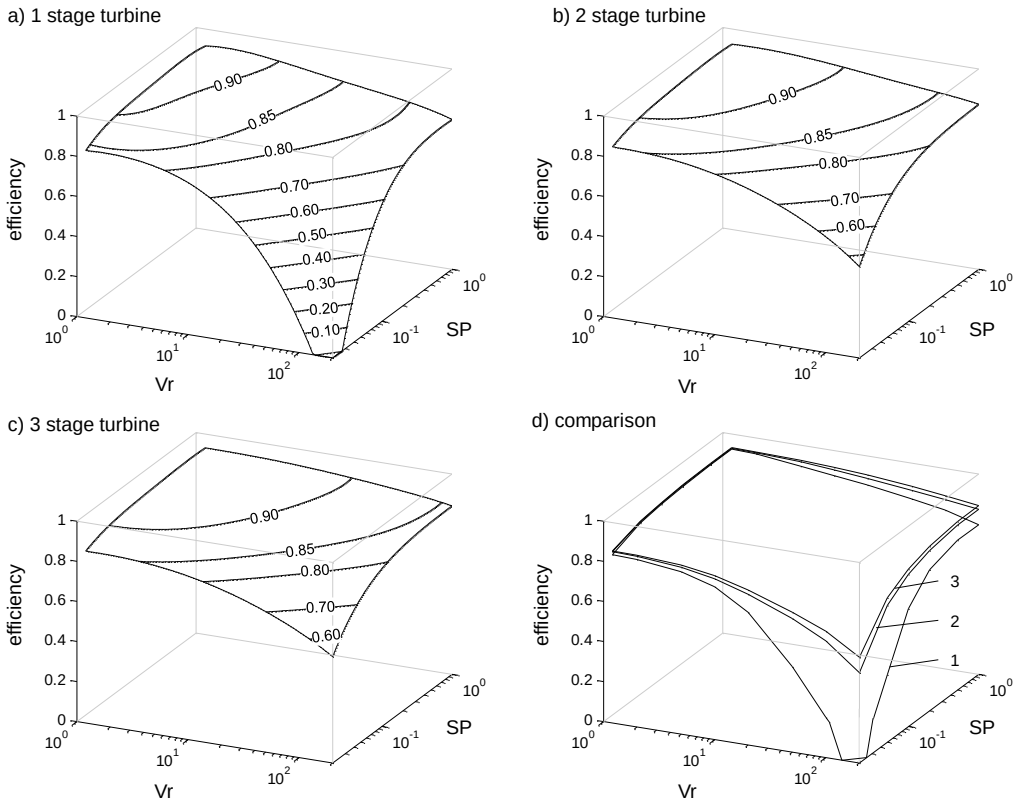

Figure 6.11 - Three-dimensional view of single stage, two stage and three stage turbines in a log-log axes

	Stages number		1	2	3
	n	F_i		A_i	
	0	const	0.90831500	0.923406	0.932274
$f(SP)$	1	$\ln(SP)$	-0.05248690	-0.0221021	-0.01243
	2	$\ln(SP)^2$	-0.04799080	-0.0233814	-0.018
	3	$\ln(SP)^3$	-0.01710380	-0.00844961	-0.00716
	4	$\ln(SP)^4$	-0.00244002	-0.0012978	-0.00118
$f(Vr)$	5	Vr	-	-0.00069293	-0.00044
	6	$\ln(Vr)$	0.04961780	0.0146911	-
	7	$\ln(Vr)^2$	-0.04894860	-0.0102795	-
	8	$\ln(Vr)^3$	0.01171650	-	-0.0016
	9	$\ln(Vr)^4$	-0.00100473	0.000317241	0.000298
Cross terms	10	$\ln(Vr)\ \ln(SP)$	0.05645970	0.0163959	0.005959
	12	$\ln(Vr)^2 \ln(SP)$	-0.01859440	-0.00515265	-0.00163
	12	$\ln(Vr)\ \ln(SP)^2$	0.01288860	0.00358361	0.001946
	13	$\ln(Vr)^3 \ln(SP)$	0.00178187	0.000554726	0.000163
	14	$\ln(Vr)^3 \ln(SP)^2$	-0.00021196	-	-
	15	$\ln(Vr)^2 \ln(SP)^3$	0.00078667	0.000293607	0.000211
	Adjusted R^2		0.99790	0.99935	0.99954

Table 6.5 – Regressed coefficients to be used in the correlation of turbine efficiency for single, two and three stage turbines

6.1.5 Comparison between discretized and global approaches

The maps of efficiency at optimized rotational speed, obtained in the previous section, are useful if the number of stages does not exceed three and if a gear box is used. In these cases, it is sufficient to use the correlation proposed to obtain a reliable estimation of turbine performance. However, in a general case the number of stages can be greater than three and some technical constraints might lead to a direct coupling with the generator. In these cases, the over mentioned maps are not sufficient to completely define the overall turbine efficiency. In this section a discretized methodology to estimate the performances of a generic turbine is introduced and the comparison with the reference efficiency is reported.

The approach consists in: (i) splitting the expansion in a selected number of stages, (ii) evaluating for every stage the efficiency which correspond to a certain set of Vr, SP and Ns and (iii) estimate the turbine global efficiency as a properly defined average of the single stage efficiencies. Respect to the work described in the previous sections, the effect of the specific speed is introduced in the efficiency correlation thus allowing the analysis of turbine stages with a non-optimized rotational speed. According to results of previous section, the analysis is limited to a maximum volume ratio per stage equal to 5 because a high efficiency turbine stage is rarely designed to work with higher values. As shown in Section 4.2 (Thermodynamic properties of organic fluids), the critical volume ratio doesn't change notably from fluid to fluid and it is always in the range of 1.65-1.75 thus working with Vr of 5 entails supersonic velocities in both stator and rotor with a consequent penalization of stage efficiency. From Figure 6.4, data related to volume ratios equal to 1.2, 2 and 5 are collected for the whole range of size parameters and specific speeds. An OLS regression is carried out in Gretl founding the variables or the combination of them which are more suitable to describe the set of selected data. Coefficients are reported in Table 6.6. An adjusted R^2 coefficient of 0.995 is found.

Maximum errors are obtained for low and high Ns that are values far from the optimal one; a plot of the residuals is reported in Figure 6.12 against Ns.

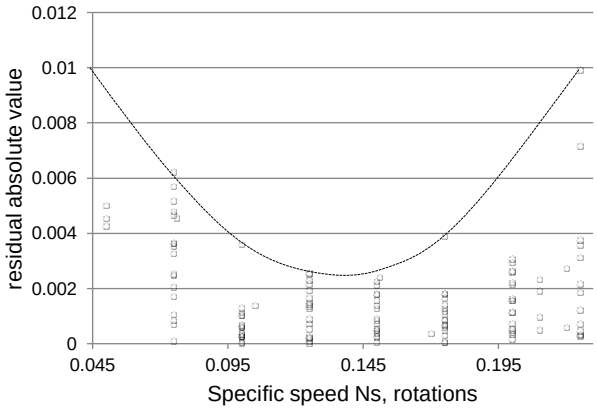

Figure 6.12 - Plot of the regression residuals against specific speed.

	n	F_i	A_i
	0	const	0.828496
$f(SP)$	1	SP	-0.083605
	2	$\ln(SP)$	0.078745
	3	$\ln(SP)^2$	0.030635
	4	$\ln(SP)^3$	0.005738
$f(Vr)$	5	Vr	0.005011
	6	$\ln(Vr)$	-0.021296
$f(Ns)$	7	Ns	2.648380
	8	Ns^2	-11.918500
	9	Ns^3	13.241800
Cross terms	10	$Ns^2 \ln(Vr)$	2.158950
	11	$Ns \ln(Vr)^2$	-0.141356
	12	$Ns^3 \ln(Vr)$	-7.013500
	13	$Ns^3 \ln(SP)$	0.659568
	14	$Ns \ln(SP)^3$	-0.002947

Table 6.6 – Regressed coefficients for the evaluation of a single stage performance as a function of SP, Vr and Ns

The validation of the discretized method is performed by comparing the results on a specific test case: a typical three stage turbine for biomass combustion applications. It is important to note that, in the discretize approach, we are using a real fluid and the thermodynamic properties are calculated along the expansion while, using the optimized performance map, only inlet and isentropic outlet condition are known and hypothesis of ideal gas is considered. Small deviations between the two solutions are expected and the goal of this comparison is to understand if it is possible to use the single stage correlation to estimate the efficiency of a multistage turbine. The main assumptions and some global expansion data are reported in Table 6.7.

fluid	toluene	Thermodynamic properties from Refprop
p_{in}, bar	10.54	Corresponding to a T_{eva}=220°C
p_{out}, bar	0.12	Corresponding to a T_{cond}=50°C
T_{in},°C	230	Corresponding to a ΔT_{sh}=10°C
m, kg/s	17.858	Corresponding to a W_{is}=3MW_{mecc}
Δh_{is}, kJ/kg	167.99	
$V_{out\ is}$, m3/s	50.26	
Vr	80.65	
beta	85.77	

Table 6.7 - Expansion inlet and outlet conditions

The overall isentropic volume ratio involves the use of a three stage turbines according to the limit over mentioned.

For the global approach, first the single stage-equivalent parameters to be used in the efficiency correlation are calculated. They result equal to SP=0.3502 and Vr=80.65 corresponding to an efficiency of 86.79% calculated for the three stage turbine. For the discretized method instead, the expansion is divided in three stages, each one with the same Vr=4.32 calculated on the isentropic expansion from the inlet point. Efficiency of the first stage is calculated by using the correlation as function of SP, Vr and Ns previously calibrated in this section. The inlet conditions for the second stage are found and the procedure is repeated. The expansion in a T-s chart is reported in Figure 6.13.

Global overall efficiency is eventually calculated dividing the sum of the mechanical works in each stage by the isentropic enthalpy drop. The result is a function of the speed of revolution which affects the specific speeds of the single stages and their efficiencies. The optimal efficiency value to be compared with the efficiency calculated with the global method is the result of an optimization procedure varying the rotational speed. Optimal speed of revolution for the present case is around 100 Hz corresponding to 6000 RPM.

In Figure 6.14, the trends of some parameters of interest for different values of RPM are reported. It is possible to note that at 3000 RPM, and so with a direct coupling with the generator, values of Ns for every stage are far below the optimal value which is around 0.15. Increasing the rotational speed, the Ns of each stage gets higher leading to high stage efficiencies and to an increase of overall performances. At around 4500 RPM the specific speed of the third stage is in the range of maximum efficiency while for the other two stages an increase of RPM is still advantageous. For 6000 RPM the maximum overall efficiency is obtained, the first and second stage are not at the maximum attainable efficiency but, for the third stage, any further increase of speed of revolution is so detrimental to penalize the overall turbine performance.

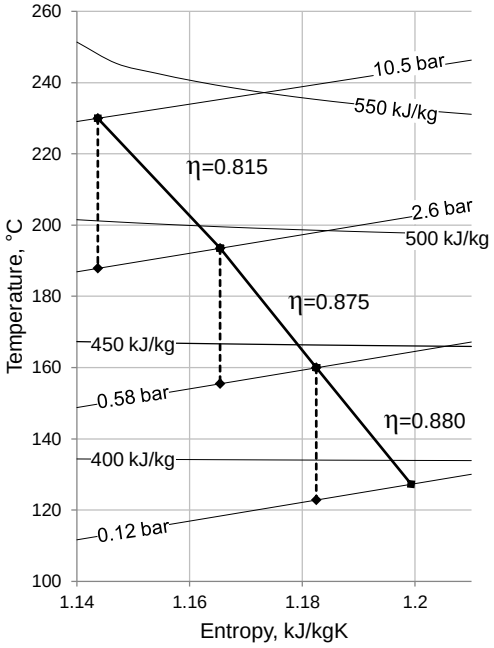

Figure 6.13 - T-s diagram of the three stages expansion calculated by a discretized approach at optimize velocity equal to 6000RPM

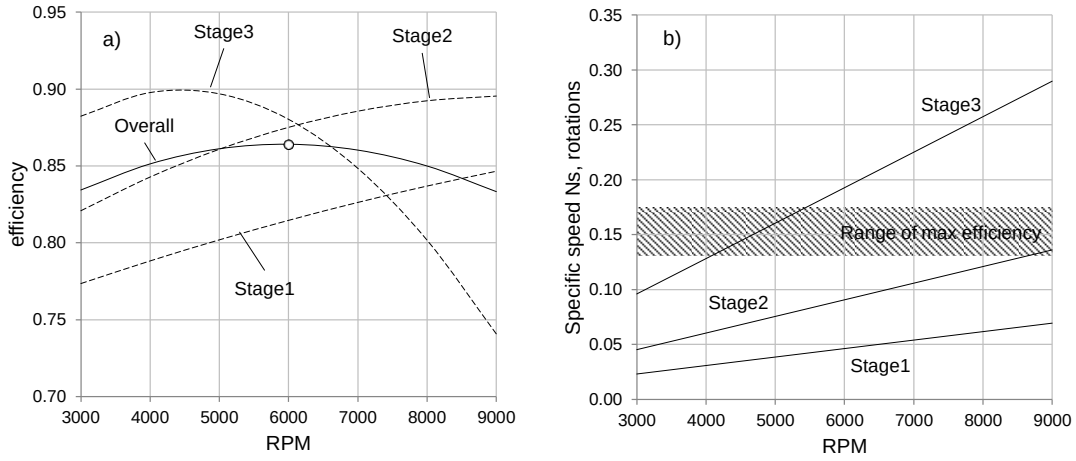

Figure 6.14 - Trends of stage efficiencies and overall turbine efficiency against rotational speed (a) and trends od specific velocities

Optimum efficiency is equal to 86.41 with a difference of less than 0.5 percentage point respect to the global approach confirming the validity of the discretized method which is implemented in the numerical code developed for this work.

6.1.6 Radial outflow turbines

A limited efficiency is achieved for high volume ratios turbines, especially for a small volumetric flow and small size parameter. The small blade height at first stage involves high secondary losses and it often requires partial admission stages. Moreover, the high change in volume flow rate results in relevant blade height variation and large flaring angles which introduce radial components of velocity with a consequent efficiency penalization. Finally, if the h/D ratio at the last stage is greater than 0.1, twisted blades are needed with the aim of optimizing the velocity triangles from blade hub to blade tip but leading to higher cost related to the more challenging design and manufacture of the machine. In order to solve these difficulties radial outflow turbines can be used. The basic idea is to expand the fluid in a series of radial stages, thus increasing the mean row diameter along the expansion. The scheme of a three stages radial outflow turbine is reported in Figure 6.15.

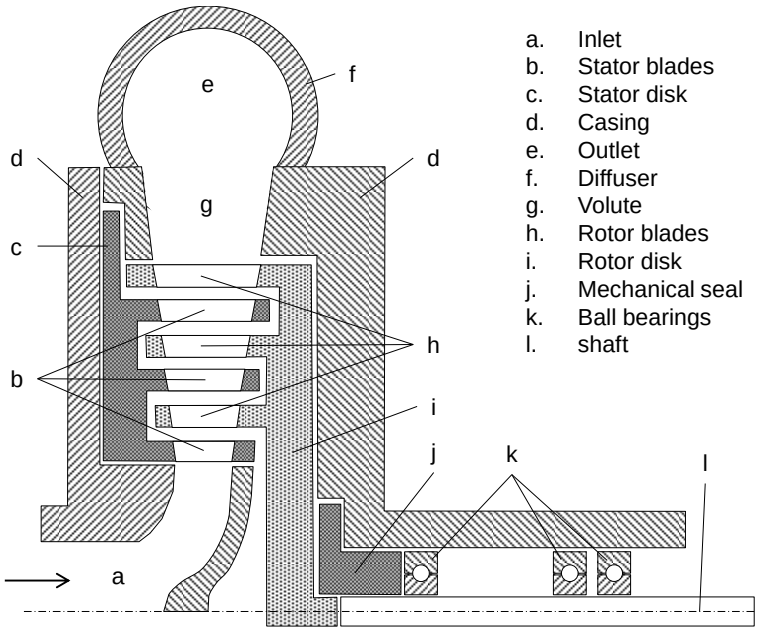

Figure 6.15 - Scheme of a three stages radial outflow turbine [4].

The radial outflow turbine is composed of casing, axial admission channel, impeller, radial diffuser and volute. All the mechanical parts are supported by the frame. The inlet vane is integrated in the casing and conveys the nozzles of the first stage. The geometry of the inlet channel is designed to avoid areas of fluid acceleration and deceleration, which would cause huge losses in the admission section. Thermal energy is transformed in mechanical energy through three rotor rows, mounted on a single disk, a peculiar

configuration typical of this radial outflow turbine. The rotor disk is coupled at one end of the shaft. The shaft, supported by rolling bearings, allows power transmission to the electric generator and supports the rotor disk. A mechanical seal, rigidly fixed to the shaft, is located between the bearings and the disk, to isolate the cycle from outside and thus to prevent organic vapor leakage or air infiltration. Rotor rows are alternated with nozzle rows, supported by a stator disk directly coupled to the casing; between those elements labyrinth seals limit leakages. At the discharge of the last rotor row the flow goes through a radial diffuser, to decrease its velocity and recover part of the kinetic energy still available at the discharge, that otherwise would be lost. Finally the flow is conveyed into the recuperator, through the volute.

This concept respect to a conventional axial turbine allows obtaining:

- A partial compensation of the volumetric flow increase, thanks to the increased section along the radius, meaning higher blades in the first stages and lower blades in the last stages with good h/D ratios all along the machine;
- Initial stages with better blade aspect ratio and no need for partial admission at the first stages, leading to efficiency improvements;
- Blade section is constant and prismatic, as the peripheral speed is constant on the entire passage section;
- Differently from the disk/diaphragm axial turbine, in a radial outflow turbine more than one rotor stage can be arranged on a single overhanging disk, giving some potential and factual advantages:
    - Better rotor dynamic thanks to the minor mass and to the reduced distance between bearings and barycentre
    - Smaller shaft section
    - Single coupling between disk and shaft
    - Simpler dynamic balance
    - Minor static and dynamic load on the bearings
    - Strain on shaft seal sizing is lower, leading to longer life of the component
    - Reduction of disk windage losses

The multistage radial outflow configuration is new in the ORC market, but the same concept has been applied to steam turbines since the late 19^{th} century by Parsons, on the first naval application of steam turbine, and later by Ljungstrom of STAL, who developed the counter rotating radial outflow steam turbine for electric power generation. In ORC field this turbine configuration was first proposed by Macchi [7] and it has been lately studied in some scientific publications [133; 134]. Nowadays, radial outflow turbines are the core business of Exergy [49] an Italian engineering company in ORC field. Exergy

proposes this concept for different applications and sizes declaring an increase of efficiency of 3-4 percentage points compared to axial flow turbines working between the same conditions. Some studies have been carried out by Exergy and Gecos group of Energy Department of Politecnico di Milano oriented to the validation of the proposed design and the efficiency increment respect to axial flow turbines.

Case study

The reference case is the $1MW_{el}$ power plant commercialized by Exergy and based on a supercritical recuperative cycle using perfluoro-2-methilpentane [5] characterized by:

- Critical Pressure p_{crit} = 19.23 bar
- Critical Temperature T_{crit}=182.15 °C
- Molar Mass MM = 338 kg/kmol

The optimization procedure described in section 6.1.1 is applied to two turbines working between the same conditions and designed in axial and radial configuration respectively. Working fluid is not implemented in Refprop database and so a dedicated file was calibrated trough the principle of corresponding states and subsequently validated with experimental data [135].

Objective function is the adjusted total-static turbine efficiency obtained considering a recovery rate of the kinetic energy of the discharge velocity axial component different for the two turbines. Φ_E is assumed to be 0.5 for axial configuration and 0.8 for the radial turbine where a greater kinetic recovery rate can be obtained with a high efficiency vane diffuser. In Table 6.8, the main assumptions common to both turbine configurations are reported.

Mass flow rate	33 kg/s
Inlet temperature	557.8 K
β	29.31
Stages number	3
Rpm	3000
Max num. blades	60(stator) 110(rotor)
Max rotor mach	1.2 (inlet) 1.4 (outlet)
Axial chord	0.01(min) 0.08 (max)
Gauge	0.003 (min) 0.02 (max)
Max flaring	30°
h/D max	0.1
Trailing edge min	0.0005
Blade wall roughness	$2\ 10^{-6}$

Table 6.8 - Assumptions valid for both radial and axial turbines for the present case study

Main results for each stage are reported in Table 6.9 for both configurations. First, it is possible to notice that the two turbines differ in enthalpy drop repartition among stages: axial turbine shows an almost homogeneous allocation with a small increase going towards the end of the machine. On the contrary, for the radial turbine, the enthalpy drop exploited by each stage strongly increases along expansion reaching in the last stage a value more than twice of the first stage without a penalization of stage efficiency. It is important to underline that in radial configuration an increase of enthalpy difference does not directly entails a high load of the last stages because of the concurrent growth of peripheral speed. In fact, optimized stage load coefficients are almost equal in both configurations with values between 3 and 3.5 representative of the possibility to obtained well design and high efficiency stages.

	$\Delta h_{is}/\Delta h_{is,TOT}$, %		η_{stage}, %		$\Delta\eta_{stage}$	k_{is}		degree of reaction	
	Rad.	Ax.	Rad.	Ax.	Rad-Ax	Rad.	Ax.	Rad.	Ax.
St 1	20.7	31.3	82.0	79.5	+2.5	3.504	3.017	0.012	0.027
St 2	31.4	33.3	85.4	85.6	-0.1	3.483	3.203	0.050	0.037
St 3	47.9	35.4	88.9	84.8	+3.9	3.387	3.268	0.260	0.377

Table 6.9 – Comparison between the optimized axial and the optimized radial turbine

In Figure 6.16 is reported a comparison between the meridional planes and the triangles of velocity for the two optimized geometries. Both configurations show a well-shaped meridional plane with a smooth increase of blade height; however it is possible to notice that the triangles of velocity are more distorted for the axial configuration where an higher value of axial discharge velocity component entails an increase of kinetic energy losses.

Finally, is possible to observe that radial configuration shows higher stage efficiency and this can be justified investigating the contribution of the different efficiency losses. In Figure 6.17 a staked bar diagram shows a comparison between axial and radial configurations, the total stage efficiency loss is divided in six different contributions.

It is possible to note that stage efficiency is higher for radial turbine in first and last stages while it is slightly lower in the second stage due to a larger value of secondary losses. Main differences are related to disk windage losses which are present in axial configuration for all the three stages and for radial turbine only on one side of the last stage and to kinetic losses that are strongly reduced in radial configuration thanks to the higher diffuser efficiency and the small axial component of discharge velocity. In

conclusion overall efficiency as define before is 84.12% for axial configuration and 88.01% for radial turbine with an increase of almost 4 per cent points.

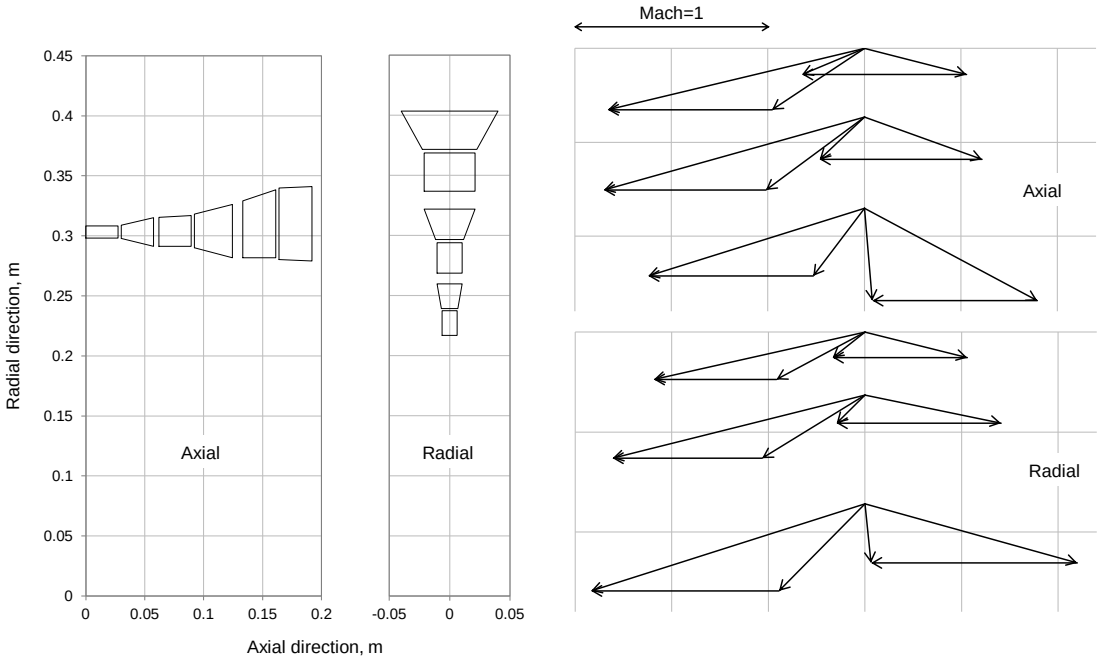

Figure 6.16 - Comparison between meridional plane (a) and velocity triangles (b) of the axial and radial turbine

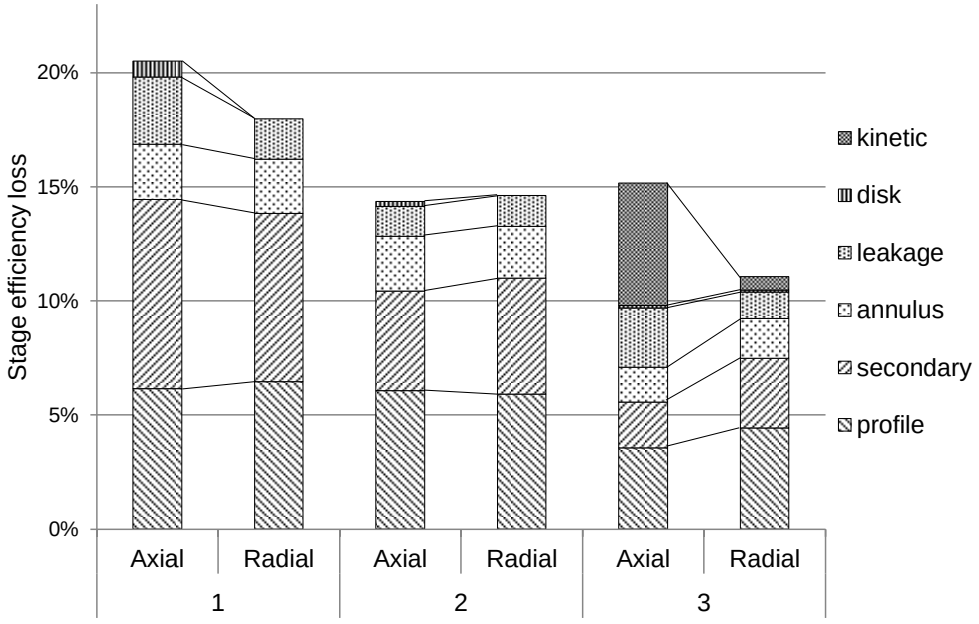

Figure 6.17 - Breakup of stage efficiency losses.

6.1.7 Micro axial flow turbines

The map of efficiency and the correlation presented in Section 6.1.3 (Results for single stage turbines) are not totally valid for micro size axial flow turbines. As already stated in Section 3.2 (Applications), there are several field of application characterized by a really small amount of available thermal power like WHR from ICE, small solar power plants and civil and domestic CHP units. In these cases, even using high critical temperature fluids with the aim of increasing the volume flow rate at turbine discharge, extremely small turbines are obtained with SP below 0.02. In this range of application, volumetric expanders might be more efficient than axial flow turbines and usually a scroll or a screw expander is used in ORCs with a power output below 100 kW_{el}.

The previous map is extended down to SP=0.0065 and the whole range in Vr, namely from 1.2 to 200, is explored: the results are reported in Figure 6.18 where the shaded area represents the field of investigation. First it is possible to notice that even an incompressible flow turbine with a really small diameter is strongly affected for SP lower than 0.02 with performances which are reduced appreciably to values lower than 60%. This is due to very low blades height and the activation of absolute limits referred to the minimum trailing edge, the minimum radial clearance and the minimum throat which lead to higher secondary, leakage and profile losses. Increasing the Vr all these effects are more marked and the performances are immediately penalized. Efficiency drops rapidly and, for Vr larger than six, it is not possible to design an expander with en efficiency greater than 50%. The trend of optimal specific speed described in previous sections is still valid and reducing the SP or increasing the Vr results in a decrement of optimal Ns. However, the presented results at optimized rotational speed are characterized by an extremely high rotational speed which entails the use of magnetic bearing, a fast generator and a power electronic system instead of a gear box solution. The analysis is not extended to multi-stage turbines because the additional cost for the design of the additional stages is not justify because of the small power output of these applications.

A comparison between single stage mini-axial flow turbines and screw volumetric expanders is proposed in section 6.3 (Comparison between axial turbines and screw expanders).

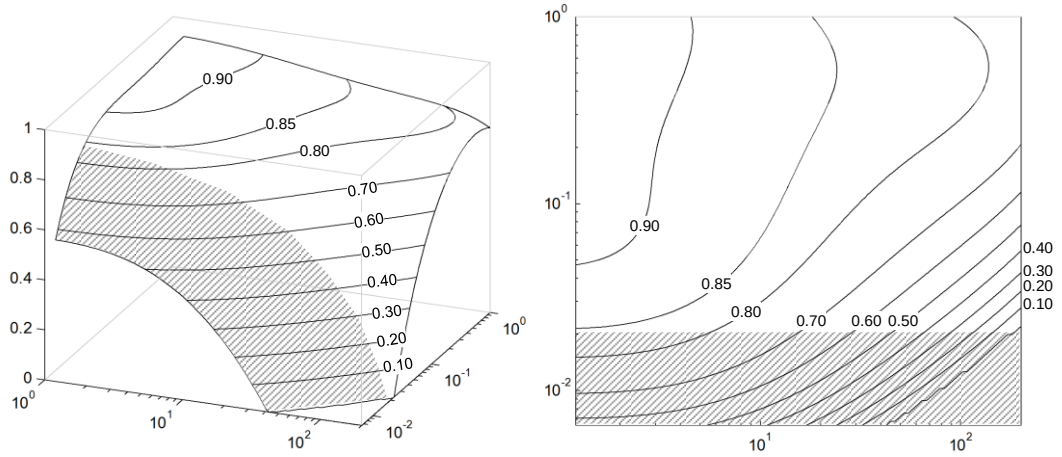

Figure 6.18 - 3D map of efficiency for axial-flow single stage turbines at optimize rotational speed. The grey area represents the solutions with SP between 0.0065 and 0.02. The anomalous trend of efficiency which can be notice at high Vr and high SP is simply numerical and due to the effect of the interpolation of the contour map, it does not affect the discussion neither on the results.

In Table 6.10 the coefficients of the regressed function are reported, the adjusted R^2 is higher than 0.995 with a maximum error around one percent point of efficiency for few solution at high Vr and very small SP.

	n	F_i	A_i
	0	const	0.930757
$f(SP)$	1	$\ln(SP)^2$	-0.02126
	2	$\ln(SP)^3$	-0.01308
	3	$\ln(SP)^4$	-0.00232
$f(Vr)$	4	Vr	-0.00219
	5	$\ln(Vr)^2$	-0.01066
	6	$\ln(Vr)^4$	0.000691
Cross terms	7	$\ln(Vr)^2 \ln(SP)$	-0.0032
	8	$\ln(Vr)^3 \ln(SP)^2$	-0.00042
	9	$\ln(Vr)^2 \ln(SP)^3$	7.72E-05

Table 6.10 - Coefficients for the correlation of optimize rotational speed efficiency for single stage axial flow turbines extended to micro applications

6.2 Positive displacement expanders

Axial turbines are likely not the more appropriate technology for small power input applications like domestic cogeneration, small solar thermal power plants in rural context and waste heat recovery in automotive sector. As highlighted in the previous section, a limited efficiency is achieved for very small size turbines due to high secondary and leakage losses. For power outputs below 100 kW_{el} positive displacement expanders are usually suggested because they might show overall performance higher than axial flow turbines. Unfortunately, volumetric expanders are not a technology widely available on the market nowadays; volumetric devices are used mainly as compressors for refrigeration and air conditioning cycles or for industrial processes and most of the references are related to this operation mode. However, as will be explained later, volumetric compressors can be operated in a reverse mode as expanders with little changes in device architecture and with limited efficiency reductions[9]. The scientific production about the topic is impressive and, in the last decades, thousands of papers and patents have been published investigating different technologies and applications, defining experimental procedures for the estimation of volumetric and machine performances and proposing numerical models to describe these devices. Despite the huge amount of studies on the topic, the level of detail of deterministic models proposed so far cannot be considered exhaustive. Most of them are semi-empirical models, they are calibrated on a single machine and the resulting information, even if useful to characterize the operation of these devices, cannot be directly extended to other similar machines. In the next sections, a bibliographic review on the topic will be presented with a focus on screw and scroll devices pointing out the attention on the limits of the scientific production and the information which would be required with the aim of making a complete description of positive displacement devices. Most interesting architectures will be discussed underlining their main features, their limits and suggested field of operation. Finally, starting from producer company catalogues, a correlation of efficiency as function of outlet isentropic volume flow and overall volume ratio is proposed for screw expanders. The correlation can be used to roughly estimate the performance of commercial compressors operated in reverse mode as expander but as explained in

[9] In next sections, no distinction is always made between volumetric compressors and expanders. If not stated otherwise the use of words like “machine” or “device” is referred to a general component without a different treatise based on the operation mode. The working principles, the main features and the efficiency loss phenomena are similar and, in most of the cases, the same considerations can be done for both compressors and expanders.

section 6.2.7 it cannot be considered as a map of maximum performances attainable with optimized volumetric expanders.

6.2.1 Working principle and index definition

Beneath the definition of positive displacement devices, many different designs and architectures are available on the market: scroll, screw and piston machines are the most common. Despite these differences, operation of volumetric machines can be divided in a limited number of stages that are communal to all of them and the same performance index can be defined. The different ideal stages are here referred to a device working in expansion mode [136] and they are represented in the P-V diagram in Figure 6.19. In the same figure even the compressor operation mode is reported.

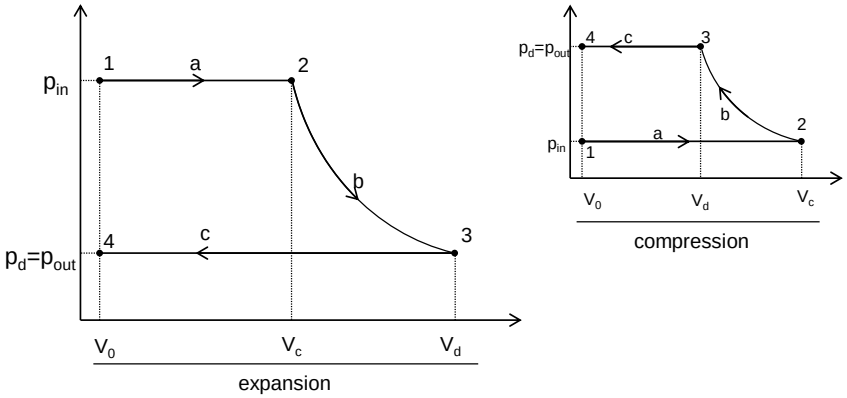

Figure 6.19 - P-V diagram of a generic volumetric device working in expansion mode (a) and in compression mode (b)

a. *Intake* (1-2): in this stage the fluid enters the machine through a valve or an admission port, filling the available internal volume V_0 which is the death volume of the machine. For some devices, like screw or scroll, the value of death volume tents to zero while for other ones, like reciprocating devices it is a finite volume represented by the minimum distance between the piston and the cylinder upper surface. Depending on the device type, the size, the fluid properties and the operation conditions a pressure drop occurs during the admission process entailing a reduction of filling efficiency ε_V[10]. Furthermore, volumetric efficiency is

[10] Volumetric efficiency (ε_v) is defined as the ratio between the actual swept volume and the theoretical one. It is affected by pressure drops, leakages, heat transfers with chamber walls and presence of death volumes. Generally the value of volumetric efficiency drops for low speed of revolution because of the increase of leakage losses and for high volume flow rate due to higher pressure drops in both intake and discharge ports.

affected by the heat transfer between the chamber walls and the working fluid. For compressors an increase of temperature and so a larger specific volume results in a smaller charge compare to the available swept volume. For expanders usually a cooling process occurs reducing the real enthalpy drop available. Volume during charging is progressively increased at constant pressure until the admission port is open;

b. *Displacement and Expansion* (2-3). When the admission port is closed by valves operation or because excluded by device rotation, the volume of fluid is trapped in. According to the geometry of the machine, the expansion chamber is displaced toward the exit port and its volume is gradually increased. In this phase efficiency losses are mainly due to leakages from one volume pocket to the next ones which reduce the volume of fluid actually interested by the expansion process;
c. *Discharging* (3-4). The expanded fluid is pushed out of the device trough a discharge port. A pressure drop occurs limiting the actual expansion and the work production. The chamber volume in this phase is reduced at constant pressure.

In compression mode, the operation is reversed but the meaning and the peculiarities of the different stages remain the same.

Differently from turbo compressors, and axial or radial flow turbines, positive displacement devices cannot be considered adiabatic machines: during the over mentioned processes heat is released to the environment and so the actual power extracted from an expander, or required in input to a compressor, has to account for these heat losses. In most of the publications, this aspect is not considered and an adiabatic or isentropic efficiency is usually presented as the ratio of the actual power output and the isentropic enthalpy head. This definition is correct only if the heat released to the environment is negligible: an assumption rarely valid even for well insulated volumetric devices due to the small mass flow rates. The general definition of efficiency for a volumetric expander, is reported in eq. 6.10 [137]

$$\eta_{exp} = \frac{h_{in} - h_{out}}{h_{in} - h_{out,is}} - \frac{Q_{amb}}{m\left(h_{in} - h_{out,is}\right)} \qquad \text{eq. 6.10}$$

However, the estimation of the Q_{amb} term is challenging if measurements of outlet temperature are not available and it requires the definition of a characteristic UA parameter of the heat transfer process between the device and the environment which presents a high uncertainty. For this reason usually in publications an approximate

definition of isentropic efficiency is used as reported in eq. 6.11, which is representative of the overall device performance in nominal condition.

$$\eta_{exp} = \frac{W_{shaft}}{h_{in} - h_{out,is}} \qquad \text{eq. 6.11}$$

The three stages of operation presented are valid for any volumetric expander working in nominal conditions, namely if the external volume ratio imposed by the cycle (π_e) matches exactly the internal volume ratio (π_i) of the machine which is defined knowing the built in volume ratio (π_{bi})[11] and the effects of pressure drops, leakages and heat transfer contribution. However, during operation it is usual that working conditions differ appreciably from the nominal ones. Off design operation of volumetric devices is critical and generally it entails a penalization of performances greater than for axial and radial turbines. For volumetric expanders, the imposition of an external volume ratio (π_e) different from the internal volume ratio (π_i) always leads to a strong efficiency loss due to over or under expansions which are represented in Figure 6.20 in P-V diagrams with reference to the nominal one reported in Figure 6.19. Off-design conditions for expanders are obtained with a variation of lower pressure while the inlet one is maintained constant. The same off-design losses referred to a compressor are reported in figure as well.

pc. *Over expansion or post compression*: it occurs when the internal expansion ratio is too high and the fluid is over expanded when the discharge port opens. The fluid in the collector enters into the device pressurizing the fluid already in the chamber. An additional work is required to push the fluid out of the device thus reducing the power production.

pe. *Under expansion or post expansion*: it occurs when the internal volume ratio of the device, is lower than the external one defined by the cycle evaporation pressure and condensation pressure. Fluid pressure at device outlet is higher than the pressure in the discharge collector and working fluid is throttled. The available enthalpy drop is not completely exploited with an associated power loss represented by the pattern filled area in Figure 6.20.b.

A number of studies are available in literature about the off-design performances of volumetric expanders [138; 139; 140; 141; 82] with the aim of numerical evaluating the

[11] For expanders the built in volume ratio (π_{bi}) is defined by the ratio between the geometrical volume at the end of intake process and the volume at the beginning of discharge process.

effect of these two losses. The trend of efficiency drop is steeper for over expansion than for under expansion.

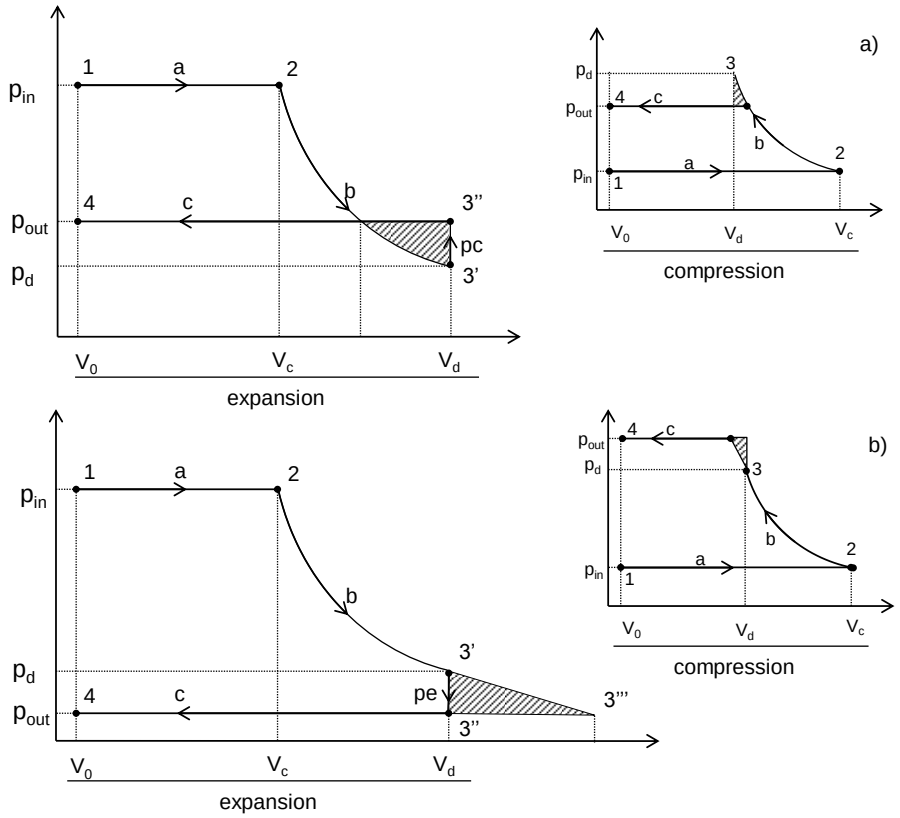

Figure 6.20 - P-V diagram for a volumetric expander in off-design conditions. Over expansion and under expansion are represented in figure (a) and (b) respectively for the expander while over compression process and under compression are represented for the compressor. In all the cases the shaded area is representative of the work loss in off design.

6.2.2 General classification

Volumetric devices are intensively studied by different universities and companies because of their large use as compressors in many different fields. In particular, two research groups lead the scientific community in this field, namely the Thermodynamic Laboratory at Liege University and the Positive Displacement Compressor Group at the City London University which are devoted to the study of these components and their work is focused on the numerical modelling and experimental activities on scroll and screw devices respectively. Most of their studies are presented at the International Compressor Engineering Conference which is hosted by Purdue University which is definitely the most prominent conference about this topic and in its proceedings all the aspect of the design and the operation of positive displacement devices are deeply analysed. However, almost the totality of the patents about scroll and screw devices are owned by companies, like Atlas Copco [142], Bitzer [143], Frascold [144] , Chicago

Pneumatic [145], Sabre [146], Man [147] and many others, which usually are not willing to convey information about the geometrical dimensions and the efficiencies of their devices. Technical catalogues, provided by these companies, are often inaccurate and rarely it is possible to retrieve consistent information about performance parameters. Despite the lack of official data from the producer, several techniques for the estimation of overall machine performances are proposed in literature and they have been applied with success to different architectures and devices configurations. It is important to underling that results obtained for a class of devices or a single model cannot be directly extended to other machines because of the different characteristic field of operation, the different volume ratios and the different maximum swept volumes of any single device configuration already available on the market. In particular, three devices architectures are the most interesting ones to be used as expanders in a ORC systems [148]:

- *Screw*: different type of screw devices are offered on the market: they are widely used as compressor in refrigeration field and as air compressors for industrial applications since, for small swept volumes, they are competitive with small centrifugal compressors. Twin screw expanders are mostly derived by commercial compressors, and they are the suggested technology for applications with a power output in the range between 3 kW_{el} and 1 MW_{el} [148] and so for small-medium size ORC. In this range screw expanders can usually handle volume ratios around 5 with good volumetric and adiabatic efficiency even if in literature and in commercial applications values greater than 7 are reported. A feature characteristic of screw devices is the possibility to vary the volume ratio in off-design acting on a slide valve and varying the dimension of the discharge port.
- *Scroll*: scroll expanders are obtained by compressors operated in reverse mode even if lately some studies focused on the design of a specific scroll expander have been presented showing a relevant increase of maximum attainable efficiency [149]. Scroll expanders can be used in micro-small ORC for remote power production or civil co-generation. Due to the necessity to limit both the diameter and the number of coils, scroll expanders are limited to swept volumes lower than 50 l/s and maximum volume ratios around 3.5. Efficiency is slightly lower respect to screw devices because of the higher impact of leakage losses and friction losses which are minimized in screw expanders since both surfaces are in motion and rolling contact is usually ensured.
- *Piston*. They are derived by reciprocating engines and they can provide volume ratios up to 14: a value that is notably higher than scroll and screw devices making the piston expanders interesting for ORC applications where usually relevant volume ratios are required. However, they are rarely used since their operation is

affected by high friction losses which lead to limited performances even if these devices are leakage-free. In addition, the valves timing is intrinsically more complicated than for other volumetric devices: in scroll and screw expanders the opening and the exclusion of the intake and discharge port is automatically defined by the device rotation while in piston expanders this is not possible and a totally new design of the valves is required in order to guarantee a correct timing with the piston motion. Swept volumes are comparable to scroll devices but differently from the other two architectures they cannot handle two phase flow fluids. A positive feature of reciprocating expanders consists in the possibility to work at very high temperatures, namely up to 400°C [148; 150], without relevant problems of thermal expansion, since are derived by endothermic engines. For both scroll and screw devices, this is not possible and maximum temperatures are nowadays around 145-150°C limiting the use of these components to medium low temperature applications. However, there is a strong interest in passing this limit because of the increasing market of high temperature heat pumps which requires volumetric devices able to work at higher temperatures [151].

In Table 6.11 a summary of the main characteristics and limits for screw, scroll and piston expanders is presented.

	screw	scroll	piston
Power output, kW	3 - 1000 [148]	5.6 - 45 [148]	
Swept volume, l/s	25-1100 [148; 152] 10-10000 [151]	1.1 - 49 [152]	1.25-75 [148]
Volume ratio	2-5 [148] -8 [153] 3.5-15(oil f.) [151] <5 [152]	1.5-4 [148] <4 [152]	6-14 [148]
Adiabatic efficiency	>80 [138]	60-70% [154]	60-80% [155]
Volumetric efficiency	>90% [151]	>90%	>90%
Maximum pressure ratio	<15 [151]	<10	<15
Maximum temperature	145-150 [148] 150-250 [138]	145-150 [148] 215 [156]	Up to 400 [148; 150]
valves	Ports Slide valve	ports	Poppet, sliding, rolling (inlet), poppet, port (outlet)

Table 6.11 - Summary of main characteristics and limits for three volumetric expander architectures

Scroll and screw devices seem to be the most reliable solutions for ORC applications and a more detailed description is provided in the next sections.

6.2.3 Screw devices

In the last four decades, the performance of screw compressor devices has been constantly increased thanks to the efforts of numerous company, university labs and single scientists who have given their own contribution to improve the design and the efficiency of this component. Since Lysholm A. proposed the first symmetric lobe profile for screw compressors in the beginning of the last century, huge steps have been made with the help of detailed models and optimization codes, bridging the efficiency gap between this devices and centrifugal compressors. In the last forty years, thousands of papers and patents have been submitted proposing new designs [157; 158], new numerical simulation models [159], new optimization techniques [160; 161] and new field of application as for example their use as expanders in the ORC field. Nowadays on the market there are only two companies which propose screw expanders for energy recovery from high pressure steam or ORC for small biomass and small WHR applications. These companies are Heliex Power [162] and Electra-Therm [50] but their market share is still small respect to other competitors and no data about the design and the performances of these components are public. On the other side, a research project called ORCNext [163] has been recently launched and it is focused on the study and the optimization of screw expanders for ORC field and the first deliverables will be available soon. In conclusion, up to now, only few scientific publications provide numerical data which allow estimating screw expanders performances. In particular, all the works presented so far investigate the possible use of a screw compressor as expanders and there are no publications where a full optimization of a screw expanders is performed starting from the design of lobe profiles to the computation of the performances with dynamic models or sophisticated 3D simulations. All this steps are commonly followed in the optimization of compressors but the market of screw expanders is not big enough to justify the design of new components, and all the results achieved in this field are protected by companies secrecy policy. The use of optimized devices certainly allows reaching higher efficiency thanks to the reduction of all the losses related to leakage and friction which can be minimized by means of the optimization of the lobe profiles and the shape of both intake and discharge ports. However, it is interesting to underline that different publications have demonstrated that good efficiency can be achieved even using compressors in reverse mode, with minimal changes on device architecture and a reduction of nominal efficiency, which can be accounted in few percentage points respect to the nominal performance computed for the compressor operation [138; 136; 141; 164].

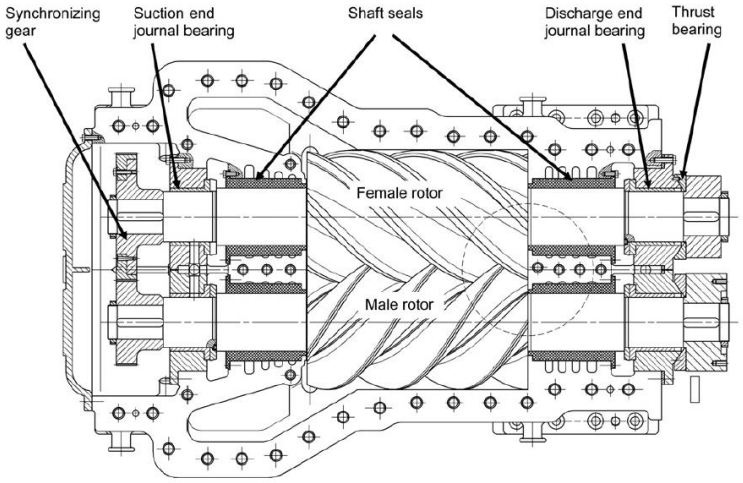

Figure 6.21 – Schematic view of a twin screw device [165]

Screw devices are formed by a pair of meshing helical rotors, surrounded by a casing as reported in Figure 6.21. The spaces between the male and the female lobes profiles and the casing, form a series of working chambers whose volume varies during device rotation. In expansion mode, fluid enters the device from the intake port filling the available space between the two rotors in the high pressure side of the device. Helical rotors are in rotation and for a certain angle of rotation the inlet port is excluded defining the inlet volume of the machine. The fluid is free to expand in a chamber delimited by the rotors and the casing, and the volume is increased moving toward the opposite extremity. On the opposite side of the screw expander a discharge port is realized to expel the expanded fluid from the machine. Power is transferred between the fluid and the rotor shafts from torque created by forces on the rotor surfaces due to the pressure, which changes along the expansion process. The overall performance of a screw expander is affected by a number of different parameters and phenomena which act together in determining the leakage losses, the friction losses, the pressure drops and eventually both the isentropic and the volumetric efficiency.

In particular, the definition of the geometry of the rotors in both radial and axial directions strongly affects the performances of a screw device: the rotor lobe profiles should be optimized taking into account the effects on the sealing line length and forces at contact point between lobes which determine leakage losses and friction losses respectively. In literature several different lobe profiles are proposed each one with different features and peculiarities. In Figure 6.22 a graphical summary of the most popular lobe profiles is proposed: the first one is the symmetrical Lysholm profile while the other ones are further improvements obtained with non-symmetrical lobes patented by SRM [166].

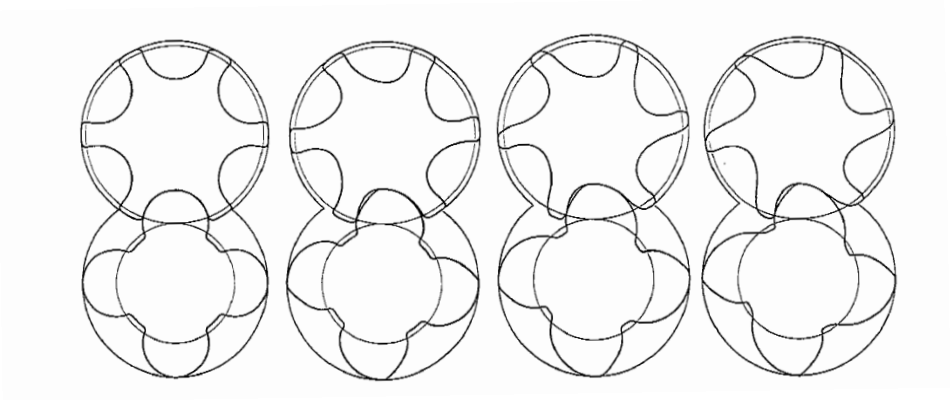

Figure 6.22 – Graphical evolution of screw rotor profiles from symmetrical Lysholm profile to modern asymmetric SRM profiles [167]

The optimization of lobe profiles design is a challenging task and dedicated tools are required in order to reach a reliable solution which is able maximize the volume flow rate while minimizing the blow hole area and limiting both the extension of the sealing line and the forces between male and female rotors [151]. The blow hole area is the small triangular area between the cusp of the casing and the two rotors and it is a leakage path where the compressed fluid can flow and expand without contributing to power production, its geometrical definition and its evolution during device operation is discussed in many papers [168; 169; 170]. The reduction of blow hole area is usually obtained by means of an increase of the length of the sealing line thus increasing the leakages through this path and the friction losses. The optimal design results from a tradeoff between these two effects and it can be faced only with optimization tools [168; 171]. Other parameters, which has to be taken into account, are the number of lobes in both male and female rotors: increasing their number allows reducing the pressure difference between two adjacent working chambers thus limiting the specific leakages above the sealing line but, on the other hand, the adoption of a high number of lobes entails a larger and slower rotor with a longer sealing line and overall increase of leakage losses. In addition adopting more lobes gives the possibility to design larger admission ports thus minimizing the pressure drops in the intake process and reducing vibration thanks to a longer contact line between the two rotors [151]. A 4-6 male female lobes configuration is traditionally adopted even if for some application high efficiency profile are proposed with 5-6 or 6-7 configurations. Finally the minimization of relative motion of rotor surfaces is crucial in order to minimize friction losses. All these aspects, plus many other effects related to wrap angle, thermal expansion and shape and positioning of the intake and the discharge ports should be considered during screw design and optimization. Many different approaches are proposed in literature for the definition of

lobes profile functions and they are mainly based on theory of gearing applied to helical gears with parallel axes [172; 173]. The most advanced lobe profiles are nowadays realized applying the envelope theorem which allows design rotors with always one point of contact during rotation and pure rolling relative motion thus limiting the friction losses [173; 174; 167]. Furthermore, it is possible, knowing the function of a rotors profile, to calculate the functional form of the conjugate segment on the other rotor with algebraic passages ensuring the perfect meshing of the male and female rotors. Lately, a rack approach has been proposed [173] which allows defining the male lobe profile on an infinite diameter pitch circle simply with a combination of linear segments and circular arches thus simplifying the machining process.

Once the rotor profile is defined, the evolution of the volume of fluid pockets has to be analytically expressed: different methodologies are suggested from the simply but relatively accurate trapezoidal rule [169], to rigorous calculation with tridimensional modeling software [159]. From these analysis, all the information required by a dynamic model are obtained, namely the function of volume pockets, the sealing line length, the blow hole area and the opening of the two ports as a function of the time or of the angle of rotation.

An interesting feature of screw expanders consists in the possibility to vary the built in volume ratio by acting on a slide valve. This is formed by a moving part of the casing which can slide axially modifying the shape of the discharge port. Differently from any other volumetric device the screw expanders are able to adapt the internal volume ratio in off-design thus strongly reducing the over and the under expansion losses. Higher pressure drops are accounted in these cases because of the larger volume flows or the smaller discharge area but considerable benefits are achieved. Some studies have been realized investigating this potentiality for screw expanders demonstrating the suitability of this solution [175; 176]. Last peculiarity of screw expanders is the possibility to handle two phase flow fluids thus allowing the expansion from saturated liquid condition and realizing an almost perfect triangular cycle. The presence of liquid in the machine has in theory a little effect on the operation and on the efficiency of these devices [177; 178; 179] but experimental data are still lacking even if in some publications an overall efficiency close to 80% has been achieved with large machines [180].

6.2.4 Scroll

The scroll machine is commonly used as a compressor in domestic or civil vapour compression cycles. It is made by two involute curves, namely the orbiting and fixed scrolls. The two scrolls are equal but they are not centred on the same axes: a small eccentricity is present for the rotating one in order to properly define separated volume pockets during rotation. For these devices the main leakage paths are represented by (i) the flank or radial leakage in the gaps between spirals walls and (ii) the tip or axial leakage between one spiral tip and the hub of other one as represented in Figure 6.23.

Scroll devices can be classified into two types: compliant and kinematically constrained. The movement of complaint scrolls is not controlled by mechanical constraints and the orbiting scroll is moved by the expanding fluid. Flank sealing is ensured by centrifugal forces which push the orbiting scrolls toward the fixed one. Lubrication for these devices is usually adopted in order to reduce friction between scrolls and to limit both flank and tip leakages. On the other hand constrained scrolls can be constrained radially, axially or both and so the movement of the orbiting scroll and the minimum distance between the two spirals during rotation are controlled.

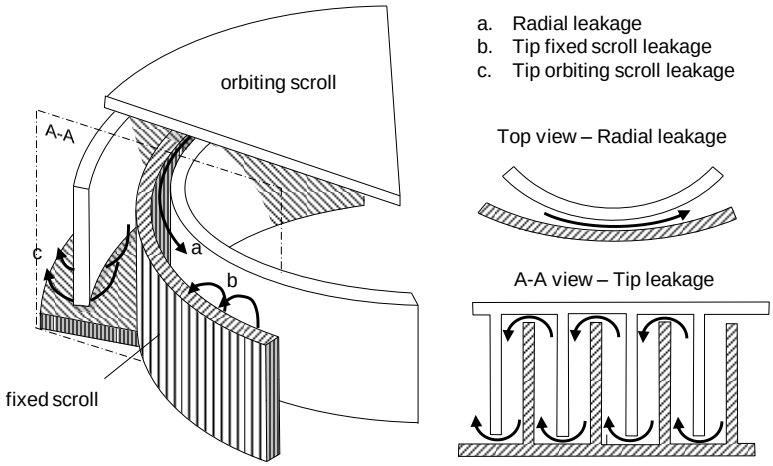

Figure 6.23 - Leakage paths in a scroll device.

Usually lubrication is not used and manufacturing tolerances and low friction materials are crucial in order to limit both flank leakage and friction losses. Diameter of scroll unit is directly related to the swept volume and so to the discharge volumetric flow and to the built in volume ratio which affect the number of coils. High diameters involve a heavy machine and tolerance issues during their manufacture. As result, the scroll expanders are suitable for small power output (namely below 5 kW_{el}) and for small volume ratios (max 3.5). Scroll expanders are not appropriate for high temperature applications or to expand

heavy and complex fluids but they are nowadays the only reliable technology for small solar power plants and civil co-generation. A schematic representation of the operation of a screw expander is reported in Figure 6.24.

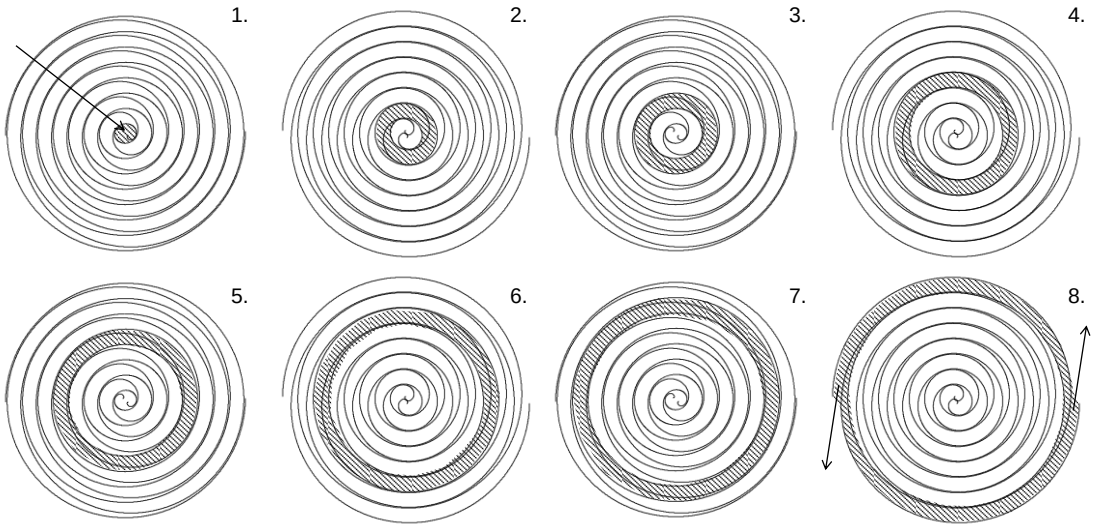

Figure 6.24 - Scroll expander functioning sequences: intake (1-2), expansion (3-7) and discharge (8).

Despite the relative high reliability of these components, most of the experimental scroll expanders studied so far are simply prototype derived from existing compressors and used in a reverse mode. This kind of experimental activities are presented in several papers [181; 141; 182; 183] and they have been demonstrated that scroll compressors can be efficiently used as expanders and higher efficiencies can be achieved only by designing a new machine [184] as expander as described in next section.

6.2.5 Models comparison

Different approaches for the modelling and the estimation of performances of volumetric devices are proposed in literature and they can be summarized in three categories depending on the level of detail considered [148]:

- *Empirical models* are based on simple equations whose coefficients have to be calibrated in order to properly describe the device performances. This approach is numerical robust and it entails a very small computational time but the results are representative of a single machine and they cannot be extended to other devices. The most common model is the Pacejka's equation which requires the calibration of two functions: one for the adiabatic efficiency and one for the volumetric efficiency as function of operational parameters like the volume ratio, the inlet

pressure and the rotational speed. Different studies are based on the use of Pacejka equation to describe the off-design operation and performances of scroll devices [137]: experimental data are required and the resulting model can be used for dynamic simulations using software based on black boxes and lumped components.

- *Semi-empirical models* are based on a set of equations able to catch the physical effects of the different phenomena occurring during a positive displacement device operation [185]. The equations represent all the basic stages of operation like the intake and discharge process, the heat transfer between the fluid and the machine or the environment, the leakage losses and the effect of over and under expansion. Each equation requires the knowledge of a set of parameters which are representative of a specific geometrical or thermodynamic quantity, and they have to be regressed on the available set of experimental data. In Figure 6.25 the scheme of the model used for the simulation of a scroll expander is reported [186]. Even this class of models, as the empirical ones, cannot be extended to other devices but can be used to perform reliable sensitivity analysis for some variable of interest and to understand the breakdown of the total efficiency loss in the different contributions.

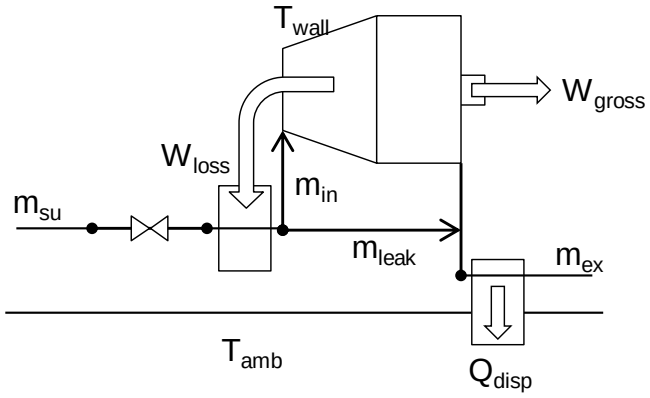

Figure 6.25 – Schematic view of the semi-deterministic model for volumetric expanders.

- *Deterministic models* are the most accurate ones but they require a relevant number of inputs, the exact knowledge of the device geometry, and a considerable computational power. Knowing the exact expander geometry it is possible to introduce in a dynamic model all the information regarding the evolution of working chamber volumes, the length of sealing lines and the relative motion of surfaces [187; 188]. These models, based on differential equations, implement mass and energy conservation and they use reliable equations of state functions

for the estimation of fluid thermodynamic properties. Furthermore, all the efficiency losses phenomena are described with rigorous models: for instance, the leakage flow rate is accounted by means of the calculation of the sonic flow expanding trough an orifice which requires the exact knowledge of the pressure difference and the leakage area between the two volume pockets. This approach is presented in various papers for the modelling of different devices: it is applied to both screw and scroll compressors and expanders [189; 190; 191] with very precise results.

An example of state of the art deterministic approach has been followed by STG international and University of Liege, which are involved in a project focused on the optimization of a scroll expander for rural thermal solar power applications. The goal of the project is to define the best scroll geometry for a high volume ratio ORC characterized by a non-constant wall thickness. The scroll geometry is mathematically described with the Gravesen and Henriksen model [192] which is based on circle involutes and can generate non-constant wall thickness scroll wrap. First, thousands of different scroll geometries have been investigated by acting on eight parameters which are varied in their range of validity. The best configurations are selected on the basis of a new figure of merit: the compactness factor which is defined as the ratio between the built in volume ratio and the normalized scroll diameter [149]. It is demonstrated that the adoption of this parameter, as objective function for the optimization process, allows selecting a limited number of promising geometries with a limited computational time. At a later stage, a detailed analysis has been performed on the optimal geometry resulted from the first investigation with a dynamic model integrated with the deterministic description of leakage and friction losses. A new optimization of the geometry is realized defining the exact wall thickness profile which allows maximizing the efficiency while respecting manufacturing constraints. The prototype of the scroll expander has been realized by Eng. Dickes in MIT labs during 2013 [184] and experimental activities are planned for 2014 when the deterministic numerical model used for the design will be validated on the actual experimental performances. The increase of efficiency, respect of the use of a scroll compressor in reverse mode, is estimated to be around 6 percentage points, 1.5 of them achieved with the optimization of the non-constant thickness wall while the rest by the exact matching of internal and external volume ratio.

This latter example well highlight the possibility in design a new optimal device for each application, but the computational power required by this approach is definitely too

onerous to be applied to a large number of devices with the numerical tools developed so far.

In conclusion, for volumetric devices various models are available for the estimation of nominal and off design performances with really good accuracy but the model results are specific to a single machine and they cannot be directly used to estimate the efficiency for a new device. Differently from axial-flow and radial inflow turbines, no similarity rules are defined in literature for volumetric compressors or expanders and no information about the efficiency loss coefficients related to geometrical ratios or specific parameters are available. The exact estimation of the performances of volumetric expanders can be realized only by complex codes which cannot be certainly introduced in a tool for ORC system optimization. In next section a simplified correlation as a function of external volume ratio and the isentropic volumetric flow is proposed for screw expanders in order to overcome the over mentioned limit.

6.2.6 Methodology for the definition screw expander efficiency

An efficiency map as function of some characteristic parameters is required with the aim of considering volumetric expanders in a numerical code for ORC optimization. The choice of independent parameters is not trivial and it requires the knowledge of the main phenomena affecting positive displacement devices. Performance maps of maximum attainable efficiencies are not available in literature for expanders but this fact is not surprising considering the relatively small market for these devices. However, this information is not available neither for volumetric compressors whose market is notably larger. The main reason of this fact is related to the secrecy policy of market leader companies: most of the volumetric devices details like scroll geometry, screw lobe profiles functions, built in volume ratios and obviously volumetric and overall efficiencies are protected by patents and it is hard to obtain this kind of information. Experimental activities could be carried out in order to acquire these data and the efficiency values but, to obtain a number of data sufficient to produce a performance map, the purchase and the test of various models is required with an increase of cost and time. For these reasons, as already mentioned, most of the studies are oriented to off-design performance definition for a given machine with the aim to calibrate models helpful for off-design and dynamic simulations. These models are limited to a single machine and they do not provide any information about the attainable efficiency of any another device with a larger size or a different volume ratio and, in conclusion, they are not directly usable to achieve the over mentioned goal.

From the literature review it is possible to deduce a series of nominal efficiency data for both scroll and screw machines (compressors and expanders). However in all the papers some information is missing and data are hard to organize. For instance, overall efficiency is usually plotted as function of the pressure ratio which is not a variable of interest with the aim of providing a general correlation. The efficiency loss due to the over or the under expansion is mainly related to volume ratio which can largely vary from fluid to fluid even if the same pressure ratio is imposed. Pressure ratio can be considered as independent variable only if the same fluid, or another one with the same complexity, is used in similar conditions. In most of the publication neither the working fluid nor the working conditions are clearly reported and it is not possible to calculate back the exact value of volume ratio corresponding to a certain pressure ratio. However, most of the working fluids commonly used with these devices are refrigerant fluids with isentropic exponent values varying in a relatively small rage and so a rough estimation of the external volume ratio it is always possible. In fact, the external volume ratio is a parameter of big interest not only to properly account off-design losses but mainly because it has a strong influence on nominal efficiency of volumetric devices. Machines with high nominal volume ratios generally show lower efficiencies because of higher friction losses (i.e. larger scroll diameters with a larger number of coils) and higher pressure drops at intake port (small areas) and at discharge port (high volume flow rates). On the other hand, pressure ratio affects leakage losses which can be correlated to volume ratio in order to consider them independent from the used working fluid. Finally, it is important to note that the nominal external volume or pressure ratio do not give any information on built in volume ratio of the machine which can be determined only by measurements or by calibration of deterministic or semi empirical models.

Another information rarely reported is the dimension of the machine or the swept volume or the volumetric flow rate at inlet or outlet port for a given rotational speed. This information is surely important in order to understand the effect of size on the maximum attainable efficiency. The increase of the size of a screw machine entails benefits because both friction and leakage losses specific to the volume flow rate gets lower with an increase of overall performances.

Other effects, like under and over expansions, are not taken into account for the moment because they are off-design effects. A volumetric expander should be selected to fit perfectly the external volume ratio imposed by the thermodynamic cycle at least in the nominal condition. Another parameter, which is not here considered, is the rotational speed because in optimal condition it should be as close as possible to the nominal one. Varying the rotational speed allows increasing or decreasing the volume flow rate but it has a detrimental effect for overall efficiency: a high speed involves an increase of

friction losses while, for a low rotational speed, leakage losses strongly limit both the volumetric and the overall efficiency.

In this section a focus on screw devices is proposed because they are recognized to be the most reliable option in a range of power output of big interest for ORC where, thanks to their performance, they can compete with micro axial-flow turbines.

In Figure 6.26 a summary of the available experimental data for screw compressors and expanders is reported as function of the built in volume ratio [193; 155; 164; 194; 136; 138], although no publication provides clearly all the information required: namely the nominal external volume ratio and the swept volume. As expected nominal efficiency decreases with the nominal volume ratio but is not possible to understand the effect of size on the device performances.

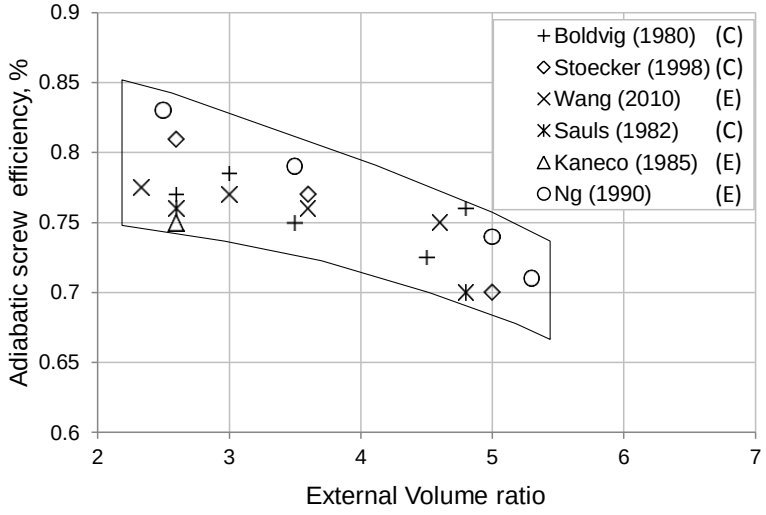

Figure 6.26 – Experimental screw efficiency for compressors and expanders against external volume ratio. In legend data labelled by (C) refers to screw compressors while data labelled with (E) to screw expansors

To bypass the previoulsy mentioned limit company catalogues could be examined extracting useful information about commercial compressors. Unfortunately, most of them don't contain real data; they do not report the needed information and many data series look suspiciously linear or proportional to independent variables. In more than one case efforts in retrieving machine efficiency from COP data have been resulted in meaningless values greater than unit and the main reason of that is related to a non-clear definition of the testing condition and because usually the size of the motor is reported instead of the actual power consumption. Fortunately European normative EN12900 implies that is mandatory to provide, for every compressor model, validated correlations for mass flow rate and power input at nominal velocity. The correlation is valid in the

range of the condensing and evaporating temperature defined by the technical limits. The functional form has ten coefficients as reported in eq. 6.12.

$$X_i = c_{1,i} + c_{2,i}T_e + c_{3,i}T_c + c_{4,i}{T_e}^2 + c_{5,i}T_eT_c + c_{6,i}{T_c}^2 + c_{7,i}{T_e}^3 + c_{8,i}T_c{T_e}^2 + c_{9,i}T_e{T_c}^2 + c_{10,i}{T_c}^3 \quad \text{eq. 6.12}$$

Where X_i is the calculated property, namely the absorbed power or the mass flow rate; T_e and T_c are the evaporation and condensation temperature respectively and $c_{j,i}$ are the correlation coefficients.

Among the European producers, Bitzer [143] provides complete information for a huge number of screw compressors models allowing to study the attainable performances for different machines working with different fluids. Knowing the compressor model, the swept volume, and the inlet condition it is possible to calculate the isentropic enthalpy head, the mass flow rate and eventually the overall device efficiency and the volumetric efficiency for each machine. Basically, from this analysis, maps of off-design at fixed RPM are obtained highlighting the effects of over and under compression and giving the possibility to define the point of optimum efficiency. The results referred to the open screw model OSK5341-K working with R22 are reported in Figure 6.27.

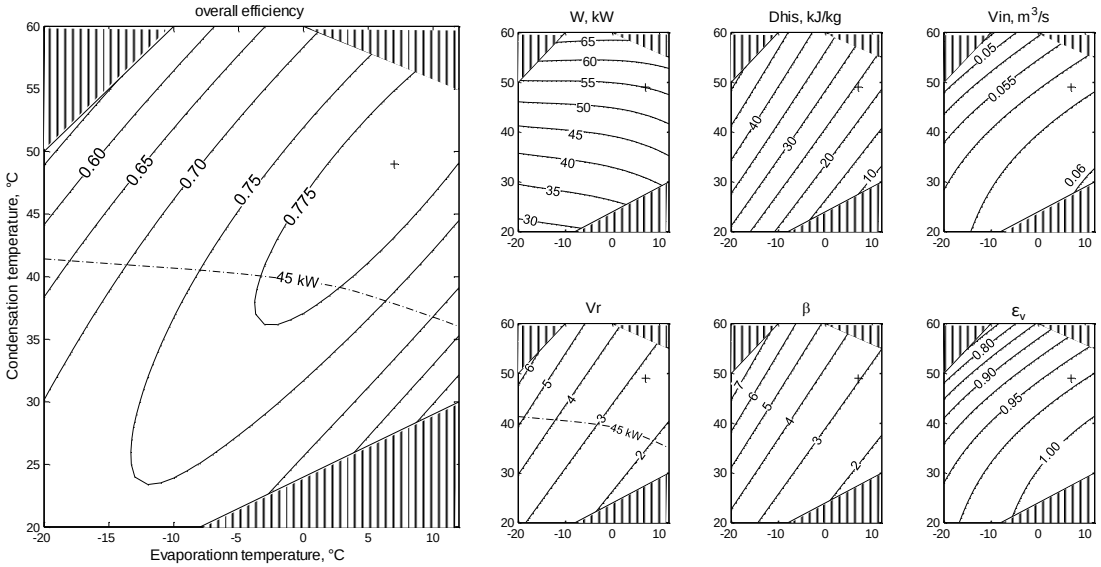

Figure 6.27 - Maps resulting from the correlation provided by the producer. The cross displayed in each plot represents the point of maximum overall efficiency. Dashed line is representative of operating points with the same power consumption.

A point of maximum overall efficiency, represented by a black cross marker, is found in correspondence of a certain combination of external volume ratio and inlet volumetric flow rate. The external volume ratio which maximizes the efficiency is close to the built in volume ratio and gives useful information on the possible application field of the selected compressor. Efficiency decreases for both higher and lower external volume ratios due to the under and the over compression processes. A trend of efficiency as function of external volume ratio for a fixed power of 45 ±0.5 kW is reported in Figure 6.28. The effect of over compression penalizes the efficiency more than the under compression resulting in a different shape of the efficiency curve.

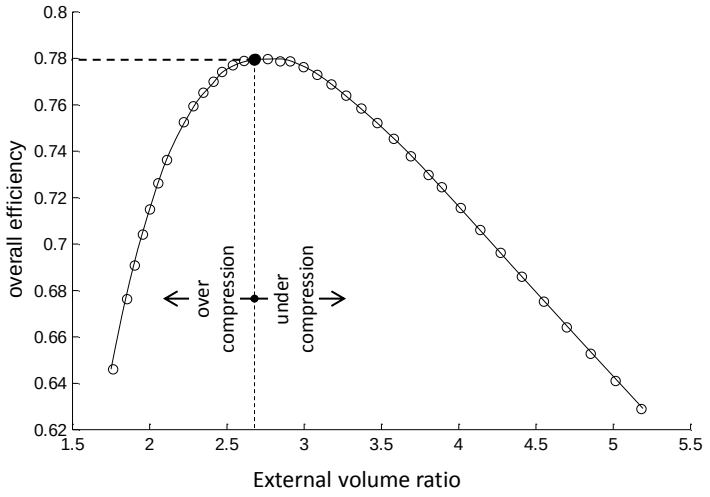

Figure 6.28 - Effects of over compression and under compression for a screw compressor working with a fixed rotational speed and the same power output.

The over mentioned procedure is applied to 100 open screw compressors working in different conditions and with six different fluids. The investigating models cover a large range in evaporation and condensation temperatures. Data of overall efficiency as function of external volume ratios and volumetric flow rate are collected but unfortunately results are not really regular and efficiency differences are noticed even among models with similar Vr and V_{in}. However, this is not completely unexpected because for this analysis data from real machines are used, accuracy of correlation is not declared and it is unknown the precision of instrumentation used for the experimental tests. For instance, a variation of inlet vapour superheating of ±2.5°C involves change in the estimated efficiency around ±1.04%, while errors on the function of mass flow rate and power input directly affect the final result.

A regression of the collected overall efficiency data as function of Vr and V_{in} is carried out in Gretl [131] and the result is displayed in Figure 6.29 together with the values calculated from producer data represented by cross markers. As expected the overall efficiency decreases for high volume ratios while benefits are obtained with bigger machines and higher swept volumes. Furthermore, the range on efficiency obtained is comparable with experimental data from references reported in Figure 6.26.

Finally, a correlation for screw expanders efficiency is proposed considering a mechanical efficiency for the compressor of 0.95 and a penalization due to the reverse operation equal to 2 percentage points. The correlation for screw expanders isentropic efficiency and the coefficients to be used are reported in eq. 6.13 and Table 6.12.

$$\eta = A_0 + A_1 \ln(V_{out}) + A_2 V_r \qquad \text{eq. 6.13}$$

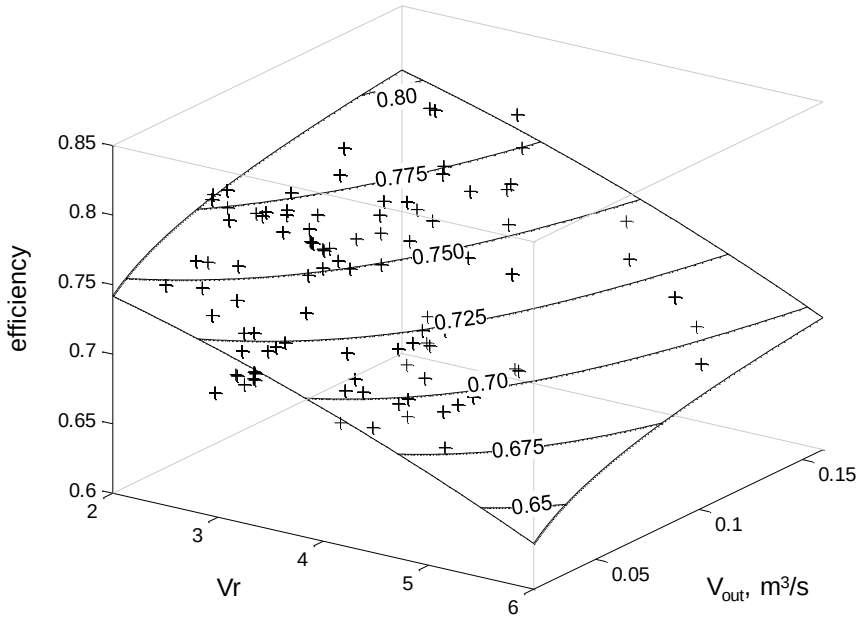

Figure 6.29 - Map of efficiency for Bitzer open screw compressors. Cross markers are representative of single device performances

A_0	0.9403305
A_1	0.0293295
A_2	-0.0266298

Table 6.12 - Coefficient values for screw expander efficiency correlation.

The suggested lower and upper bounds for the two independent variables are related to commercial devices as reported in Table 6.11 and the use of this correlation at volume ratios higher than 7 should be carefully performed because off-design effects have to be taken into account. Useful information about this aspect can be obtained from literature [138] where the off-design performances of different screw expanders having built in volume ratios between 2 and 5.2 are compared. Off-design data are obtained from two publications realized by Mycom [195] and Steidel [196] where the potential of screw expanders for vapour and high quality steam is investigated. The efficiency data are calculated and the trend against pressure ratio is reported for five devices. Three devices of the Mycom set are here considered: the lowest volume ratio screw expander is excluded because it is not possible to graphically obtain the maximum efficiency while the Steidel device does not show the off design trend for post expansion. It is interesting to notice that the efficiency variations in off-design, normalized on specific axes, show the same trend for the 2.5, 3.5 and 5 built-in volume ratio Mycon devices suggesting that the relative off-design behaviour is substantially equal for all these devices. The results are reported in Figure 6.30 and are regressed by a logarithmic trend line function with a R^2 coefficient higher than 0.99. In conclusion, the previously mentioned correlation can be adjusted for Vr higher than 7 with a correction factor expressed by eq. 6.14.

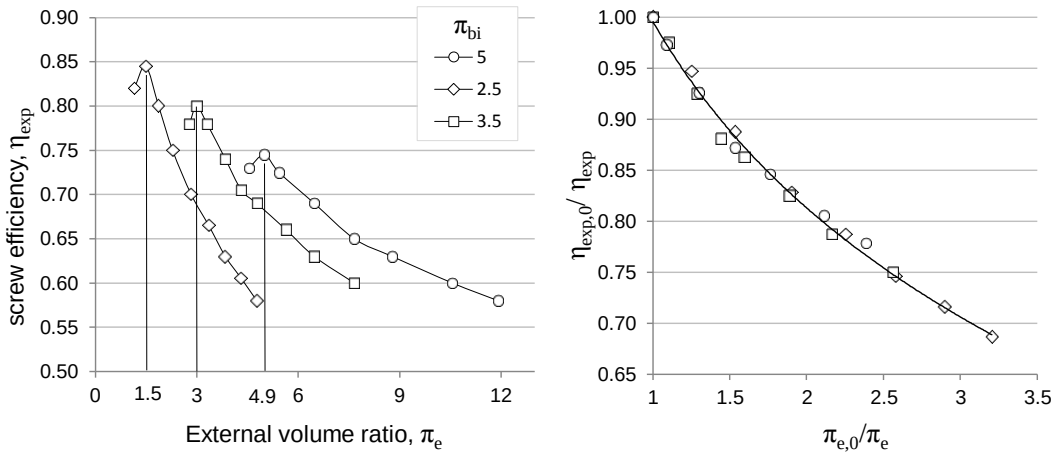

Figure 6.30 –Under expansion off-design performances for screw expanders in absolute and relative axes

$$Fc = 1 - 0.264 \ln\left(\frac{Vr}{7}\right) \qquad \text{eq. 6.14}$$

6.2.7 Final remarks

It is important to underline that the correlation of efficiency for screw expanders proposed in the previous section cannot be considered as a reference for state-of-the art for full optimized screw expanders for a number of reasons:

- Nowadays screw expanders are not produced by any company except by ElectraTherm and Helixpower but their components have not been tested so far from independent institutions as university or research centres and so no data are available about the performance of full optimized screw expander devices.
- All the information regarding screw expanders are derived by experimental campaigns on screw compressors in reverse operation. Experimental campaigns have been demonstrated the reliability of this approach with overall maximum performances close to the compressor nominal one. Additional losses are caused by a non-optimized shape of the intake and discharge ports and additional throttling losses. Results are thus representative of screw compressors in expansion operation whose efficiency is certainly lower than a device optimized to work as expander.
- The trend of efficiency for screw compressors is obtained calculating the point of maximum efficiency for many models and working fluids starting from producer data. Polynomial functions accuracy can greatly affect the final result and in any case the value of efficiency for compressor is usually far from the maximum one achievable for a device with the same volume ratio and the same swept volume because many other aspects are considered during the design. Since these devices are commonly used as compressor for refrigerant cycles their efficiency might be penalized in order to obtain a more reliable device which requires a limited maintenance. Regressed values are thus representative of commercial screw compressors and not of maximum attainable compressor efficiency.
- The extension of the correlation to expanders entails various approximations which affect partially the accuracy of the final result. In particular, it is not possible to correctly quantify the efficiency reduction shifting from compression operation to the expansion one. In addition, the effects of pressure losses in intake and discharge ports play an opposite role depending on the operation mode. A compressor has a built in volume ratio greater than the external one while for an expander the opposite. This entails that the map of performances should be translated to higher external volume ratios in order to evaluate a screw expander performance. However, pressure drops have a different weight depending on the size and on the built in volume ratio but no data in literature are available and this

aspect is here neglected considering these effects already included in the previous assumptions.

Despite the over mentioned approximation and limits the proposed correlation is a first attempt for the definition of a correlation of efficiency for screw expanders as function of both size and volume ratio. No other examples are available in literature but the results obtained are in good agreement with the experimental values obtained from other publications and reported in Figure 6.26. Accuracy enhancement is possible only when new experimental data will be available or general semi-deterministic models will be calibrated giving information about the weight of the different efficiency losses as function of geometrical ratios or specific parameters.

6.3 Comparison between axial turbines and screw expanders

An exhaustive comparison between axial turbines and screw expanders is quite challenging because the efficiency of these two devices is affected by different parameters, namely Vr and V_{out} for volumetric device and Vr, Ns and SP for turbine stages. These parameters are obviously influenced by the fluid properties and the cycle parameters like minimum and maximum temperature and plant configuration. The high variability of thermodynamic properties for the available working fluids and the number of different possible applications and sizes entail that each case has to be examined by itself in order to outline in which conditions is more reliable the use of a volumetric expander instead of an axial turbine. Furthermore, it is crucial to define all the problem constraints in order to examine the two solutions in a clear way without favoring excessively one of them. In this section a comparative study about the use of two different types of expanders is proposed for a rural solar power application.

The reference case is the $3kW_{el}$ solar power plant proposed by STG international [88] for electrification of rural villages in developing countries. Small concentration factor parabolic solar trough collectors are used with a maximum HTF temperature in the range between 150-160°C. The thermal power is released to an ORC working with R245fa in a saturated subcritical cycle where the expansion is realized by a scroll compressor used in reverse mode which is the only volumetric device suitable for this range of power output. The experimental activities in Florida have been demonstrated the reliability of the concept on the small scale opening the scenario to scale-up of the plant up to higher plant sizes. Screw expanders and small size axial-flow turbines can be used in a range of power output between few kW_{el} to 200 kW_{el} and the task is to define the boundary which defines where the volumetric devices might be more efficient than turbo machines. In this analysis working fluid is always R245fa with a fixed condensing temperature equal to

40°C compatible with the use of an air cooled condenser. Investigated solutions have an evaporating temperature in the range 70-130°C which entails volume ratios up to values slightly above the maximum one for screw devices. Isentropic power output is varied between 5 and 100 kW_{el}. The analysis is realized comparing the performance of the screw expander and a single stage axial-flow turbine rotating at optimized speed. Single stage turbines are here considered because of the small size of the plant and the small volume ratios do not justify the use of multi-stage turbines. A power electronic efficiency of 0.97 is assumed for the axial flow turbine while the screw expander is directly connected to the generator.

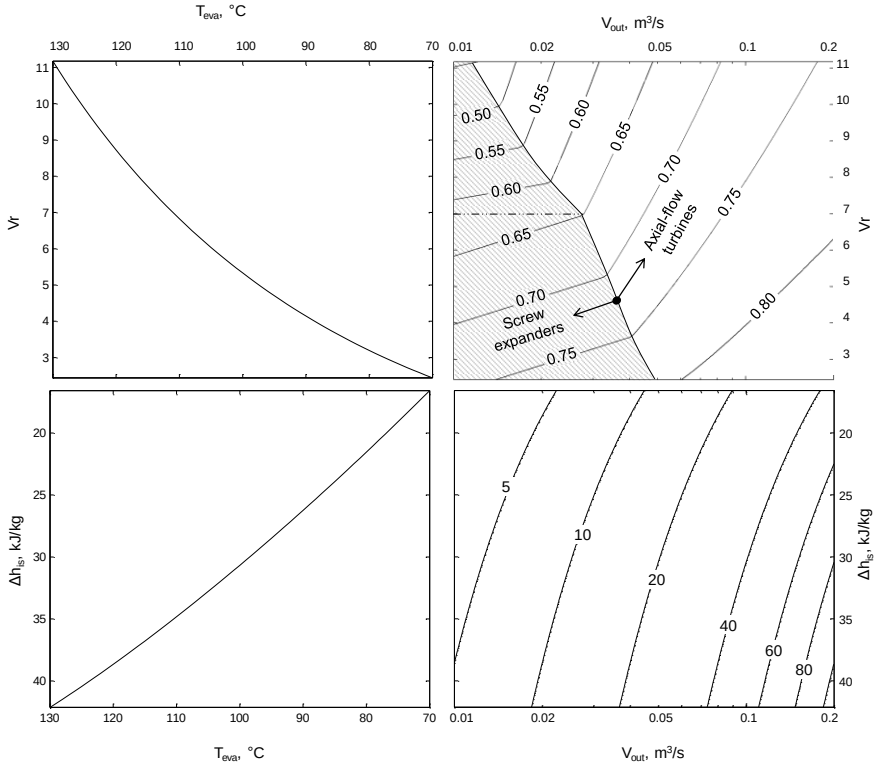

Figure 6.31 – Trend of Volume ratio against evaporation temperature (top-left), trend of isentropic enthalpy drop against evaporation temperature (bottom-left), contour map of isentropic power (bottom-right) and contour map of maximum attainable efficiency using a screw expander or a micro single stage axial flow turbine (top-right). The shaded area represent the region where screw device is more efficient than the turbine.

In Figure 6.31 the trends of different parameters are shown. In the top left corner and in the bottom left corner the isentropic volume ratio and isentropic enthalpy drop are reported against the evaporation temperature. The trend is not linear for both parameters and it is important to note that, in the investigated range of temperatures, the volume ratio reach values higher than 7 which is the upper bound for the nominal screw efficiency correlation. Above this value the volumetric efficiency is adjusted with the correction factor reported in eq. 6.14. The isentropic power is reported in the bottom right corner and

it covers the range of commercial screw compressor devices. Finally, in the top right corner the maximum attainable efficiency by using a screw expander or single stage axial-flow turbine is reported. In this latter diagram the solid line divides the map in two portions: the grey area represents the region where the screw expander is more efficient than the axial flow turbine while in the white one the opposite. For volume ratios higher than 7 the off design correction is applied to the screw devices leading to lower efficiencies and limiting their use only to very low volume flows where axial turbines are excessively penalized by high secondary and leakage losses. In conclusion, smaller is the volume flow rate more competitive is the screw expander and for gross power output of 10-15kW_{el} volumetric devices are the suggested expander for this application. The contour map of efficiency of Figure 6.31 is reported as tridimensional surface in Figure 6.32 in order to better understand the trends of efficiency for both screw expanders and axial flow turbines.

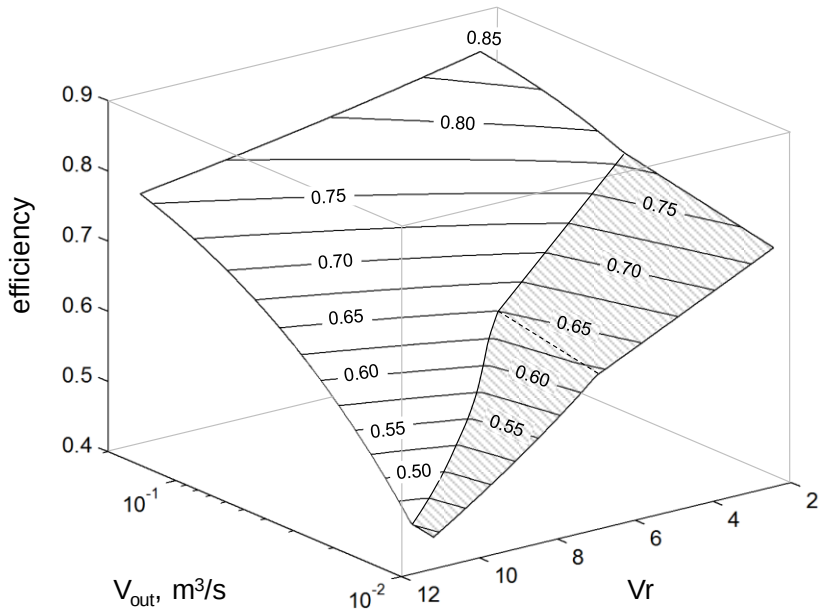

Figure 6.32 – Surface of maximum efficiency using a screw expander (shaded area) or an axial flow turbine (white)

The dashed line represent the points on the screw map characterized by a volume ratio equal to 7, above this limit it is possible to notice the change of slope due to the off-design correction. In Figure 6.33, the contour map of the difference between the screw expander efficiency and the turbine efficiency is reported: the increment at low volume flow rates is relevant reaching values close to 15 percentage points. However limiting the volume ratio to 7 and so considering available devices without off design effects it is possible to extend the field of operation of screw expander to higher volume flow rates if

the corresponding efficiency penalization (up to 8 percentage points) respect to the axial flow turbines is compensated by a less expensive equipment or a lower maintenance cost.

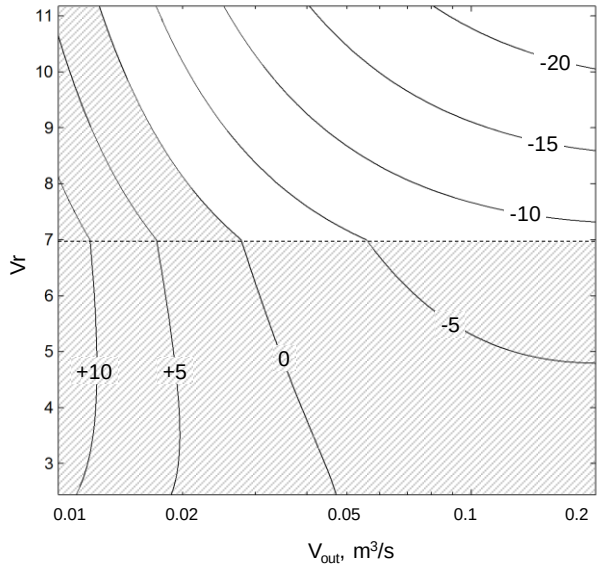

Figure 6.33 – Difference between screw and axial turbine efficiency. The shaded area is representative of the conditions where the screw expander is, or might be, affordable respect to a micro-high speed turbine

Finally, the trend of turbine SP against to the volume flow rate and the volume ratio is reported in order to justify the trend of turbine efficiency which depends on SP and Vr.

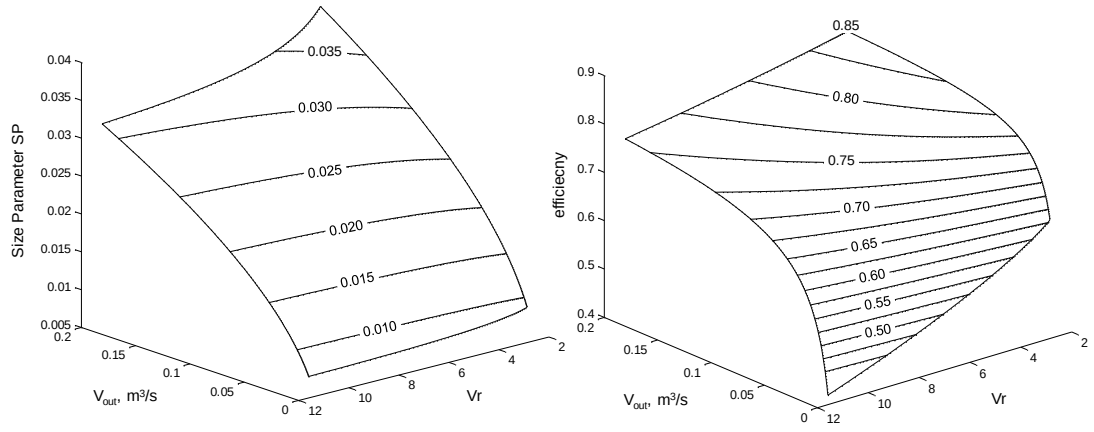

Figure 6.34 – Surface of SP values and turbine efficiency varying Vr and V_{out}

6.4 Other components

A brief overview of the other components commonly used in ORC is reported in the next sections.

6.4.1 Primary heat exchanger

A particular attention must be reserved to the heat exchangers, which typically contribute for the largest fraction of power block cost. The primary heat exchanger, where heat is introduced in the cycle, has to be designed according to the trade-off between different opposite effects. The increasing of surface is positive from a thermodynamic point of view, since it allows limiting the entropy generation and achieving higher performances, but it leads to a more expensive equipment with a contrasting effect on the cost of electricity. Shell&Tubes are the most common heat exchanger type in ORC field and they are used for the economizer and the superheater (when the hot stream is liquid). The hairpin shell and tube, reported in Figure 6.35, is an example of this kind of units: basically it is a heat exchanger with a very high L/D aspect ratio folded on itself. It allows for a large thermal duty in a single unit with an almost perfect counter current streams disposition and small mean temperature differences.

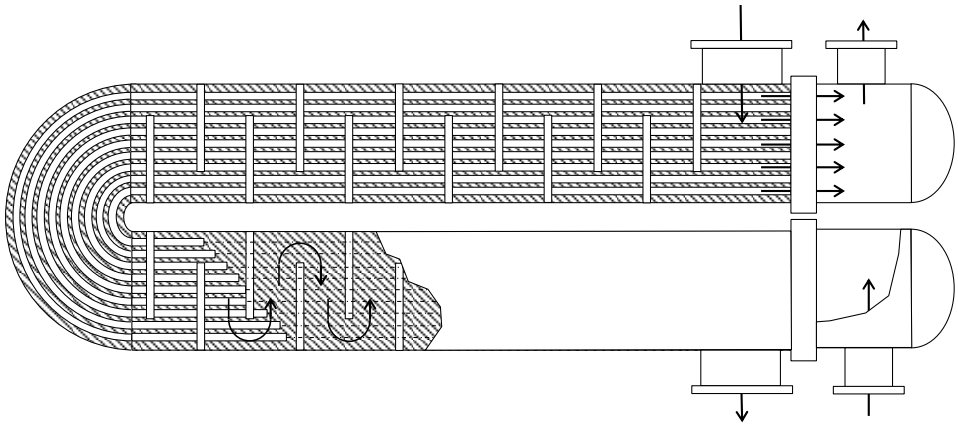

Figure 6.35 - Hairpin Shell&Tubes heat exchanger

For evaporators and water cooled condensers instead, a kettle reboiler and pool condensers are usually adopted if mixtures are not used as working fluid. For small scale applications, instead, plate-fins or brazed plate heat exchangers can be used since they are more economical compared to S&T units.

Carbon steel is the most common material for these components even if other alloy can be used in presence of corrosive fluids.

6.4.2 Air condensers

The condenser has to reject to the environment a large fraction of the power input, because of the relatively low thermodynamic efficiency of ORCs. In case of air cooled condensers (ACC), its cost can be around the 20% of the power block cost and so its design should be carefully evaluated. A larger surface allows reducing the condensation pressure and increasing the power output, however it leads to a higher equipment cost, a larger footprint and to a higher electric consumption of the fans. The design of this component is derived from HVAC industry. An ACC is formed by a couple of copper finned tube banks made by few (up to 5) rows and multiple passages. Ambient air is conveyed by a series of fans placed on the top of the unit. Small tubes diameter and advanced fins design, can give important advantages in terms of total weight and internal volume (important to reduce the amount of fluid charged in the plant). Finally a solution which is offered by LU-VE [197] consists in a "wet and dry" ACC. If the ambient air temperature becomes too high to maintain the cooling capacity, the system starts to spray the required amount of water onto the fins. In this way, the duty of the condenser is dramatically improved since the ambient temperature is brought down to the wet bulb temperature with relevant energy advantages. Usually the transition from dry to wet operation is set to 20°C.

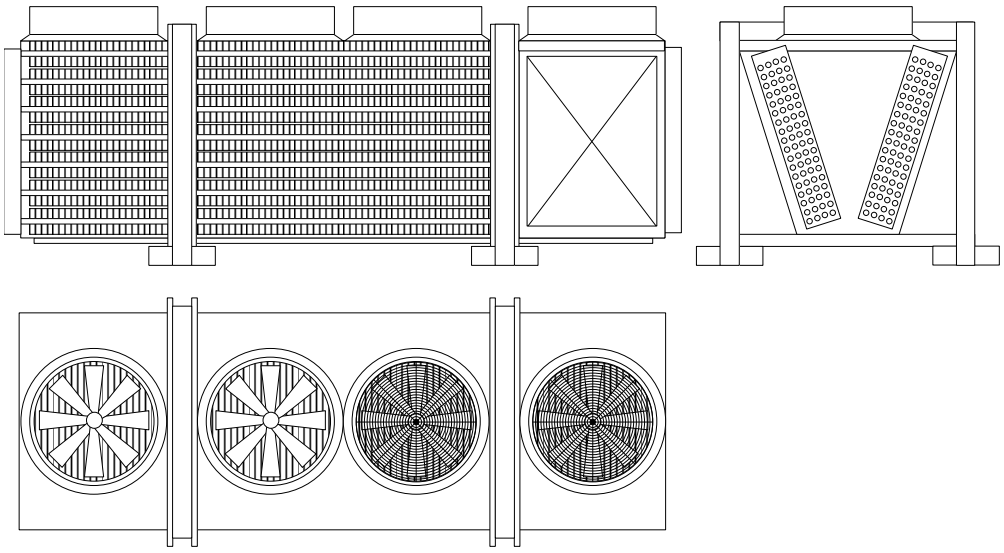

Figure 6.36 - Air Cooled condenser sketch.

6.4.3 Recuperator

The recuperator is component particularly important in high temperature applications and in those cases characterized by a high minimum temperature of the heat source. For high temperature sources usually complex working fluids are used involving small temperature drops along the expansion and so a large thermal power available at turbine discharge. A recuperative preheating of the pumped liquid is important to obtain high efficiencies limiting the temperature differences in the PHE. Recuperator is usually formed by a finned tubes heat exchanger in order to improve the film transfer coefficient on the tube external side, where vapour flows. This technology is derived by HVAC (Heating, Ventilation, and Air Conditioning) industry and recuperators are realized by several liquid circuits arranged on different staggered rows forming a tube bank. Tubes are finned with continuous plates, organic liquid flows perpendicular to the vapour and usually multi-passage paths are adopted. The external-internal surface ratio is generally around 15-17. Fins are always realized in copper except for aggressive fluids like ammonia, while tubes material depends on the operating temperature. For temperatures below 200°C tubes are made by copper while for higher temperatures cupronickel 90/10 is used. Recuperator is placed just after the turbine diffuser in order to reduce pressure losses in the piping between the two components.

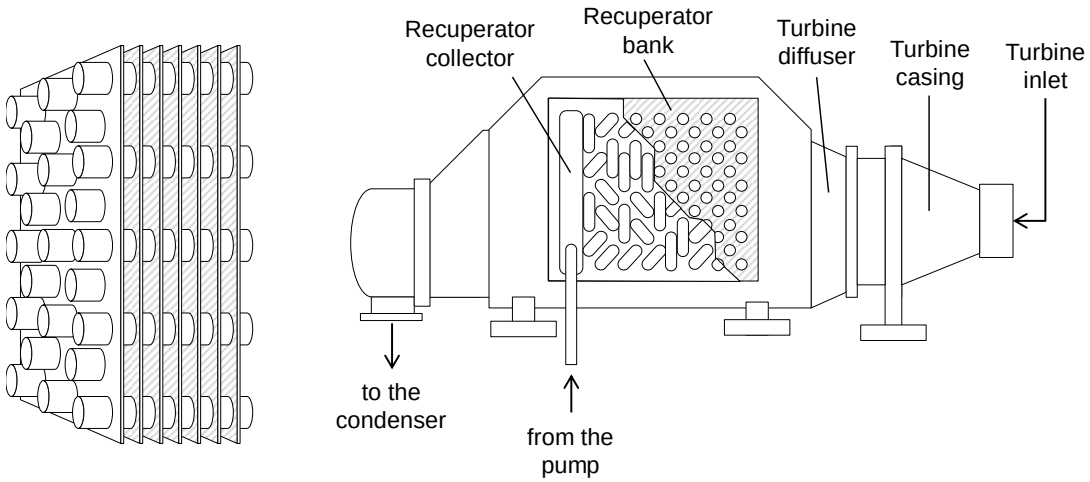

Figure 6.37 – Schematic representation of regenerator finned tube bank typical of a ORC recuperator and its disposition ant turbine outlet.

6.4.4 HRSG

In WHR from industrial processes usually the heat source is a stream of hot gases and so S&T heat exchangers are not the most appropriate component because of the low overall heat transfer coefficient resulting from the use of plain or low finned tubes. The best technical solution is to use a HRSG (Heat Recovery Steam Generator) unit totally similar to the components commonly used in combined cycles. They are formed by a bundle of vertical finned tubes arranged in several rows. Evaporator unit has a steam drum on the top of the tube bank where the two phases are separated. Liquid stream flows into an unheated tube which is called down-comer from the upper drum to the lower liquid drum. Fluid remains in liquid phase because its pressure is increased by the liquid head. From the lower drum fluid is conveyed to a series of rising tubes in parallel where the working fluid absorbs heat from the hot gases and it is partially vaporized. Finned tubes are used to enhance the film heat transfer coefficient on the external side where hot gases flow.

6.4.5 Pumps

ORC pump are usually variable speed multistage centrifugal pumps and their design is relatively easy because of the great knowledge and the wide use of this component in power production, chemistry and refinery fields. Depending on the cycle configuration, fluid selection and cycle design parameters, the pump might show a consumption which is a relevant share of the turbine gross power output (up to 20-30% in supercritical cycles with high critical pressure fluids). In this case, the pump efficiency is a crucial parameter and the component has to be carefully designed in order to achieve higher cycle efficiency. An innovative technology is the hydrodynamic pump which allows avoiding the leakage of fluid and the contact with air. This technology permits to activate the pump without a direct mechanical connection, but thanks to a magnetic field.

6.4.6 Generators, gear boxes and power electronic systems

No particular observation can be done on these components since they are similar to those commonly used in industrial field and power generation.

"Three non-aligned points

can be connected by an infinite number of straight lines,

if the points are sufficient big or

if the lines are thick enough"

Ernesto Pedrocchi

7 Cost correlations

With the aim to perform techno-economic optimization, thus minimizing the Levelized Cost of Electricity (LCOE), cost information for all the cycle components are needed. Cost of the equipment, Balance of Plant cost (BOP) and the fixed investment cost related to the exploitation of a certain heat source should be known with a good accuracy in order to obtain reliable final results. Rough errors in the calibration of cost correlation functions can lead to results far from the optimal in terms of both absolute final LCOE and of values of cycle design parameters and optimal solution might entail configurations which are almost infeasible from a technical point of view. For instance, if the cost function for the air condenser results in a large under-estimation of component cost, the optimization routine will push both approach point and pinch point temperature differences to their lower bounds achieving a higher efficiency but entailing an extremely wide heat exchanger surfaces. Another example is related to turbine cost correlation when high critical temperature fluids are used: as already stated in section 4.2.5 (Effects on component design and cycle configuration) low condensing temperatures lead to very low condensing pressures and an exponential increase of both the volume flow rate and the mean diameter at the turbine last stage. Furthermore, the isentropic volume ratio is increased requiring a higher number of stages as well. If the turbine cost correlation does not take into account the size of the turbomachine and the number of stages, the optimization algorithm will push the condensation temperature to very low values in order to exploit a higher enthalpy drop and increase the power production but leading to a non-feasible design of the turbine.

Despite the importance to obtain reliable cost correlations, this topic is not widely discussed in scientific literature and general, and possibly smooth, capital cost functions are difficult to find. Furthermore available data usually refer to a very specific field or to a small range of temperature and pressures. Engineering companies and component producers are the only figures who can provide affordable data but internal secrecy policy tends to keep the economic information strictly reserved and this kind of information is rarely conveyed. The goal of this section is to organize the relatively small scientific literature about this topic and to calibrate a series of cost correlations, one for each ORC component, which are used in the ORCO software.

Three main references are usually adopted to obtain cost correlations in this work; they propose different approaches and some more details about them are further reported in order to help the reader to better understand the next sections:

- Perry [198]: is the most used and reliable handbook about chemical engineering process and it contains a chapter about equipment cost correlations. Different approaches are proposed by this text and we refer to the *Exponential Method* which is commonly used in engineering for fast cost estimations. The cost of equipment is calculated starting from the cost of a similar component, knowing its size or its capacity. A power factor is used on the ratio of capacities in order to account for scale economies attainable with larger equipment, which generally shows a lower specific cost. The reference formula is reported in eq. 7.1

$$C_2 = C_1 \left(\frac{q_2}{q_1}\right)^n \qquad \text{eq. 7.1}$$

  Where C_1 and q_1 are respectively the capital cost and the capacity of the reference component while q_2 is the capacity of the component whose cost is calculated. Exponent n introduces a deviation from the linear trend considering size effect on the equipment cost. The lower the value of the exponent, the lower the specific cost of the component increasing the size or the capacity, and for this reason n is generally lower than unit. For instance, typical values for motors or generators are around 0.6-0.7 while for air cooled condenser they are close to unit because of the modularity of this component. An intrinsic drawback of this approach is related to the definition of just one reference point and one exponent. Therefore, errors in their estimation introduce high deviation of the calculated cost. In addition, the use of exponential laws far from the reference point can lead to relevant under or over-estimation of component cost.
- Turton [199]: is another common textbook for the design of chemical and synthesis processes. It presents a detailed methodology for the calculation of equipment cost for many components of interest in ORC field. The approach followed is more accurate compared to Perry's one and results do not present drifts for values far from the reference one. In Turton, the base cost functions are obtained by using the capital equipment-coasting program CAPCOST [200], which is based on the module factor approach originally introduced by Guthrie [201; 202] and later modified by Ulrich [203]. Data are regressed and cost correlations are presented in the logarithmic form reported in eq. 7.2.

$$\log_{10}\left(C_p^0\right) = K_1 + K_2 \log_{10}(A) + K_3 [\log_{10}(A)]^2 \qquad \text{eq. 7.2}$$

Where C_p^0 is the base equipment cost for a component operating at ambient pressure and made of carbon steel and A is the capacity or the size of the component. A lower and upper bound for every function is declared.
Effects of pressure and labor are taken into account by multiplying the base cost for a certain bare module factor F_{BM} calculated with eq. 7.3

$$F_{BM} = B_1 + B_2 F_M F_P \qquad \text{eq. 7.3}$$

Where $F_M$and $F_P$are the material and the pressure factor respectively.
Different material factors are listed for each component depending on the material used for the construction. Data proposed by Turton are calculated as the average of values from reference [202; 202; 203]. Pressure factor instead is calculated with the formula reported in eq. 7.4

$$\log_{10}(F_P) = C_1 + C_2 \log_{10}(P) + C_3 [\log_{10}(P)]^2 \qquad \text{eq. 7.4}$$

Where P is the pressure in bar gauge inside the tube or inside the shell depending on the side where the high pressure fluid is placed. Pressure factors are always greater than unit and extrapolation outside of the validity range should be done with caution. The trend of pressure factor for a shell& tube heat exchanger is represented in Figure 7.1 considering the thickness increment just on tube material and on both shell and tube. C_x coefficients are reported in figure as well. Correction is applied only for fluid pressure 5 bars greater than the ambient one.

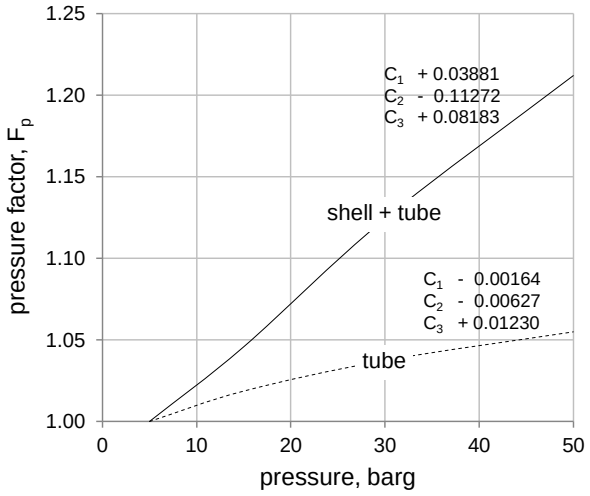

Figure 7.1 - Pressure factors for Shell&Tubes heat exchangers if the thickness increment is applied on tube material or on both tube and shell. Coefficients reported in figure refer to eq. 7.4

Finally the cost of a general component results from eq. 7.5.

$$C_{BM} = F_{BM} C_p^0 \qquad \text{eq. 7.5}$$

- NETL report [204]: this is the result of a work funded by the United States Government and it follows an approach similar to Turton for the estimation of base equipment cost. Data are provided as curves of capital cost against size for different components. Since the curves are reported only graphically, the numerical data are obtained by the author from these charts and eventually regressed in the logarithmic form proposed by Turton and reported in eq. 7.2. The accuracy claimed in the report is +50%/-30% and it is recommended for order of magnitude cost estimations. In NETL report, ICARUS Process Evaluator software is also used and some results for Shell&Tube heat exchangers are reported.
  Bulk material and installation labor costs are estimated with a series of multiplicative factors to take into account foundations, insulation, instrumentation and other expenses. Depending on the type of streams handled, different values are proposed varying the temperature and the pressure. The final cost of a general component is calculated by eq. 7.6.

$$C_{BM} = C_p^0 (1 + F_{DL}) \sum_{i=1}^{n} \left(1 + a_i (1 + b_i)\right) \qquad \text{eq. 7.6}$$

  Where C_p^0 is obtained graphically from the charts in the report, $F_{DL}$is the distributive labor factor equal to 0.2 for heat exchangers and other ORC components and a_i and b_i are the distributive factors for bulk material and labor for the different n terms previously mentioned.
  Finally, multiplicative factors for converting carbon steel to other equivalent alloys cost are considered and values are reported in Table 7.1
- The last source of information comes from a previous work [2] where different exponential laws are calibrated for different components in a limited range of validity for the techno-economic evaluation of binary geothermal power plants.

Material	Pumps	Other Equipment
All Carbon Steel 1.00 1.0	1	1
Stainless Steel, Type 410	1.43	2
Stainless Steel, Type 304	1.7	2.8
Stainless Steel, Type 316	1.8	2.9
Stainless Steel, Type 310	2	3.33
Rubber-lined Steel 1.43	1.43	1.25
Bronze	1.54	
Monel	3.33	

Material	Heat Exchangers
Carbon Steel Shell and Tubes	1
Carbon Steel Shell, Aluminum Tubes	1.25
Carbon Steel Shell, Monel Tubes	2.08
Carbon Steel Shell, 304 Stainless Steel Tubes	1.67
304 Stainless Steel Shell and Tubes	2.86

Table 7.1 - factors for converting carbon steel to equivalent alloy costs as reported in [204]

In the next sections two components are discussed in detail, namely the Shell&Tube (S&T) heat exchanger and the axial turbine. For the other components a brief summary of the data collected and the final cost correlations are simply proposed.

7.1 Shell & tube heat exchangers

Economizers, evaporators, superheaters and once trough supercritical PHE are usually designed as S&T heat exchangers. For ORC, the ratio between the total heat transfer surfaces and the power production is larger than in conventional steam Rankine cycles due to the low efficiency of the thermodynamic cycle. In ORC the share of total cost for heat exchangers is relevant and their cost functions should be calibrated carefully in order to obtain reliable final results. Information from different references are compared in order to understand similarities and discrepancies among them and define a new and more general cost correlation.

First, the analysis of Turton data is performed. In this reference three different base cost functions are defined, namely for floating head, fixed head and U tube S&T heat exchangers. They slightly differ one from each others as reported in Figure 7.2 where the trends for the specific cost and absolute cost are shown in USD^{2001} as defined in the original reference. With an OLS regression, a new logarithmic correlation is proposed fitting the three series, also reported in Figure 7.2. The fitted curve is used to compare Turton cost data with the other references available in literature.

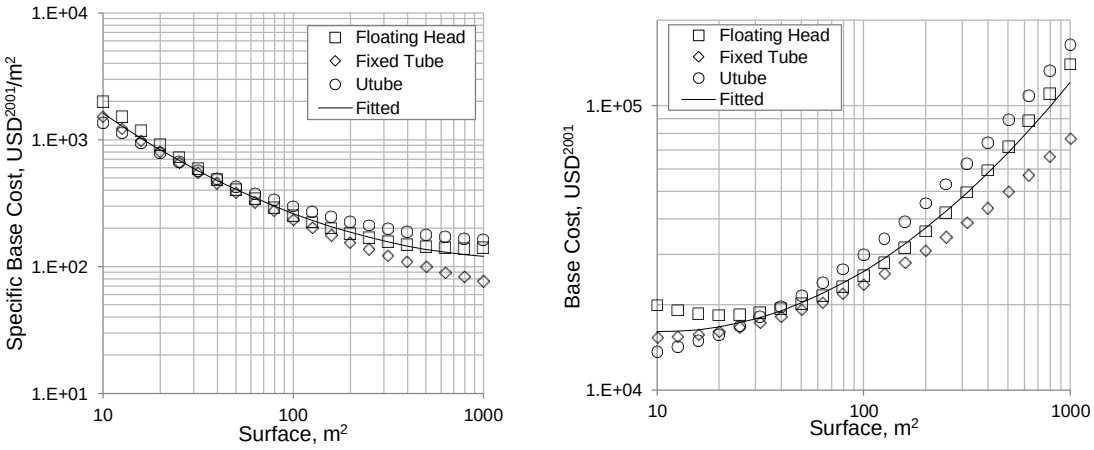

Figure 7.2 - Specific cost and total cost for different S&T heat exchangers as reported by Turton. The solid line represents the regressed function used for the comparison with the other references

NETL cost function is obtained graphically from the corresponding chart in the report where the trend of the component base cost as function of the heat exchanger surface is reported in USD^{1998}.

The different base costs from Turton and NETL converted in USD^{2013} are reported in Figure 7.3 together with the exponential functions proposed by Perry. Three functions are proposed in this last reference for the same heat exchanger types discussed by Turton. The base S&T is the floating head one, whose cost can be calculated with the coefficients values reported in Table 7.2.

Coefficients for C_p^0	C_1	21.700 USD^{1997}	eq. 7.1
	q_1	93 m^2	
	n	0.59	
	Range of validity	1.9-1860 m^2	

Table 7.2 - Coefficients and range of validity for S&T exponential law as proposed by Perry

Fixed head and U tube S&T costs are obtained by multiplying floating head S&T cost by 0.85 and 0.87 respectively.

It is possible to note the good agreement among all the references, between Turton and NETL there is a small difference at low surfaces while they are almost overlapped at large areas, where there is the upper bound for the Turton correlation. Perry trend is obviously different because it is obtained by an exponential method but, even if it underestimates the cost at both small and large surfaces, the reference point of the equation perfectly fits the other two correlations.

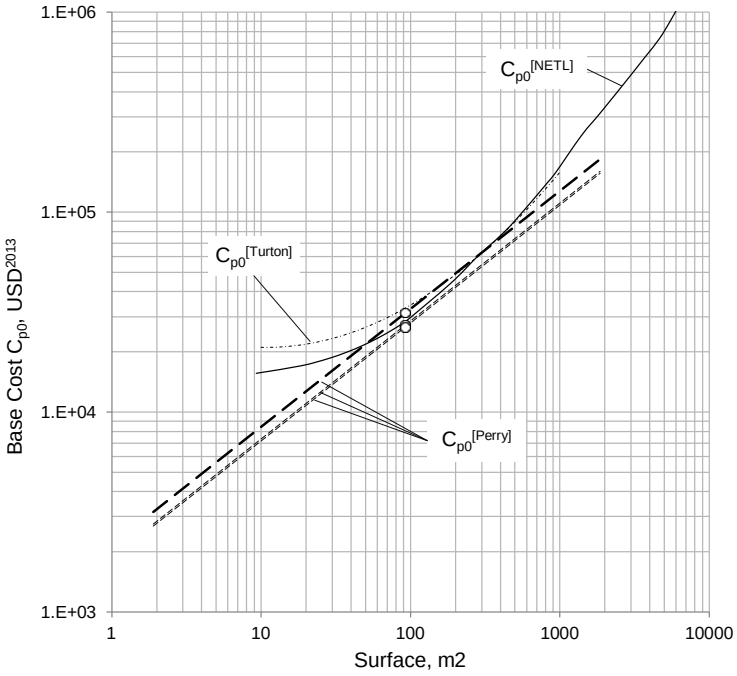

Figure 7.3 – Comparison between the different S&T heat exchanger base cost correlations proposed in literature. For Perry correlation the marker represents the reference point

At the second step the effect of material and labor are added to both Turton and NETL base cost curves in order to obtain a comparison among the results provided by the two different methodologies. Results are reported in Figure 7.4, together with other two references. ICARUS curve is taken from NETL report where different heat exchangers have been designed with the corresponding software: non-smooth trend is due to real limits and technical constraints considered by the tool. The other curve, labeled as Astolfi, comes from a previous work on ORC technology, where a first attempt of cost correlation was proposed. The functional form is the same of Perry in eq. 7.1 and it is centered in a different reference point defined thanks to personal communications with an ORC engineering company. The exponent used in this case is 0.9 and the correlation is suitable to evaluate the cost of S&T for larger size power plants where the increase of heat transfer area is obtained by adding new units in series or in parallel instead of enlarging a single heat exchangers.

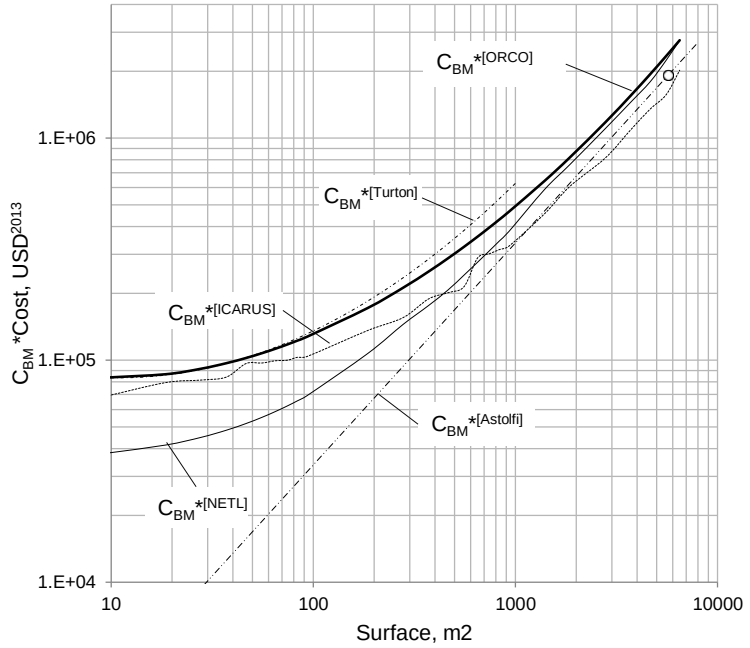

Figure 7.4 – Total S&T cost against heat exchanger surface trends from literature. The thicker curve is the proposed correlation for S&T heat exchangers to be used in ORCO

Accounting for material and labor factors, cost correlations show a similar overall trend but they appreciably differ at low surfaces where the NETL approach underestimates heat exchanger cost respect to both Turton and ICARUS results. For large surfaces, instead, the different trends get similar and comparable in both values and slope. Finally a new correlation is proposed for S&T heat exchangers trying to consider all the references in the range where they appear to be more reliable. In particular a higher weight is given to Turton and ICARUS data at small area and to Perry and Astolfi at larger surface where Turton correlation is out of the range of validity. The new cost correlation is fitted with the logarithmic form of eq. 7.2 and the regressed coefficients are reported in Table 7.3

Coefficients for $C_{BM}{}^{*}$	K_1	5.10496720	eq. 7.2
	K_2	-0.37366325	
	K_3	0.18991667	
Coefficients for F_p	C_1	-3.35099	eq. 7.4
	C_2	1.915216	
	C_3	-0.28169	
	Range of validity	25-5000 m^2	

Table 7.3 – Shell and tube cost correlation coefficients for bare module cost and pressure factor.

For the proposed correlation the trend of total cost and specific cost against heat exchanger surface is reported in Figure 7.5. The total cost increases with an almost linear trend except at low surfaces, namely below 800 m^2, while the specific cost becomes almost constant for heat exchanger surfaces larger than 2000 m^2. For surfaces larger than 5000 m^2 the specific cost is considered constant and so the total cost rises proportionally to the surface.

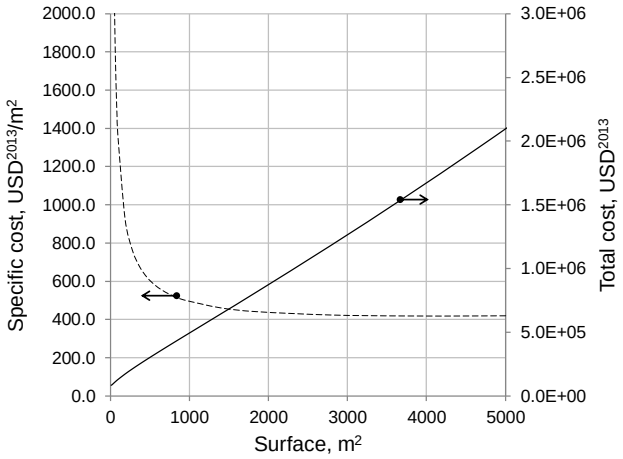

Figure 7.5 - Trends for the total cost and specific cost of Shell& tubes heat exchangers without considering pressure effects

The proposed cost correlation is valid if no pressure effects are taken into account and unfortunately the set of available data does not allow obtaining a new formulation for the total bare module cost simply trough algebraic manipulation of Turton equations. The proposed final correlation is reported in eq. 7.7 where F_P is calculated with eq. 7.4.

$$C_{BM} = C^*_{BM}(1 + F_P) \qquad \text{eq. 7.7}$$

The function for F_P, as proposed by Turton, is valid for values of P in the range of 5-140 bar gauge. The new coefficients for F_P are retrieved and reported in Table 7.3, while the trend of the pressure factor is reported in Figure 7.6. This term is important for supercritical cycle with fluids having relatively low critical temperature, for instance, for R134a whose critical pressure is around 45 bar, the correction factor can account for more than 10% of the total PHE cost.

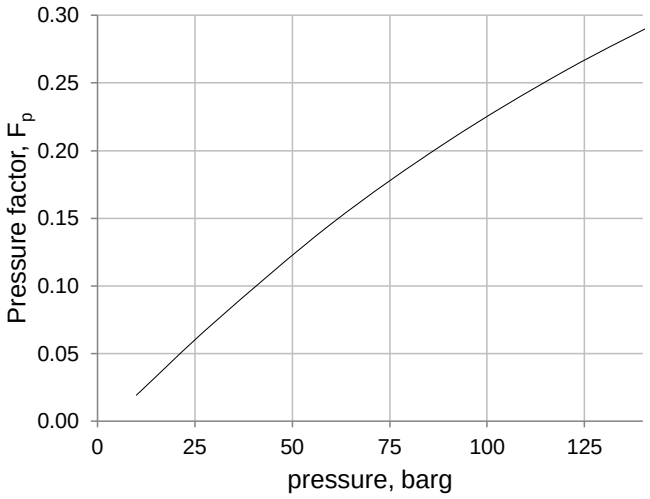

Figure 7.6 - Pressure factor for S&T heat exchanger to be used in eq. 7.7

The same correlation can be used for the evaluation of both kettle reboiler and low finned tube S&T heat exchangers by means of the introduction of two correction factors. For kettle reboiler cost, C_{BM} should be multiplied for 1.35 [198] while for low finned heat exchanger a multiplying factor equal to 1.7 [42] is adopted considering a the additional material and labour costs.

Finally, calculations were carried out using Thermoflex PEACE components [43] and Aspen EDR tool [42] and designing several different heat exchangers. Unfortunately this approach did not provide useful data due to the discontinuous trend of the collected results. The reason of this is related to the structure of these codes: they perform a heat exchanger optimization based on pseudo Bell-Delaware method [36; 37] considering TEMA standard [205] for the selection of both shell and tube diameters, rear and front head etc. From one side, the result is certainly more reliable because only components from a referenced catalogue are used but, from the other side, the use of discrete values for the optimization variables entails a discontinuous objective function and a more challenging optimization problem. In conclusion, heat exchangers with similar duty might result in different configurations leading to different costs and justifying the discontinuous trend over mentioned.

7.2 Axial turbine

Axial turbine is the key component of an ORC system but unfortunately there is a very small availability of public data of cost about it. The market is shared between few companies which have strict reserve policy and they are extremely reluctant in releasing information. The same lack in available data is present for steam turbines in spite of their wider use in power plant applications. In this section a correlation for the cost of ORC turbines is derived, combining steam turbine drives cost data with information about ORC devices.

The trends of cost for steam turbine drives of turbo-pumps groups are reported in Figure 7.7. Data come from NETL report and Turton and costs are reported in USD^{2013} against shaft power in kW. In the NETL report, two correlations are available for high (700-25000 kW) and low shaft power (7-700kW) respectively, while in Turton an intermediate range is considered. It is interesting to note how in log-log axes the three trends are relatively comparable, even if they certainly refer to different conditions at both turbine inlet and outlet. Instead of using all these three references a new correlation is first regressed as representative of this component.

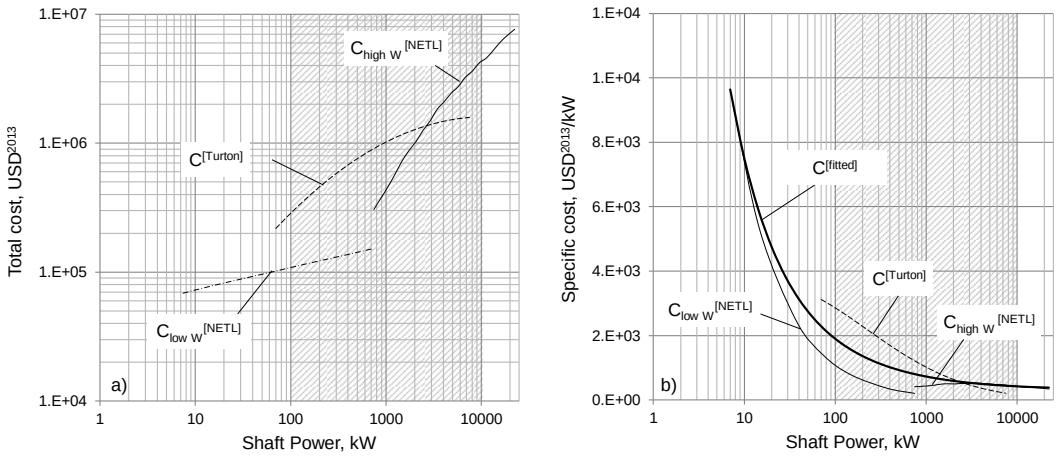

Figure 7.7 - Trends of steam turbine drive total cost against shaft power (a) for three references and corresponding trends of specific cost (b). In figure b the thicker solid line is the proposed regressed function for steam turbine drives.

An OLS regression on the specific cost is performed fitting the three coefficients required by the logarithmic functional form already reported in eq. 7.2 and used by Turton to describe the base cost of different components. The trend of the specific cost resulting from this new cost correlation is reported in Figure 7.7.b and compared with the data obtained from the literature. For steam turbine drives there is a good agreement at both low and high powers with NETL results, while in the range between 100 kW and 2 MW

the proposed function is between the Turton and the NETL ones. The values for the regressed coefficients are reported in Table 7.4.

Coefficients for C_{BM}	K_1	4.65209	eq. 7.2
	K_2	0.13348	
	K_3	0.08996	
Range of validity		7.5kW-10MW	

Table 7.4 - Regressed coefficients for the correlation of cost for steam turbine drives.

Results achieved so far are useful only for the calculation of the cost of a small axial steam turbine and the same correlation cannot be directly used for estimation of ORC turbine cost. As already stated in Section 4.2.5 (Effects on component design and cycle configuration) organic fluids allow designing turbines with a limited number of stages thanks to the low isentropic enthalpy drop in expansion and machines with more than three stages are rarely adopted. On the contrary, using water as working fluid requires a larger number of stages in order to limit the load coefficients and maintain a high overall efficiency. Another difference is related to the volume flow rates at turbine discharge and so to the dimension of the last stage: for steam turbine drives volume flow rate is mainly affected by shaft power and condensing pressure while for ORC completely different values can be obtained using different fluids. In this latter, case critical properties of the working fluid strongly affect the size of the turbine even for the same gross power output and the same temperature of condensation. The task is to define a correlation which is valid for both ORC turbines and light fluids, like water or ammonia, taking into account not only the shaft power but also the number of stages and the SP of the last stage which are representative of the axial and the radial dimension of the turbine.

Four additional ORC turbines are considered exploring different sizes and applications. Main assumptions and results are reported in Table 7.5 listing the turbines in ascending order respect to gross power.

Cases A and C are representative of two simil-Turboden turbines used in a commercial biomass co-generative power plants. A light siloxane is used as working fluid in a saturated cycle working between 220°C and 90°C. Due to the small inlet volumetric flow rate, partial admission is used for the smallest size turbine (~650 kW) while for largest one (2.3 MW) a reasonable sizing of the first row blades is obtained even with total admission. The case B is representative of a particular turbine which expands a non-conventional working fluid $TiCl_4$. From a previous study [66], a supercritical non-recuperative cycle is selected as the most suitable solution for really high temperature

applications where the heat source can be exploited down to low temperatures. Finally, case D represents a medium size binary geothermal power plant for the exploitation of a 150°C hot brine.

	A	B	C	D
application	biomass	WHR	Biomass	geothermal
Working fluid	MM	TiCl4	MM	R134a
Plant layout	saturated	supercritical	Saturated	supercritical
Gross power, kW	640	1230	2300	6000
Number of stages	2	3	2	2
SP of the last stage	0.157	0.19	0.287	0.18
admission	partial	total	Total	total
Expected specific cost, USD^{2013}/kW	450	420	330	260

Table 7.5 - ORC turbines reference cases assumptions and results. The ORC turbines are designed with Axtur. The value of expected specific cost is selected by assuming a turbine cost share around 30% of a reasonable specific cost of the power block (without BOP) for every case.

The proposed functional form is reported in eq. 7.8 and it is formed by two terms. The first one is representative of a fixed cost independent of the axial and radial dimension of the turbine and it is function of the turbine gross power output. It takes into account the cost of the project engineering, the purchase of mechanic and rolling bearings, the shaft cost and the installed instrumentation. The second one is a function of the number of stages and of the last stage size parameter; furthermore it accounts all the expenses for stages design and manufacturing.

$$C_{turb} = C_1(W)^{n_1} + C_2\left(\frac{SP}{SP_0}\right)^{n_2}(n_{st})^{n_3} \qquad \text{eq. 7.8}$$

Where power W is in MW and SP_0 is assumed equal to 0.18. The five coefficients (C_1, C_2, n_1, n_2, n_3) have to be calibrated fitting cost data.

For steam turbine drives, the last stage SP and the number of stages are calculated with an inlet pressure of 27,58 bar (400 psig as reported in NETL report) and assuming an inlet and condensing temperatures of 400°C and 50°C respectively. The number of stages is computed considering a maximum isentropic enthalpy drop per stage slightly higher than 153 kJ/kg. This value corresponds to stages with a peripheral speed equal to 350 m/s and a load coefficient of 2.5 according to eq. 7.9.

$$k_{is} = \frac{\Delta h_{is}}{u^2/2} \qquad \text{eq. 7.9}$$

Six stages are obtained for all the steam turbine drives while the trend of last stage SP is reported in Figure 7.8.

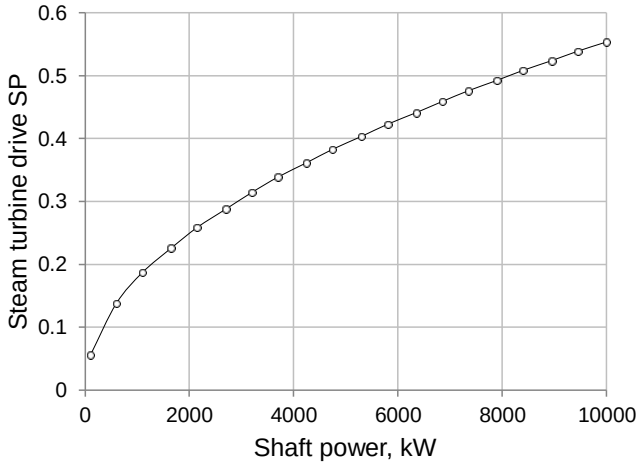

Figure 7.8 - Trend of SP for steam turbine drives in the range 100 kW - 10 MW.

Twenty points are considered with a linear spacing between 500 kW and 10 MW which is the typical range for ORC applications. In order to balance the weight of the two data sets, errors of ORC turbines are multiplied by five. The values of the regressed coefficients are reported in Table 7.6.

Term 1 $f(W)$	C_1	240000
	n_1	0.99
Term 2 $f(n_{st}, SP)$	C_2	61750
	n_2	1.06
	n_3	1.18

Table 7.6 - Coefficients for the correlation of turbine cost reported in eq. 7.8

Actual and fitted cost values are displayed in Figure 7.9. A good agreement, with maximum relative errors lower than 4%, is obtained for the selected turbines which cover a wide range in shaft power, number of stages and size parameters confirming the reliability of the proposed correlation.

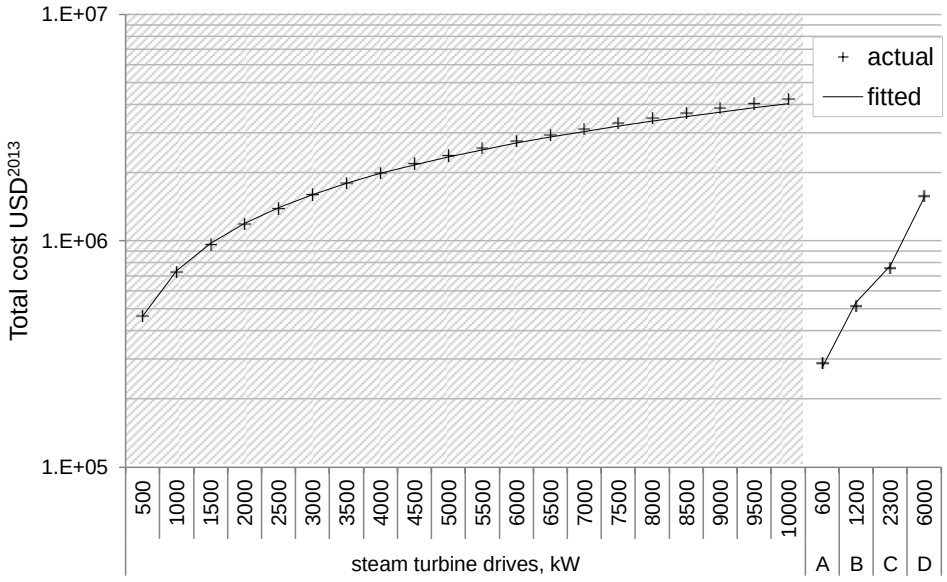

Figure 7.9 - Fitted vs actual total cost for steam turbine drives (shaded area) and ORC turbines (white area)

Finally, it is possible to analyze the total cost breakup among the two terms of the proposed correlation. Results are reported in Figure 7.10 and it is possible to note how both terms contribute to define the total cost of the turbine: relative cost for stages manufacturing is very high for low power steam turbines with a relevant number of stages, while this term gets lower for bigger devices with values close to 40% for 10 MW drives. Similar conclusions are valid for ORC turbines, where usually the cost share related to the overall project is higher due to the limited number of stages.

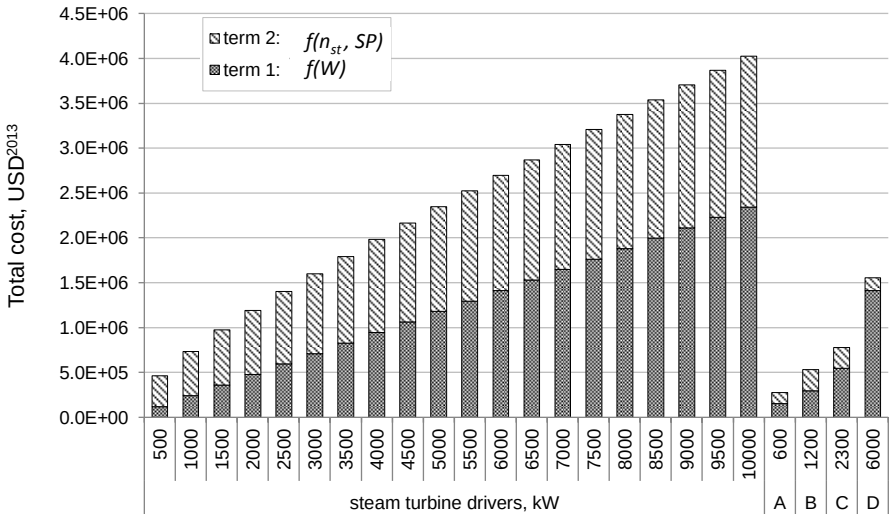

Figure 7.10 - Total cost breakup for steam turbine drives and ORC turbines.

In addition, the parametric trend of the specific cost is reported in Figure 7.11 for turbines with a different number of stages, different sizes and different shaft power. As expected, by increasing the shaft power, the specific cost is always reduced, the overall project is more expensive but it is not so challenging as for very small turbines where ad hoc components are required. The number of stages strongly affects the specific cost because it is associated to a more complicated design of the turbine with the contextual optimization of a higher number of blade profiles. Axial dimension increases, leading to manufacturing and assembly extra costs. An increase of size parameter leads higher diameters and higher costs for disks additional material and a larger blade surface to be machined.

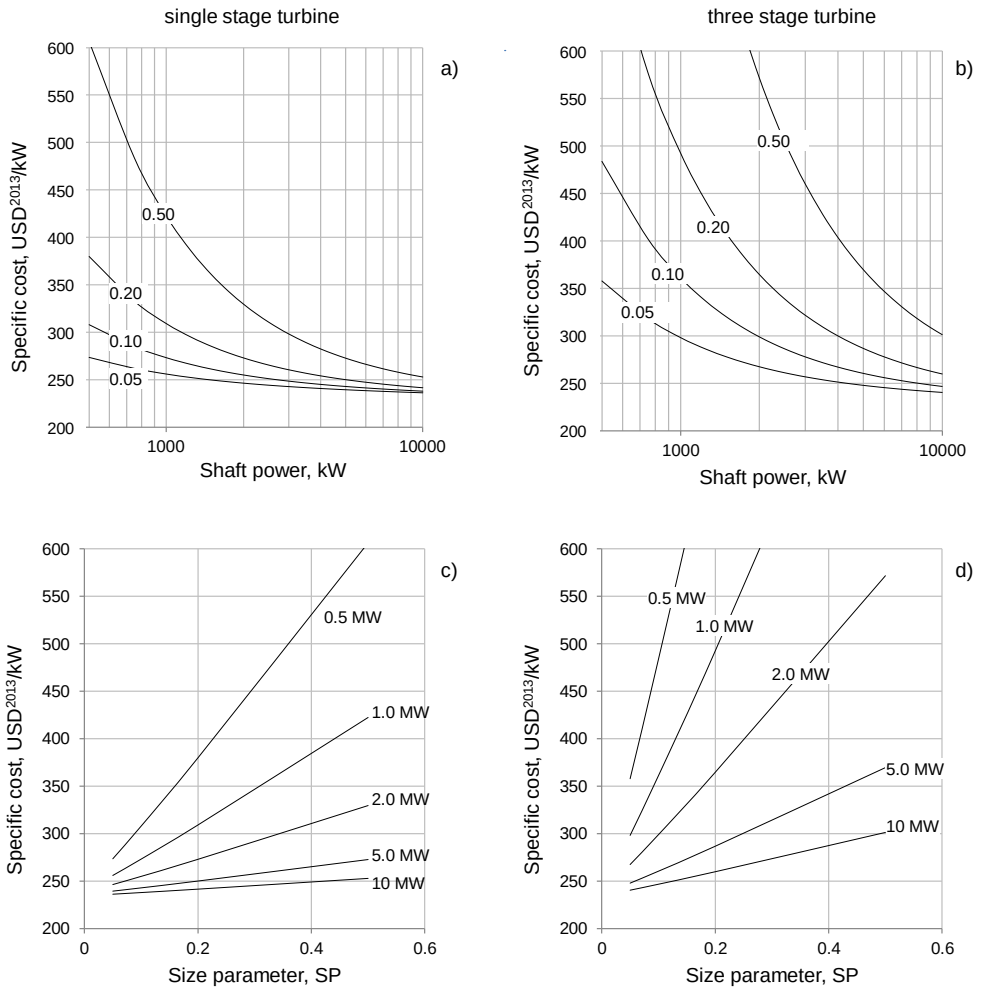

Figure 7.11 - SP based parametric trends of specific cost against shaft power for a single stage (a) and a three stage turbine (b). Shaft power based parametric trends against SP for the same two turbines(c-d)

7.3 Proposed correlations for other components

In this section the cost correlations for the other components general used in the ORC field are shortly presented.

7.3.1 Recuperator

Recuperator is usually a finned tube bundle and its cost is not correctly described by the correlation of cost of the S&T or the air cooled condensers. In addition this component is relatively specific in ORC applications while in steam Rankine cycles, where usually the turbine outlet temperature is close to the saturation one, the heating of compressed liquid is performed by regenerative bleedings from the turbine. From a confidential communication with a market leader in this field, information about a commercial device are available and the proposed correlation is expressed by an exponential law centred on the reference case. Both tubes and fins are realized in copper and no relevant cost increase is expected by adopting cupronickel tubes[12].

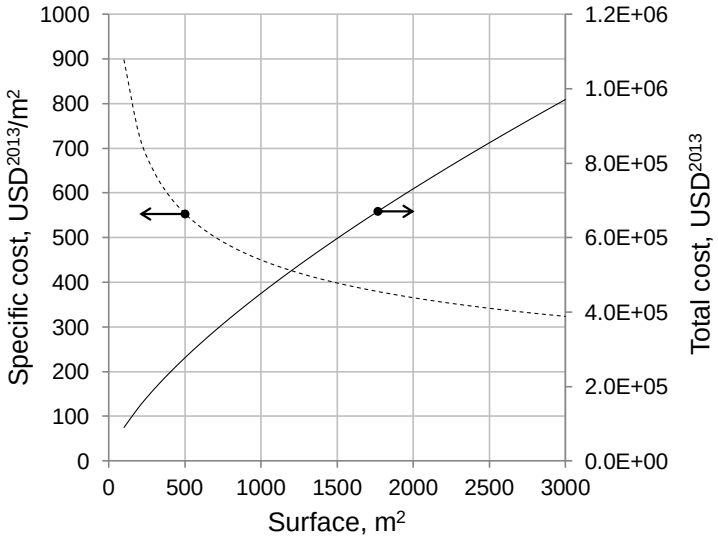

Figure 7.12 - Trend of specific cost and absolute cost for recuperator

$$C = 450000\left(\frac{A}{1000}\right)^{0.7} \qquad \text{eq. 7.10}$$

[12] The ratio between tube and fin metal masses is around 1:3 for finned surfaces area ratio of 16-17. The differential cost of adopting a cupronickel 90/10 alloy can be accounted in around 2.5% by considering that nickel cost is twice the copper one.

7.3.2 Screw expander

The correlation of cost for screw expander is derived by information about compressor cost. More than 100 data about air compressors have been retrieved by catalogues, internet online shops and personal communication with producers in a range between 3.7 and 184 kW. The cost is reported as function of the inlet swept volume ratio which is actually the variable which more affect the size and the cost of a screw compressor. From this information, the cost correlation for screw expanders is calibrated as function of the outlet volume flow rate. The trend of absolute cost and specific cost are reported in Figure 7.13 for different models commercialized by 5 companies. The effect of volume ratio on component cost is not taken into account since usually this parameter entails a different shape of the intake or discharge ports but it does not change the actual size of the device and different volume ratios can be obtained with a non-relevant impact on the device cost.

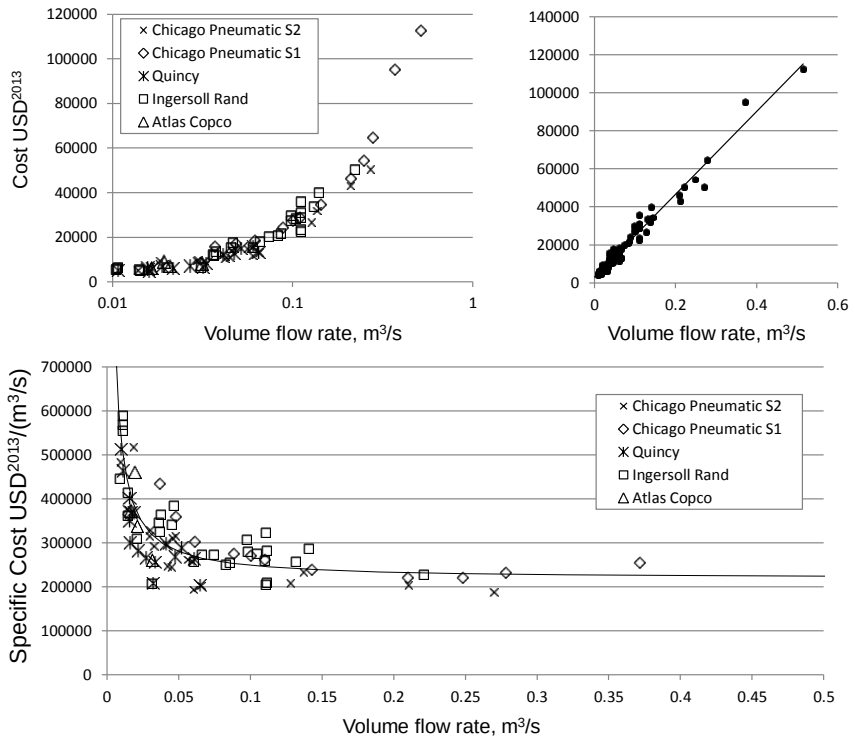

Figure 7.13 - Cost function for screw compressor/expanders. Absolute cost against outlet volume flow rate logarithm (a), fitting trend line (b) and specific cost against outlet volume flow rate (c)

Data are fitted by a linear regression with a R^2 of 0.983. the correlation for screw device cost is reported in eq. 7.11.

$$C = 3143.7 + 217423\, V_{out} \qquad \text{eq. 7.11}$$

7.3.3 Air cooled condenser

A correlation of cost for air cooled condensers ACC is proposed in both Turton and NETL reports. In addition, an exponential law is available from a previous work and centered on a nominal data obtained by a confidential communication with a leader market company. Trends of total cost and specific cost are reported in Figure 7.14 for both base cost and bare material cost. Two Turton curves are reported for ACC carbon steel and aluminum tubes.

There is a good agreement among NETL and Turton results in the range of 10-1000 m^2, while the correlation from Astolfi is well calibrated for larger heat exchanger surfaces compared to Turton upper limit. In conclusion this latter one is selected as the most reliable correlation for ACC component. The coefficients to be used in eq. 7.2 and eq. 7.3 are reported in Table 7.7 while pressure factor F_M is assumed equal to unit because correction is not applied if the pressure inside the tubes is lower than 10 barg.

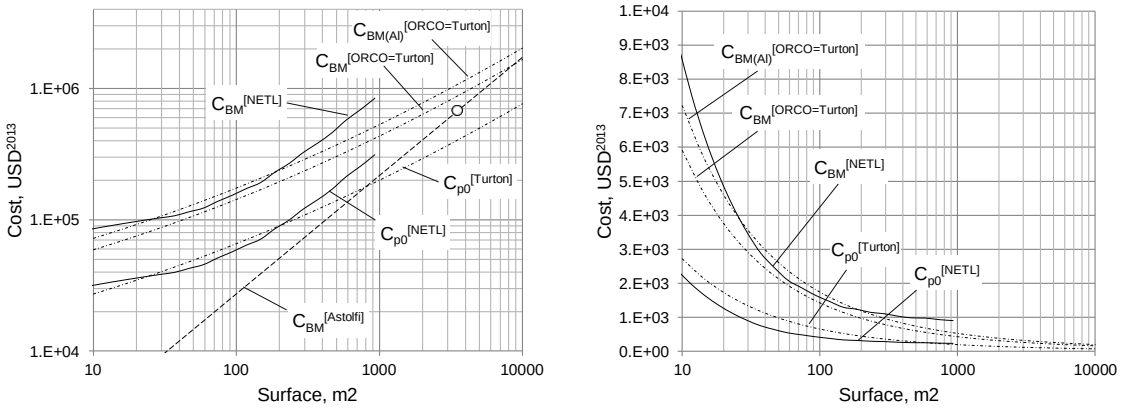

Figure 7.14 - Total cost (a) and specific cost (b) trends for ACC. The correlation used in ORCO is the Turton one

Coefficients for C_p^0	K_1	4.150806	eq. 7.2
	K_2	0.234145	
	K_3	0.049692	
Coefficients for C_{BM}	B_1	0.96	eq. 7.3
	B_2	1.21	
	F_M	1(CS) – 1.8(Al)	
Range of validity		10-10000m^2	

Table 7.7- Coefficients for ACC cost correlation

7.3.4 Pump

Costs correlation for the pump is reported in all the three considered references as reported in Figure 7.15. Perry exponential law tends to underestimate the component cost even because it does not consider the cost of the electrical drive and so it cannot be directly compared to the other correlations. The other two curves show a good agreement in both total cost and specific cost axes against shaft power. A new correlation for the bare material cost without pressure effect is calibrated, in the logarithmic form proposed by Turton. The proposed function represents both Turton data, in the very low power range, and NETL data for high power consumptions. Effect of pressure is accounted with the same approach proposed for the S&T component by using eq. 7.7. Coefficients are reported in Table 7.8.

Coefficients for $C_{BM}{}^{*}$	K_1	3.985497	eq. 7.2
	K_2	0.000294	
	K_3	0.143086	
Coefficients for F_p	C_1	-3.86967	eq. 7.7
	C_2	2.953313	
	C_3	-0.76214	
Range of validity		1kW-1MW	

Table 7.8 - Coefficients for Pump cost correlation

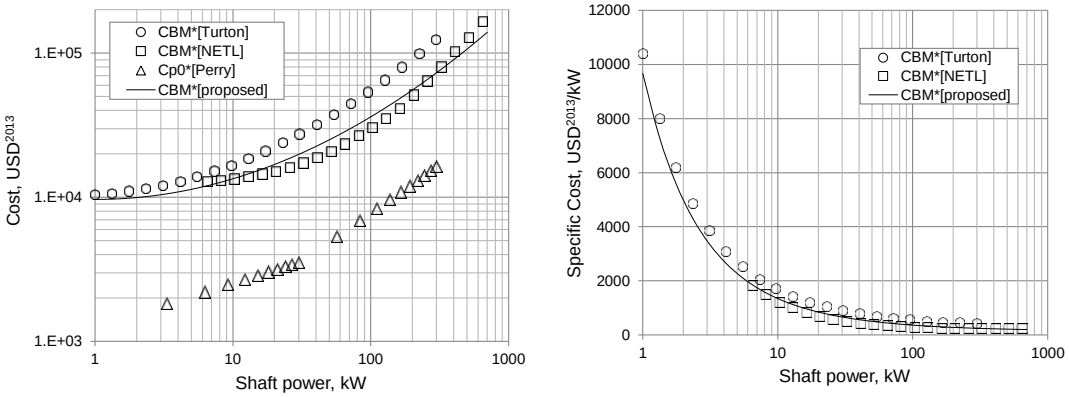

Figure 7.15 - Trends of purchase cost (a) and specific cost (b) for pump component.

7.3.5 Fan

Fans are used to blow air in the ACC or hot gases in WHR applications and, compared to the other components of an ORC, its share on the total plant cost is almost negligible. Two data series are proposed in literature and displayed in Figure 7.16. Their trends are quite different and data reported in specific cost axes show a unusual trend for high volume flow rate. This high grade of uncertainty is not really relevant because of the relatively small cost of the component and a new logarithmic correlation is proposed regressing data from literature. The regressed function fits properly the Turton data for the low volumetric flow rates while it tends to NETL results for the higher values of the considered range showing a reasonable monotonic trend. Coefficients are reported in Table 7.9.

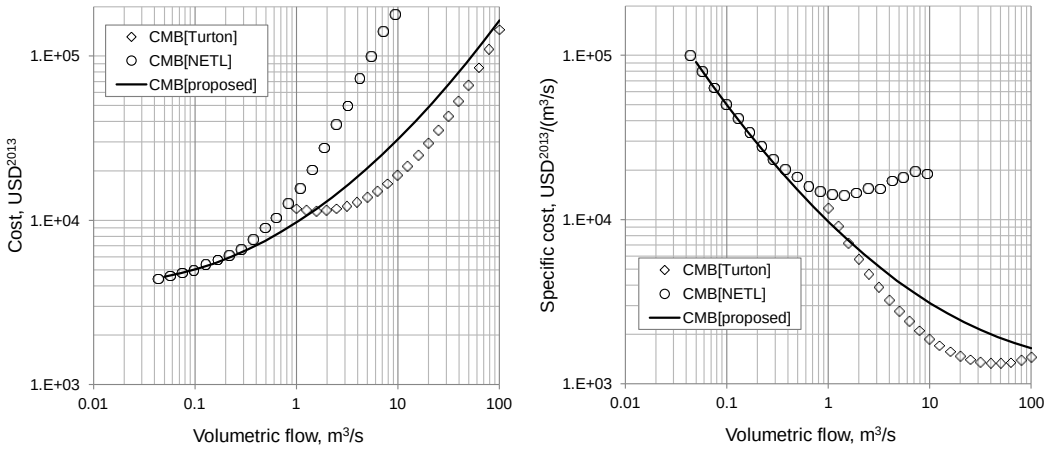

Figure 7.16 - Trends of purchase cost (a) and specific cost (b) for fan component

Coefficients for C_{BM}	K_1	3.987619	eq. 7.2
	K_2	0.396461	
	K_3	0.109338	
Range of validity		0.06-100m^3/s	

Table 7.9 - Coefficients for fan cost correlation

7.3.6 Generator and gear box

Information about electrical drives are reported in Turton for three different devices differing on cooling system. These data refer to motors and not to generators and the range of shaft power is limited to 2.5 MW. Extrapolation up to 10 MW, which is the upper limit for ORC field, might entail relevant errors in the estimation of the generator cost. In Astolfi [2] an exponential law is proposed, which is centered on a generator size equal to 5 MW while in Perry [198] two correlations for electrical motors in two different ranges of shaft power are reported but the upper limit of them is far below the typical ORC specifications. The trends of the four correlations are shown in Figure 7.17 for both total and specific cost against generator shaft power.

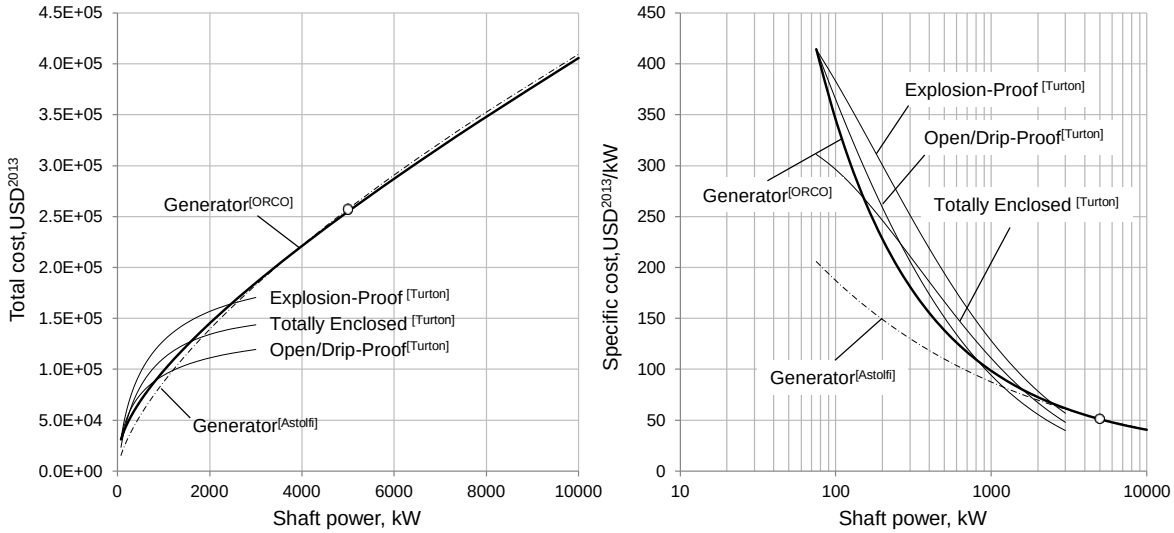

Figure 7.17 – Total cost (a) and specific cost (b) for generator component

It is possible to note that the specific cost trends are comparable even if the Turton data refer to electrical motors instead of generators. The exponential law by Astolfi tends to underestimate the cost of generator in the range below 1 MW while extrapolation of Turton trends over 3 MW results in a excessively small specific cost for big generators. A new cost function is proposed interpolating the available data in the logarithmic form reported in equation eq. 7.2. Coefficients are displayed in Table 7.10 together with gear box ones.

For gear box component no data are available in the considered references and as proposed in Astolfi gearbox is around 40% of the cost of the generator.

		Generator	Gear Box	
Coefficients for C_{BM}	K_1	4.105466	3.707701	eq. 7.2
	K_2	0.057044	0.056923	
	K_3	0.079664	0.079684	
Range of validity			80kW-10MW	

Table 7.10 - Coefficients for generator and gear box cost correlations

7.3.7 HRSG

The calibration of a cost correlation for vertical finned tubes heat exchangers like those used in HRSG unit of combined cycles is a challenging task because these components are usually customized for each single plant as function of the gas temperature, the available thermal power and the cycle configuration. Commercial catalogues are not available and all the information are retrieved manipulating data from reference and running Thermoflex software designing HRSG assembly for different sizes.

First a review on budget prices for total cost for combined cycles and gas turbines, including BOP and construction, is carried out using data reported in Gas Turbine World 2013 Handbook [206]. Here, a correlation of specific cost for simple cycle commercial gas turbine is proposed and reported in Figure 7.18 next to the trend of total cost. The curve is regressed by the logarithmic functional form proposed by Turton and the results are displayed by the solid lines.

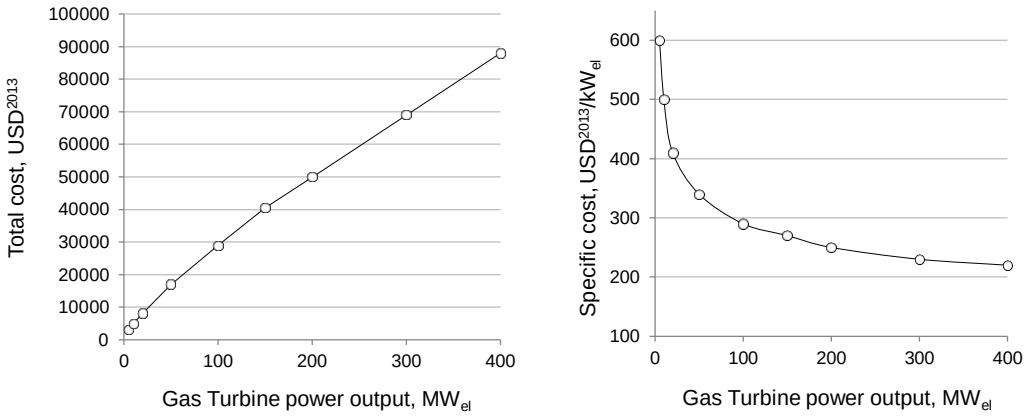

Figure 7.18 – Total cost and specific cost of gas turbine unit in simple cycle against power output

From the same reference, data regarding combined cycles cost and the share of gas turbine and steam turbine power are available. Information are collected for several combined cycles in a range of steam turbine power output between 5 MW_{el} and 30 MW_{el},

which is the range of application of ORC for WHR applications from industrial plants. By means of the cost correlation for the gas turbine previously defined, the total and the specific cost for the steam cycle are obtained. The results for 25 commercial heat recovery steam cycles are reported in Figure 7.19 in terms of total and specific cost.

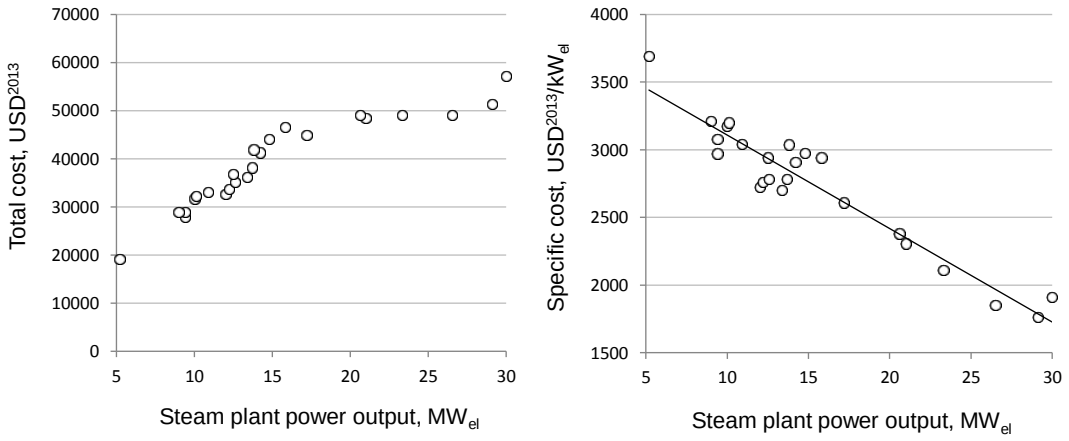

Figure 7.19 – Trend of total cost and specific cost for 25 steam cycle of commercial combined cycles in the range between 5 and 30 MWel

It is possible to note that the specific cost of the steam section of combined cycles is a decreasing function of power output in the considered range. For small plants the specific cost is higher than 3500 USD^{2013}/kW_{el} while it decreases down to 1500 USD^{2013}/kW_{el} for plants with a power output around 30 MW_{el}. These values will be used later as term of comparison for the specific cost of HRSG.

In Thermoflex, five HRSG units with the same configuration are designed for different available thermal powers. An economizer, an evaporator and a superheating section are assembled together. The hot gas temperature ranges between 385 °C and 200 °C as representative of the waste heat available from a cement production plant. Water steam is produced with a pressure of 40 bar and a maximum temperature of 360 °C assuming a pinch point temperature difference of approximately 10 °C. Four sizes are investigated between 20 and 100 MW_{th}. From Thermoflex output it is possible to obtain indication about the total cost of the HRSG unit and heat exchanger surface for each tube bank.

The specific cost of the HRSG is a decreasing function of the thermal power and it is interesting to note that reporting these values to the power output considering an average efficiency equal to 30%, values around 1500 USD^{2013}/kW_{el} result for small sizes applications and around 800 USD^{2013}/kW_{el} for bigger plants, corresponding to a share

slightly lower than the 50% of the total cost for the steam plant of commercial combined cycles retrieved from reference.

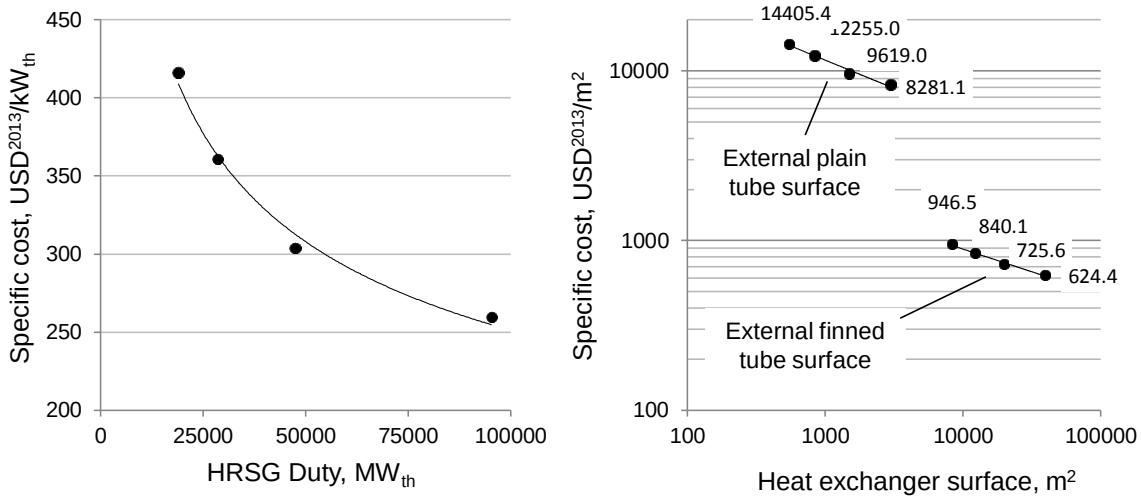

Figure 7.20 - Trend of specific cost respect to thermal power (a) and trend of specific cost respect to plain tube surface or external finned surface (b) for HRG unit designed with ThermoFlex

These values are confirmed by data reported in "Cost and performance baseline for fossil energy plants" NETL report [207] where the cost breakdown for a heat recovery steam cycle is expressed in detail. A synthesis of the costs share of HRS (excluding stack), the steam turbine, and the condenser (excluding the cooling water tower) and BOP costs is reported in Table 7.11.

	Cost USD^{2010}x1000	Share
HRSG	~44500	44.7%
Turbine	~33000	33.2%
Condenser	~6500	6.5%
BOP	~15.500	15.6%

Table 7.11 - Plant cost breakdown for the steam cycle of a big combined cycle power plant [207]

The trend of specific cost of HRSG respect to the total tube surface and the total finned surface is reported in Figure 7.20. It is possible to notice that the specific cost for square meter of heat exchanger surface is extremely high especially if referred to the plain tube outside area. This is due to the fact that in HRSG, differently of S&T heat exchanger, the tube material is just a share of the total cost. It is important to underline that using a correlation for HRSG cost related to only surface extension entails a non-realistic result in the optimization, since the algorithm will try to limit the cost of the HRSG increasing the temperature difference and leading to pinch points greatly larger than those commonly adopted for this technology. On the other hand a correlation simply related to thermal

power does not catch the effect of surface increase involving an extreme design of the heat exchangers with pinch point temperature differences pushed to the lower bound.

The suggested solution is to divide the cost of a HRSG unit in two terms, as reported in eq. 7.12.

The first term of the correlation is the tube cost material which is considered function of pressure and plain tube external surface. This correlation is defined multiplying the S&T correlation for a corrective factor which has to be calibrated. S&T cost correlation includes the cost of the tube bundle and the shell while in HRSG the shell is not present but there is and additional cost for the drum fins material. Since the area ratios commonly used in these components entails a ratio between fins mass and tube mass around 3 the correction factor to be used should be around this value. The second term is representative of the size of the casing, the insulating material and the expenses for the assembly: it is supposed to be function of the perimeter of the frontal area of the HRSG. In particular since the film heat transfer coefficient of the hot gas is assumed constant, it entails similar average gas velocity and so the HRSG perimeter is proportional to the square root of the volumetric flow. This second term is calibrated on a logarithmic function in order to fit economic data obtained by Thermoflex. Several different calibration are investigated and among them the most reasonable one has a material factor equal to five, while the coefficients for the second term are reported in Table 7.12.

$$C_{HRSG} = \sum_{\substack{eco \\ eva \\ sh}} C_1(A) + C_2(\dot{V}) \qquad \text{eq. 7.12}$$

Coefficients for C_2	K_1	6.10523	eq. 7.2
	K_2	0.00080	
	K_3	0.61496	

Table 7.12 - Coefficients for the calculation of the fixed cost of a HRSG unit

Share of the material term is around 25-30% of total HRSG cost according to Thermoflex output.

A validation of the proposed correlation is carried out designing two pressure levels and single level steam water cycles for different sizes and comparing the result with those retrieved from reference. Maximum temperature of the hot gas is set to 500°C according to small gas turbine total outlet temperature from catalogue [206] and minimum temperature is 100°C. Five plants are designed imposing pinch point and approach point

temperature differences equal to 10°C and 25°C respectively and a comparison between the obtained specific costs and the reference one are reported in Figure 7.21.

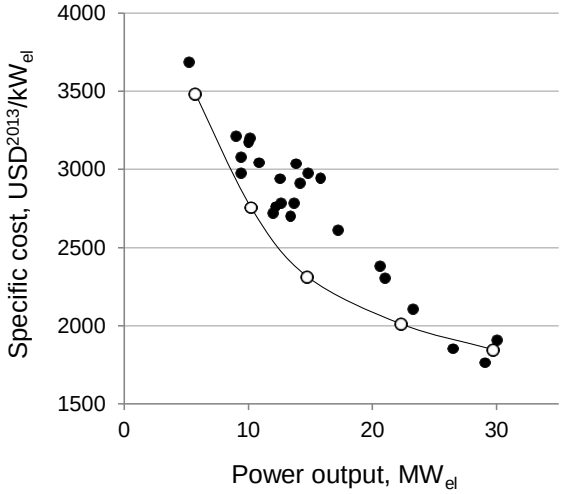

Figure 7.21 – Results obtained with the proposed correlation (solid line and white markers) are validated with the data from reference [206].

7.3.8 BOP

Balance of Plant include all the expenses for placement of the concrete foundation, the installation of the components, the piping, the measurement and control apparatus and several other expenses. BOP is usually assumed as a fixed percentage of the plant cost but since in this work different cycles are analyzed, BOP is divided in two contributions: a fixed component equal to the 15% of plant cost including all the fixed costs plus another part which depends on the number of pressure levels: in fact two pressure levels cycles requires extra costs for the additional piping and the additional instrumentation. Each pressure level accounts for another 15%.

7.4 Film and overall heat transfer coefficients

It is important to underline once again that the detailed design of a heat exchangers is not required if the aim of the study is to compare different pant designs and to select a small number of promising combinations of working fluids and cycle configurations for a given application. This approach is furthermore helpful in order to understand general trends in working cycle selection procedure and to produce approximate but realistic comparisons between different solutions. As already stated before, pressure drops can be assumed constant independently of working fluid and component size, commercial well designed heat exchangers usually show pressure drops in a relatively small range and different

constant values can be assumed for gaseous and vapor streams, liquid streams and two phase flow streams. Some more indication is reported in section 8.2.1 (Cycle definition) where the default values used in ORCO are listed. Same considerations can be done for the overall heat transfer coefficient U whose value can be accurately estimated only by knowing the exact geometry of the heat exchanger and the fluid thermodynamic and transport properties. Computational issues do not allow introducing neither an approximate sizing of the heat exchangers in an optimization routine because of the large number of additional variables and the presence of multiple local minimums even if some examples of this approach are available in literature [35]. In addition, even using the last version of Refprop, the transport properties are unknown for several working fluids typically used in the ORC field. The global heat transfer coefficient is affected by the nature of the two streams, their composition and their phase. Furthermore it is affected by heat exchanger geometry and flows directions (counter-current flow, cross flow or a mixed configuration). The availability of reliable values of U is crucial since all the cost correlations, presented in previous sections for the heat exchangers, are expressed as function of the total tubes area, which can be estimated only by assuming a reference value of the overall heat transfer coefficient. For a generic heat exchanger, the duty Q and the mean logarithmic temperature difference ΔT_{mln} can be calculated by eq. 7.13 and eq. 7.14 with reference to the general T-Q diagram reported in Figure 7.2. Heat exchanger surface A can be eventually calculated with eq. 7.15.

$$Q = m_h c_{p,h} \Delta T_h (1 - \eta_{th}) = m_c c_{p,c} \Delta T_c \qquad \text{eq. 7.13}$$

$$\Delta T_{mln} = \frac{\Delta T_1 - \Delta T_2}{\ln\left(\frac{\Delta T_1}{\Delta T_2}\right)} \qquad \text{eq. 7.14}$$

$$Q = UA\Delta T_{mln} \qquad \text{eq. 7.15}$$

The value of the global heat transfer coefficient can be obtained from reference for different types of heat exchangers or otherwise it can be estimated by knowing the two streams film coefficients, the fouling factors and the material resistivity as expressed by eq. 7.16. U can be defined respect to both the internal or the external heat exchanger surfaces whose values are relatively close for plain tubes while they appreciably differ for finned ones. Since our cost correlations are defined respect to the plain tube outside surface, the calculation of the reference global heat transfer coefficients has to be referred to this surface.

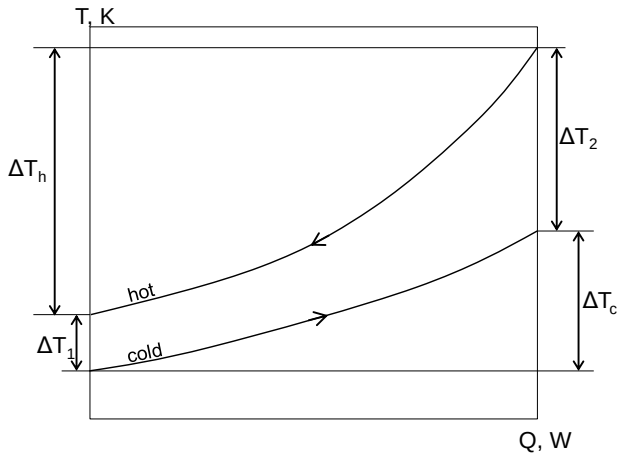

Figure 7.22 - Definition of temperature differences in a counter-flow heat exchanger to be used in eq. 7.13 and eq. 7.14

In eq. 7.16 the general formula for the calculation of U referred to the plain tube external surface $A_{ext,pt}$ is reported.

$$U = \left(\frac{1}{h_{int} \frac{A_{int,pt}}{A_{ext,pt}} \chi_{int}} + \frac{1}{h_{ext} \frac{A_{ext,t}}{A_{ext,pt}} \chi_{ext}} + \frac{R_{f,int}}{\frac{A_{int,pt}}{A_{ext,pt}}} + \frac{R_{f,ext}}{\frac{A_{ext,t}}{A_{ext,pt}}} + R_m \right)^{-1} \quad \text{eq. 7.16}$$

Where

- h_{int} and h_{ext} are the internal and external film heat transfer coefficients which are generally unknown
- χ_{int} and χ_{ext} are the film heat transfert enhanced factors which can be present if the internal or the external surfaces of the tubes presents a characteristic texture or pattern. For instance, for air cooled condenser the internal tube surface has a number of micro swirl fins in order to break the fluid boundary layer, to avoid phase stratification by keeping the liquid phase always on the tube surface, to increase the turbulence and in conclusion improve the heat transfer process by a factor which can be in the range of 2-5.
- $A_{int,pt}$, $A_{ext,pt}$ are the internal and external plain tube surfaces while $A_{ext,t}$ is the actual outside heat transfer, which accounts for the presence of fins. The ratio of $\frac{A_{int,pt}}{A_{ext,pt}}$ is usually around 0.87 while the value of $\frac{A_{ext,t}}{A_{ext,pt}}$ is equal to unit for plain tubes and it can reach values up to 14 for finned tubes.
- $R_{f,int}$ and $R_{f,ext}$ are the fouling resistance coefficients which account for the fouling deposition during operation. R_f depends on the fluid type, the content of

salts, particles or dust and usually an average value between two cleaning cycles is assumed as representative of in-service operation.

- R_m is the material resistance which can be usually neglected because of the very small contribution to the overall resistivity.

The goal is to estimate a suitable value of the film heat transfer coefficient h for all the fluid streams which generally interest ORC field in order to be able to calculate the global U for all the different applications. Unfortunately is not easy to retrieve a reference film heat transfer coefficient for non-conventional fluids like condensing and boiling hydrocarbons, and values where reported are defined in a large range of values [208; 209; 210]. On the other hand values of U for different applications can be collected from literature [211; 210] and some characteristic values for the global heat transfer coefficient can be collected for several combinations of hot and cold fluid types in S&T heat exchangers. These values are referred to the outside plane tube surface but in all the references the location of hot and cold fluid is not expressed, entailing an additional uncertainty. Furthermore they are representative of in-service operation after the fouling process has already been taken place and so, resistivity coefficients are required in order to retrieve the values of internal and external film coefficients.

Fouling resistivity coefficients for different fluids are reported by TEMA standards [205] and Perry chemicals [198]. In Table 7.13 the in-service average U values for different primary heat exchangers are reported while in Table 7.14 the same quantity is reported for condenser units. R_f values are displayed in Table 7.15.

W/m^{2}K		Hot stream		
		Water	Oil	Gas
Cold stream	Organic liquid	600	500	99
	Organic boiling	600	500	99
	Organic vapor	500	400	93
	Water liquid	950	700	105
	Water boiling	900	675	105
	Water vapor	500	400	93

Table 7.13 – Averaged global heat transfer coefficients for different combination of fluids in S&T heat exchangers with plain tubes for PHE [211]

W/m^{2}K		Hot stream			
		Organic vapor	Organic condensing	Water vapor	Water condensing
Cold stream	air	765	105	1200	105
	water	100	55	107	55

Table 7.14 - Averaged global heat transfer coefficients for different combination of fluids in S&T heat exchangers with plain tubes for condenser [211]

fluid	R_f m^{2}K/W
Distilled water	0.00009
Organic fluid	0.00018
Oil	0.00018
Brine	0.0004
Exhaust gas	0.0015
Air	0.00035

Table 7.15 – Fouling resistance coefficients for different fluids

By minimizing the error on the average U it is possible to estimate the values of h for each single stream. The retrieved values are reported in Table 7.16. Hot streams are always placed in shell side while working fluid flows into the tubes. Plain tubes are considered according to reference specifications.

stream	U W/m^{2}K
Water liquid	7500
Water boiling	7000
Water vapor HP	800
Water condensing	10000
Water vapor LP	125
Organic liquid	1900
Organic boiling	1900
Organic vapor HP	600
Organic condensing	2500
Organic vapor LP	125
Oil	1000
Brine	2200
Exhaust gas	125
Air	125

Table 7.16 – Regressed values of film heat transfer coefficients for different fluids commonly used in ORCs

The average values obtained can be compared with other data from reference in Figure 7.23 and it can be noticed how all the proposed values are within the range defined by literature.

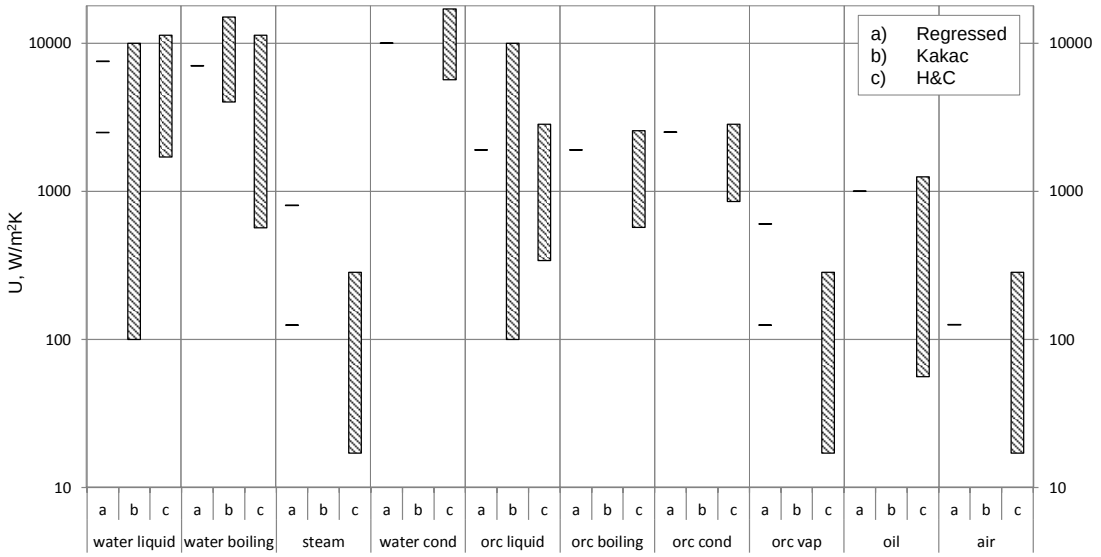

Figure 7.23 - Comparison between regressed values of film heat transfer coefficients (h) and ranges from literature

Finally the calculated values of U for different heat exchangers are reported in Table 7.17 and Table 7.18. Area ratios are assumed respectively equal to 0.87 for internal tube surface, 3.7 for low finned tube in S&T heat exchangers, 12 for WHR finned tubes and 14 for finned surface of ACC and recuperator. An internal texture is adopted in ACC tubes in order to enhance the film heat transfer coefficient.

7.5 Extrapolation outside of validity range

A correlation of cost is defined for every component of a generic ORC system on the basis of the available literature. The proposed correlations are valid within a certain validity range and extrapolation should be done with careful. In particular, the use of logarithmic functions for sizes below the lower bound might entail a stronger over estimation of component cost. For example, the specific cost predicted by the proposed correlation of a S&T heat exchanger having a surface of 5 m^2 is more than 17000 USD^{2013}/m^2, which is a value excessively high. The proposed approach is to use the general correlation in the validity range, while to apply an exponential law otherwise. The reference point for the correlation is the lower or the upper bound depending on the direction of the extrapolation. Two different exponents are considered: for extrapolations below the lower bound a value of 0.67 is assumed, representative of typical size economies for components manufacture. For extrapolations above the upper limit the exponent is equal to 0.9, since the increase of capacity is obtained with the use of a higher number of devices in series or parallel configuration. An example of the extrapolation for S&T heat exchanger is reported in figure where it is possible to highlight the differences

between the use of the logarithmic correlation outside of the limit and the use of an exponential function.

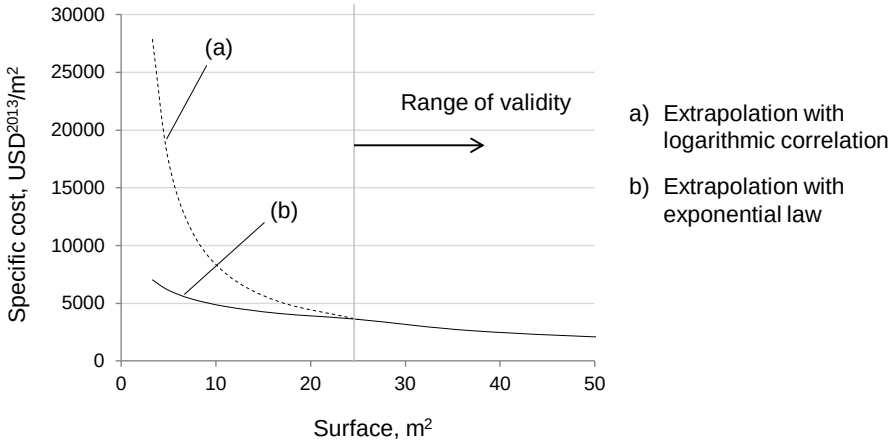

Figure 7.24 - comparison between extrapolation outside the range of validity using the general correlation (dashed line) or with an exponential law (solid line)

7.6 Cost of the fluid

Working fluid purchase is not considered in this work because it requires the estimation of the volume of the plant and a preliminary sizing of the heat exchangers and the piping. This level of detail, as already explained in Section 2.1.3 (System optimization), is beyond the aim of this work but some information about the economic issues related to the use of different fluids are here reported.

From personal communications with companies and organic fluid producers the following aspects can be highlighted:

- The share of the working fluid cost on the total plant cost is not always negligible and it can reach 10% of the plant cost, without BOP, if a non-flammable and non-toxic fluid is used.
- Main cost difference is between flammable and non-flammable fluids: flammable fluids, namely all the linear and cyclic alkanes cost around 2.5 USD^{2013}/kg while the other ones, like refrigerant fluids cost at least 15 USD^{2013}/kg. R134a is the only exception because it is a fluid produced in large amount and it cost is around 5 USD^{2013}/kg. Heavy perfluorinated fluids instead are extremely expensive (more than 100 USD^{2013}/kg) since are usually sold in small quantities and their market is limited.
- Another difference is the density of these compounds, flammable fluids are relatively light (~ 600kg/m^3) while fluorinated compounds have a density which is

approximately twice than hydrocarbons entailing for the same plant volume a higher amount of fluid. The hypothesis of constant value is almost correct when kettle reboilers and pool condensing heat exchangers are used but cannot be always applied, for instance if a for supercritical cycle is used.

- Using a non-flammable fluid (e.g. R245fa vs pentane) leads to a cost for the working fluid at least twelve times more than using a flammable fluid, with a relevant impact on power block economics. On the other hand the use of flammable fluids requires additional safety protection, an expensive anti-fire system and additional authorizations which make the whole project more expensive. Nevertheless these additional costs are generally not so high to level off the economic advantage of using a cheaper fluid. All these considerations are strongly site dependent and additional costs greatly vary from country to country and a general conclusion cannot be achieved. For example in Europe a series of strict normative, the 96/82/EC and the 2012/18/UE also called Seveso II-III Directives[13], regulate the use of flammable and toxic compounds in industrial field. As a result, the installation of ORC using dangerous working fluids is strongly discouraged and requires a longer authorization process, it has to face the NIMBY reactions by the population and needs more expensive equipment. The only exception is the binary geothermal power plants in Italy, which are excluded from the Seveso Directive from July 2013.

[13] The Seveso directive was adopted by EU after the Seveso disaster in 1976 which interested a small chemical plant in the north of Italy. A relevant amount of TCDD, an extremely toxic compound (NFPA Healthy 4) was released in the environment causing an frightening exposure in population.

	fluid		side		h, W/m^{2}K		Fouling, m^{2}K/W		A ratio		Enhancement F		U, W/m^{2}K
	hot	cold	hot	cold	hot	cold	hot	cold	hot	cold	hot	cold	
PHE S&T	Brine	Water L.	Tube (p. t.)	Shell (p. t.)	2200	7500	0.0004	0.00009	0.87	1	1	1	829.15
		Water B.				7000							822.65
		Water V. HP		Shell (l. f. t.)		800				3.7			743.56
		ORC L.		Shell (p. t.)		1900		0.00018		1			592.05
		ORC B.				1900							592.05
		ORC V. HP		Shell (l. f. t.)		600				3.7			674.84
PHE S&T	Oil	Water L.	Shell (p. t.)	Tube (p. t.)	1000	7500	0.00018	0.00009	1	0.87	1	1	695.97
		Water B.				7000							690.71
		Water V. HP	Tube (p. t.)	Shell (l. f. t.)		800			0.87	3.7			581.68
		ORC L.	Shell (p. t.)	Tube (p. t.)		1900		0.00018	1	0.87			501.94
		ORC B.				1900							501.94
		ORC V. HP	Tube (p. t.)	Shell (l. f. t.)		600			0.87	3.7			538.76
PHE WHR	Exhaust gas	Water L.	WHR (f. t.)	Tube (p. t.)	125	7500	0.0015	0.00009	12	0.87			953.74
		Water B.				7000							943.88
		Water V. HP				800							428.69
		ORC L.				1900		0.00018					623.47
		ORC B.				1900							623.47
		ORC V. HP				600							343.01

Table 7.17 - Hypothesis and definition of the global heat transfer coefficient in PHE for different combinations of hot and cold fluid

	fluid		side		h, W/m^{2}K		Fouling, m^{2}K/W		A ratio		Enhancement F		U, W/m^{2}K
	hot	cold	hot	cold	hot	cold	hot	cold	hot	cold	hot	cold	
COND ACC	Water C.	Air	Tube (t. t.)	Bank (f. t.)	10000	125	0.00009	0.00035	0.87	14	4	1	1372.35
	Water V. LP				125								303.13
	ORC C.				2500	125	0.00018						1088.82
	ORC V. LP				125								303.13
COND S&T	Water C.	Water L	Tube (p. t.)	Shell (p. t.)	10000	7500	0.00009	0.0004	0.87	1	1		1330.08
	Water V. LP				125								98.66
	ORC C.				2500		0.00018						833.1019
	ORC V. LP				125								98.66
REC	Water V.	Water L.	Bank (f. t.)	Tube (p. t.)	800	7500	0.00009	0.00009	14	0.87	1	1	2836.50
	ORC V.	ORC L.	Bank (f. t.)	Tube (p. t.)	600	1900	0.00018	0.00018					1059.13
TOP	Exhaust gas	Oil	WHR (f. t.)	Tube (p. t.)	125	1000	0.0015	0.00018	12	0.869565	1	1	465.40

Table 7.18 - Hypothesis and definition of the global heat transfer coefficient in condenser, recuperator and WHR heat exchanger for different combinations of hot and cold fluid

"Art and science have their meeting-point in method"

Edward Bulwer-Lytton

8 Analysis approach and code structure

In this chapter the comprehensive approach at the basis of this thesis work is presented with all the features implemented in ORCO (Organic Rankine Cycle Optimization) software for the systematic techno-economical optimization of ORC systems.

8.1 Analysis approach

For a given heat source the optimal combination of working fluid, plant layout and cycle parameters have to be defined. Cycle parameters like the evaporation and the condensation temperatures and the pinch point temperature differences in the heat exchangers are optimized by an opportune routine while the investigation of different combination of working fluid and plant layout is faced with an exhaustive approach. In order to reduce the number of cases to be examined by a brute-force search it is sufficient to examine for each fluid only one cycle configuration for each class[14] letting the optimization routine free to suppress or to inhibit a certain component. In example, for two pressure levels cycles, it is possible to have a superheating on both levels and to use a recuperator but is not necessary to explore eight different cycle configurations because it is sufficient to optimize the most comprehensive one. If the use of some component is detrimental in terms of power production maximization or LCOE reduction it is automatically excluded from the final solution, and the only difference between the achieved solution and the actual optimal one are the additional pressure drops of the inhibited components. An example about this aspect is reported in Section 9.1.1 (Algorithm selection for thermodynamic and techno/economic optimization) where a two pressure levels cycle working with pentane is optimized from a thermodynamic point of view leading to the exclusion of both superheaters.

[14] With reference to Chapter 5 (Thermodynamic cycle configurations) cycle configuration can be classified in four groups: 1 pressure level cycles (both subcritical and supercritical), two pressure levels cycles and flash trilateral cycles.

In Figure 8.1 the basic scheme of the suggested approach is presented.

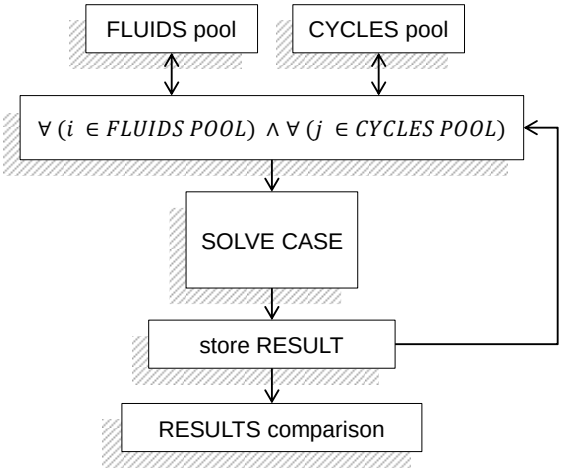

Figure 8.1 - basic scheme of the methodology used in ORCO: all the possible combinations of working fluid and cycle layout are investigated and final results are compared with the aim of defining the best cycle configuration for each working fluid and the best global solution.

8.2 Code structure and case resolution

The scope of this section is presenting the ORCO software and its features. All the information about some code details, even already mentioned in the previous chapters, are here briefly reported in order to give an general presentation of the code.

ORCO is able to perform both techno-thermodynamic and techno-economic optimizations of ORCs, analyzing several cycle configurations and using as working fluid many different pure fluids and mixtures. The basic steps for the initialization of ORCO and the main stages of code execution are reported in Figure 8.2. Details regard each stage are further reported.

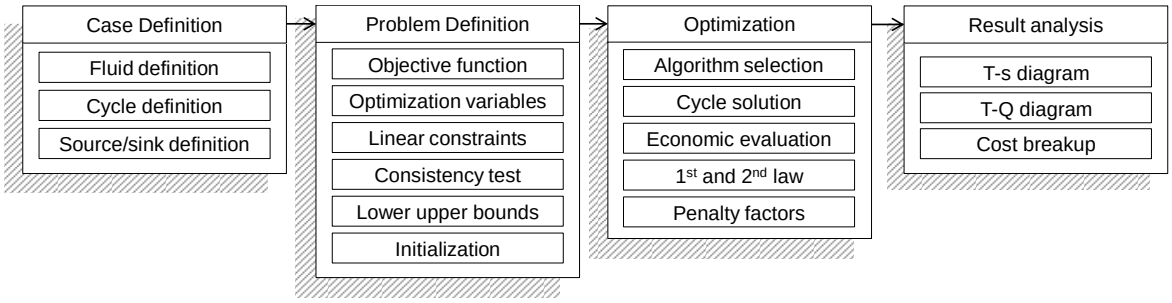

Figure 8.2 - Steps required for ORC initialization and execution

8.2.1 Case definition

First ORCO requires the definition of both working fluid and cycle configuration. In addition, all the fixed parameters like components efficiency, pressure drops and characteristics of the hot and cold stream are defined in order to completely described all the boundaries of the investigated case.

Fluid definition

Refprop 9.1 [106] database is integrated in ORCO tool, allowing the use of many different working fluids and their mixtures. Refprop is the definitely the most reliable software for the estimation of fluid thermodynamic properties because of the high accuracy of the equation of state and the good stability of the saturation routines. It is developed by the NIST (National Institute for Standards and Technology) and it implements multi-parameter equation of state in reduced Helmotz energy form. This family of equation of state was first proposed by Span and Wagner [212; 213; 214; 215] and further improved by Lemmon with the introduction of new terms and a better calibration of equation coefficients [216; 217]. The equations of state in Refprop are always up to date and the calibration of parameters is constantly revised on the basis of new publication and new data available from experimental campaigns. More than 120 pure fluids and more than 70 pre-implemented mixtures are available in Refprop database and, furthermore, any user define mixture can be created. Most of the available pure fluids can find application in ORC field and the complete list is reported in Table 4.3 and Table 4.4. No relevant issues about the use of Refprop is reported except for calculation of thermodynamic properties in some regions of the state diagram where the routines are more unstable and fail to reach the convergence; these areas are usually close to critical point and for very low pressures in two phase region. In most of the cases instability is due to internal tolerance criteria or maximum number of iterations and usually this problem can be dodge changing the set of input variables. Another issue is related to the lack in transport and physic properties, like conductivity and viscosity, which are not defined for all the available fluids due to scarcity of experimental data. This is a problem which has to be faced if the code will be extended with an evaluation of film transfer coefficient depending on the working fluid.

Some more recommendations are required if a new mixture is selected. Refprop implements the GERG-2004 [218] mixing coefficients have been already set for many different combination of fluid in mixture and these parameters can be reasonably extended to other similar blends. In particular Refprop shows a good accuracy for mixtures of hydrocarbons and more in general for mixtures of fluids chemically similar.

On the other hand in cases where two very different fluids are mixed together, the lack in well calibrated interaction coefficients leads to instability of saturation routine and relevant errors in the evaluation of chemical equilibrium especially in phase transition. A validation of Refprop results on the basis of experimental data from literature is crucial in order to limit the analysis to those mixtures which are well described. Two examples are proposed, the first one is a mixture of ethane and butane representative of a blend of compounds chemically similar: both of them are linear hydrocarbons and almost non-polar molecules. The second one instead, reported in section 9.2 (Use of mixtures for Biomass plants), is a mixture characterized by a light and simple molecule, the ethanol, having atoms with free electron pairs and the possibility to create hydrogen bounds, and an aromatic hydrocarbon, the toluene. The results for the mixture of ethane and butane are compared with experimental data collected from four different publications [219; 220; 221; 222] reporting data of seven isothermal VLE (Vapour Liquid Equilibrium) diagrams. A graphical summary is proposed in Figure 8.3 and it is possible to notice the good accuracy of Refprop calculation even for temperatures higher than the critical temperature of pure ethane (32.17°C).

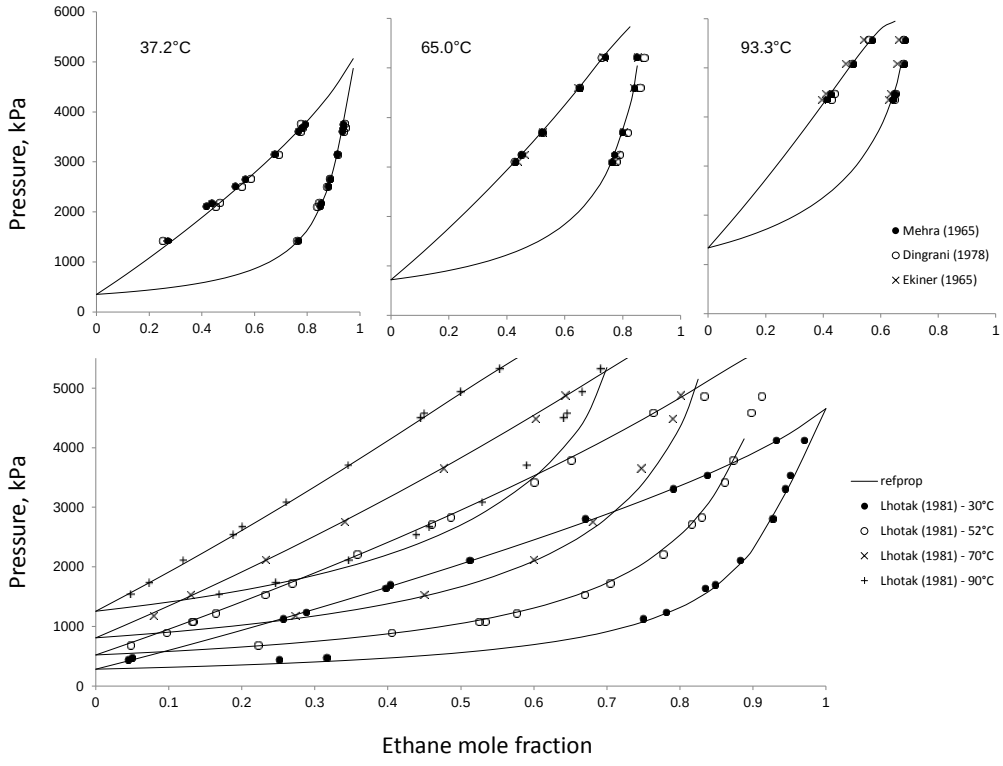

Figure 8.3 - Comparison between Refprop results and experimental data for a mixture of ethane and butane on seven isothermal VLE diagrams from 30°C and 93.3°C.

Cycle definition

With ORCO all the cycle configurations described in Section 5 (Thermodynamic cycle configurations) can be investigated. The user can easily customize any desired thermodynamic cycle simply acting on a series of parameters which are briefly listed in Table 8.1.

Parameter	options	note
Cycle Configuration	One pressure level cycle Two pressure levels cycle Flash trilateral cycle	Three general configurations are defined because they require different steps for the thermodynamic cycle solution
Type of Pressure Level	Subcritical Subcritical once-through supercritical	(ECO+ EVA+SH) → ΔT_{sc} is considered Single PHE → $\Delta T_{sc} = 0$
Turbine admission	Saturated vapour Superheated vapour Throttled Saturated liquid	ΔT_{sh} is equal to zero ΔT_{sh} is defined by the user or the optimization routine Throttling from saturated liquid to saturated vapour (CFC) Two phase flow expansion → triangular cycle
Recuperator	Yes No	Recuperator can be used in both pressure levels if the turbines are placed in series
Expander type	Axial turbine Screw expander	See section 6.1 (Axial flow turbines) See section 6.2.3 (Screw devices)
Expander efficiency	Fixed Calculated at 50 Hz Calculated at opt. RPM	- - Used only for axial turbines
Turbines configuration	Series Parallel	Only for two pressure levels cycle
Superheating constraint	Yes No	Only for two pressure levels cycle: LP superheating is constrained to HP turbine outlet

Table 8.1 - List of ORCO parameters for definition of the cycle configuration

Furthermore the user has to define the matching with the heat source, this parameter does not affect the design of the thermodynamic cycle which is completely defined by the over mentioned variables, but it allows exploring three different cases:

- *Direct heat introduction*: the heat is directly introduced to the working fluid, no HTF (Heat Transfer Fluid) and no additional heat exchangers are required. An example is a direct concentrating solar power plant where the working fluid flows in the solar field collector tubes.

- *Binary$_{1L}$ (single level heat introduction)*: the thermal power is released by a hot fluid. Typical examples are geothermal power plants, solar power plant where an opportune HTF is used into the solar field and direct WHR from hot gases.
- *Binary$_{2L}$ (two levels heat introduction)*: if the thermal power is transferred from a high temperature stream to a medium temperature fluid, which one eventually releases heat to the ORC. Biomass combustion is an example of this configuration since a loop of synthetic oil is commonly used to transfer thermal power from the biomass boiler to the ORC.

Plant layout schemes and T-Q diagrams are reported in Figure 8.4 to give a graphical representation of the difference between the three heat source matching options. The cooling stream in the condenser is labeled as BS (Bottom Stream) while the hot streams are named respectively as MS and TS (Medium Stream and Top Stream).

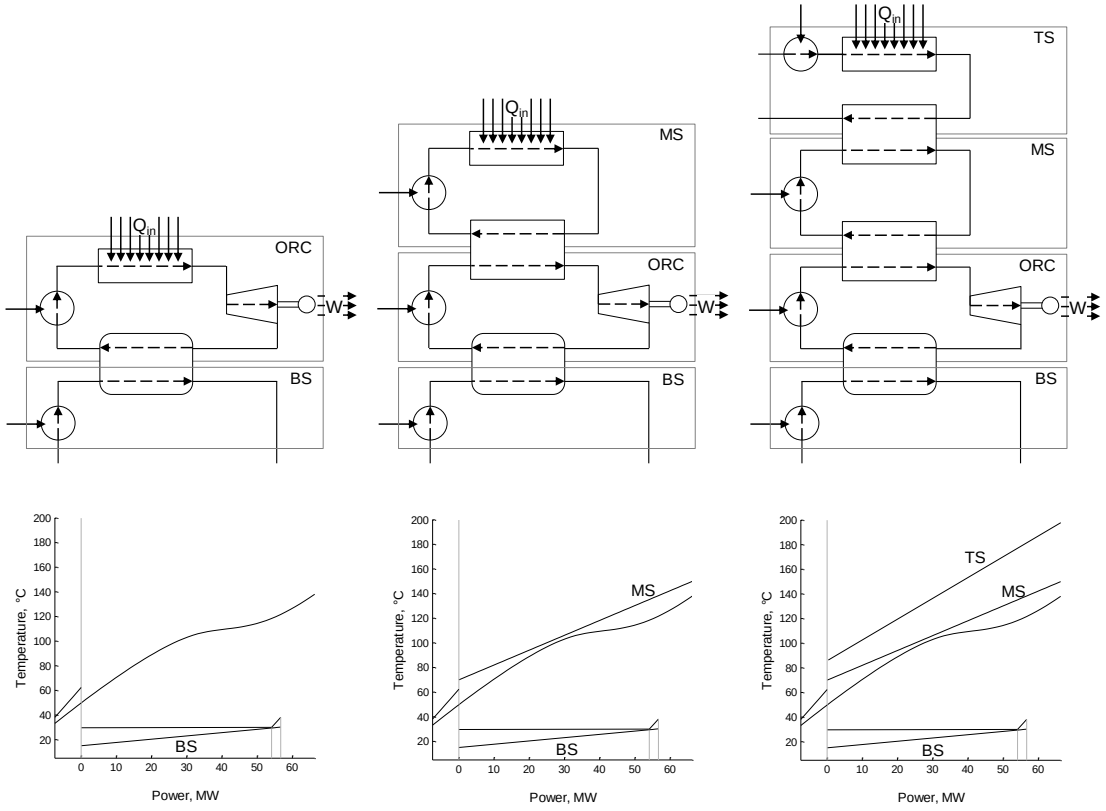

Figure 8.4 - Three different matching options with the heat source. (a) direct heat introduction, (b) binary (one level): heat is released to the ORC by a medium temperature stream (MS), (c) binary (two levels): if the MS is an intermediate temperature stream and the heat is provided by a higher temperature stream (TS)

Acting on cycle design variables the user can easily define more than 100 different plant layouts.

At this stage all the fixed pressure drops and the efficiencies for each component are defined. Pressure drops are constant in the present study because, as already stated in section 2.1.3 (System optimization), the introduction of the design of each heat exchanger inside of the optimization routine leads to doubtful results, due to a more complex problem which is affected by a larger number of optimization variables, by the presence of multiple local minimum and very different weights of the design parameters on the final solution. In addition, an optimization of this type is not compatible with the scope of this work: ORCO is realized with the aim to help ORC designers in selecting the most suitable combination of working fluid and cycle configuration. At this level of detail it is reasonable to consider well designed heat exchangers with comparable pressure drops [211]. An absolute pressure drop is considered for all liquid streams while a relative pressure drop is considered for vapor ones. For two phase flow components, namely the evaporators and the condenser, the pressure drop is defined by means of an equivalent temperature drop.

In addition the efficiency of most of the components, like the generator and the pumps, can be considered independent of the size of the plant, the application and the working fluid. Main assumptions about component efficiency and pressure drops set as default in ORCO are reported in Table 8.2.

The turbine efficiency is fixed only in preliminary calculations while in the final results expander performance should be always computed. Furthermore with an axial flow turbine an additional constraint related to the expansion region is introduced: turbines are not design to work with two phase flow, the presence of droplets at the peripheral velocities of commercial machines involve hammering and damaging of blade surfaces with a more probable detachment of boundary layer and an overall low efficiency of the turbine stages interested by the phenomenon. The maximum fraction of liquid allowed is 0.07 and a correction of efficiency is applied for stages working with a vapor quality lower than unit.

Last parameter to be defined is the overall constraint of the plant, namely the fixed variable which determines the size of the plant. A fixed value can be defined for the mass flow rate of working fluid or for one of the mass flow rates of the hot streams; otherwise it is possible to fix the gross power of the turbine, the net power of the thermodynamic cycle or the available thermal power from the heat source. All the other absolute quantities are determined on the basis of this parameter.

Temperature and pressure drops	
ΔT_{cond}	0.3°C
Δp_{des}	1%
Δp_{eco}	50kPa
ΔT_{eva}	1°C
Δp_{sh}	2%
Δp_{SHE}	5%
$\Delta p_{rec,HS}$	2%
$\Delta p_{rec,CS}$	50kPa
ΔT_{sc}	1.5
Heat losses from heat exchangers	
Q_{loss}	0.01
Component efficiency	
$\eta_{is,turb}$	0.85
$\eta_{mec,\ turb}$	0.97
$\eta_{el,\ gen}$	0.98
$\eta_{gear\ box}$	0.97
η_{pump}	0.70
η_{fan}	0.70
$\eta_{mec,\ pump/fan}$	0.98
$\eta_{el,\ mot}$	0.97
constraint	
Max quality along expansion 0.93	

Table 8.2 - Main fixed assumptions in ORCO related to pressure drops, heat exchangers heat losses and components efficiency.

Heat sources and heat sink definition

This stage is fundamental in order to properly define a certain case study and it requires the characterization of both hot and cold sources and all the cycle design parameters which are not interested by optimization. As already mentioned in section 3.4 (Typical heat source temperature profiles and limits) all the streams except the working fluid are described with an incompressible liquid or an ideal gas model depending on the nature of the fluid. In particular for all the cases analyzed in further sections five different streams are considered as reported in Table 8.3. Data for HTF are retrieved by Dowtherm catalogue [223] while for geothermal brine information are obtained from scientific publication [113] technical reports [224; 225].

For each stream the user has to define the inlet temperature, the sink temperature, the sink pressure and the pressure drops in heat exchangers and heat introduction processes in order to properly evaluate the auxiliaries power consumption.

	model	Cp, kJ/kgK	ρ, kg/m^3	MM, kg/kmol	T_{sink}, °C
Cooling water	(1)	4186	1000	18	T_{amb}
Geothermal brine	(1)	3800-4250	880-1200	18-20	$T_{lim,brine}$
HTF synthetic oil	(1)	1500-2500	1000-600	100-200	$T_{lim,oil}$
Cooling air	(2)	1000	1.2	28.9	T_{amb}
Hot gases	(2)	1200	1.3	31	$T_{lim,stack}$

Table 8.3 – Typical non-working fluids available in ORCO and their properties. (1) refers to incompressible liquid model while (2) to the ideal gas model. Any new fluid can be defined by the user.

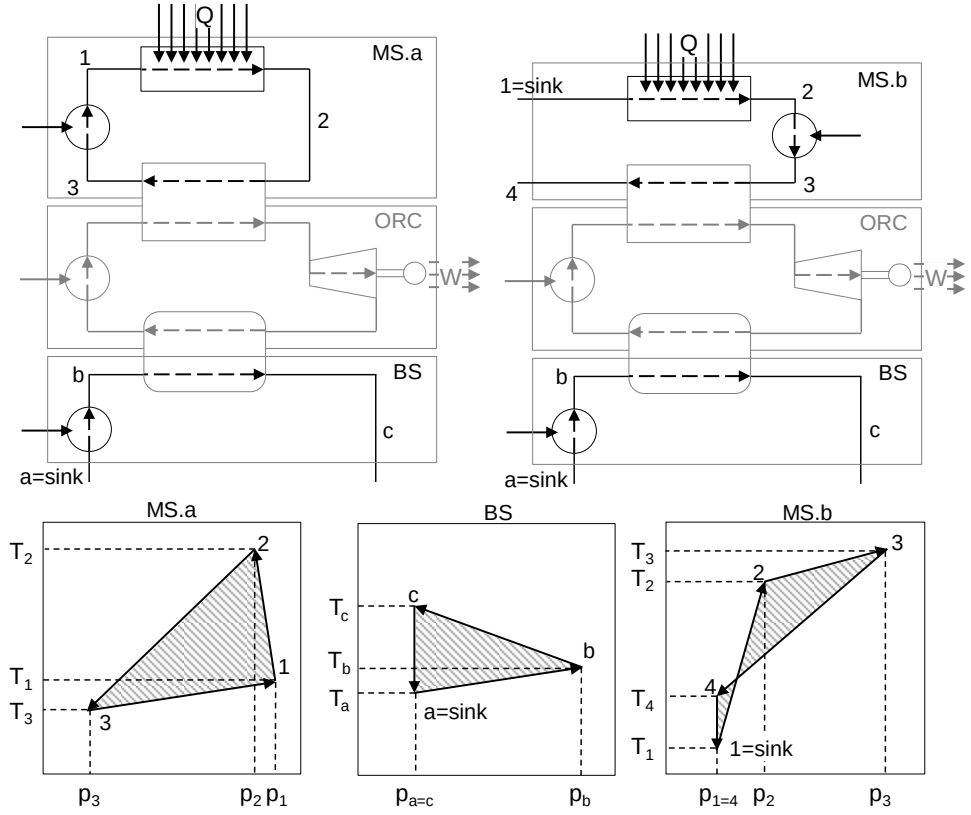

Figure 8.5 - Loop circulation of the medium temperature stream in a solar power application (a) and free circulation in a geothermal case. T-P diagrams are representative of a medium temperature stream in loop circulation (c1), the bottom stream (c2) and a medium stream in free circulation(c3)

The sink temperature for a certain stream has a different meaning depending on the plant configuration and the final design obtained from the optimization. For bottom streams, like cooling water or cooling air, the sink temperature is equal to the ambient temperature and the stream, after leaving the condenser, is brought back to ambient conditions by means of a mixing process. For hot sources, instead, this parameter has a dual meaning depending on the type of fluid circulation. In *free circulation* mode the fluid minimum temperature is constrained to the sink temperature but, if the fluid leaves the last heat

exchanger of the ORC with an higher temperature, it is cooled down by a mixing process to the sink value. This is a typical case for geothermal brines or hot flue gases. On the other hand if the fluid is in *loop circulation* the sink temperature is simply the fluid temperature lower bound. The fluid after being cooling down in the PHE is sent back to the system without any additional cooling. This case is representative of a solar power plant where the HTF fluid is heated in the solar field and releases heat to the working fluid in a loop circulation. The representation of the two circulations in the T-P diagram is reported in Figure 8.5 with reference to a solar and a geothermal energy exploitation.

8.2.2 Optimization Problem Definition

Any different cycle configuration is optimized by a suitable numerical algorithm which acts on a set of optimization variables in order to minimize or maximize a certain objective function. The optimization variables can be bounded or unbounded and a set of linear constraints can be defined between them. Furthermore nonlinear constraints should be imposed if some limit cannot be directly express as function of the optimization variables: these limits are usually accounted as penalty factors on the objective function value in order to penalize those solutions which don't respect one or more limits.

Objective function

The objective function for an optimization problem is the variable which is maximized or minimized during the optimization process. For ORC two main classes of objective functions can be defined if the goal is to maximize the plant performances or to minimize the cost of electricity. Obviously these two objective functions are not coincident since usually a higher efficiency is achieved with more expensive equipment.

Techno-thermodynamic optimization

Different objective function can be considered as representative of the thermodynamic performance of a ORC system but all of them are equivalent in terms of trend and maximum point even if the absolute value changes according to the evaluated quantity.

- *Net power output*: calculated as the difference between the gross turbine power output and the power consumption of the pumps and the auxiliaries of the system
- *Plant efficiency*: is equal to the ratio between the net power output and the maximum available thermal power. It is different from the cycle efficiency since in this latter one the possible non total exploitation of the heat source is not considered.

- *Second law efficiency*: is calculated dividing the net power output by the exergy of the heat source or the maximum power output attainable with a reversible cycle.
- *Specific power*: is calculated as the ratio between the net power production and the mass flow rate of the heat source, which is proportional to the maximum available thermal power or the heat source exergy.

Techno-economic optimization

The objective function of a techno-economic optimization is not univocal since it depends on the system and the application which is investigated. Different objective functions can be defined depending on the type of the heat source and on the assumptions at the basis of the financial evaluation of the investment. A brief summary of the possible economic objective functions is here proposed starting from the more exhaustive to the simplest one.

- *Capital budgeting analysis or investment appraisal*: This approach is the most general one and it is based on the analysis of the investment and the calculation of the IRR (Internal Rate of Return) which is a parameter commonly used in capital budgeting and it allows comparing plants with different total cost, different power production and different variable costs since it is representative of the profitability of a certain investment. It is defined as the "rate of return" that makes the NPV (Net Present Value)[15] equal to zero at the end of the plant life and it is equal to the minimum acceptable rate of return or cost of capital. First the total cost of the plant is calculated as an overnight cost, rescaling the expenses incurred during the years of construction to the night before the first start up. This value represents the negative y intercept of the curves represented in Figure 8.6 which show the capital budgeting analysis applied to two different investments. Each year part of the investment is covered by the cash flow resulting by the selling of the electricity minus the O&M (operation and maintenance) costs. DPVs (Discounted Present Values) are used in order to take into account the effect of time value of money on future earnings.

$$DPV = \frac{FV}{(1+r)^t} \qquad \text{eq. 8.1}$$

[15] The NPV, namely the value or the magnitude of an investment is not a suitable financial indicator since it doesn't give any information about the risk of a certain investment. Large NPV can be obtained for investments characterized by a more expensive plant cost and a longer payback time which might be actually less profitable than other one with lower NPV

Where FV is the future value, t is the year and r is the inflation rate.
From the analysis of the trend of the NPV during the years it is possible to evaluate the payback time of the investment and the NPV at the end of the plant life. IRR is hence calculated varying r in order to set to zero the last NPV. Higher is the value of IRR higher is the profitability of the investment. In figure the capital budgeting analysis for two plants differing in investment (A=20M$, B=40M$) and power production (A=18MW, B=30MW) is reported. Common hypothesis are the selling price of electricity (0.03$/kWhel) and the hours of operation (7000heq). The Solid lines correspond toa capital cost of 3.5% while dashed lines are obtained with the corresponding values of IRR. It is possible to note that plant B shows a higher NPV at the end of its lifetime but its IRR is notably lower than plant A.

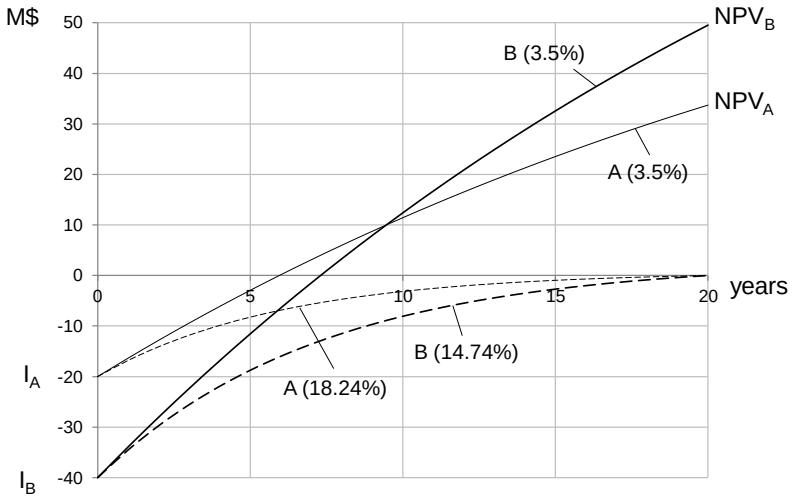

Figure 8.6 - Capital budgeting analysis for two different plants

This approach requires the assumption of the price of electricity to compare different solutions and it is, for this reason, site dependent and general conclusions are hard to obtain.
Furthermore the use of IRR as index for the plant profitability has some drawbacks since its maximization involves distortions in the achieved solutions. With an optimization of IRR, low PBT (Pay Back Time) investments looks more profitable than other ones which can reach, at the end of life time, a NPV notably higher and small and likely less advanced plants are preferable. A suggestion is to consider a maximization of NPV with a constraint on minimum PBT or a multi-objective optimization with a contextual maximization of both IRR and NPV.

- *Levelized cost of electricity*: the LCOE is expressed in USD for kWh_{el} produced and it represents, for a given technology, the minimum electricity price which allows to break even the project at the end of it lifetime. it is an economical index which accounts for all the plant life the expensed related to the construction and the variable cost of operation represented by fuel consumption and O&M costs. It is calculated by eq. 8.2 and it doesn't require the definition of the price of electricity.

$$LCOE = \frac{\sum_{t=1}^{n} \frac{I_t^f + O\&M_t^f + FC_t^v + O\&M_t^v - MI_t^f}{(1+r)^t}}{\sum_{t=1}^{n} \frac{E_t}{(1+r)^t}} \qquad \text{eq. 8.2}$$

Where the terms with superscript f are related to yearly fixed expenses while superscript v denotes variable expenses calculated multiplying the energy production for the specific variable cost:

- I_t^f is the fixed investment cost for the year t of operation
- $O\&M_t^f$ is the fixed operation and maintenance cost
- $FC_t^v = fc^v\, E_t$ is the fuel consumption cost for the production of an amount E_t of energy, fc^v is the specific cost in USD/kW_{el}
- $O\&M_t^v = o\&m^v\, E_t$ is the operation and maintenance cost for the production of an amount E_t of energy, $o\&m^v$ is the corresponding specific cost in USD/kW_{el}
- $MI_t^v = mi^v\, E_t$ is the monetary incentive for the production of an amount E_t of energy, mi^v is the specific incentive in USD/kW_{el}

Another way to evaluate the LCOE consist in the evaluation of two terms: the first one is related to a share of the total plant investment cost and fixed yearly costs while the second one instead is related to the cost of the energy production due to fuel consumption and variable expenses and monetary incentives for green technologies. The goal of this approach is to normalize the whole life of a power plant to the an equivalent first year of operation allowing to compare different technologies or different solutions which differ one to each other in terms of capital cost, power output [226]. The share of capital cost which is considered at the first year is calculated by eq. 8.3.

$$CI^f = I_{TOT} CCF \qquad \text{eq. 8.3}$$

Where CCF is the first year Capital Charge Factor which usually ranges between 10% and 15% depending on the financial risk assumptions and the lifetime of the plant.

The LCOE is hence calculated by and it represent the slope of the straight line connecting the origin of axes with the final point of total expense of a plant for one year of operation as represented in

$$LCOE = \frac{C^f + C^v}{E} = \frac{C^f + c^v E}{E} = \frac{[I_{TOT} CCF + O\&M^f] + [(fc^v + o\&m^v - mi)\ E]}{E} \quad \text{eq. 8.4}$$

Different plants can be compared in terms of LCOE without any assumption on price of electricity and plants with a lower LCOE are intrinsically more competitive on the market.

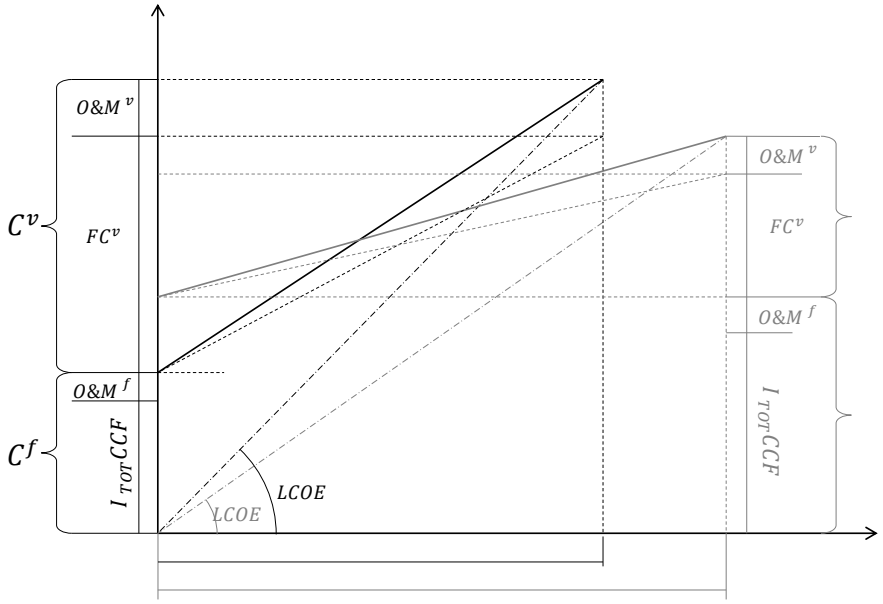

Figure 8.7 - LCOE graphical representation for two power plants

- *Specific cost of the plant*: Is the most intuitive one an it is calculated simply by dividing the total cost of the plant (cost of the power block plus the cost of the heat source) by the net power of the system. It is proportional to the LCOE if the variable costs related to fuel consumption is not considered like in solar and geothermal energy, and O&M cost are neglected

Furthermore, from a general point of view, the objective function can entail the minimization of different variables. In automotive field for example it is crucial to take into account the volume and the weight of the plant since the space available on trucks is limited, in this case the objective function might consider the plant efficiency, the plant volume and the plant cost. The result of the optimization in this latter case is not a single solution but a locus of minimum, called Pareto front, formed by different solutions with roughly the same value of the overall objective function but different breakdown of the terms. Among these solutions further consideration can be done by considering additional limits which allow excluding some results and to identify a small number of promising configurations [227; 228]. Same consideration is valid even for ORC installed on ships or on oil refinery plants [35]. Other multivariable optimizations can account for minimization environmental impact considering for example carbon dioxide emissions.

Design and Optimization variables definition

As already stated in in previous section two type of analysis can be realized with ORCO: (i) a techno-thermodynamic optimization or a (ii) techno-economic optimization. The first one is carried out with the goal to maximize the power output, the second one otherwise is oriented to the minimization of LCOE. Depending on the type of the analysis, some cycle parameters are fixed while other ones must be optimized. In the simplest case, if the goal of the study is to validate a certain cycle configuration or to realize sensitivity analysis, all the cycle parameters required for the complete definition of a cycle configuration are set by the user. In the technical-economic optimization, instead up to ten variables are considered for the two pressure levels cycle.

All the thermodynamic points of the ORC can be sequentially calculated with the definition of ten design parameters, independently if they are set by the user or by the optimization algorithm. It is important to note that most of the design variables can be defined in different ways, for instance the maximum temperature of a subcritical superheated cycle can be defined directly by its value or by defining an approach point temperature difference respect to the hot source inlet condition or finally by selecting a temperature increment in superheating. The same considerations can be done for the maximum and the minimum pressure of the cycle and, from a general point of view, all the definitions are perfectly equivalent. However a smart selection of the set of the independent variables allows defining linear constraints between the parameters and it helps the optimization algorithm to reach the final solution with a better precision and a reduced computational time. The variables used in ORCO are listed below with a short description on the effects they have on the cycle assessment.

- *Condensation temperature,* T_{cond}: This parameter defines the temperature of the saturated vapour at condenser inlet thus affecting the minimum pressure of the cycle. Reducing this parameter leads to an increase in the gross power output thanks to a bigger turbine pressure and enthalpy drops. On the other hand it entails a rise of both the ORC pump and the condenser fans consumption. In addition, the logarithmic temperature difference in the condenser is reduced leading to larger heat exchange surface and a bigger size of the turbine due to the higher volume flow rates with a relevant increase of the power block cost. This parameter is considered fixed in techno-thermodynamic optimization because its effect on power production is substantially monotonic and a reduction of the condensing temperature usually leads to higher efficiencies even if the auxiliary consumption increases.
- *Level Temperature,* T_x *or* T_{eva}: it is the variable which fixes the maximum pressure of the cycle and it is defined as the temperature of vapor in saturated condition for the subcritical cycles. For supercritical cycles instead, it defines a fictitious point right above the critical point which is used to define the turbine inlet pressure. This parameter strongly affects the cycle thermodynamic efficiency, the working fluid mass flow rate and PHE heat transfer area. This parameter is an optimization variable even for thermodynamic optimization as described in Section 9.1.1 (Two examples of thermodynamic optimization). Two values are required for two pressure levels cycles.
- *Superheating temperature increment,* ΔT_{sh}: this parameter, together with the value of level temperature, sets the maximum temperature of the cycle. Its effect on the power production is non-univocal and even in thermodynamic optimization it should be optimized. Two values are required for two pressure levels cycles.
- *Pinch point temperature difference in the recuperator,* $\Delta T_{pp,rec}$: This parameter influences the regenerator effectiveness. The optimization of this parameter is important in presence of a limit on the heat source minimum temperature because a proper recuperator design allows obtaining the best compromise between cycle efficiency and the exploitation of the available thermal power. Two values are required for two pressure levels cycles.
- *Mass flow rate ratio,* M_r: it is the ratio between the mass flow rate at the low pressure level and mass flow rate at the high pressure level. In thermodynamic optimization it is varied in order to obtain the same pinch point temperature difference in both high pressure and low pressure levels while, in techno-economic optimization, it allows imposing different values of pinch point on the two levels thus optimizing the size of the PHE. Mass flow rate ratio strongly

affects the final solution and it is a parameter required only for two pressure levels cycle.

- *Outlet temperature of the hot source*, $T_{out,HS}$: it is equivalent to define the pinch point temperature difference in the PHE only if this condition is not located at the hot side of the heat exchanger. In techno-economical optimization for very inexpensive heat sources, the optimal cycle has generally a poor efficiency with a pinch point temperature difference which can be larger than the approach point as reported in Figure 8.8: a solution that cannot be realized if the value of pinch point is defined instead of the outlet temperature of the heat source. By reducing $T_{out,HS}$ the heat recovery and the overall plant efficiency increase, but, on the other hand, the PHE area and cost also increase with contrasting effects on LCOE.
- *Pinch point temperature difference in the condenser*, $\Delta T_{pp,cond}$: it is defined as the minimum temperature difference between the saturated vapor in the condenser and the cooling air or the cooling water. By reducing this parameter, a lower air flow rate is used with reduced fan consumption, but a higher heat transfer area is required, leading to a higher condenser cost.

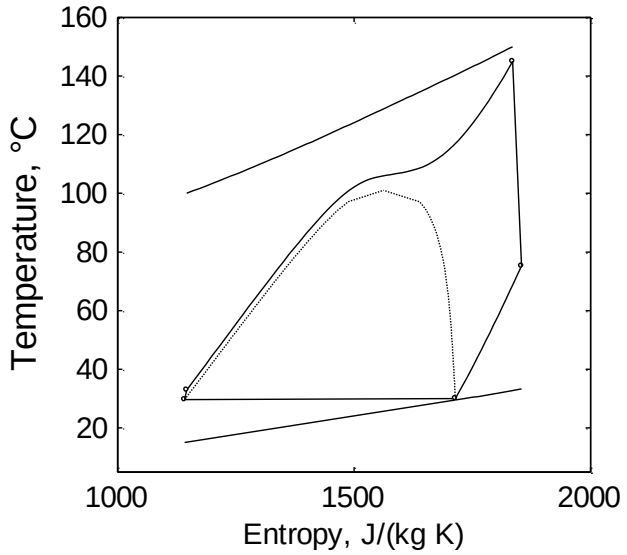

Figure 8.8 - A supercritical cycle optimized for a very inexpensive heat source: minimization of LCOE is obtained by a reduction of power production and cost of PHE.

The user can freely customize the set of optimization variables, defining which parameters are fixed and which ones has to be optimized. A Summary of the suggested optimization variables usually considered for the three general cycle configurations on the basis of the objective function is reported In Table 8.4.

	One pressure level		Two pressure levels		Flash trilateral	
	Techno-thermo	Techno-eco	Techno-thermo	Techno-eco	Techno-thermo	Techno-eco
T_{cond}		X		X		X
$T_{x,LP}$	X	X	X	X	X	X
$\Delta T_{sh,LP}$	X	X	X	X		
$\Delta T_{pp,rec,LP}$		X		X		X
$T_{x,HP}$			X	X	X	X
$\Delta T_{sh,HP}$			X	X		
$\Delta T_{pp,rec,HP}$				X		
M_r			X	X		
$T_{out,HS}$		X		X		X
$\Delta T_{pp,cond}$		X		X		X
n	2	6	5	10	2	6

Table 8.4 – Suggested optimization variables depending on the cycle configuration and the objective function

Linear constraints between variables

Another important step in optimization consists in the definition, if it is possible, of linear constraints between variables. This potentiality is extremely important because by setting large maximum and minimum bounds for every variable, some regions of non-feasible design might be explorer by the solver, with the necessity to introduce controls in order to avoid code crashing and penalty factors to take them into account (see Section 8.2.5-Penalty factor for more details). In example, if power output is optimized for a subcritical cycle, the evaporation pressure and the superheating temperature difference are the two optimization variables. Let's consider a working fluid with a high critical temperature: the evaporation temperature lower bound is close to the condensing temperature while the upper bound is very close to the inlet temperature of the heat source. The superheating temperature increment instead must be in a range which allows achieving the maximum cycle temperature even for the minimum evaporation temperature. As result there is a wide range of values which are not compatible and they result in non-feasible design of the PHE with a maximum cycle temperature higher than the inlet temperature of the heat source. Same consideration is valid for the evaporation temperatures in a two pressure levels cycle.

In these cases additional boundaries can be expressed by linear constraints between variables which force the optimization algorithm to search the final solution in the field of feasible solutions excluding a priori some parameters combinations. From eq. 8.5 to eq. 8.8 these constraints are reported for a generic two pressure levels cycle with superheating on both levels.

$$\forall i \in (LP, HP) \rightarrow T_{eva,i} + \Delta T_{sh,i} \leq T_{in,MS} - \Delta T_{pp,PHE} - \Delta T_{ap-pp} \quad \text{eq. 8.5}$$

$$T_{eva,LP} \leq T_{eva,HP} - \Delta T_{HP-LP} \quad \text{eq. 8.6}$$

$$T_{cond} \leq T_{eva,LP} - \Delta T_{LP-cond} \quad \text{eq. 8.7}$$

$$\Delta T_{pp,cond} \leq T_{cond} - T_{in,BS} - \Delta T_{ap-pp} \quad \text{eq. 8.8}$$

Where the values of ΔT_{ap-pp}, ΔT_{HP-LP} and $\Delta T_{LP-cond}$ are required in order to guarantee always feasible solutions. In particular it is important to have a minimum gap between two adjacent pressure levels thus obtaining a minimum pressure ratio for the turbine. In addition it is crucial to avoid solutions with both MS and BS characterized by very small temperature changes thus entailing an uncontrolled soaring of both mass flow rate and auxiliaries consumption.

Consistency test

Fixed cycle design variables, choice of cycle layout and working fluid characteristics are checked together with the values of maximum temperature of the heat source and ambient temperature. If a conflict between certain variables is notice the code automatically changes a parameter in order to solve the incongruence or it stops the execution. For instance, if the working fluid is a wet fluid, no saturated cycles are allowed due to the limit related to an expansion with a limited liquid fraction while for fluids with a critical temperature higher than the maximum temperature of the heat source, the supercritical cycle is not feasible.

Lower and upper bounds

For each optimization variable the maximum and the minimum allowable values have to be defined according to the cycle configuration and the other fixed parameters. The assumption used for the calculation of lower and upper bound for each variable are further described.

- T_{cond}: the temperature of condensation limits are defined by means of the assumption of a minimum and maximum approach point temperature difference at condenser unit. Suggested values depend on the cooling medium used in the

condenser and the type of application. If ambient air or cooling water are used, values of 5 and 50°C can be adopted as minimum and maximum values for $\Delta T_{ap,cond}$, while if a cogenerative power plant is analyzed they should be defined according to the temperature of the hot water for district heating. Finally, if a mixture is considered, the minimum value of $\Delta T_{ap,cond}$ has to be defined in order to match the glide of working fluid in condensation and avoid negative pinch point at the saturated liquid extremity;

- $T_{x,LP}$, $T_{x,HP}$: the temperature limits of the two pressure levels depends on cycle configuration as the scheme reported in Table 8.5 for a generic single level cycle, while the constraints between the two temperature levels have been introduced before as linear constraints. For saturated cycles and overhanging saturation lines an adjunctive limit is considered if the constraint of dry expansion is imposed: in this case the maximum evaporation temperature is determined by exploring different saturated vapor points along the Andrew line and finding the evaporation temperature which involves a vertical slope on vapor side. If the critical temperature is assumed as upper or lower bound it is helpful to consider a certain temperature difference ΔT_i in order to do not investigate a region very close to the critical point where generally equations of state show instability and convergence issues. For supercritical cycles the maximum temperature is defined by means of the definition of a maximum pressure which is conventionally assumed equal to the pressure upper limit for the equation of state.

level	Subcritical level	Supercritical level
Turbine admission	Superheated, saturated vapor, throttled, saturated liquid	
LB	$T_{cond} + \Delta T_i$	$T_{crit} + \Delta T_i$
UB	$min(T_{crit} - \Delta T_i, T_{in,HS} - \Delta T_i, T_{max,wf})$	$min(3\ p_{crit}, p_{max,wf}\ )\ s_{crit}$

Table 8.5 - Definition of lower and upper bound for level temperature variable: comparison between subcritical and supercritical single level cycles.

- ΔT_{sh}: the superheating lower bound is always equal to zero in order to let the optimizer free to converge to a saturated vapor admission; the upper bound is assumed large enough to reach a temperature close to the maximum temperature of the heat source when the minimum evaporation temperature is imposed;
- $\Delta T_{pp,rec}$: the lower limit for the pinch point temperature difference at recuperator is set equal to 0.1°C thus considering a really high efficacy of the heat exchanger while the upper bound should be defined according to the application and configuration cycle. The maximum value for this parameter should be larger than

the maximum temperature gap between turbine outlet and condensation temperature in the most extreme case in order to let the optimization free to suppress the recuperator;

- M_r: the ratio between high pressure and lower pressure mass flow rates can be varied between 0.05 and 0.95;
- $T_{out,HS}$: the outlet temperature of the hot source is always greater than the minimum limit temperature defined according to the type of the heat source while the maximum bound is close to the inlet temperature;
- $\Delta T_{pp,cond}$: even this parameter, like T_{cond}, has to be set with reference to the type of cooling stream and the type of application. Reasonable lower bounds are 0.1 and 1 for air cooled condenser and water cooled condenser respectively. The upper bound is free and it is limited by a linear constraint with the other variables.

Other lower and upper bound can be related to additional constraints while a minimum condensing pressure or a maximum pressure of the cycle.

Initialization

Last step before starting the optimization is to generate a feasible initial point for the algorithm. This step is crucial and a bad initialization of the optimization routine leads to non-accurate solution: the algorithm, starting from a point far from the optimal one, takes more time in finding the solution and it is more probable that it stops in a local minimum instead to find the real global one. Furthermore it is always a good practice to initialize the algorithm with values different form the lower or the upper bounds in order to not constrain excessively the routine in the first iterations.

It is always suggested to perform some test cases varying the initial point in order to understand how this assumption affects the final solution. In ORCO some default settings are already implemented using eq. 8.9 where the values for the coefficient χ are reported in Table 8.6.

$$X_i = LB_i + \chi(UB_i - LB_i) \qquad \text{eq. 8.9}$$

	single pressure level sub	sup	2 pressure level	Flash trilateral
$T_{x,LP}$	1.5/2	1/10	1/3	1/2
$T_{x,HP}$	-		2/3	1.5/2
T_{cond}	0.5			
$\Delta T_{sh,LP,HP}$	1/2			
$\Delta T_{pp,rec,LP,HP}$	1/2			
M_r	1/2			
$T_{out,HS}$	1/4			
$\Delta T_{pp,cond}$	1/6			

Table 8.6 - Values of χ for the calculation of the initial point

8.2.3 Optimization

Optimization is a crucial step in ORC systems design and the correct choice of the most suitable algorithm has to be faced carefully in order to obtain reliable results since the solution accuracy depends on the on the objective function, the presence of discontinuities and local minimum. In this section a brief overview of the optimization algorithms available in Matlab is presented with a comparison of their performances on a couple of test cases.

Optimization algorithm selection

In Matlab environment [45], several different non-linear optimization algorithms are already implemented with the possibility to solve different kind of numerical problems. However these algorithms greatly differ one to each other in terms of stability, final solution accuracy and computational time. The definition of the most suitable algorithm for the optimization of a certain problem is an open task because every algorithm has different benefits and drawbacks: some of them are more indicated to solve large size problems, other ones can escape easier from local minimum, and finally other ones are negatively affected by long computational time. In ORC optimization the problem is generally bounded since for each variable both lower and upper bounds can be defined and linear constraints between variables can be expressed. Three algorithms are the most suitable ones to solve this kind of problems [229]

- *fmincon*: it is an algorithm suitable for the solution of small-medium size problems and it is gradient-based method which calculates the Hessian after each function evaluation. It is a powerful method when the objective function is smooth without discontinuities or deep local minimum.

- *Pattern-search* [230; 231; 232]: is a direct-search derivative-free algorithm. At each iteration the algorithm creates a mesh of point around the temporary optimal point and it evaluates the objective function in this pool. After it moves according to the best solution it found. The procedure for mesh generation, its size and orientation are fundamental in order to have a reliable solution and currently adaptive meshes method are used [233]. This algorithm is suitable for the solution of medium size problem and it should be able to escape from local minimum and to handle discontinuities.
- *Genetic algorithm*: it is a meta-heuristic method. In each step of a genetic algorithm is based on the generation of a number of inputs, also called a population of individuals, and the evaluation of their objective function. After that, the solutions are listed on the basis of a certain criteria, the fitness function, and a new population is generated by mixing the input variable of the selected individuals of the previous iteration. Crossover and mutation functions define how the new population is created miming the reproduction process of a living organisms. They are method suitable for the optimization of very large size problem and they requires a large number of iterations

All the over mentioned optimization algorithms allow defining lower and upper bounds for every variables reducing the size of the admissible domain of solutions and increasing the stability of the code. In addition a starting point can be specified initializing the algorithm close to the optimal solution thus reducing the computational time and increasing the accuracy of the final solution.

8.2.4 Thermodynamic cycle solution

The resolution of the ORC form a thermodynamic point of view requires an iterative procedure if the efficiency of the expander is computed. Furthermore the routine can be divided in different sub sections and two of them require and additional internal iteration to fix the pinch point temperature difference at the primary heat exchanger and to optimize the turbine efficiency by varying the rotational speed. The two routines for the two internal loops are written by the author in order to reduce the computational time.

A graphical representation of the steps required to compute a single configuration is reported in Figure 8.9.

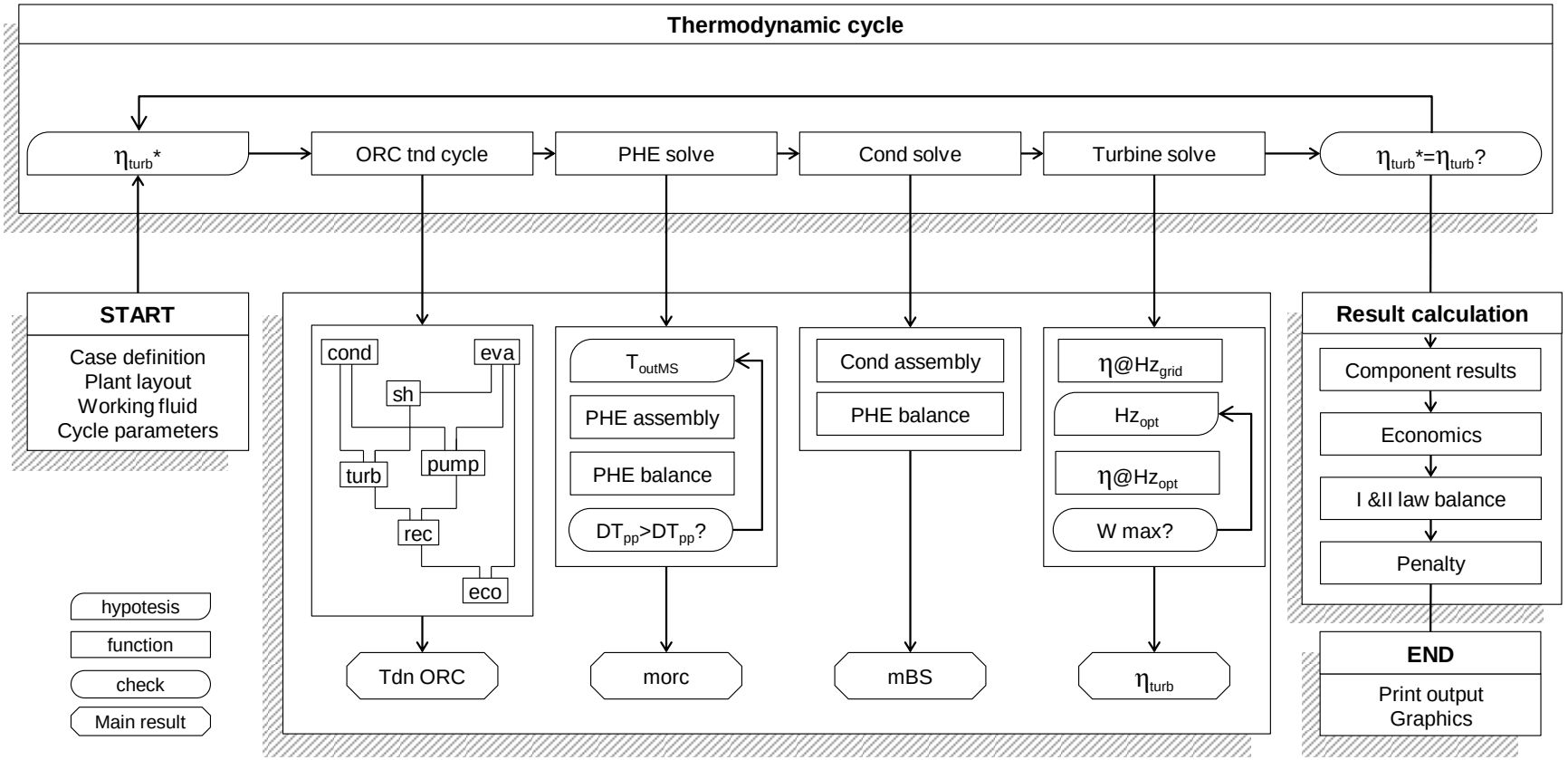

Figure 8.9 – Schematic view of the solution process for a single configuration.

ORC thermodynamic cycle

The first step required is the calculation of all the working fluid thermodynamic points, namely the inlet and outlet condition from each component. In this stage no iterative procedure is required and, with the set of design parameters presented in section 8.2.1 (Heat sources and heat sink definition), all the points are computed sequentially. This is valid for all the cycle configuration implanted in ORCO but the code can be easily modified with aim of investigating new plant layouts. Each component is represented by a specific function which calculates the outlet condition receiving in input the inlet condition and a set of exogenous parameters like the component efficiency, the pressure drops and so on. Each function is completely independent and new plant configurations can be realized just by writing the sequence of component priority and by the definition of streams chain. In Figure 8.9 an example is presented for a single level subcritical cycle: Condenser outlet condition is completely defined by the design parameter T_{cond}, as well for the evaporator component since T_{eva} is imposed. Knowing the superheater inlet condition, the outlet one is defined by the ΔT_{sh} and the turbine can be hence calculated because the outlet pressure is already known. Energy balance at recuperator allows calculating the cold stream outlet condition from this component. Finally the economizer and the desuperheating are calculated in order to close the thermodynamic cycle on both low pressure and high pressure sides.

For other plant layouts sequence of calculation is different and other component are used like a flash tank in the flash trilateral configuration; furthermore depending on both the configuration and the set of design parameters some components might be automatically suppresses like the superheater, the recuperator, the economizer and the desuperheater. For instance, if a very large $\Delta T_{pp,rec}$ is imposed by the optimization routine, the recuperator is not feasible since the pinch point temperature difference is larger than the gap between the inlet temperatures of the hot and the cold stream. Recuperator is hence suppressed, no heat is transferred and an isenthalpic lamination is accounted on both streams. Another example is for strongly superheated subcritical cycles using a low evaporation temperature: the thermal power available at turbine outlet is higher than the power required to heat the cold fluid up to the evaporation temperature. In this case it is not possible to exploit the whole heat because otherwise evaporation occurs in the recuperator. This is not a feasible condition for most of the plant configurations where usually a well-defined separation between single phase and two phase heat exchangers is required in order to solve problems of stratification, flow circulation and blowdown of

liquid in the previous components. In order to avoid this solutions $\Delta T_{pp,rec}$ is adjusted to obtain an saturated liquid at recuperator outlet condition.

PHE and condenser solve

Since both the inlet and the outlet conditions for each component are known it is possible to assembly the primary heat exchanger and to match the heat source temperature profile with the working fluid. PHE is formed by a sequence of heat exchangers which are, starting from the low temperature, the economizer, the evaporator and the superheater. If a two pressure levels cycle is considered the heat exchangers of the low pressure are placed before the high pressure ones according to their temperature level. Each heat exchanger is discretized in several different sections whose number depends on component type, on temperature difference between the two extremities and on enthalpy difference. For both the evaporator and the condenser a number of section equal to 20 is considered in order to properly characterize the temperature profile for mixtures, while for the single phase streams a discretization based on a fixed ΔH per section is imposed. In particular the ΔH step is found with the calculation of the enthalpy change corresponding to a temperature variation of 3°C on both extremities and adopting the minimum value among them. This approach guarantees a sufficient discretization for supercritical cycles where the imposition of a fixed temperature step might lead to a poor detail around the critical point. In Figure 8.10 the comparison between the two discretization approaches is proposed for R161 transcritical transition. In Figure 8.10.a a fixed ΔT is imposed and it is possible to note the poor quality around the critical point where small temperature changes entail high enthalpy and entropy variations. In Figure 8.10.b the auto-adapted discretization is adopted and it is possible to note how the spacing between the nodes gets smaller around the critical point where is more important to describe the temperature profile. In Figure 8.10.c and Figure 8.10.d the enthalpy and temperature variations respect the total change are reported and it is possible to notice that whit the fixed temperature step more than 30% of the total enthalpy change is covered in a single section. A proper discretization allows reducing the computational time and to properly locate the pinch point temperature difference in supercritical PHE.

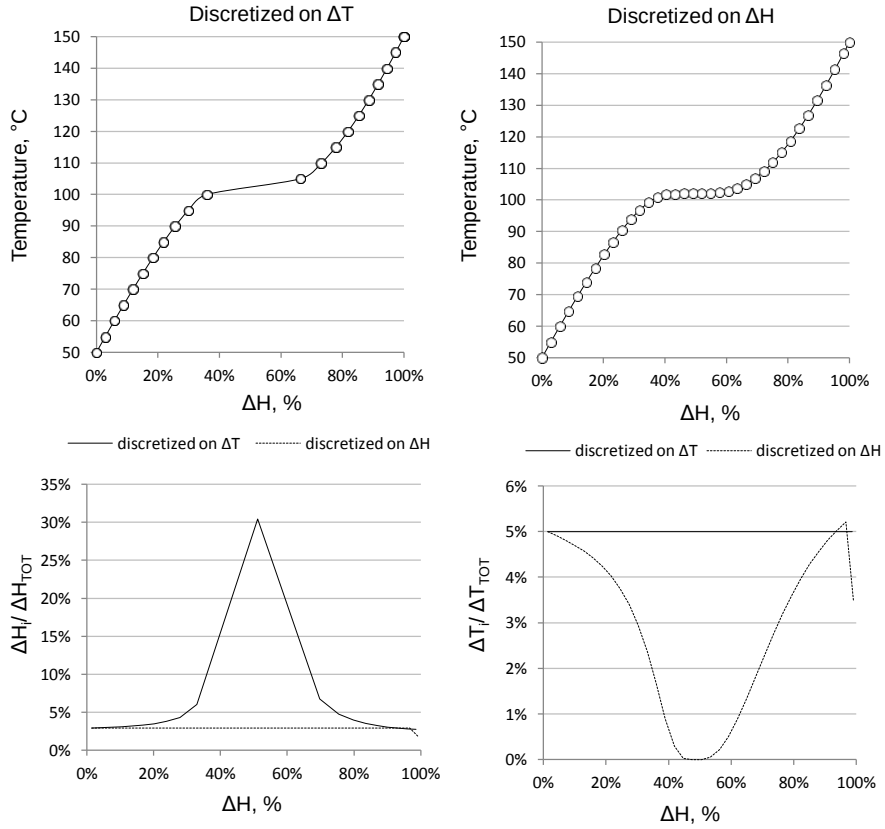

Figure 8.10 - Comparison between two different discretization approaches for R161.

The discretized heat exchangers are assembly together in a single PHE and the hot stream conditions are calculated from the energy balance form each section. The ratio of mass flow rate between working fluid and hot stream is calculated and since one of them is defined as exogenous variable even the other one is known. Temperature differences are computed at the extremities of each section and the pinch point temperature difference is obtained. If the value of ΔT_{pp} is lower than the minimum one an internal iteration is realized varying the outlet temperature of the hot stream with the aim to respect this constraint.

A similar approach is followed for the condenser assembling the two phase flow heat exchanger and the desuperheater unit and imposing a certain $\Delta T_{pp,cond}$. Iteration is not required if constant or a linear heat capacity for the cooling stream is considered and the working fluid is not a mixture with a large temperature glide.

Turbine solve

Turbine is the key component of ORC systems and in ORCO it is analyzed more in detail in order to estimate its efficiency and its size. Starting from the inlet conditions and the exhaust pressure, the isentropic enthalpy drop and volume flow ratio along the expansion are computed. The number of turbine stages is estimated by setting two limits, namely: (i) the stage maximum volume flow ratio and (ii) the maximum allowable stage enthalpy drop. Only one of the two limits is active depending on the application and on the nature of the fluid. According to results presented in section 4.2 (Thermodynamic properties of organic fluids) and considering only organic fluids, namely hydrocarbons, fluorinated compounds and siloxanes, the increase of complexity is usually connected to an increase of molar weight and critical temperatures. As result for the same evaporation and condensation temperatures the isentropic volume ratios becomes bigger while usually the overall isentropic enthalpy drop is limited. In this case a maximum $V_{r,stage}$ admissible for each stage is assumed equal to 4 in order to contain the flaring angles and the blade height variations across the rotor blade. This allows limiting the penalties due to high Mach numbers, supersonic velocities and shock waves. If the total V_r is larger than this limit, the expansion is divided into the minimum number of stages with respect the over mentioned constraint.

The second constraint is set in order to limit the mechanical stresses. Fluids with high molecular weight show relatively small turbine enthalpy drops and they give the possibility to design a turbine with moderate peripheral speeds and reduced mechanical stresses. Low molecular weight fluids instead, like water or ammonia, show high enthalpy drops along the expansion. For this reason, a limitation related to the maximum enthalpy drop exploitable for each stage is introduced, equal to 65 kJ/kg. This value is derived by assuming a 50% reaction degree stages with a load coefficient (k_{is}) equal to 2 and a mean peripheral speed of 255 m/s according to eq. 7.9. If this limit is exceeded, the expansion is divided into the minimum number of stages with the same enthalpy drop.

Once the number of stages is determined, it is possible to compute the size parameter SP, the specific speed Ns at grid frequency and the efficiency of each stage according to the approach explained and validated in section 6.1.5 (Comparison between discretized and global approaches). The overall power output is then computed by summing the work for all the stages and the efficiency at grid frequency is eventually calculated.

For really small or really large turbines directly connected to the generator, the stages specific speeds are far from the optimal one (~0.1-0.15) thus entailing a low isentropic efficiency and the use of a gear box can be really profitable. The efficiency can be

optimized by varying the rotational speed with an internal optimization routine. For high speed turbines a gear box is usually adopted with the possibility to explore a large range of rotational speeds with continuity. For low rotational speed turbines instead the optimal velocity can be found adopting a generator with a number of pairs of poles greater than two and so only discrete values of rotational speeds are allowed, otherwise a gearbox can be used but an additional mechanical loss has is accounted. Finally for micro axial turbines a fast generator is usually adopted with a power electronic system. If a two pressure levels cycle is considered the two turbines are one the same shaft and thus they have the same rotational speed.

Turbine stage efficiency is eventually corrected depending on the vapour quality x_v: the penalization is proportional to the fraction of liquid at stage outlet according to eq. 8.10.

$$\eta_{is,t} = \eta_{is,t}(x_v) \;\; if \; x_v \leq 1 \qquad \text{eq. 8.10}$$

For the volumetric expander the efficiency is simply computed by eq. 6.13 and eq. 6.14.

8.2.5 Result calculation

Once all the thermodynamic points of the cycle are calculated it is possible to evaluate the cost of each component, to verify the I and II law balances and to eventually introduce penalty factors in order to account the violation of some constraints.

Economics

Power block cost is evaluated with the cost functions presented in Chapter 7 (Cost correlations). Additional information are required about the cost of the heat source which can represent a relevant share, up to more than 50%, of the total plant cost. Examples are the geothermal energy exploitation where the cost of exploration campaigns, drilling of wells and preparation of the field are operation extremely expensive and solar energy where the cost of solar field can easily overcome the power block cost. In some other application instead heat source is almost free, like in WHR and no additional costs to the power block equipment should be considered. Some more information about the cost of geothermal wells, biomass burner and low cost solar collectors for rural applications are reported in Chapter 9 (Model validation and test cases).

I & II law balance and efficiency definitions

Since all the thermodynamic points are calculated and both inlet and outlet conditions from each component are known, it is possible to evaluate performance indexes and verified the first and the second law balances. These balances can be applied to the whole plant or to different subsystems focused only the working fluid system or including more components. The first law balance for a generic ORC system can be represented with a Sankey chart as reported in Figure 8.11 for a plant where both the Top temperature Stream (TS) and the Medium temperature Stream (MS) are present.

Four different system boundaries can be defined:

- *Working fluid system*: represent the enthalpy balance on the working fluid and can be used to check for the presence of errors. It is defined by eq. 8.11.

$$Q_{in}^{wf} + \sum_{\substack{lp \\ hp}}^{j} W_{mec}^{pump,wf,j} = \sum_{\substack{lp \\ hp}}^{j} W_{mec}^{turb,wf,j} + \sum_{\substack{lp \\ hp}}^{j} Q_{loss}^{rec} + Q_{cond} \qquad \text{eq. 8.11}$$

  Where Q_{in}^{wf} is the thermal power introduced in the working fluid in the PHE, $W_{mec}^{pump,wf,j}$ and $W_{mec}^{turb,wf,j}$ are the mechanical powers of the pumps and the turbines of the thermodynamic cycle, Q_{loss}^{rec} is the heat released to the environment from the recuperator due to non-perfect insulation and Q_{cond} is the heat released at the condenser.

- *ORC system*: represent the energy balance for the ORC system where the heat losses in the PHE ($Q_{loss}^{i,j}$), the mechanical and electrical losses of pump and motors ($W_{loss}^{pump,wf,j}$, $W_{loss}^{mot,wf,j}$), of the generator (W_{loss}^{gen} and W_{loss}^{gbox}), of the turbine ($W_{loss}^{turb,wf,j}$) and the consumption of condenser auxiliaries ($W_{el}^{pump,bs}$) are accounted as expressed by eq. 8.12. On the other hand, the consumption for the auxiliaries of both medium temperature and top temperature streams are not here considered as well as the recovery efficiency of the available heat.

$$Q_{in}^{cyc} = W_{el}^{cyc} + \sum_{\substack{eco \\ eva \\ sh}}^{i} \sum_{\substack{lp \\ hp}}^{j} Q_{loss}^{i,j} + \sum_{\substack{lp \\ hp}}^{j} Q_{loss}^{rec,j} + \sum_{\substack{lp \\ hp}}^{j} W_{loss}^{mot,wf,j} + \sum_{\substack{lp \\ hp}}^{j} W_{} \qquad \text{eq. 8.12}$$
$$+ \sum_{\substack{lp \\ hp}}^{j} W_{loss}^{turb,wf,j} + W_{loss}^{gbox} + W_{loss}^{gen} + W_{el}^{pump,bs} + Q_{cond}$$

From this balance it is possible to define the cycle efficiency (η_{cyc}):

$$\eta_{cyc} = \frac{W_{el}^{cyc}}{Q_{in}^{cyc}}$$

$$\eta_{cyc} = \frac{\left[\begin{array}{c} Q_{in}^{cyc} - \sum_{\substack{eco \\ eva \\ sh}}^{i} \sum_{\substack{lp \\ hp}}^{j} Q_{loss}^{i,j} - \sum_{\substack{lp \\ hp}}^{j} Q_{loss}^{rec,j} - \sum_{\substack{lp \\ hp}}^{j} W_{loss}^{mot,wf,j} - \sum_{\substack{lp \\ hp}}^{j} W_{loss}^{pump,wf,j} \\ - \sum_{\substack{lp \\ hp}}^{j} W_{loss}^{turb,wf,j} - W_{loss}^{gbox} - W_{loss}^{gen} - W_{el}^{pump,bs} - Q_{cond} \end{array}\right]}{Q_{in}^{cyc}} \quad \text{eq. 8.13}$$

Which can be reduced to eq. 8.14 by the definition of a series of efficiency losses expressed by equations from eq. 8.15 to eq. 8.19.

$$\eta_{cyc} = 1 - \Delta\eta_{loss}^{PHE} - \Delta\eta_{loss}^{rec} - \Delta\eta_{loss}^{m-e} - \Delta\eta_{aux}^{pump,bs} - \Delta\eta_{cond} \quad \text{eq. 8.14}$$

$$\Delta\eta_{loss}^{PHE} = \frac{\sum_{\substack{eco \\ eva \\ sh}}^{i} \sum_{\substack{lp \\ hp}}^{j} Q_{loss}^{i,j}}{Q_{in}^{cyc}} \quad \text{eq. 8.15}$$

$$\Delta\eta_{loss}^{rec} = \frac{\sum_{\substack{lp \\ hp}}^{j} Q_{loss}^{rec,j}}{Q_{in}^{cyc}} \quad \text{eq. 8.16}$$

$$\Delta\eta_{loss}^{m-e} = \frac{\sum_{\substack{lp \\ hp}}^{j} W_{loss}^{mot,wf,j} + \sum_{\substack{lp \\ hp}}^{j} W_{loss}^{pump,wf,j} + \sum_{\substack{lp \\ hp}}^{j} W_{loss}^{turb,wf,j} + W_{loss}^{gbox} + W_{loss}^{gen}}{Q_{in}^{cyc}} \quad \text{eq. 8.17}$$

$$\Delta\eta_{aux}^{pump,bs} = \frac{W_{el}^{pump,bs}}{Q_{in}^{cyc}} \quad \text{eq. 8.18}$$

$$\Delta\eta_{cond} = \frac{Q_{cond}}{Q_{in}^{cyc}} \quad \text{eq. 8.19}$$

- *Plant Medium Stream boundary*: consumption and losses of pump for the Medium temperature Stream are consider plus the recovery ratio of the available thermal power. The net electrical power from this system is obtained by subtracting to the ORC power output the consumption of medium temperature stream pump.

$$W_{el}^{p,ms} = W_{el}^{cyc} - W_{el}^{mot,ms} \quad \text{eq. 8.20}$$

Which brings to the definition of plant efficiency ($\eta_{p,ms}$) reported in eq. 8.24

$$\eta_{p,ms} = \frac{W_{el}^{p,ms}}{Q_{in}^{ms}} = \frac{W_{el}^{cyc} - W_{el}^{mot,ms}}{Q_{in}^{ms}} \quad \text{eq. 8.21}$$

$$\eta_{rec,ms} = \frac{Q_{in}^{cyc}}{Q_{in}^{ms}} \quad \text{eq. 8.22}$$

$$\varepsilon_{el}^{ms} = \frac{W_{el}^{mot,ms}}{W_{el}^{cyc}} \quad \text{eq. 8.23}$$

$$\eta_{p,ms} = \eta_{cyc}\, \eta_{rec,ms}\, (1 - \varepsilon_{el}^{ms}) \quad \text{eq. 8.24}$$

- *Plant Top Stream boundary*: same consideration of the previous case but with a larger boundary enveloping the whole system

$$W_{el}^{p,ms} = W_{el}^{cyc} - W_{el}^{mot,ms} - W_{el}^{mot,ts} \quad \text{eq. 8.25}$$

$$\eta_{p,ts} = \frac{W_{el}^{p,ts}}{Q_{in}^{ms}} = \frac{W_{el}^{cyc} - W_{el}^{mot,ms} - W_{el}^{mot,ts}}{Q_{in}^{ms}} \quad \text{eq. 8.26}$$

$$\eta_{rec,ts} = \frac{Q_{in}^{ms}}{Q_{in}^{ts}} \quad \text{eq. 8.27}$$

$$\varepsilon_{el}^{ts} = \frac{W_{el}^{mot,ts}}{W_{el}^{cyc}} \quad \text{eq. 8.28}$$

$$\eta_{p,ms} = \eta_{cyc}\, \eta_{rec,ms}\, \eta_{rec,ts}\, (1 - \varepsilon_{el}^{ms} - \varepsilon_{el}^{ts}) \quad \text{eq. 8.29}$$

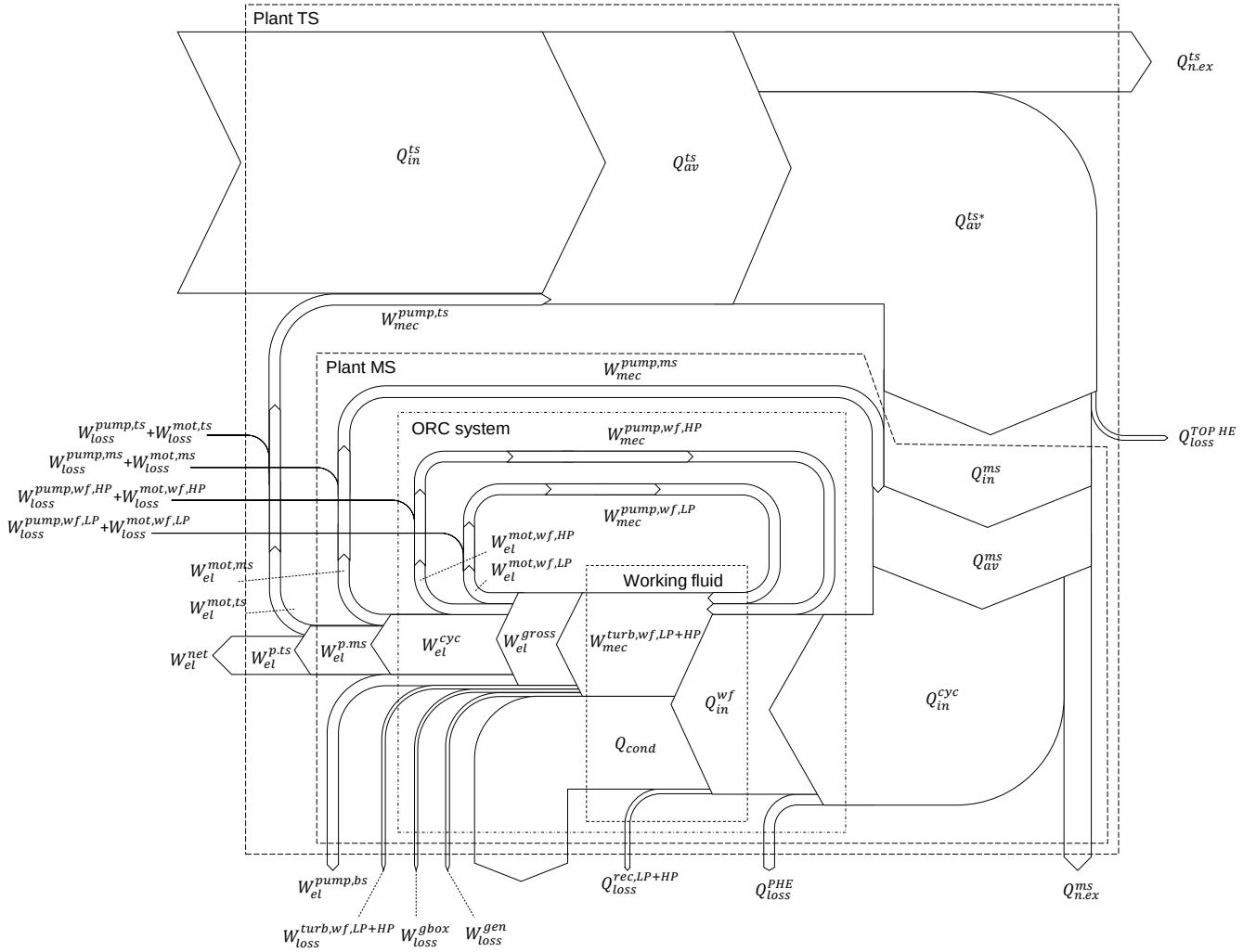

Figure 8.11 - Sankey diagram for a general ORC system where both Medium temperature and Top temperature streams are present

Second law balance is obtained computing the entropy generation in each process.

The main reason of efficiency losses are:

- *Heat transfer with local temperature differences between the two streams*: in all the heat exchangers, the PHE, the recuperator and the condenser.
- *Fluidodynamic losses*: in all the machines characterized by a non-isentropic process, namely the pumps, the turbine and the fan of ACC.
- *Heat losses*: due to a non-perfect insulation of heat exchangers.
- *Mechanical and electrical losses*: mainly due to friction, they represent a direct loss of power production.
- *Mixing losses*: when two streams in different thermodynamic condition are mixed together. A typical case is a non-total recovery of a geothermal brine available heat, and the mixing of cooling air or cooling water into the environment after the condenser.

The II law efficiency losses are referred to the maximum power which can be produced by a variable temperature heat source with a series of reversible processes is equal to the exergy variation of the hot stream.

$$W_{id} = m_{HS}(ex_{in} - ex_{out}) = m_{HS}[(h_{in} - h_{out}) - T_0(s_{in} - s_{out})] \quad \text{eq. 8.30}$$

It is interesting to note that for an ideal gas or an incompressible fluid, if no pressure drops are present and a constant specific heat is defined, the previous equation can be written as reported in eq. 8.31.

$$W_{id} = m_{HS}\left[cp(T_{in} - T_{out}) - T_0 cp \ln\left(\frac{T_{in}}{T_{out}}\right)\right] \quad \text{eq. 8.31}$$

Which can be simplified by collecting the term $Q_{in,max} = cp(T_{in} - T_{out})$

$$W_{id} = Q_{in,max}\left(1 - \frac{T_0}{(T_{in} - T_{out})/\ln\left(\frac{T_{in}}{T_{out}}\right)}\right) \quad \text{eq. 8.32}$$

Which correspond to the definition of Lorentz efficiency reported in Section 5.10 (

Lorentz cycle)

Penalty factor

Penalty factors are used to correct the final solution if some nonlinear constraint are violated or if the value of an optimization variable is adjusted in order to solve a conflict and achieved a feasible solution. According to the type of plant layouts available in ORCO three main reasons of penalty correction factors are considered:

- *Wet expansion*. Since all the thermodynamic points of the cycle have been calculated a check on the quality along the expansion is realized. For wet fluids it is sufficient to evaluate the quality at turbine outlet while for dry fluids in theory the expansion can cross the two phase region and so a discretization of the expansion is required only if the specific entropy at turbine inlet is lower than the specific entropy at the point where the Andrews saturation line is vertical. If the maximum liquid fraction is higher than the limit the correspondent penalty factor is calculated;
- *Modification of outlet temperature of heat source.* In techno-economic optimizations the outlet temperature of the heat source is not fixed or determined by an imposed $\Delta T_{pp,PHE}$. The $T_{out,HS}$. is an optimization variable which acts modifying the thermal input and so the net power produced by the cycle while on the other one it allows reducing the size and the cost of the PHE. The lower bound of this temperature is set according to the nature of the heat source as mentioned in section 3.4 (Typical heat source temperature profiles and limits) and so for some combinations of the optimization variables a unfeasible solution might be found with the hot stream temperature profile crossing the cold one in the PHE. In this case the outlet temperature is modified by the code in order to respect the minimum $\Delta T_{pp,PHE}$ defined for the techno-economic optimization. A penalty factor is introduced to take into account this correction and to avoid solutions with the same objective function value if they are obtained by manipulation of the control variables;
- *Pinch point temperature difference in the recuperators.* Same consideration can be made for this parameter when exploring the whole range between the lower and upper bound one of the cases mentioned in Section 8.2.4 (ORC thermodynamic cycle) are highlighted.

The equation used for the calculation of the penalty factors are reported from eq. 8.33 to eq. 8.35: a penalty proportional to the square of the relative distance between the actual value and the limit value or the input variable is considered in order to help those

algorithms which cannot handle discontinuities in the objective function. The different weights for the penalties are set according to the necessity to consider the wet expansion as a numerical barrier and to exclude those solutions which violate this limit, while for the other two variables the penalty factor is accounted as a warning. A final check on the penalties values is performed verifying that the optimization algorithm actually avoid solutions which don't respect one or more limits.

$$P_i = 100 \left(\frac{x_{exp}^{lim} - x_{exp}^{act}}{x_{exp}^{lim}} \right)^2 \; if \left[x_{exp}^{act} < x_{exp}^{lim} \right] \qquad \text{eq. 8.33}$$

$$P_i = 0.01 \left(\frac{T_{out,HS}^{act} - T_{out,HS}^{imp}}{T_{out,HS}^{imp}} \right)^2 \; if \left[T_{out,HS}^{act} > T_{out,HS}^{imp} \right] \qquad \text{eq. 8.34}$$

$$P_i = 0.01 \left(\frac{\Delta T_{pp,rec}^{act} - T_{pp,rec}^{imp}}{T_{pp,rec}^{imp}} \right)^2 \; if \left[\Delta T_{pp,rec}^{act} > T_{out,HS}^{imp} \right] \qquad \text{eq. 8.35}$$

The objective function value is hence corrected with the sum of the penalty factors.

$$F_{obj} = \begin{cases} -W_{net} \left(1 - \sum P_i \right) \; if \; thermodynamic \; optimization \\ LCOE \left(1 + \sum P_i \right) \; if \; technoeconomic \; optimization \end{cases} \qquad \text{eq. 8.36}$$

“I have not failed.

I've just found 10,000 ways that won't work”

Edison, T.A.

9 Model validation and test cases

The systematic approach presented in the previous chapters is tested on four test cases investigating two applications where ORCs are commonly used, like the exploitation of geothermal energy and biomass combustion, and two fields where the upset of ORC technology is still large, like WHR from cement industry and small direct solar thermal power systems.

9.1 Hot geothermal brines

Geothermal hot brines are available in many areas around the world, especially in North America (Arizona, Nevada and California), in Central America (Mexico, Costa Rica, Guatemala and El Salvador), in Europe (Italy and Germany), in Turkey and in Far East and Oceania (Philippines, Australia and New Zealand). The temperature of the hot geothermal brine usually ranges between 120 and 180°C depending on the site, the type of rocks surrounding the well and the depth of the geothermal reservoir. An average temperature is assumed to be 140-150°C which is the temperature of several wells in North America and Turkey but higher temperature brines are found in Central America, for example in Berlin (El Salvador) where a 9.3 MW_{el} ORC binary power is installed to exploit a 180°C geothermal brine. In this section the reference case is a 200kg/s 150°C geothermal brine with an ambient temperature of 15°C but lower and higher temperature of the brine are investigated as well in order to achieve a more general conclusion. A limit on the reinjection temperature equal to 70°C and an ACC unit is used.

As mentioned in section 3.3 (Hot geothermal brines) and in section 5.2 (One pressure level cycles) most of binary geothermal plants are based on a single evaporation level subcritical cycle with a saturated, or slightly superheated, turbine admission. This plant layout is the most common in ORC applications, nevertheless if the hot source is characterized by a large available temperature variation it is not the most suitable one because it entails large efficiency losses in the heat introduction process which is characterized by large temperature differences. From a thermodynamic point of view superheated cycles, using low critical temperature fluids, can reduce these losses thanks to the heat introduction at higher temperature in the superheater section with a consequent efficiency increase. A further improvement is to adopt supercritical cycles where the smooth transition above the critical point allows minimizing the mean logarithmic

temperature difference in the PHE. Finally two pressure level cycles are proposed on the marked but they are rarely adopted because of their higher complexity.

In this section a comparison between subcritical, supercritical and two pressure levels cycles is performed from a techno-thermodynamic and a techno-economic point of view highlighting the importance of using reliable correlation for the estimation of turbine efficiency. In addition, for the thermodynamic optimization three different cases are examined imposing a fixed turbine efficiency (i), calculating the performances with a direct coupling with the generator (ii) and finally optimizing the rotational speed (iii).

All the assumptions related to pressure drops and component performances are reported in Table 8.2.

Algorithm selection for thermodynamic and techno/economic optimization

The selection of the most suitable optimization algorithm should be performed with one or more test cases and comparing the results obtained with different optimization strategies. Some algorithms are more suitable than others to solve a certain problem depending on the shape of the objective function, the presence of local minimum and discontinuities. Thermodynamic optimization with a fixed turbine efficiency usually act on a limited number of variables (up to 6 for two pressure levels cycles) and presents a relatively smooth solution surface. Local minima are always present but there are no discontinuities. This allows using algorithms based on the derivate calculation like the basic matlab *fmincon*. On the other hand, economic optimizations present discontinuities when turbines with a different number of stages are used and when some components are suppressed by the optimization routine. In these cases other algorithms can perform better than *fmincon* like the *pattern-search* or the *genetic-algorithm*. Here two test cases are proposed: a thermodynamic optimization (i) and a techno-economic optimization (ii) are applied to a two pressure levels cycle for geothermal energy exploitation. In the first case the selection of the best algorithm is performed by comparing the final solutions with the reference optimal solution which can be easily achieved with a parametric analysis. In the second case only a some consideration is reported since the larger number of optimization variables does not allow a graphical representation. Assumptions common to both test cases are reported in Table 9.1.

For the thermodynamic optimization five variables must be considered since the thermodynamic cycle has both pressure levels subcritical. Superheating is considered on both levels. Working fluid is pentane and the three algorithms presented in section 8.2.3

(Optimization algorithm selection) are compared. The reference solution is found investigating cycles without superheating[16] and imposing different values of mass flow ratio thus optimizing only the two evaporation temperatures. M_r is the most critical variable since small changes of its value strongly affect the pinch point temperature differences in the PHE and the overall final solution. A recuperator is adopted at low temperature and a minimum pinch point temperature difference in the PHE equal to 3°C is considered.

fluid	pentane
$T_{in,HS}$	150°C
$T_{limit,HS}$	70°C
m_{HS}	200 kg/s
T_{amb}	15°C
T_{cond}	30°C
$\Delta T_{pp,cond}$	0.5°C
$\Delta T_{pp,rec}$	5°C

Table 9.1 - General assumptions for the optimization test cases

In Figure 9.1 the trend of the optimal solutions of a two pressure levels saturated cycle is reported against M_r and the two dotted lines define a range of ±0.5% error. The maximum is found in correspondence of a mass flow ratio close to 0.4 corresponding to a net power output slightly higher than 8.4 MW_{el} and a $DT_{pp,PHE}$ equal to the minimum one in both pressure levels. The markers are representative of the final solutions achieved by the three different algorithms and the values of the optimized variables are reported in Table 9.2.

	W_{net}, MW_{el}	M_r	$T_{eva,LP}$,°C	$\Delta T_{sh,LP}$	$T_{eva,HP}$,°C	$\Delta T_{sh,HP}$
inizialization	7.212395	0.5	68.5	10	107	10
fmincon	8.392582	0.391301	81.5527	0.009396	114.544	0
pattern-search	8.143362	0.5	76.01563	0.000002	115.9346	19.47371
genetic-algorithm	8.193192	0.455302	78.47449	0	114.8113	14.22435

Table 9.2 – Variables and objective function values at initialization and optimal point for the three optimization algorithms

[16] For high critical temperature fluids in saturated cycle configuration, superheating is usually detrimental [10; 20]

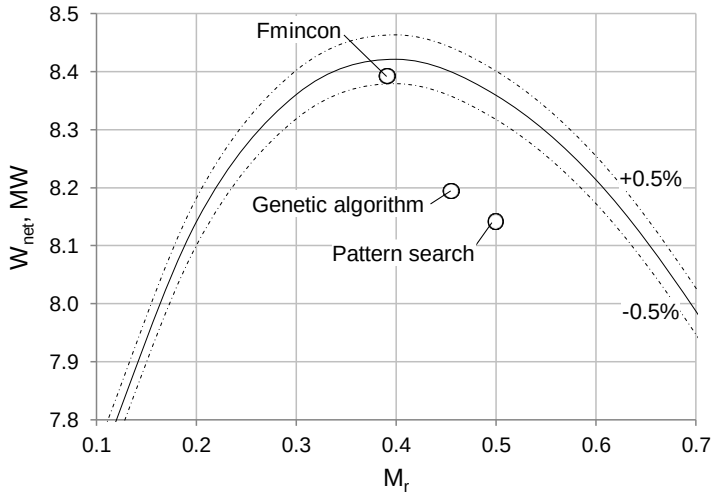

Figure 9.1 - Comparison between the final solutions achieved by the three optimization algorithms and the reference solution for the considered test case. Dotted lines are represents an error of ±0.5%

It is interesting to note how only *fmincon* is able to find the real optimum of the problem and the final small error is mainly related to the presence of additional pressure drops in the superheater which are not considered in the reference case. The optimal value of M_r is correctly found. In order to understand the differences between the three algorithms the trends of the optimization paths for both the objective function and the optimization variables are reported in Figure 9.2. It is interesting to note that the initialization point is pretty close to the final solution, represented by the *fmincon* solution: both evaporation temperatures are close to the optimal value and superheating is initialized at 10°C and so in the very low side of its variability range defined by the lower and upper bounds. As result the initial power output is 12% lower than the optimal value, a gap which is totally bridged by *fmincon* algorithm and only partially by the other two routines.

From the optimization paths it is possible to note how *fmincon* applies contextual small changes to all the variables reaching a final solution where both superheating temperature increments are set to zero. *Pattern-search* fails mainly because it starts acting only on some variables leaving M_r substantially unchanged until the solution is likely in local minimum. Any change of M_r from this point entails a decreasing of power output and so the final value of the mass flow rate ratio remains equal to 0.5. The low pressure superheating is properly set to zero while the high pressure one is far from the optimal value since it is increased to 20°C. Furthermore *pattern-search* requires a number of iterations almost twice than *fmincon* algorithm. *Genetic-algorithm* is able to reach a better result than *pattern-search* but it fails in the optimization of superheating temperature

difference in high pressure level and, even if it catches the trend of M_r, it quits the computation with a value remarkable higher than the optimal one. The number of iterations greatly exceeds the other two algorithms.

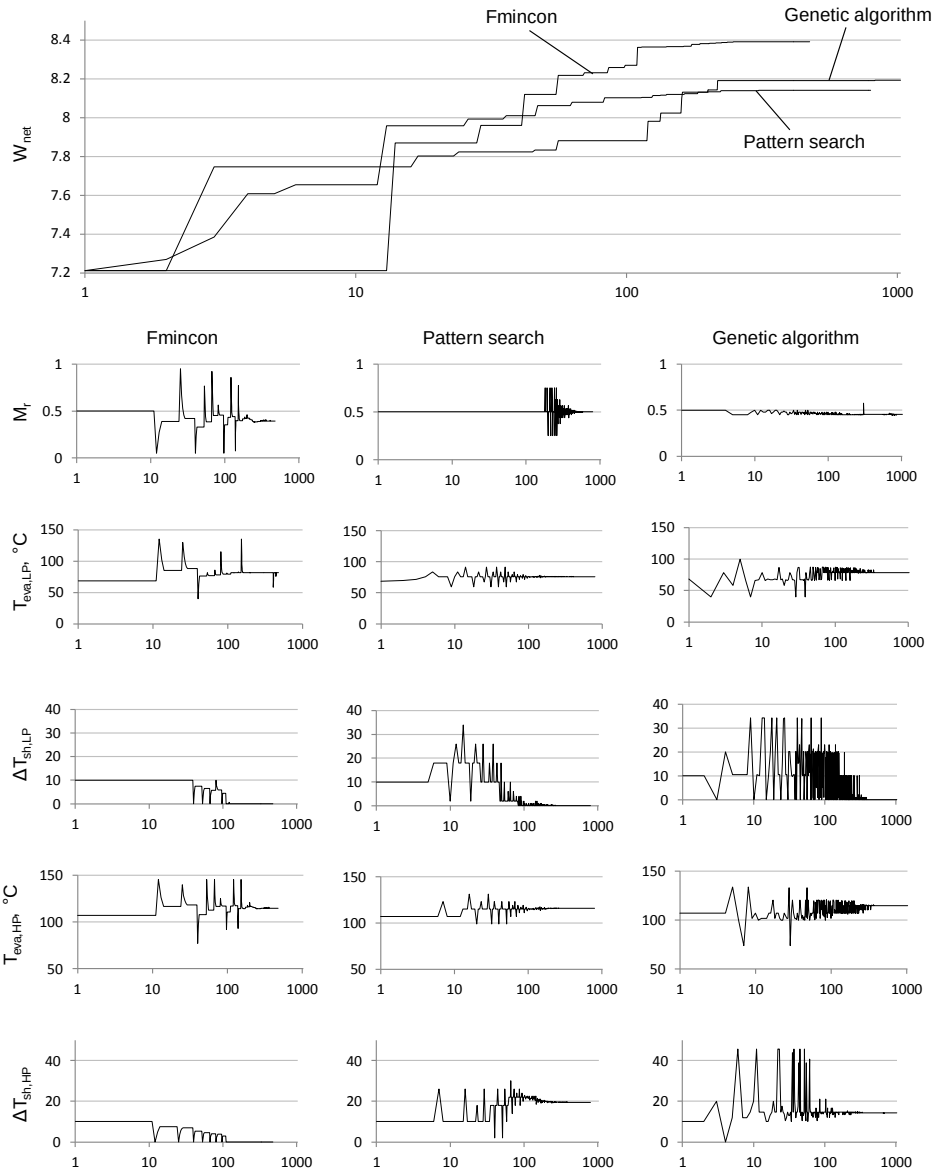

Figure 9.2 - Trends of optimization paths for objective function and optimization variables for three algorithms

The second example is the techno-economic optimization applied to the same reference case: in addition to evaporation temperatures, superheating temperature differences and mass flow rate ratio, even condensing temperature and pinch point temperature differences in both the condenser and the recuperator and the outlet temperature of geothermal brine are varied. The number of stages, and so the cost of each turbine,

changes with the volume ratio which is strictly related to the values of evaporation temperatures and pressure of condensation.

The trend of specific cost is displayed in Figure 9.3 exploring different combinations of evaporation temperatures while maintaining fixed the other variables.

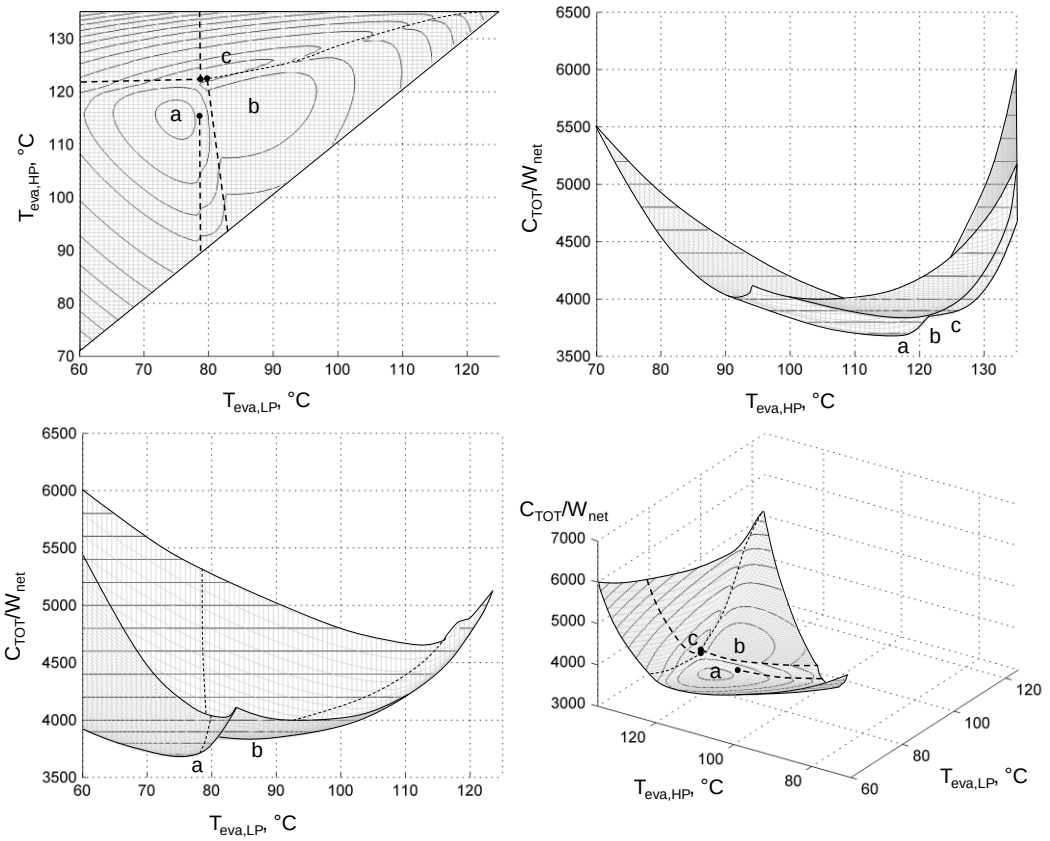

Figure 9.3 - Surface of objective function for the techno-economic test case. Local minimum are labelled with letters b and c, while the global optimum with letter a. Dotted lines show the presence of discontinuities

It is possible to notice that the objective function presents at least three local minimum and several discontinuities represented in figure by dotted lines. In this case it is not possible to represent the optimization paths due to the larger size of the problem but it is possible to highlight that *fmincon* algorithm is not suitable to solve this kind of problem, it is affected by the presence of discontinuities and it stops prematurely the execution in a point close to a ridge. In particular it acts on just few variables in the first hundreds of iteration moving far from the optimal point. *Genetic-algorithm* takes a long number of iteration before approaching a point relatively close to the real optimum: with a better definition of the algorithm parameters (size of the population, migration and mutation factors) it is certainly possible to obtain a better solution. The most suitable algorithm is

the *pattern-search* which is able to reach the optimal solution in a number of iterations slightly smaller than 10000.

In the next calculations a combination of *fmincon* and *pattern-search* algorithms is used in order to take advantage from the peculiarities of these two methods. *Genetic-algorithm* is not used because is negatively affected by the small size of the problem and it requires an excessive computational time.

9.1.1 Techno -thermodynamic optimization

The techno-thermodynamic optimization is carried out in different steps: first the different solutions are investigated with a hypothesis commonly adopted in literature, namely a fixed turbine efficiency, later this assumption is removed and two cases are compared, one with a direct coupling with the generator and the other one with a turbine at optimized rotational speed.

Two examples of thermodynamic optimization

As above mentioned, in thermodynamic optimization it is necessary to consider at least two optimization variables for single pressure level cycles, namely the turbine inlet pressure and the maximum temperature of the cycle. The reason is not trivial and the optimal values differ appreciably among the different solutions depending on the critical temperature of the working fluid respect to the temperature of the heat source and depending on the plant layout. This is one of the differences between ORCs and common steam cycles where usually the maximum cycle temperature is fixed considering a maximum allowable temperature for the superheater tube material or a minimum approach point temperature difference with the hot source which is fixed by techno-economic reasons. In order to highlight the influence of the two optimization parameters on the final thermodynamic performance, the results for two different cases corresponding to a supercritical regenerative cycle with R134a and a R245fa subcritical regenerative cycle are presented in Figure 9.4, Figure 9.5 and Figure 9.6. The geothermal brine temperature is fixed equal to 150°C and the rejection temperature is limited to 70°C, a minimum pinch point temperature difference in PHE equal to 3°C is considered. Different combinations of $p_{in,turb}$ and $\Delta T_{ap,PHE}$ are investigated for both cases.

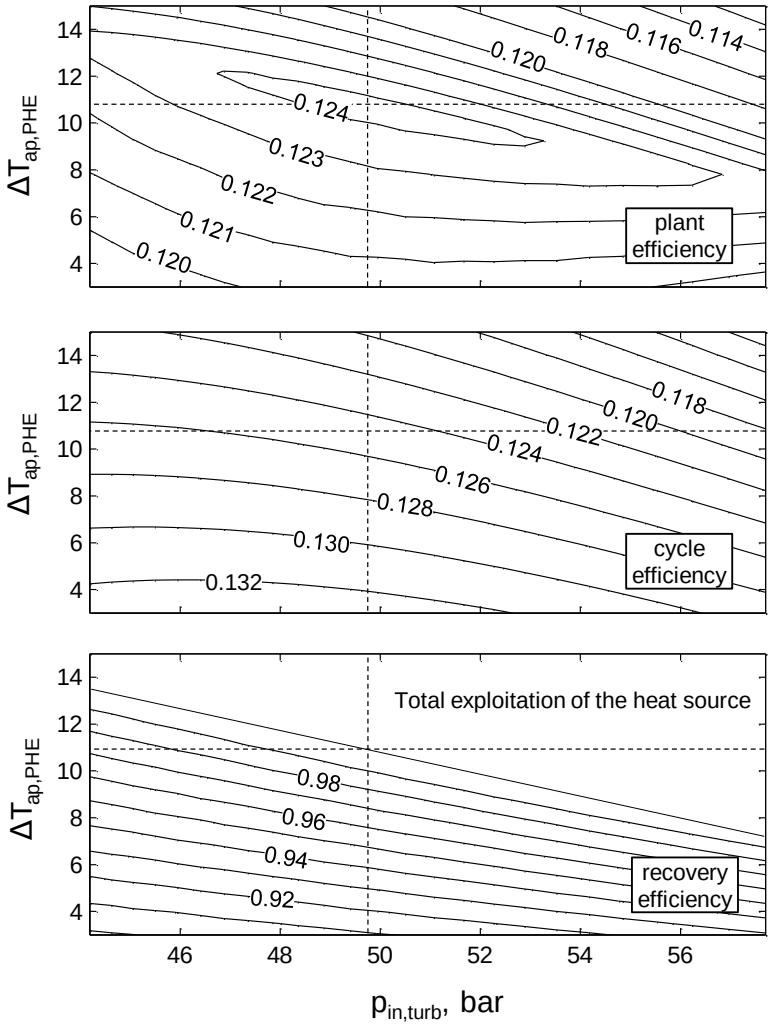

Figure 9.4 – Results for a supercritical R134a cycle. Contour maps for plant efficiency (a), cycle efficiency (b) and recovery efficiency (c) varying the maximum pressure of the cycle and the approach point temperature difference in the PHE

From the contour diagrams in Figure 9.4 referred to R134a supercritical cycles, it is possible to note that the optimal results are obtained for the cycles with the best compromise between cycle efficiency and recovery efficiency. For a given $p_{in,turb}$, reducing $\Delta T_{ap,PHE}$ (i.e. increasing the turbine inlet temperature) allows reaching higher values of the cycle efficiency, but above a certain limit yields a lower heat recovery from geothermal brine. Optimum value of $\Delta T_{ap,PHE}$ is higher than the lower bound and, for a given turbine inlet pressure, it is near the maximum value for which a heat recovery efficiency of 100% is obtained.

The results for R245fa are presented in Figure 9.5 where parametric curves for different values of ΔT_{sh} are reported and compared with the values which can be obtained for a

saturated cycle. By observing the trend of one of the reported curves, it is possible to note that at low evaporation pressures, geothermal brine is totally exploited with a pinch point temperature difference higher than the minimal value. An evaporation temperature increase is convenient because it entails higher cycle efficiency. This occurs up to a certain pressure and beyond this value the plant efficiency suddenly starts decreasing, or at least a marked change of slope for low ΔT_{sh} values can be notice. Here, the minimum pinch point temperature difference in PHE becomes the active constraint and geothermal brine reinjection temperature is higher than the limit entailing a recovery efficiency drop with detrimental effects on cycle performance. As widely observed in the literature for organic fluids, it is evident that, for high critical temperature fluids, saturated cycles is the optimal solution and the superheating is detrimental for thermodynamic performance [10; 20].

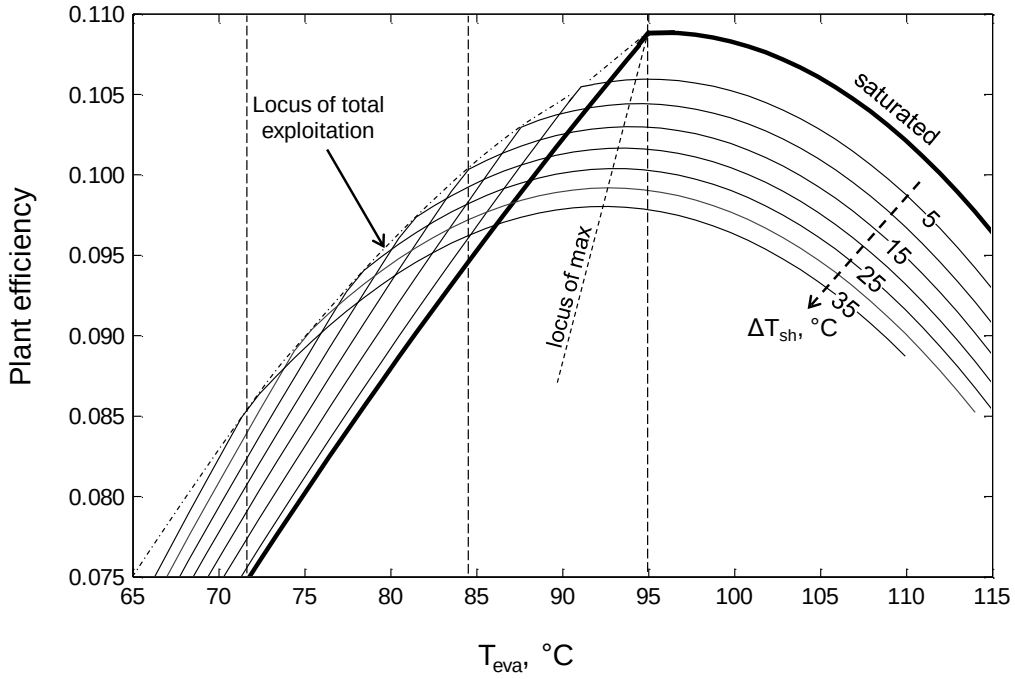

Figure 9.5 - Plant efficiency for a subcritical cycle with R245fa for different evaporation temperatures and superheating temperature increments. The thicker line is representative of the saturated cycle while with dashed lines are connected the locus of maximum efficiencies and the locus of total exploitation of the heat source.

The situation is illustrated in Figure 9.6, where the influence of superheating is analysed for three turbine inlet pressures: while at low pressure increasing the superheating is beneficial, mostly due to lower irreversibilities in the heat introduction in the evaporation phase and in the economizer, for higher pressure the reduced exergy losses in heat exchangers are overcompensated by the higher residual exergy in the brine discharged. This analysis, repeated for different fluids with high critical temperature and overhanging

saturation line, suggests that the best performance is generally reached for saturated cycle with the higher value of evaporation pressure consistent with the rejection temperature constraint.

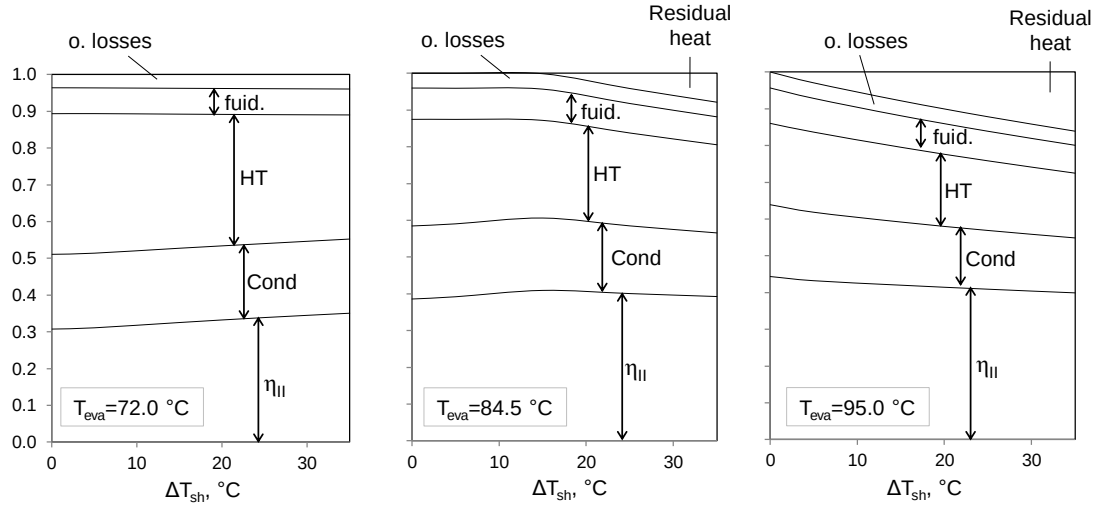

Figure 9.6 - Second law analysis breakdown for three different evaporation temperatures.

Thermodynamic optimization with a fixed turbine efficiency

As reported from tables Table 2.1 to Table 2.3 most of the analysis in literature are carried out considering a fixed efficiency for the turbine, independently of the working fluid and the cycle parameters. This assumption is approximately valid only if the rotational speed is not fixed and the number of stages is selected without any techno-economic constraints. A very high overall efficiency can be always obtained by optimizing the rotational speed and by increasing the number of stages thus limiting the volume variation across a single row. In this section a fixed isentropic efficiency equal to 85% is assumed as representative of average performance in geothermal field but for some fluids the maximum achievable efficiency can be higher than this imposed value, thus involving non-optimized final solutions. On the other hand for fluids characterized by large volume ratios, the assumption of a fixed value of efficiency might lead to turbines with a large and non-feasible (from an economic point of view) number of stages. This assumption will be removed in the next sections but it is useful now in order to present some thermodynamic results for the three considered cycle configurations and underling how different assumptions can affect the optimal solution.

Results for the subcritical configuration are reported in Figure 9.7 where the trend of specific power calculated as the ratio between net plant power and brine flow rate is displayed against a reduced temperature parameter. This parameter is defined as the ratio between the critical temperature of the fluid and the maximum temperature of the

geothermal brine in Kelvin degrees. Reporting the results against this reduced temperature is useful to compare solutions with different temperatures of the geothermal source and to define general criteria in fluid and cycle selection.

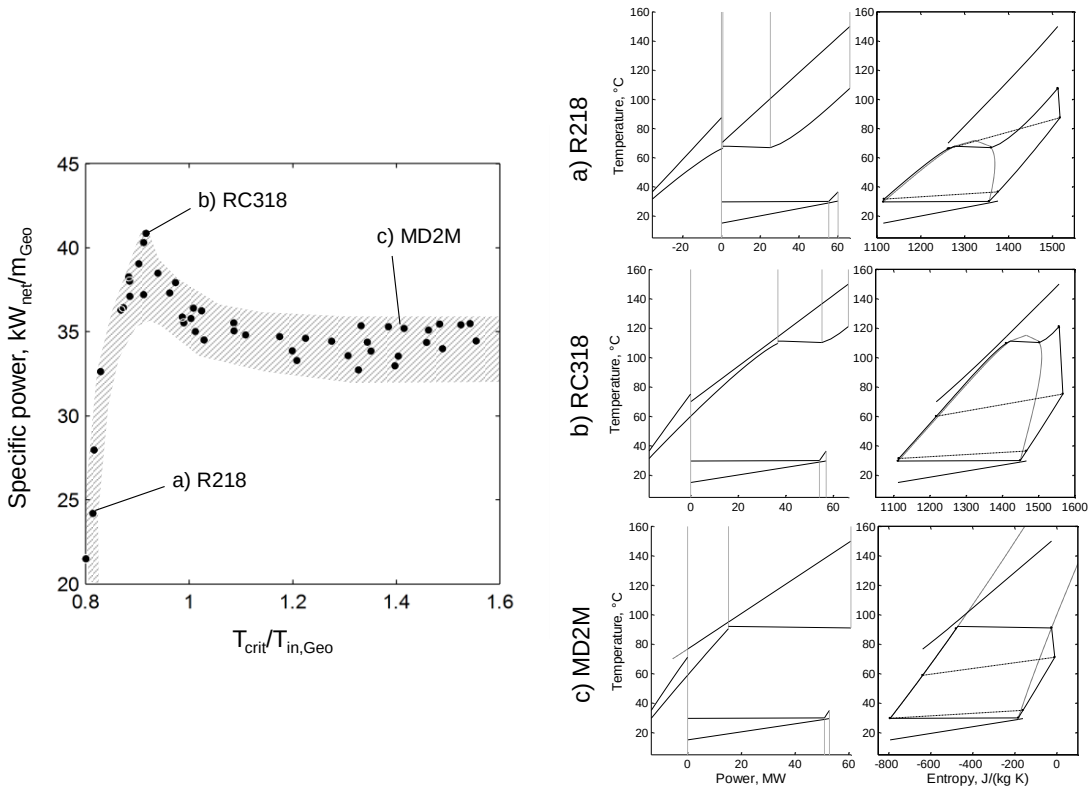

Figure 9.7 - Specific power for subcritical cycles optimized by varying evaporation temperature and superheating temperature difference. The T-Q diagram and the T-s diagram is proposed for three fluids representative of a low critical temperature fluid (R218), a high critical temperature fluid (MD2M) and the optimal fluid (RC318)

Each marker is representative of the optimal solution for a subcritical cycle configuration obtained by acting on two variables: the evaporation temperature and the superheating temperature increment. Using fluids with a low critical temperature (e.g. R218) entails a limitation of power output mainly because of limited evaporation temperature (i) and the correction of the pinch point temperature difference in the recuperator (ii) in order to avoid evaporation in this component. As result, the temperature differences in both recuperator and PHE are larger than the minimum, and the maximum temperature of the cycle is limited in order to maintain a lower outlet temperature from the turbine. In this way it is possible to exploit the whole available heat in the recuperator without increasing the duty of the condenser and the efficiency losses due to a higher weight of the desuperheating section. For fluids with a critical point lower than the reinjection temperature an even stronger penalization occurs because the pinch point temperature

difference in the PHE is larger than the minimum one. For fluids with a critical temperature higher than the brine maximum temperature (MD2M), instead, the adoption of a superheating is detrimental as already demonstrated in Section 8.2.1 (Two examples of thermodynamic optimization) for pentane fluid and for $T_{in,geo}/T_{crit}$ larger than unit all the optimal cycles show a saturated vapor condition at turbine inlet. No effects of fluid thermodynamic properties on turbine efficiency are here considered and all these cycles show almost the same performance because they work between the same condensing (fixed) and evaporation (optimized) temperature and they basically refer to the same ideal Carnot efficiency.

In Figure 9.8.a and Figure 9.8.b it is possible to observe the optimized trends of both temperature increment in superheating and the evaporation temperature. The ΔT_{sh} decreases with the critical temperature reaching null values for reduce temperature close to unit. Evaporation temperatures are instead limited by the critical temperature of the fluid for $T_{in,geo}/T_{crit}$ lower than 0.9 while for greater values this parameter assumes an almost constant trend. It is interesting to note that the optimal evaporation temperature value is higher than the ideal Carnot one calculated with eq. 5.7 and corresponding to a value of 76°C because of the presence of an economizer section and a condensing temperature higher than the ambient one.

It is evident that subcritical superheated cycles working with fluid with critical temperatures lower than the brine temperature tends to supercritical cycles. The optimal working fluid is RC318 whose optimal evaporation temperature is pushed toward the upper bound and possible advantages are achievable by the adoption of a higher maximum pressure. The specific power for optimal supercritical cycles is reported in Figure 9.9 and compared with the previous results: supercritical cycle can reach higher performances thanks to a better matching between the heat source and the working fluid in the PHE. Efficiency increment is larger for low critical temperature fluids where no limitation of the recuperator is now considered.

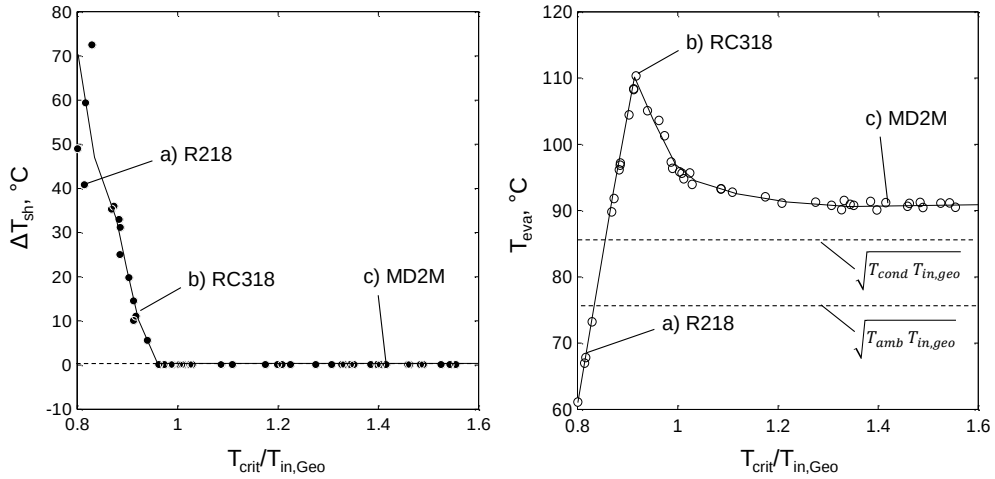

Figure 9.8 – Optimized temperature increment in superheating (a) and optimized evaporation temperature (b) for single level subcritical cycles

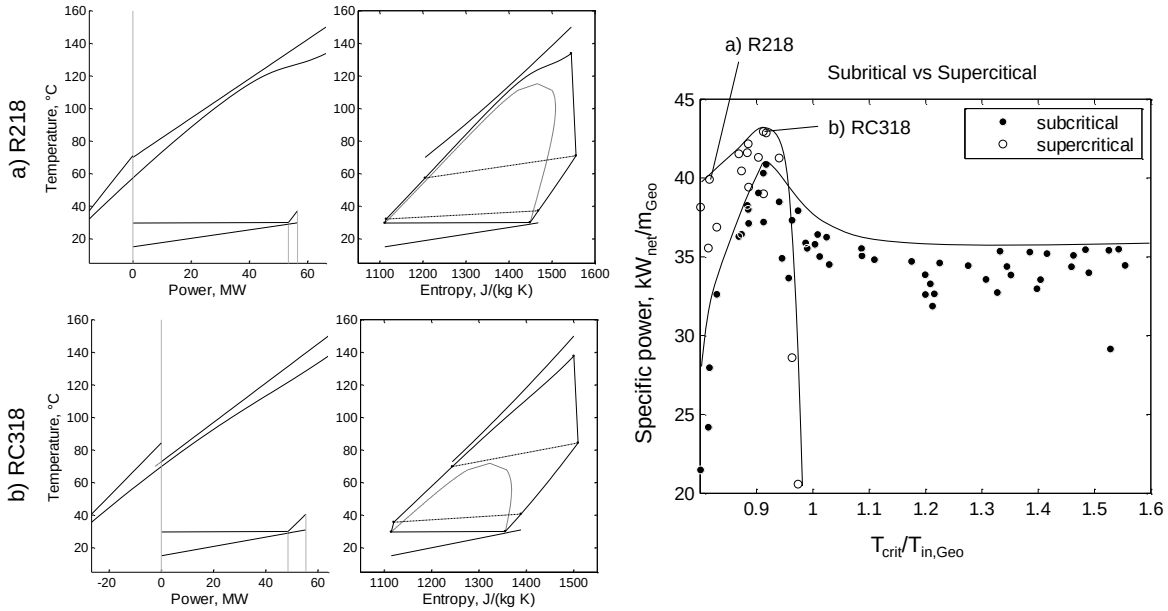

Figure 9.9 - Comparison between performance achievable for supercritical and subcritical single level cycles (a)

Finally two pressure levels cycles are considered even if they are rarely proposed for the exploitation of geothermal brines. With this plant layout it is possible to reduce the efficiency losses in the heat introduction process and achieve and higher power production. In Figure 9.10 the optimal results for the two pressure levels cycles are reported: the results are obtained by acting on five variables namely the two evaporation temperatures, the superheating increments and the ratio between the high pressure and the low pressure mass flow rates. The maximum specific power is close to the supercritical cycle one but the same result is achieved with a more complex plant layout and a more

complex operation where the levels of the condenser hot well and of the both evaporators have to be controlled.

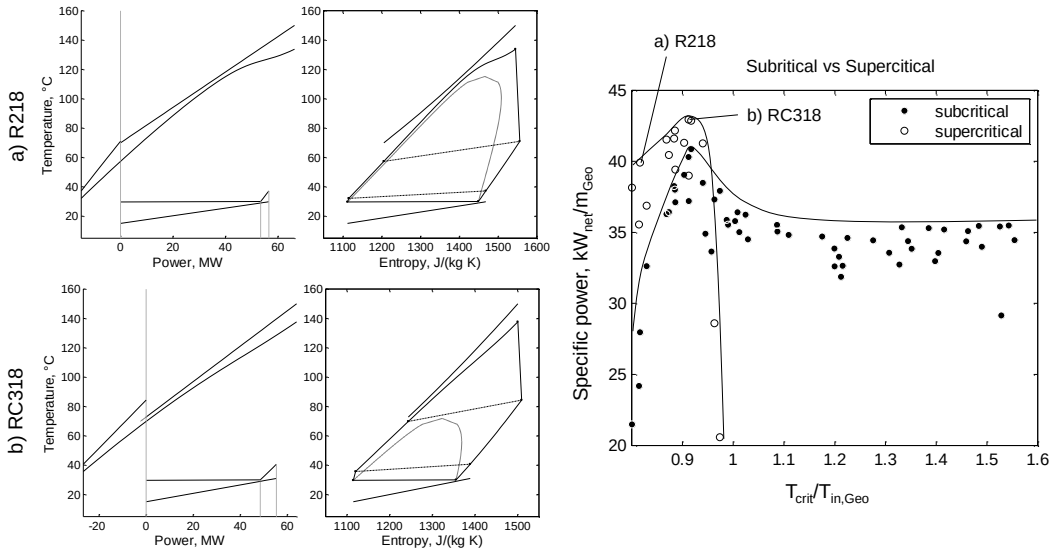

Figure 9.10 – Performance of optimized two pressure levels cycles and T-Q and T-s diagrams for two fluid: RC318 and MD2M

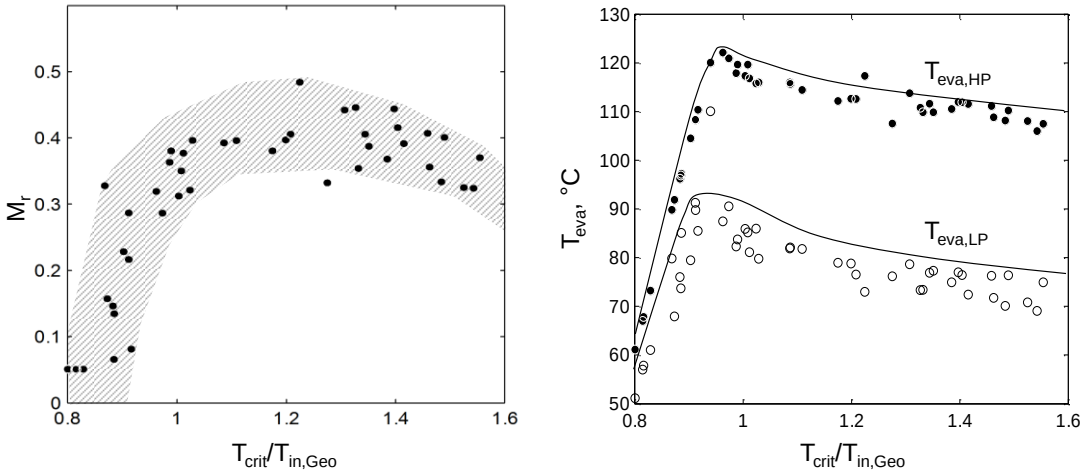

Figure 9.11 – Optimized LP/HP mass flow rate ratio (a) and optimized evaporation temperatures (b) for two pressure levels cycle

The optimal values for the evaporation temperatures are reported in Figure 9.11.a while the value of mass flow rate ratio is reported in Figure 9.11.b. It is possible to notice that

for low critical temperature fluids the two evaporation temperature are almost equal and the difference between them is pushed to the lower bound (10°C) furthermore the mass flow ratio tends to zero leading to solutions which tends to the single level superheated subcritical cycles as shown for the RC318 case. For high critical temperatures fluids instead the two evaporation temperatures are notably different with a difference almost constant varying the fluid with a value around 30°C.

From a thermodynamic point of view and with a fixed turbine efficiency supercritical cycles lead to higher performances compared to both single level and two levels subcritical cycles.

Techno-thermodynamic optimization with turbine directly coupled with the generator

A typical simplification which is usually done in the study of ORC system is to consider the turbine efficiency constant independently of the working fluid used and the parameters of the thermodynamic cycle. In particular, as will be better explained later, an almost constant efficiency can be obtained only if a gear box, a multi poles generator or a power electronic system are used and the rotational speed is optimized. With a direct coupling with the generator, the assumption of turbine fixed efficiency can lead to large errors and final misleading final results, as can be noticed by observing Figure 9.12.a, where the expander performance is reported for the subcritical optimal solutions. It is important to underline that these values are obtained with a different combination of evaporation temperature and superheating respect to the previous case because the optimization is carried out considering the effects of cycle parameters on turbine efficiency and in some cases the possibility to enhance the turbine efficiency is obtained by means of a reduction of evaporation temperature. A very high efficiency can be obtained for a large number of fluids but it is possible to notice that for some low critical temperature fluids and for high temperature fluids the turbine isentropic efficiency drops because of the non-optimized rotational speed. In addition, for high critical temperature fluids the volume ratio is large and multi stage turbines are adopted. In Figure 9.12.b the number of stages is reported while in Figure 9.12.c the stage specific speed, or the mean specific speed for multistage turbines is reported showing that some turbines have a Ns value lower than the optimal one while others show values greatly above 0.1-0.15. Efficiency decrement is higher for multistage turbines where the last stage is strongly penalized by large volume flows at turbine outlet.

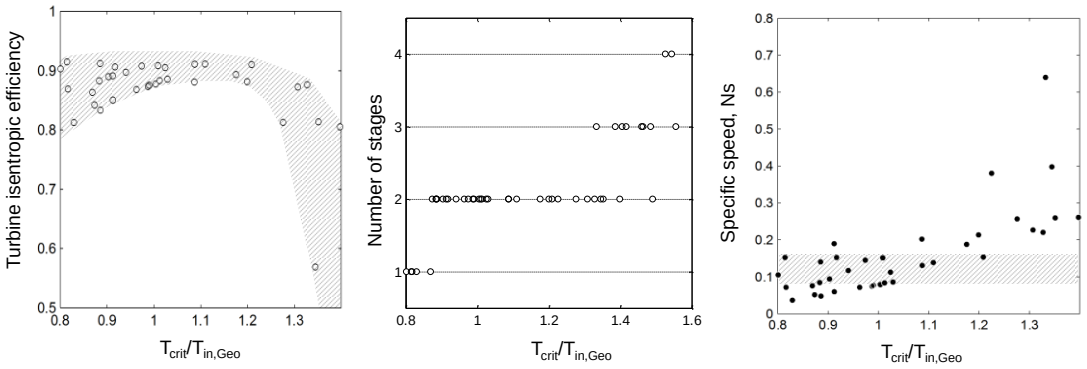

Figure 9.12 – Maximum attainable isentropic turbine efficiency for a direct coupling with the generator (a), number of stages of the turbine (b) and mean stages specific speed (c) for a subcritical cycle

Techno-thermodynamic with turbine efficiency calculated at optimal rotational speed.

The same cases are analyzed optimizing the rotational speed with the procedure introduced in section 6.1.5 (Comparison between discretized and global approaches) and recalled in section 8.2.3 (Turbine solve). Always with reference to the subcritical cycle it is possible to observe how the optimal rotational speed is equal to 3000 RPM for many solutions but fast turbines are needed for low critical temperature fluids and low rotational speeds are required for high critical temperature fluids as reported in Figure 9.13.

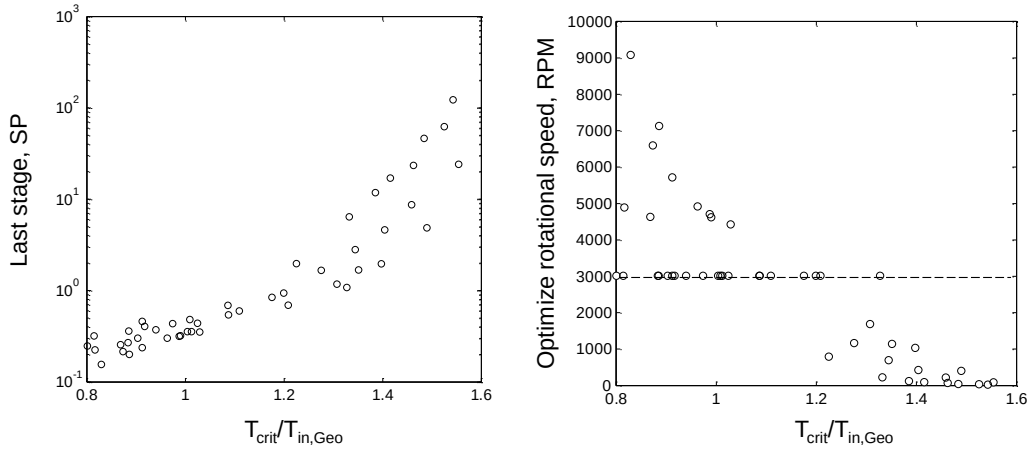

Figure 9.13 – Increment of last stage SP for high critical temperature fluid (a) and optimized turbine rotational speed (b)

Optimized turbine efficiencies are obviously higher respect to those solutions with direct coupling with the generator but a decrease of performances is highlighted for high critical temperature fluids characterized by multistage turbines due to the trade-off between stages with very different optimal rotational speed. This effect is even larger for two

pressure level cycles where the rotational speed is determined considering both turbines on the same shaft and the optimal rotational speed results from a trade-off between the high pressure and the low pressure turbines characterized by stages with a very different size parameter and very different optimal specific speed. These effects result in a penalization of the plant efficiency for high critical temperature fluids as shown in Figure 9.14 where the comparison between the optimal solutions for both subcritical and supercritical single level cycles and two pressure levels cycles is reported for the fixed turbine efficiency case, for the case with a direct coupling to the generator thus rotating at 3000 RPM and with the results obtained at optimized rotational speed. It can be noticed that the optimal cycle is always in supercritical configuration using a fluid with a critical temperature close to the inlet temperature of the geothermal brine. Efficiency of subcritical cycles (both single and two pressure levels) decreases for high critical temperature fluids due to the penalization of turbine efficiency over mentioned. In addition Size Parameter of the last stage notably increases leading to a higher cost of the turbine.

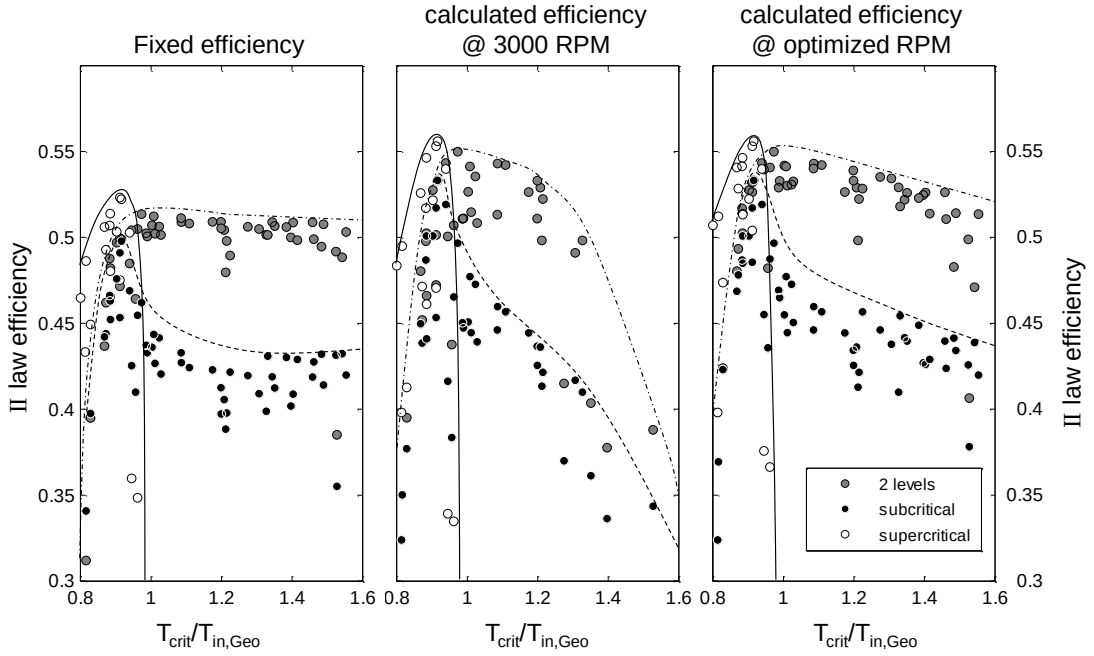

Figure 9.14 – Comparison between the optimal cycles from a thermodynamic point of view with different hypothesis on the turbine efficiency

Referring to Figure 9.14.c the maximum attainable efficiency is obtained for a supercritical cycle working with RC318, Main cycle parameters and results are reported in Table 9.3 for the three best fluids while the T-Q diagram are represented in Figure 9.15.

ranking	1	2	3
fluid	RC318	C4F10	R236ea
cycle	Supercritical recuperative	Supercritical recuperative	2 pressure levels
$T_{in,geo}/T_{crit}$	0.9178	0.913	0.975
Cycle efficiency	13.66%	13.59%	13.51%
Recovery efficiency	100%	100%	100%
Plant efficiency	13.62%	13.55%	13.47%
Specific power, kWel/(kg/s)	45.59	45.35	45.10

Table 9.3 - Best combination of working fluid and cycle configuration for the exploitation of a 150°C geothermal brine

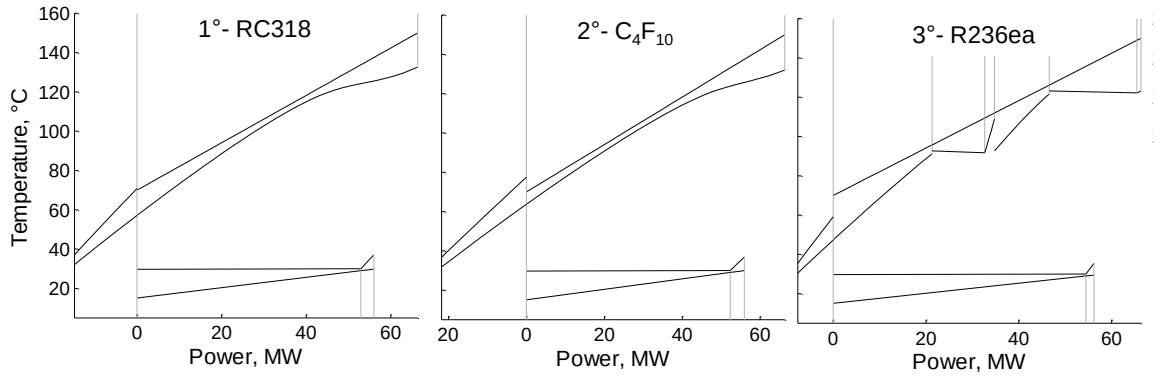

Figure 9.15 - T-Q diagrams of the first three best plants for the exploitation of a 150°C geothermal brine

Comparison between 120°C-150°C-180°C geothermal brines

The techno-thermodynamic optimization is carried out for all the available fluids, considering different geothermal brine temperatures between 120°C and 180°C, representative of different geothermal fields. As on the previous case the analysis is repeated with minimum reinjection temperature of 70°C. All the calculations refer to solutions with turbine efficiency calculated at optimal rotational speed.

A graphical comparison among three investigated cases (120°C-150°C and 180°C) is reported in Figure 9.16, in terms on specific power and second law efficiency where each point represents the best cycle configuration for a given working fluid. Firstly, it is possible to note that, for the different geothermal brines considered, a similar trend is obtained against the $T_{in,geo}/T_{crit}$ ratio for both the 150°C and the 180°C cases. The same behaviour is obtained for all the temperatures greater than 140°C but the results are not reported in figure due to graphical reasons. This peculiarity is quite interesting and it suggests the possibility to define some global rules in the simultaneous selection of cycle configuration and working fluid.

The optimal fluid has a critical temperature which lies in a very narrow range between 0.88 and 0.92 of the geothermal brine temperature with a supercritical cycle. The only exception is the lowest geothermal brine temperature considered (120°C), the optimal fluid is heptane in 2 pressure levels cycle, which has a critical temperature higher than the maximum temperature of the geothermal brine. This can be explained considering the low temperature difference available for geothermal brine cooling, corresponding to the exploitation of a heat source at almost constant temperature, which leads to no advantage in the adoption of a supercritical "nearly triangular" cycle. In addition, supercritical cycles with low critical temperature fluid lead to high maximum pressures and a relevant pump power consumption. Nevertheless the 120°C geothermal brine allows designing a large number of cycles with competitive performances and subcritical single level cycles can achieve an efficiency comparable to the best solution but with a simpler plant layout.

Recuperator pinch point is optimized by the algorithm and its value is always pushed to the lower bound (5°C) because a limit in reinjection temperature is here considered and so the use of an efficient recuperator allows reducing the mean logarithmic temperature difference in the economizer, a higher mass flow rate and a higher power production without limiting the exploitation of the geothermal brine.

From a thermodynamic point of view it is hence possible to conclude that, for a given geothermal source, a pre-selection can be made among a small number of working fluids which allows, in supercritical configuration, to achieve the highest performances. However, the adoption of supercritical cycles leads to higher values of $\sum UA / W_{net}$ compared to both single level subcritical cycle and two pressure levels plants. Therefore, higher heat exchange area and cost can be expected for optimized supercritical cycles, highlighting the importance of an economic analysis to define the optimal combination of fluid and plant configuration.

Brine temperature	120°C	150°C	180°C
fluid	heptane	RC318	R236ea
cycle	2 pressure levels	Supercritical recuperative	Supercritical recuperative
Tcrit/Tin,geo	1.3739	0.9178	0.9102
Cycle efficiency	11.19%	13.66%	15.64%
Recovery efficiency	100%	100%	100%
Plant efficiency	11.13%	13.62%	15.61%
Specific power, kWel/(kg/s)	23.28	45.59	72.01

Table 9.4 – Optimal plants for the exploitation of geothermal brines with maximum temperature of 120, 150 and 180°C

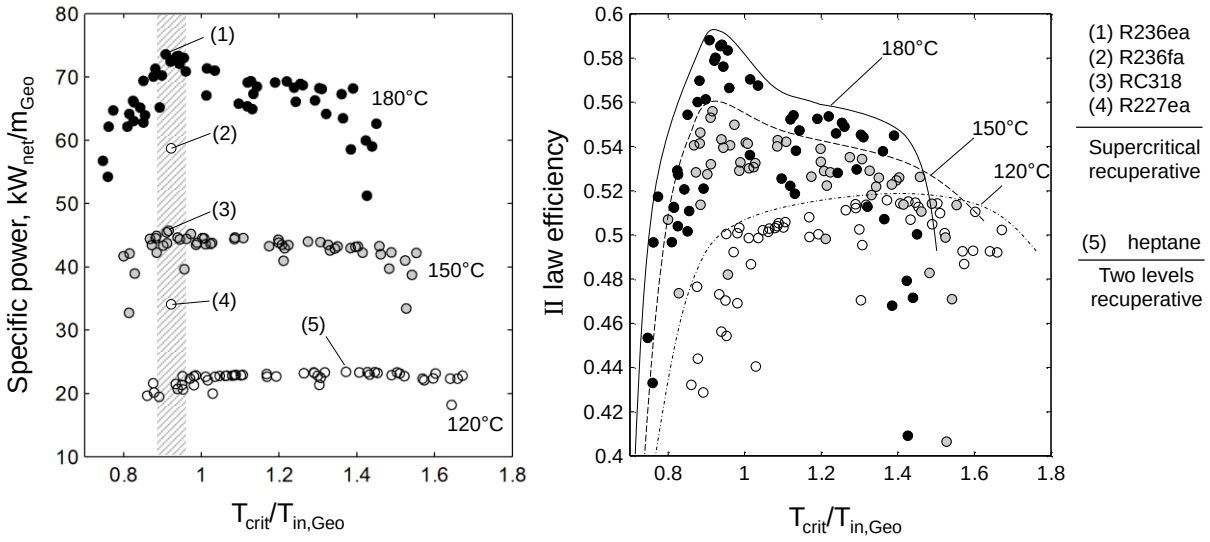

Figure 9.16 –Comparison between the maximum achievable performances using subcritical, supercritical and two pressure levels cycles for temperature of the geothermal brine ranging between 180 and 120°C

Effect of molecular complexity

Finally, some considerations on the influence of molecular complexity on the optimal fluid selection can be made. Complex fluids have similar specific heat in vapour and liquid phase, therefore their Andrews saturation line becomes overhanging. This characteristic allows designing PHE with very small ΔT_{mln} taking advantage from the relatively small heat capacity variation below and over the critical point.

This last point can be explained by considering two fluids with a similar critical temperature but different molecular complexity. The selected fluids are C_4F_{10} and R152a, whose backbone chains have four and two carbon atoms respectively. C_4F_{10} is a cycloalkane fully substituted by fluorine atoms, while R152a chemical formula is F_2HC-CH_3. Results obtained for the thermodynamic optimization are reported in Table 9.5, while T-s and T-Q diagrams are shown in Figure 9.17. Using a more complex fluid like C_4F_{10} gives the possibility to reduce heat transfer irreversibilities in PHE while the adoption of a regenerator allows increasing the cycle thermodynamic efficiency without penalizing the heat recovery efficiency. On the other hand, the use of C_4F_{10} demands for larger PHE heat transfer area and cost, highlighting once again the importance of economic analyses in a comprehensive optimization procedure. In Table 9.5, results of the second law analysis are also reported. In both cases, losses related to heat discharged by the condenser have the greatest impact, highlighting the importance of irreversibilities in heat rejection for cycles with a limited efficiency. As expected, the main difference is associated to the PHE, with a strong exergy losses reduction by moving towards higher

complexity fluids. Finally, the effect of the recovery efficiency is reflected in the brine residual heat loss, which contributes reducing the efficiency of R152a, even considering the additional losses in the regenerator present only for C_4F_{10}.

	152a	C_4F_{10}
Trid	0.913	0.913
prid	1.020	1.266
General performance indexes		
Wnet plant, kW_{el}	8266.84	9070.49
Specific Cost, USD^{2013}/kW_{el}	3562.88	4506.46
Specific Power, $kW_{el}/(kg/s)$	41.33	45.35
ΔT_{mln}	9.3	4.78
Specific UA, $(W/m^2)/kW_{el}$	2.16982	3.06296
efficiencies		
cycle efficiency	12.6%	13.6%
recovery efficiency	98.4%	100.0%
plant efficiency	12.4%	13.6%

UA, W/m^2	152a	C_4F_{10}
Condenser	10923	10215
Desuperheating	-	1170
Recuperator	-	2537
PHE	7014	13860
Second law balance		
etaII	50.4%	55.3%
Condenser	19.6%	19.0%
Geothermal mix	1.1%	0.0%
Heat transfer	14.0%	9.6%
Heat losses	1.0%	1.2%
fluidodynamic	10.2%	10.7%
Mechanic-electric	3.8%	4.2%

Table 9.5 - Comparison between a complex fluid (C4F10) and a simply fluid (R152a) having a similar critical temperature

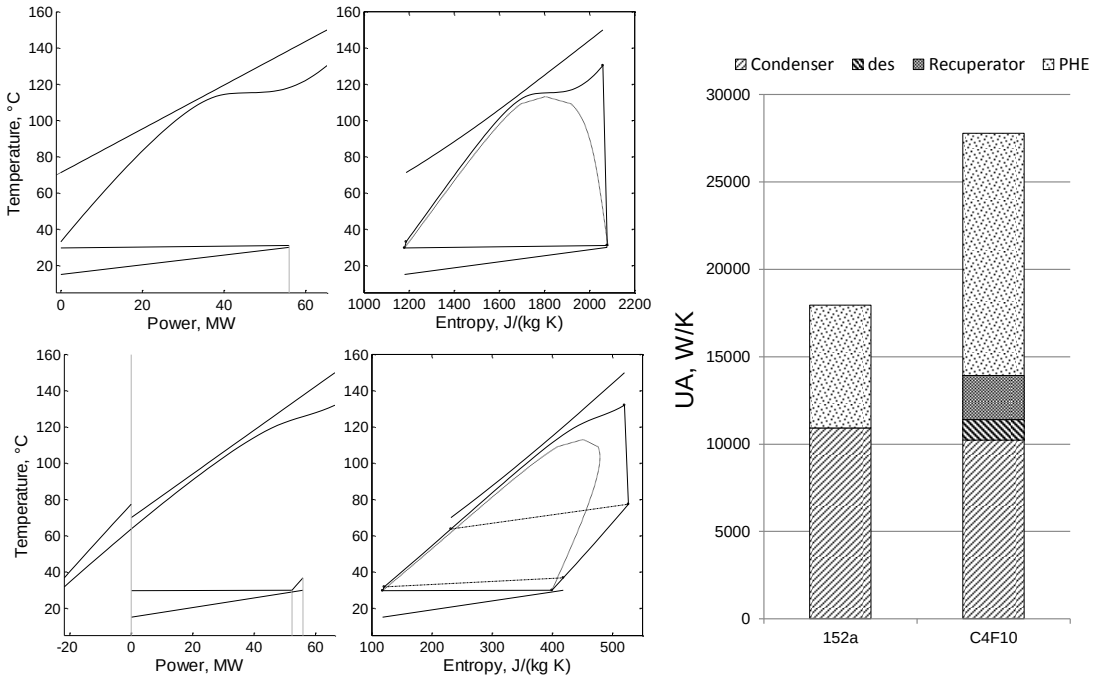

Figure 9.17 - T-Q and T-s diagrams for R152a and C4F10 and breakdown of UA

9.1.2 Techno-economic optimization

The techno-economic optimization is carried out with the aim of minimizing the specific cost of the plant. Thus the procedure takes into account the optimization of the heat exchanger surfaces, the turbine size and its efficiency and the effect of large fixed cost related to the exploitation of a geothermal reservoir. In geothermal fields the cost for the exploration campaigns, the drilling of the wells and the construction of all the required infrastructures is a relevant share of the final plant cost (up to 50%). For a 20MWel conventional geothermal plant the field development can range between 71-87 million USD^{2013} [234] with a cost breakdown as reported in Table 9.6.

operation	Cost USD^{2013}	Specific Cost USD^{2013}/kW$_{el}$
Site scouting and geophysical exploration	1.4-2.8	70-140
Exploratory drilling	28-42	1400-2800
Drilling	42	2800
Total	71.4-86.8	4270-5740

Table 9.6 – Cost breakdown for geothermal wells exploration and drilling expenses

In the next calculations only the drilling cost is considered and since different geothermal wells are investigated with temperatures of brine varying between 120 and 180°C a general correlation for source cost is proposed. By considering a favourable thermal gradient (ΔT_{geo}) of 50°C/km [235] and a specific cost of drilling (C_{drill}) equal to 1.2 million USD^{2013}/km including one production and one reinjection well with a mass flow rate of 100kg/s, the cost of the geothermal field is hence accounted by eq. 9.1

$$C_{geo} = \frac{m_{geo}}{100} \Delta T_{geo} \left(T_{geo} - T_{amb}\right) C_{drill} \qquad \text{eq. 9.1}$$

This results in a cost of around 16.2 million USD^{2013} for the reference case with a 150°C geothermal brine.

Preliminary analysis

A preliminary economic optimization procedure was carried out with four fluids having very different thermodynamic properties in order to validate the correlations adopted in a wide range of conditions and to verify the influence of the various parameters which mainly affect the final optimal solution. A geothermal brine with a temperature at PHE inlet equal to 150°C and a reinjection temperature equal to 70°C is taken as reference case.

Fluids here considered are R134a, ammonia, water and D5, a medium-large weight siloxane. R134a, despite its GWP, is commonly used as refrigerant fluid and as working fluid for supercritical regenerative cycles. Ammonia, thanks to its thermodynamic properties, gives the possibility to obtain a compact design of the components and may be profitable from an economic point of view. However, it is rarely used in power plants due to its flammability and toxicity. Water is the most common fluid used for power generation, but it is not competitive for medium-low temperature heat sources and small sizes, mostly because of the uneconomical turbine design. The selected configuration for ammonia and water consists of a subcritical superheated cycle with the adoption of a gearbox. Finally, D5 is considered in order to investigate the difficulties which can occur when using complex fluids with a high critical temperature. A subcritical superheated cycle is adopted, allowing the solver to converge to a saturated configuration acting on ΔT_{sh}.

In Table 9.7, the calculated efficiencies and values of the optimized parameters resulting from the thermodynamic and from the economic optimization are reported while in Figure 9.18 the comparison between thermodynamic and economic optimizations is presented for the four investigated fluids. Wide stacked bars are referred to absolute component cost repartition while tight bars show the change in total plant specific cost and power block specific cost.

Final results for R134a show a lower T_{cond} (i.e. a lower $\Delta T_{ap,cond}$) than the value adopted in the thermodynamic optimization with a consequent increase of both air condenser area and fans consumption. On the hot side, optimal maximum pressure (i.e. T_x) decreases while $\Delta T_{ap,PHE}$ and $\Delta T_{pp,PHE}$ increase entailing a higher value of $\Delta T_{mln,PHE}$, which allows reducing the cost of the primary heat exchanger, accepting lower cycle efficiency. Thanks to the optimization of $\Delta T_{pp,rec}$, geothermal brine is completely exploited in both cases. The main effect of economic optimization is a reduction of absolute total plant cost but also a lower value of both total plant (-12.65%) and power block (-27.14%) specific costs, even if net power production decreases.

The optimization procedure applied to ammonia entails a reduction of the condensing temperature (almost identical to the one found for R134a) with an almost constant evaporating pressure resulting in a higher power production. Power block cost increases because of the lower ΔT_{mln} in the condenser while for the PHE it remains almost constant but power block specific cost is slightly reduced, thanks to the higher power output. It is also important to note that the absolute power block cost is lower for ammonia than for R134a because subcritical cycles always lead to higher ΔT_{mln} and lower PHE costs. In addition also the ammonia turbine is cheaper than the R134a one, because of its small SP,

even if it is designed with a higher number of stages (4 vs. 2). The total plant specific cost finally decreases according to the higher plant efficiency. In both cases component cost repartitions show that primary heat exchanger, condenser and turbine cover almost the 75% of total power block cost. The final specific cost is lower for R134a, thanks to its higher efficiency.

As expected the results obtained for water and D5 are very different. With water as working fluid the optimized cycle show a low evaporation temperature in order to respect the constraint on minimum vapour quality at turbine discharge. Turbine is more expensive than for both R134a and ammonia because of the larger number of stages and the larger size parameter. The optimization algorithm has a small possibility to change this solution: an increase of evaporation temperature entails a reduction of recovery efficiency and a non-total exploitation of the geothermal source, in addition expansion wouldn't respect the vapour quality limit with a strong penalization of turbine performances. Both condensing temperature and evaporation temperature are slightly increased with the aim of reducing turbine cost while maintaining a good power production.

D5 is selected as representative of high complexity fluids. It features an overhanging saturation line and the optimization numerically converges to a saturated cycle, which is the most advantageous configuration also from the economic point of view due to the higher $\Delta T_{pp,PHE}$. The main difficulty found in using high critical temperature fluids is the very low condensing pressure and the consequently high specific volume at turbine exhaust, causing a high cost of this component. For this fluid, the turbine is largely the most expensive component and economic optimization leads to an increase in both evaporation and condensing pressure, with the main goal of reducing the turbine size. Recovery rate drops because of the higher evaporation temperature, entailing a lower plant efficiency and power production. The overall power block cost and total plant specific costs decrease, but reaching values which are more than twice than the R134a and ammonia ones.

In conclusion water and D5 are economically unsuitable for medium low temperature geothermal sources. In particular, water is more indicated for high temperature heat sources with net power of at least 5 MW, in order to reduce criticalities (small volume flow rates) in the design of the first turbine stage. On the other hand, D5 and other siloxanes and complex hydrocarbons are attractive for high temperature small-scale cogenerative applications, where the higher condensing temperature and pressure lead to a favourable size of the last turbine stage.

	R134a		ammonia		water		D5	
System efficiency								
cycle efficiency	13.30%	12.74%	11.50%	11.93%	9.30%	9.48%	13.13%	9.42%
plant efficiency	13.26%	12.70%	10.67%	11.25%	9.26%	9.30%	10.38%	6.41%
recovery efficiency	100.04%	100.04%	93.21%	94.71%	100.04%	98.54%	79.38%	68.54%
plant II law	0.5411	0.5182	0.4354	0.4591	0.3778	0.3794	0.4234	0.2617
General results								
Wnet plant	8879.4	8504.6	7145.8	7534.2	6200.2	6226.4	6948.4	4294.8
Specific Cost PB	1592.4	1160.3	1241.2	1154.1	1726.2	1672.6	6981.8	3490.9
Specific Cost TOT	3827.0	3342.7	3796.7	3570.9	4760.0	4679.9	11321.4	8170.4
Design parameters								
T_{cond}	30	24.29	30	24.29	30	30.65	30	54.43
T_{eva} or T_x	108.42	102.06	86.37	86.74	71.17	72.95	99.72	107.74
$\Delta T_{ap,PHE}$	10.98	17.82	4.5	4.47	4.5	2.0	50.28	42.26
$\Delta T_{pp,rec}$	5	11.85	5	5	-	-	5	17.67
$\Delta T_{pp,PHE}$	3	8.08	3	3.73	3	2.48	3	2
$\Delta T_{pp,cond}$	1	2.20	1	1.91	1	2.31	1	10
$T_{out,geo}$	70	70	70	74.27	70	71.21	70	95.20
$\Delta T_{mln,PHE}$	7.51	15.34	17.16	18.47	21.86	20.31	14.67	12.32
Turbine results								
Turbine efficiency	0.899	0.8993	0.8976	0.8955	0.8845	0.8841	0.8803	0.8865
Number of stages	2	2	4	4	5	5	3	2
Rotational speed	3000	3000	11343.4	11771.9	1605.6	1681.8	74.7	175.7
Size parameter	0.1601 0.249	0.168 0.262	0.0987 0.1538	0.0962 0.1604	0.8701 1.8575	0.831 1.7997	5.1655 16.8215	3.5129 7.0556
Specific speed	0.0927 0.1354	0.093 0.137	0.079 0.1356	0.0751 0.141	0.0834 0.2228	0.0823 0.2237	0.0602 0.1998	0.087 0.1762

Table 9.7 - Absolute cost repartition (left axis) and specific cost (right axis) achievable for four test fluids exploiting a 150°C geothermal brine

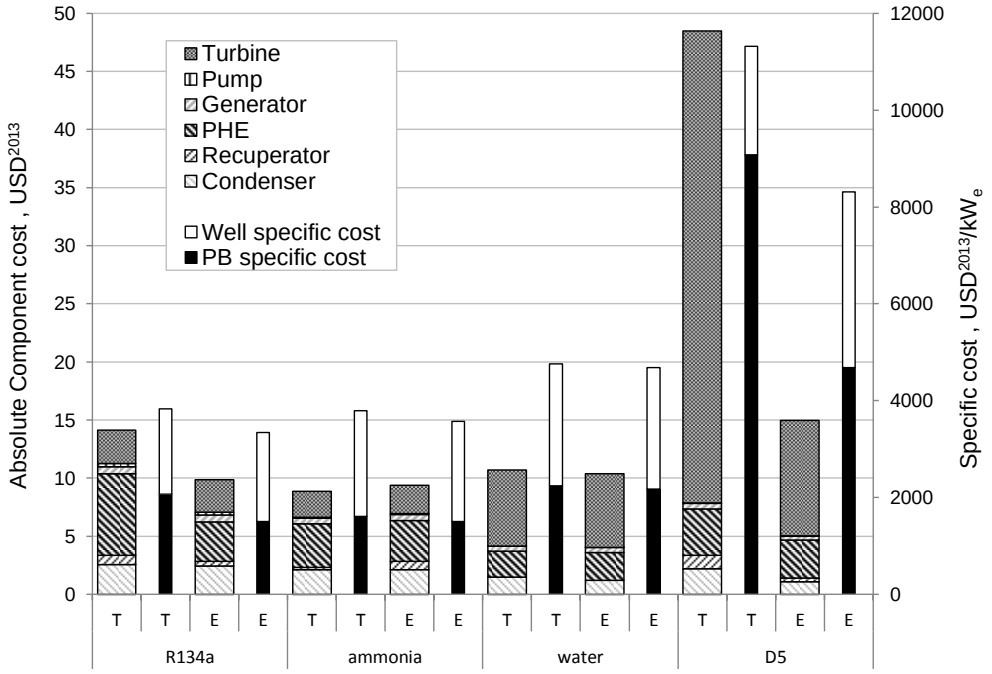

Figure 9.18 - Absolute cost repartition (left axis) and specific cost (right axis) achievable for four test fluids exploiting a 150°C geothermal brine

Comparison between 120°C-150°C-180°C geothermal brines

The economic optimization routine is applied to all the considered fluids for the three selected geothermal brine inlet temperatures 120, 150 and 180°C. Both single level (supercritical and subcritical cycles) and two levels cycles are considered.

In Figure 9.19.a, the decrement of total specific cost attainable with an economic optimization is reported and it is possible to notice that a relevant reduction of specific cost, larger than 200 USD^{2013}/KW_{el} is always possible but more marked results are highlighted using high or low critical temperature fluids. In particular for fluids with a $T_{in,geo}/T_{crit}$ parameter lower than unit the optimal cycle is still supercritical but the efficiency is strongly penalized due to a reduction of maximum pressure and temperature. In Figure 9.19.b it is possible to notice how the sharp peak characteristic of the optimized supercritical cycles levels off and the trend of optimal solutions is smoother. For fluids with a reduced temperature between 1.1 and 1.4 the optimized plants are similar to those optimized by a thermodynamic point of view while for high critical temperature fluids instead the reduction of specific cost is obtained by means of a reduction of efficiency as mentioned for D5 fluid in previous section.

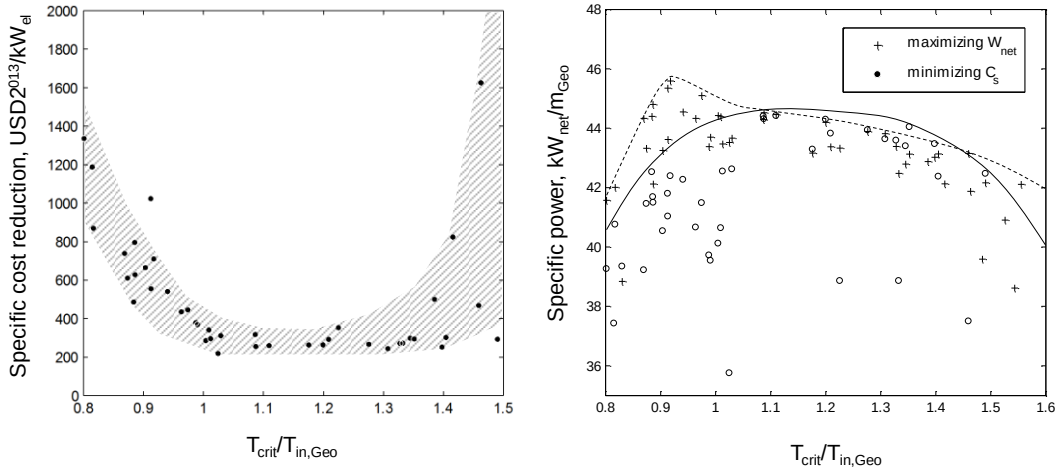

Figure 9.19 – Reduction of plant specific cost attainable (a) and specific power output variation (b) with a techno-economical optimization vs a techno-thermodynamic optimization.

The second law efficiency for the cycles optimized from an economic point of view are reported Figure 9.20 for geothermal brines having maximum temperatures equal to 120, 150 and 180°C. From a comparison between Figure 9.20 and Figure 9.14, it is possible to notice that the optimization algorithm acts in the same way independently of the temperature of the hot source: supercritical cycles with low critical temperature fluids are now penalized respect to two pressure levels cycles which can reach a higher power production. For high critical temperature fluids the trend remains similar to the thermodynamic optimization since the issues related to turbine efficiency and size are emphasized by component cost.

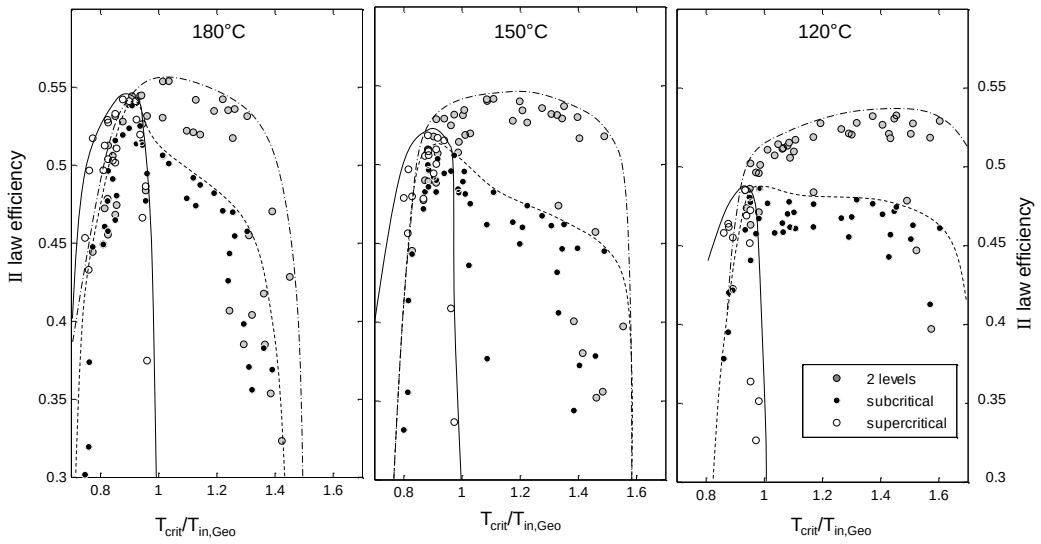

Figure 9.20 – Second law efficiency for techno-economic optimization applied to 180, 150 and 120°C geothermal brines

The total specific cost is reported in Figure 9.21. For the 150°C it is possible to note a rather regular trend of the total plant specific cost on $T_{in,geo}/T_{crit}$ parameter. The minimum is found in the range between 0.8-0.9, where several cycles with different fluids can achieve good economics. For values of $T_{in,geo}/T_{crit}$ lower than 0.8, the cost of optimized solutions rapidly increases due to the reduction of plant performances as already found from the thermodynamic analysis. For values above 0.9, costs rise as well for single level subcritical cycles, due to the lower efficiency of subcritical saturated cycles and to the strong increase of turbine cost which mainly affects the final solution. Two pressure levels cycles show a lower cost than the subcritical single level ones thanks to a higher power production and a larger number of optimization variables which allows exploring a wider range of solutions. These cycles have a specific cost competitive with the supercritical cycles but the higher BOP and the use of kettle reboilers affect the final solution. In the 150°C geothermal brine case, the optimal solution is a R134a supercritical regenerative cycle with no gearbox. For this fluid, a well-designed two-stage turbine directly jointed with the generator can be used. For ammonia, results also deserve to be discussed: the optimal cycle is subcritical with a very small recuperator and a high level of superheating. In this case, the adoption of a speed reducer is advantageous and the mechanical losses associated to this component are more than compensated by the increased turbine efficiency. Optimal rotational speed is around 11000 RPM and allows increasing the specific speed Ns of the last stage, which would be far from the optimum value without the adoption of a speed reducer. In all the investigated applications, fluids with high critical temperatures show extreme values of outlet volume flow rates, which entail optimized rotational speed far below 3000 RPM. In these cases, the adoption of multi-pole generator is certainly advantageous, but turbine size and cost increase a lot, leading to non-competitive costs. As already mentioned, this kind of fluids are more indicated for back pressure co-generative power plants where an increase of the condensing pressure allows keeping a reasonable diameter of the last turbine stage.

Finally, for fluids with $T_{in,geo}/T_{crit}$ just above 0.9, supercritical cycles have specific costs higher than subcritical ones, even if they allow achieving higher performances. Supercritical cycles are kept close to the saturation line and optimal $p_{in,turb}$ and $T_{ap,PHE}$ vary in narrow ranges, due to the constraint keeping the expansion in the superheated vapour region. In these cases, the economic optimization cannot effectively increase $T_{mln,PHE}$ without changing $T_{reinj,geo}$ and subcritical cycles can achieve lower specific costs because of the lack of this constraint.

For the two extreme temperatures the same trend previously described can be recognized. The optimal solution for the 180°C brine is a regenerative supercritical cycle, which entails the same considerations already discussed for 150°C brine optimal solution. Different aspects can be instead highlighted for the 120°C brine case, where the optimal solution is always a supercritical cycle but some two pressure and single pressure levels cycles can compete in terms of plant specific cost because of the better exploitation of heat source characterized by a small temperature variation.

In Table 9.8 for the best cycle results for geothermal brine temperatures of 120, 150 and 180°C are reported while T-Q diagrams are displayed in Figure 9.22.

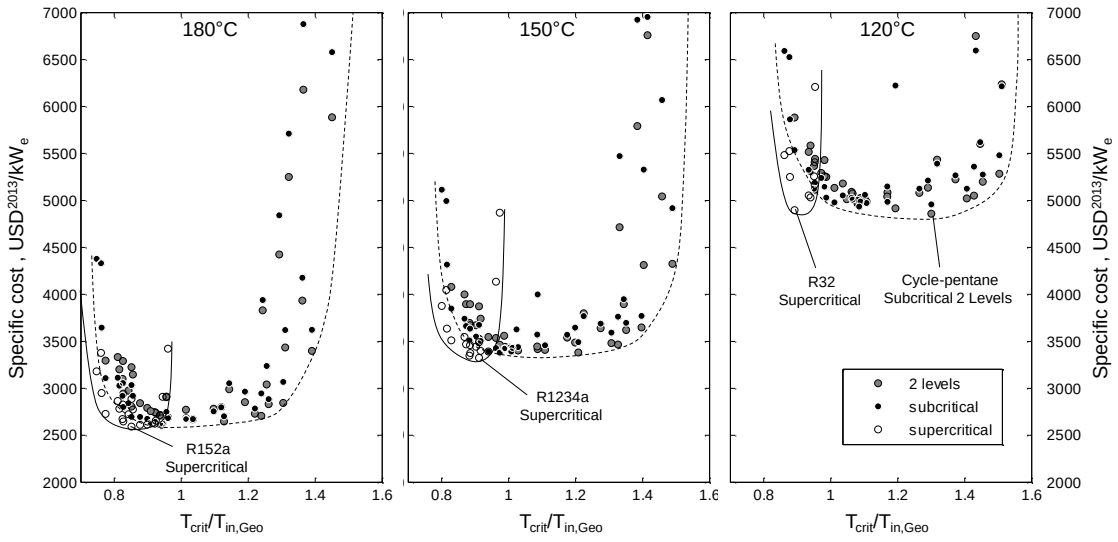

Figure 9.21 – Plant specific cost for binary geothermal power plants with geothermal brine temperature varying between 120 and 180°C

Brine temperature	120°C	150°C	180°C
fluid	R32	R134a	R152a
cycle	Supercritical non-recuperative	Supercritical recuperative	Supercritical recuperative
$T_{in,geo}/T_{crit}$	0.8934	0.884	0.853
Cycle efficiency	9.89%	12.74%	14.49%
Recovery efficiency	100%	100%	100%
Plant efficiency	9.82%	12.70%	14.46%
Specific power, $kW_{el}/(kg/s)$	20.54	42.52	66.58
Specific Cost PB USD^{2013}/ kW_{el}	1427	1160	909
Specific Cost TOT USD^{2013}/ kW_{el}	4892	3343	2588

Table 9.8 - Optimal techno-economical solutions for the exploitation of geothermal brines with temperature of 120, 150 and 180°C

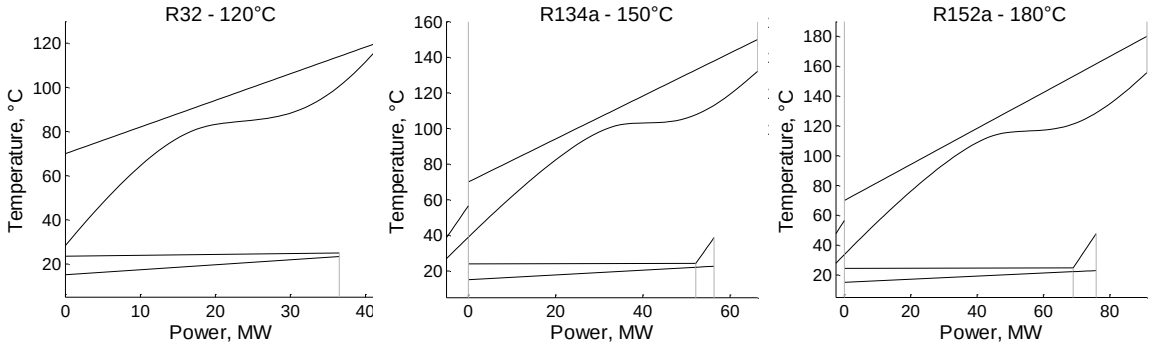

Figure 9.22 - Optimal techno-economical T-Q diagrams for the exploitation of geothermal brines with temperature of 120, 150 and 180°C

Optimal results for all cycles and for each brine temperature are reported in Figure 9.23. Circle markers refer to economic optimization results, while cross markers are representative of values obtained from thermodynamic optimization. First, it is possible to see the reduction of total plant specific cost as a result of the economic optimization procedure. In many cases this difference seems to be quite small, but it is important to remember that the well cost strongly affects the final solution for geothermal binary power plants. In particular, for the assumed exploration and drilling costs, economic and thermodynamic optimum are quite similar, due to the need of amortizing a large initial investment cost. Moreover, values computed in the thermodynamic optimization are obtained with different turbine designs which lead to solutions not always directly comparable.

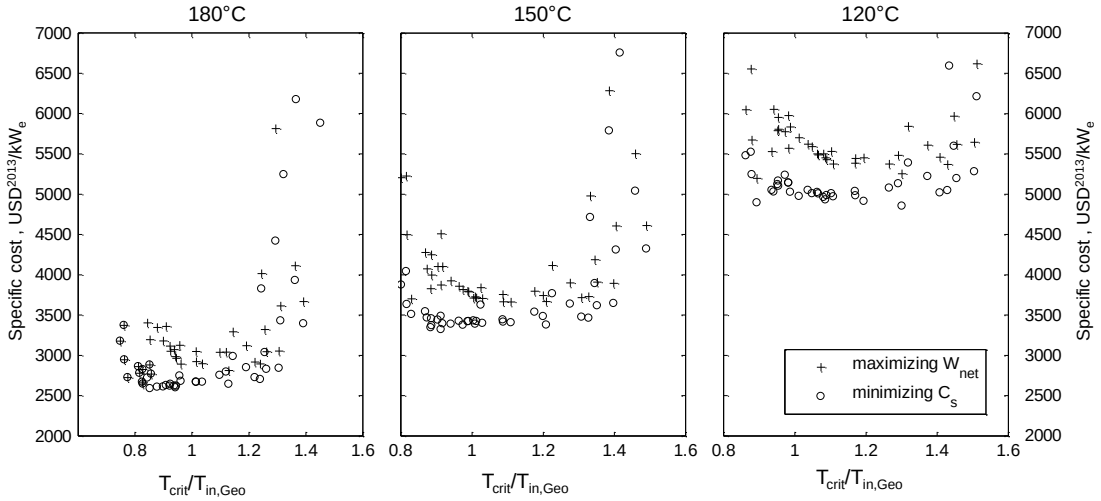

Figure 9.23 – Plant specific cost reduction attainable with a techno-thermodynamic vs a techno-economic optimization

Conclusions

Results can be summarized in the following statements:

- The choice of fluid and cycle configuration is crucial in order to minimize the total plant specific cost: important performance and cost variations result between optimal and non-optimal cycles.
- The techno-economic optimization provides results different from the ones obtained from the thermodynamic analysis, confirming its primary importance in the optimization of ORC plants. However, it is confirmed that for sufficient maximum geothermal brine ΔT (in presence of a high brine temperatures or low minimum reinjection temperatures), supercritical cycles perform better also from the economic point of view.
- Optimal fluids have $T_{in,geo}/T_{crit}$ parameter close (slightly lower) to the ones found for the thermodynamic analysis, but advantages related to supercritical cycles over subcritical ones are less evident.
- Adopting fluids with $T_{in,geo}/T_{crit}$ parameter lower than 0.8 in supercritical configuration entails higher plant costs due to the poor cycle efficiency, while for values above 1.3 the specific costs rise mainly because of the increase of the turbine cost.
- Gear box is not always profitable; for the investigated cases it can be conveniently adopted for low molecular complexity fluids (e.g. water, ammonia, R161) to obtain acceptable turbine efficiencies.
- High critical temperature fluids require turbines with a low speed of revolution in order to have specific speed near the optimal value and hence the adoption of a multi-pole generator.
- Sensitivity analysis on geothermal well cost shows that the optimal cycle parameters do not change appreciably by changing the geothermal well cost, at least when its contribution on total cost is not lower than half of the cost of the power block.
- An increase of the relative cost of the geothermal well push the economic optimization towards cycles with higher efficiencies and higher power block absolute costs

9.2 Use of mixtures for Biomass plants

In biomass applications, ORCs commonly use a pure working fluids (i.e. siloxanes or long chain alkanes) in a saturated recuperative configuration. In particular, the selected evaporation temperature is the result of the cycle efficiency optimization through the evaluation of the trade-off between the maximization of both the power production and the heat recovery from the synthetic oil used as HTF (Heat Transfer Fluid) in the biomass burner. The performance of the ORC can be improved by the adoption of multicomponent blends as working fluids. However complex analytical tools are needed to design such ORC units and, in particular, the selection of a mixture characterized by a proper temperature glide is not trivial because requires the evaluation of the miscibility of mixture components, its thermal stability and the study of the heat transfer coefficients in phase transition. In this section the design of a superheated recuperative ORC coupled with a small capacity biomass fired boiler is investigated comparing the performances attainable with pure toluene vs mixture of toluene and ethanol.

As already mentioned in Section 4.2.6 (Use of mixtures vs pure fluids) the use of mixtures can be extremely attractive when both hot and cold sinks are characterized by a variable temperature profile. An applicative case, which fully satisfies these conditions, is represented by a biomass fuelled ORC in a co-generative configuration, where heat resulting from the biomass chemical energy conversion is transferred to a synthetic oil used as HTF. In most of the cases the mass flow rate of the HTF and its maximum temperature are defined by the biomass burner manufacturer, thus, these variables have been fixed in this study. Oil maximum and minimum temperature are 300°C and 200°C respectively and mass flow rate is calculated in order to obtain an heat input of 20 MW_{th} namely the thermal power input of the biggest ORC unit installed by Turboden [48]. In the condenser unit hot water is produced for co-generative purposes, rising its temperature from 50°C to 90°C. The simulated plant is a CHP subcritical cycle and the layout scheme is the same for both pure fluids and mixtures.

As regards components specifications, a fixed isentropic efficiency for pump is assumed equal to 0.7 while the performance of the turbine is calculated at optimized rotational speed. A techno-economic optimization is performed by acting on four design parameters, namely the evaporation and the condensation temperatures, the approach point temperature difference in the PHE and the pinch point temperature difference in the recuperator. Since the condensing temperature is defined at the saturated vapor condition, by fixing this value even the pinch point at the condenser is defined. For no one of the mixtures here considered the temperature glide in condensation is higher than the cooling water temperature variation and so pinch point condition is always in correspondence of

the saturated vapor condition. The minimum $\Delta T_{pp,cond}$ is 10°C while in the other heat exchangers this parameter is optimized.

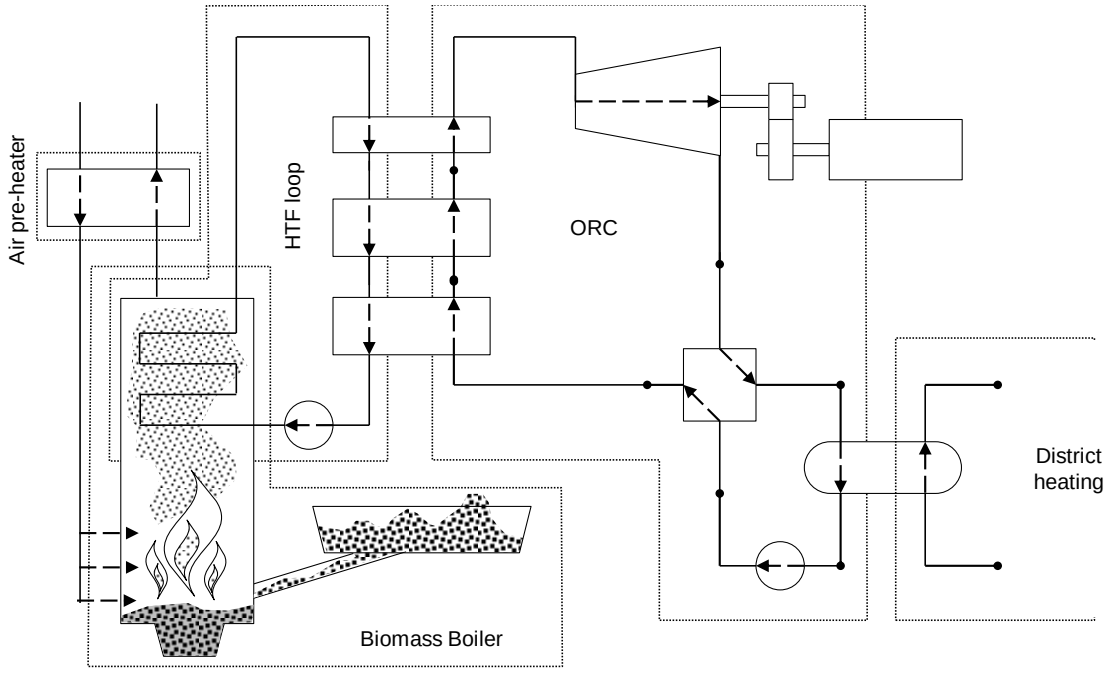

Figure 9.24 - Plant layout scheme of a ORC coupled with a biomass boiler and HTF loop

Fluid selection

A preliminary study has been carried out considering binary mixtures defined by combination of more than 30 fluids with the purpose of finding out a mixture with a considerably high temperature glide in phase transition. The selected mixture is an ethanol/toluene blend since it shows relevant temperature glides in both evaporation and condensation allowing a good matching with both HTF and cooling water temperature profiles. Pure toluene is commonly used in commercial applications [51] because of the overhanging shape of its saturation line, because of its critical temperature being not extremely high and its limited cost. Ethanol on the other hand is a light and polar molecule characterized by a bell shaped saturation line which can create hydrogen bounds because of the availability of free electrons pairs. The prediction capability of Refprop is tested on the experimental data available in literature [236; 237; 238] and a graphical comparison is reported in Figure 9.25.

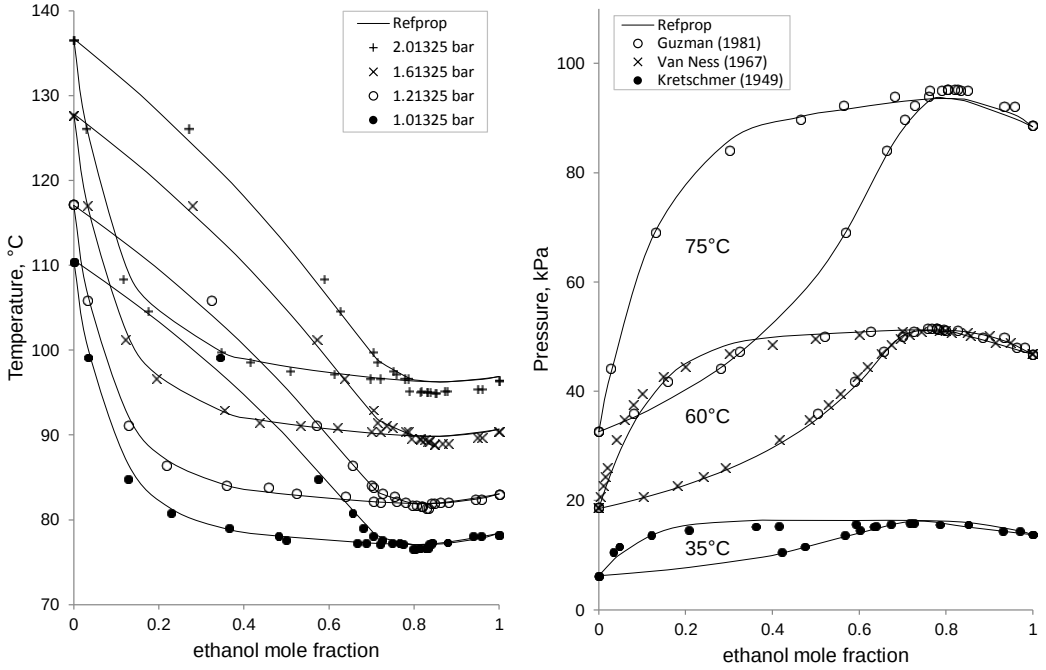

Figure 9.25 – comparison between Refprop results and data from literature for a mixture of toluene and ethanol

The mixing rules implemented in Refprop are reliable for the estimation of thermodynamic properties of this mixture where strong non-ideal effects are present. Results are quite accurate and discrepancies around the azeotropic point are not significant for this study since only mixture far from the azeotropic point are here considered in order to take advantage from their temperature glide in phase transition.

Unfortunately the limiting maximum temperature at which experimental data are available (140°C) shows the necessity to carry out experimental activities at higher temperatures. The trend of attainable temperature glides at higher pressure, calculated with Refprop, is reported in Figure 9.26 against the average temperature of phase transition for different mixture compositions. Peculiarity of this mixture is the possibility to have a higher temperature glide in evaporation than in condensation. For instance, using a mixture with a fraction of ethanol in the range between 20 and 30% it is possible to obtain temperature glides around 22 °C in condensation and values 10°C higher in evaporation, which is surely a positive aspect since the cooling water has a temperature variation smaller than the HTF (50°C vs 100°C).

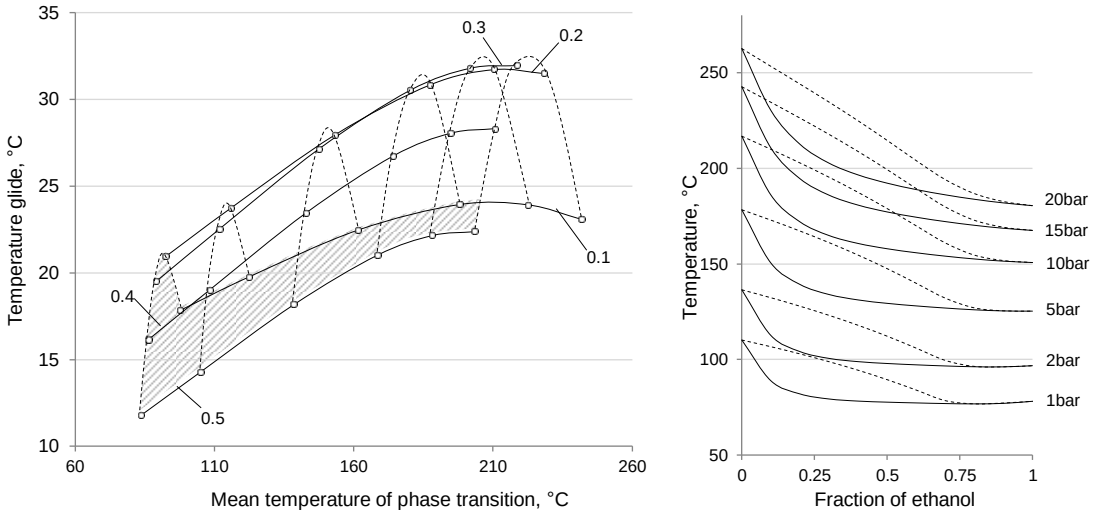

Figure 9.26 – Maximum temperature glide attainable at different mean temperatures of phase transition for five mixture compositions (a) and the correspondent VLE diagrams (b)

Economic Assumptions

The investment cost of a cogenerative biomass power plant is formed mainly by two terms: the first one is related to the ORC power block while the other one to the biomass furnace and the HTF loop. Furthermore, in order to evaluate a reliable cost of the technology, the cost related to the consumption of biomass has to be considered. The size of the ORC power block is object of the techno-economic optimization and reliable values for biomass furnace and wood cost have to be defined. For both terms there is a great variability depending on the producer, the maximum temperature of the HTF loop, the type of biomass and the country where the plant is going to operate.

Information about commercial Turboden biomass cogenerative power plants can be found in literature [239] and most interesting results are proposed in Table 9.9. Data are fitted with a logarithmic function in order to extrapolate a reasonable value for a plant having the specification of our reference case. Data of cost includes ORC, biomass furnace, thermal oil boiler, fuel handling, civil works, connection to the grid, engineering, The net electricity value has been considered as a the electric energy produced minus the ORC own consumption and thermal oil circuit own consumption [239].

Trend of total cost and specific cost are reported in Figure 9.27 against net electric power, data are extrapolated up to 4 MWel which is the size considered in this study.

Model	Wnet kW_{el}	Total cost USD^{2013}	Specific cost USD^{2013}/kW_{el}	Biomass cons. kg/h
Turboden 22 Split	1803	10141875	5625	4753
Turboden 18 Split	1469	8997625	6125	3871
Turboden 14 Split	1007	7426625	7375	2655
Turboden 10 Split	771	6457125	8375	2032
Turboden 7 Split	572	5648500	9875	1508
Turboden 6 Split	486	5346000	11000	1281
Turboden 4 Split	345	4398750	12750	909

Table 9.9 - Data of seven commercial biomass CHP unit base on a ORC produced by Turboden [239].

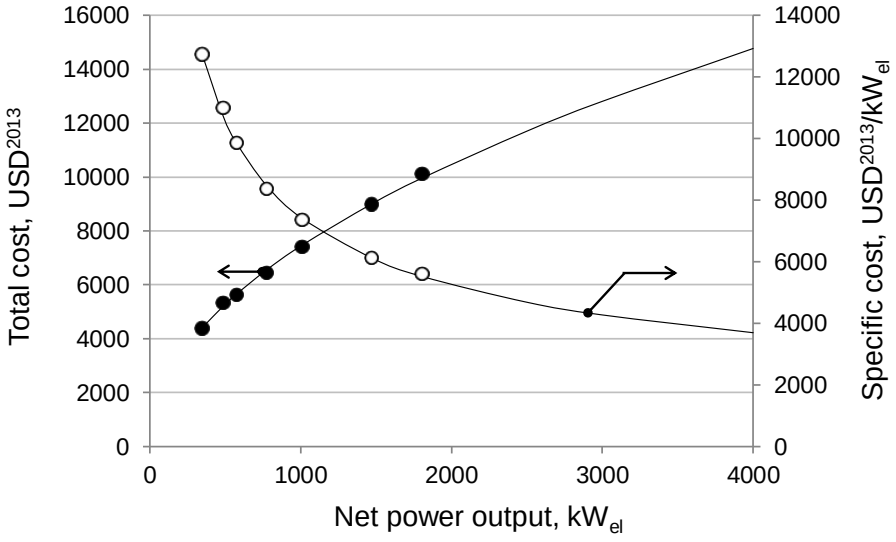

Figure 9.27 - Trend of specific cost and total cost for commercial CHP biomass fired ORC from Turboden

In the same publication [239] a cost of biomass equal to 10 €/MWh_{th} is assumed as representative of availability of unused biomass. In other publications instead different values are proposed [240] in a range between 15 and 25 €/MWh_{th} for waste biomass and biomass directly harvested from the wood in European countries. Other data are available from website of a biomass producer in UK [241] with prices varying from 0.02 USD/kWh_{th} to 0.09 USD/kWh_{th} depending on the type of the biomass and humidity content. Finally results presented in a report delivered by the Biomass Trade Center [242] highlight a strong variability depending on the country considered and the type of biomass (pellets or chips) with values between 10 €/MWh_{th} for wood chips in Romania up to 40 €/MWh_{th} for wood pellets in Austria or Ireland.

For the biomass boiler cost instead a value between 700 and 1600 USD/kW_{el}[17] is reported in a publication investigating the potential of biomass fired ORC in Brazil [243] for a plant with an ORC having efficiency equal to 18%. Finally all the over mentioned references declare furnace efficiency between 85% and 87%.

The LCOE of the plant can be calculated by

$$LCOE = \frac{(C_{fu} + C_{orc})CCF + C_b}{W_{el} h_{op}} = \frac{(c_f CCF + c_b \, h_{op}/\eta_f)Q_f + C_{orc} CCF}{W_{el} h_{op}} \qquad \text{eq. 9.2}$$

Where the specific cost of the biomass (c_b) is equal to 0.02 USD/kWh_{th} and the specific cost of the furnace (c_f) is set to 380 USD/kW_{th} (~1900 USD/kW_{el}). The number of hours of operation (h_{op}) is 7000 in a year and the furnace efficiency (η_f) is equal to 86%. CCF is set to 12%.

These economic assumptions are relatively optimistic and different values can be found depending on the market considered. The higher the fixed cost related to the biomass furnace and the biomass consumption, the higher the advantage of adopting high efficient solutions, since this reduces the total cost of electricity, favoring the use of mixtures In conclusion, a low fixed cost, as in this case, allows performing the comparison between pure toluene and mixtures in a more conservative way and the advantage in using mixtures is simply enhanced by a higher cost of the furnace or the biomass.

Results

Different mixture compositions are investigated and for each one a techno-economic optimization is carried out. Adding small fraction of ethanol immediately results in a relevant temperature glide in both evaporation and condensation reducing the ΔT_{mln} in these components and limiting the second law efficiency losses due to heat transfer. The evolution of T-Q and T-s diagrams is reported in Figure 9.28 for mixtures with a fraction of ethanol ranging from 0.1 to 0.6 and compared with the optimal result for pure toluene. It is possible to notice that a small amount of ethanol strongly affects the temperature glide in phase transitions with a relevant temperature difference in both condensations and evaporation. As a general consideration, increasing the amount of ethanol leads to lower critical temperatures and a phase transition characterized by a smaller heat of vaporization. Furthermore the temperature difference in expansion gets bigger, limiting

[17] Cost includes the biomass furnace and part of the auxiliary equipment but without BOP

the amount of heat available at the recuperator. Saturated liquid temperature in condenser hot well is reduced involving a lower inlet temperature in the economizer and a higher duty of this last component. Superheating is suggested in order to increase cycle efficiency since the HTF is always cooled down to its minimum lower temperature.

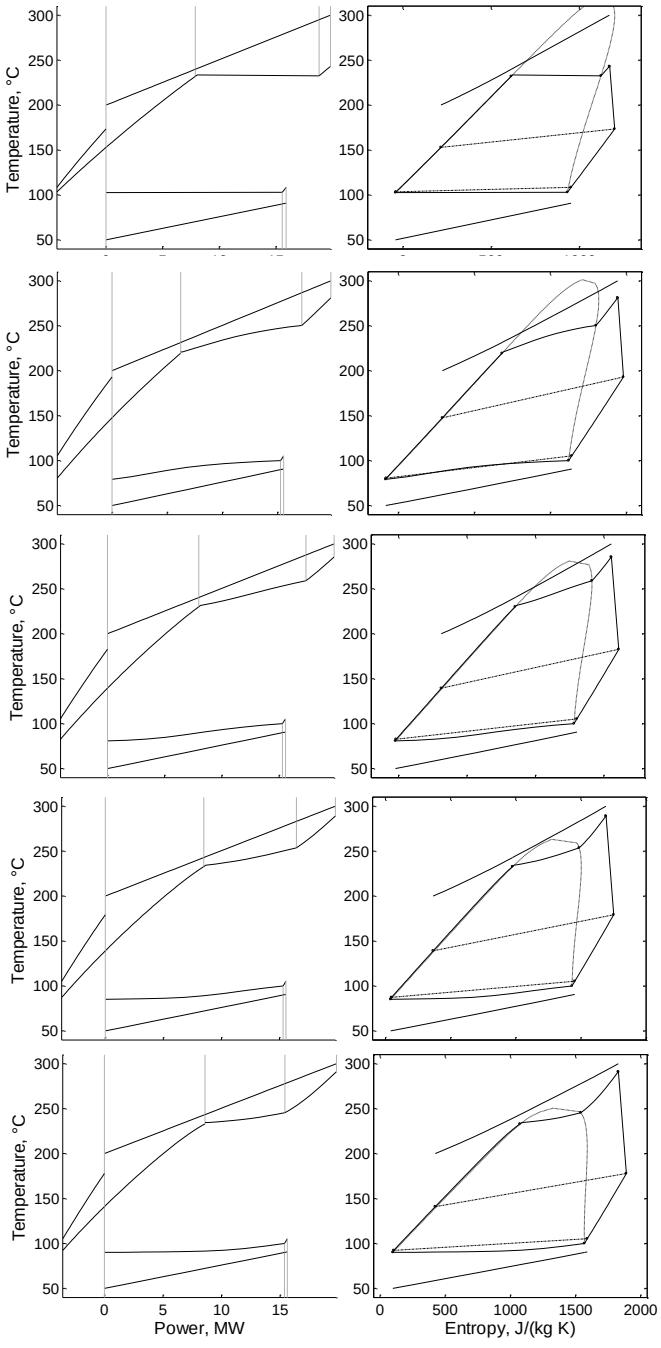

PURE TOLUENE

The optimal cycle is a subcritical cycle with an almost saturated condition at turbine inlet. Both evaporation and condensation are characterized by an isothermobaric phase transition leading to large temperature differences in these components. Pinch point temperature difference in the recuperator is pushed to the lower bound involving a high surface.

TOLUENE 0.9-0.1 ETHANOL

A relatively small fraction of ethanol involves relevant temperature changes in phase transition. Recuperator pinch point is larger than the minimum because of the colder temperature at condenser hot well

TOLUENE 0.8-0.2 ETHANOL

A higher temperature drop in expansion is highlighted limiting the inlet temperature at the economizer, superheating is used to enhance the cycle performances by means of the reduction of mean logarithmic temperature difference in the PHE

TOLUENE 0.7-0.3 ETHANOL

A further increasing of ethanol fraction leads to small temperature glides in condensation with an increasing of mean logarithmic temperature difference in the condenser and higher second law efficiency losses

TOLUENE 0.6-0.4 ETHANOL

The critical temperature gets lower and the cycle adopts a higher superheating. Pinch point temperature difference in the recuperator is reduced and the weight of economizer on total PHE duty is relevant

Figure 9.28 – Variation of T-Q and T-s diagrams increasing the ethanol fraction in toluene-ethanol mixtures

It is interesting to notice that, if the fraction of ethanol is further increased, the optimal cycle would probably require a supercritical transition with positive effects on the efficiency. Nevertheless the temperature glide in condensation is strongly reduced leading to a lower net power production.

Table 9.10 shows some performance results allowing a comparison between the use of pure toluene and mixtures of toluene/ethanol as working fluids. First it is possible to highlight that the power output as well the plant efficiency has a maximum for a mixture with a fraction of ethanol around 25% with a performance increase of more than 8.8% respect to the pure toluene case. This efficiency increment might be even larger with a thermodynamic optimization since here the performances of the cycles are affected by economic reasons related to the extension of heat exchanger surfaces and cost. The Specific cost of the investigated cases are quite close to the values predicted by data from Turboden (Figure 9.27) and, for the pure toluene case, a specific cost 10% lower is obtained. A difference which can be explained considering that the prices reported in Table 9.9 [239] refers to the commercial price (a discount is always attainable during the project definition) and the exact cost of key component are unknown affecting the final solution. Finally it is interesting to note that the LCOE obtained are in the range between 0.06 and 0.29 USD/kWh$_{el}$ reported in the IRENA report [244] for this technology. It is interesting to note that the capital cost share on the LCOE is around the 31% of the total LCOE but this value is strongly affected by the economic assumptions. The value of LCOE, calculated with a monetary incentive (MI) equal to 50 USD/MWh$_{el}$, is reported in the last row of Table 9.10.

	fraction of toluene						
	1	0.95	0.8	0.75	0.7	0.65	0.6
W_{net} plant, kW_{el}	3651.89	3885.74	3963.13	3973.58	3965.28	3942.58	3907.82
plant efficiency	18.3%	19.4%	19.8%	19.9%	19.8%	19.7%	19.5%
Cost TOT, 1e6 USD^{2013}	12.21	12.52	12.65	12.65	12.64	12.61	12.57
Specific Cost TOT USD^{2013}/kW_{el}	3342.39	3222.15	3192.00	3184.17	3187.34	3198.73	3215.61
LCOE, USD^{2013}/kWh_{el}	0.1847	0.1749	0.1721	0.1716	0.1719	0.1728	0.1741
LCOE, USD^{2013}/kWh_{el} (with MI)	0.1347	0.1249	0.1221	0.1216	0.1219	0.1228	0.1241

Table 9.10 - General results for optimized plants using mixtures with different compositions

The use of mixtures allows achieving higher efficiencies mainly because of reduced heat transfer second law losses in both the Primary Heat Exchanger (PHE) and the condenser. It is important to remember that the PHE is formed by three different units (the economizer, the evaporator and the superheater) thus the positive effects of the temperature glide in phase transition are fully exploited only in a limited share of the total

duty. The ΔT_{mln} of evaporation section is strongly reduced though maintaining an almost fixed pinch point temperature difference while the trend of ΔT_{mln} for the whole PHE show a minimum for a 20% ethanol mixture. This can be explained considering that increasing the ethanol molar fraction entails a lower turbine outlet temperature and so a lower inlet temperature in the economizer which is a component characterized by large temperature differences between the hot stream and the working fluid. For mixtures with more than 30% of ethanol content, the economizer duty overcomes the evaporator one and the resulting global ΔT_{mln} starts to increase, justifying the maximum in the trend of PHE UA parameter. Afterwards, mixtures with more than 60% of ethanol content show a lower efficiency because of their low critical temperature which limits the evaporation temperature. The condenser and the recuperator show opposite trends of the UA and ΔT_{mln} parameters. For the condenser the temperature glide is fully exploited and the mean temperature difference is strongly reduced with mixtures having a fraction of ethanol up to 30%, beyond this composition the temperature glide reduces because of the proximity of the azeotropic point. For the recuperator instead the UA parameter is first strongly reduced by the larger ΔT_{pp} while for amount of ethanol higher than 20% it starts to increase again due to the effect of a lower glide in condensation.

		fraction of toluene						
		1	0.95	0.8	0.75	0.7	0.65	0.6
COND	Cost, USD^{2013}	639.65	714.64	766.49	771.56	769.16	759.14	742.21
	Duty, MW_{th}	15.74	15.49	15.41	15.40	15.40	15.43	15.47
	ΔT_{pp}, °C	13	10	10	10	10	10	10
	ΔT_{mln}, °C	27.84	21.92	17.97	17.58	17.57	17.94	18.69
	UA_{ext}, kW/m^{2}K	565.15	706.60	857.33	875.86	876.81	860.08	827.33
	A, m^2	1093.14	1288.25	1427.36	1441.33	1435.43	1409.32	1364.9
REC	Cost, USD^{2013}	389.52	215.20	208.21	211.67	217.05	224.73	235.85
	Duty, MW_{th}	4.34	4.19	4.11	3.92	3.75	3.61	3.55
	ΔT_{pp}, °C	5	21.43	22.67	20.48	18.05	15.53	12.99
	ΔT_{mln}, °C	11.35	29.18	32.13	30.14	27.85	25.42	23.05
	UA_{ext}, kW/m^{2}K	382.23	143.74	127.81	129.94	134.52	142.03	154.11
	A, m^2	699.27	262.96	233.82	237.71	246.09	259.83	281.94
PHE	Cost, USD^{2013}	1020.65	1134.87	1208.39	1209.35	1208.61	1206.84	1199.30
	Duty, MW_{th}	19.81	19.81	19.81	19.81	19.81	19.81	19.81
	ΔT_{pp}, °C	6.21	8.58	8.76	8.54	8.49	8.59	8.9
	ΔT_{mln}, °C	23.40	21.31	20.71	20.84	20.96	21.06	21.27
	UA_{ext}, kW/m^{2}K	846.55	929.34	956.55	950.52	945.18	940.69	931.00
	A, m^2	1436.46	1580.58	1663.38	1665.09	1667.56	1670.80	1664.05
PHE DUTY BREAK	Eco %	39.8%	41.2%	40.3%	41.7%	42.8%	43.6%	43.3%
	Eva %	55.1%	53.6%	47.3%	43.8%	40.3%	36.9%	34.5%
	Sh %	5.1%	5.2%	12.4%	14.5%	16.9%	19.5%	22.2%
TOTAL HE Area		3228.87	3131.79	3324.56	3344.13	3349.08	3339.95	3310.89

Table 9.11 - Detailed results on Heat Exchanger size and specifications for mixtures having different compositions

The lower overall temperature difference in the heat exchangers for the mixture with a molar fraction of ethanol around 0.3 justifies the maximization of cycle efficiency which reaches a value +8.8% higher than the pure toluene cycle. In accordance to what previously said, this increase in efficiency and power production is obtained with an enlarged total heat exchangers surface and so a higher cost of the equipment.

In addition to the effects on heat exchanger sizing, the use of mixtures entails a different design of the turbine. Increasing the ethanol molar fraction a higher maximum temperature of the cycle can be achieved but both higher volume ratios and isentropic enthalpy drops along the expansion are obtained which leads to high stage load coefficients and increased flaring angles. In particular for pure toluene a two stage turbine is used while for mixtures three stages are required to exploit the overall volume ratio respecting the constrains of blade height variation for each stage. On the other hand the use of mixtures allows the reduction of the mass flow rate which, together with a higher condensing pressure, results in a lower volume flow rate and thus a smaller size and cost of the turbine. Results are reported in Table 9.12: it is possible to underline that the turbine efficiency is first slightly improved by the adoption of a three stages configuration while for mixtures with a large fraction of ethanol the efficiency gets progressively lower because of the higher number of stages with different size parameters and non-optimized specific speeds. A large amount of ethanol leads to higher optimal rotational speed because of the smaller SP caused by the reduction in volume flow rate and isentropic enthalpy drop. The smaller SP especially at the first stage leads to the efficiency decrement over mentioned. The most expensive turbine (which is also the more efficient) is obtained for a 5% of ethanol mixture since it has large size parameters and three stages; increasing the ethanol fraction the cost is reduced thanks to the smaller size parameters but the toluene turbine remains the cheapest one. The trend of turbine cost variation respect to the pure ethanol case is reported in Figure 9.29.b.

	fraction of toluene						
	1	0.95	0.8	0.75	0.7	0.65	0.6
M, kg/s	42.473	36.911	32.2725	31.2139	30.2599	29.3857	28.5795
effciency	88.14%	88.25%	87.58%	87.48%	87.41%	87.38%	87.40%
Vr	15.5404	24.9281	28.5365	28.1583	27.2436	25.9139	23.9863
Δhis, kJ/kg	106.0321	130.536	160.1313	166.5323	171.9052	176.4181	180.0179
N stages	2	3	3	3	3	3	3
SP, min/max	0.149-0.289	0.104-0.289	0.081-0.239	0.077-0.226	0.074-0.215	0.071-0.204	0.069-0.195
Ns, min/max	0.077-0.142	0.064-0.164	0.060-0.165	0.060-0.164	0.059-0.163	0.059-0.162	0.060-0.161
RPM	6940	7350	9770	10470	11130	11770	12330
Cost, USD^{2013}	1152.09	1358.79	1323.42	1311.97	1296.94	1279.15	1258.79

Table 9.12 - Turbine results using different toluene-ethanol mixtures

In conclusion mixtures of toluene and ethanol can achieve higher efficiencies but with a more expensive power plant. The total plant specific cost is reduced with a minimum corresponding to a 25% ethanol mixture which shows a specific cost 4.73% lower than the pure toluene case. The reduction of LCOE is more marked reaching values of -7.05% since using mixtures a higher power production is attainable.

However, mixtures usually show a lower film heat transfer coefficient in phase transition due to non-contextual evaporation (or condensation) of the two components and the formation of composition gradients. Simulations performed with Aspen for this mixture[18] have highlighted a progressive reduction of h for mixture which tends to a values 50% lower than pure toluene. A reduction of global heat transfer coefficient U can be evaluated equal to 25% in condensation and to 40% in evaporation adopting the same assumptions defined in section 7.4 (Film and overall heat transfer coefficients). Neglecting the size effect on component cost (a small reduction of specific cost is still attainable) and further enhancements achievable with a new optimization a simplified sensitivity analysis is proposed in Figure 9.29.a. The relative reduction of LCOE can be accounted in more than one percentage point respect to the previous case since the heat exchanger cost have a limited cost share on the total plant cost and an even smaller weight on the LCOE where the biomass consumption cost is considered

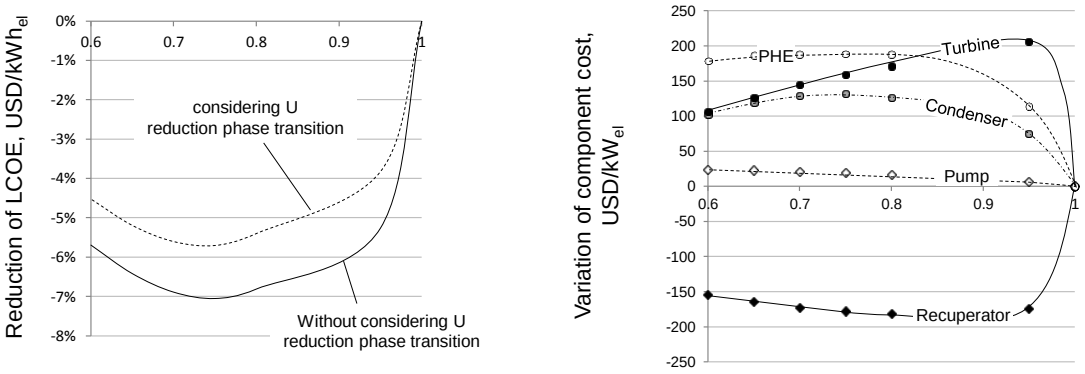

Figure 9.29 - Specific cost reduction attainable using toluene-ethanol mixtures vs pure toluene with an assumption of constant film heat transfer coefficient in phase transition and with a penalization for mixtures (a) variation of specific cost of plant components varying the amount of ethanol in mixture

[18] The numerical results obtained by Aspen are affected by mixing rules (in this case Huron-Vidal) and accuracy of the thermo physical properties of pure fluids. Results are calculated minimizing the cost of the heat exchanger with a maximum allowable pressure drop on both streams. It is important to notice that in scientific literature reduction between 3 and 40% are highlighted for mixture of light refrigerant fluids [111] and mixtures of ethanol and water [112]

Finally a comparison in terms of second law efficiency is proposed in Table 9.13. It can be highlighted that increasing the ethanol fraction:

- the condenser loss is strongly reduced according to the lower ΔT_{mln} in this component when mixtures are used. The minimum is found in correspondence of a 25% ethanol mixture, beyond this value the glide in condensation decreases leading to larger efficiency losses;
- recuperator loss is immediately increased because of the larger ΔT_{pp} caused by a lower saturated liquid temperature at condenser outlet. Increasing the ethanol fraction involves higher temperature drops in the expansion and so a reduction of the available thermal power;
- Economizer loss is increased because of the lower inlet temperature and the higher temperature differences;
- Evaporator loss is always reduced due to the presence of a temperature glide and the reduction of the heat of vaporization approaching the critical point;
- Superheater loss is relatively constant since using mixtures its duty is increased while the ΔT_{mln} is reduced;
- Fluid-dynamics losses are related to the expansion and compression losses in the turbine and the pump. These losses are larger for mixtures because of the lower turbine efficiency and the higher head of the pump.

	fraction of toluene						
	1	0.95	0.8	0.75	0.7	0.65	0.6
etaII	54.53%	57.90%	59.01%	59.16%	59.04%	58.71%	58.21%
Condenser	20.14%	15.51%	12.39%	12.37%	12.69%	13.29%	14.13%
Recuperator	2.01%	4.11%	4.39%	3.99%	3.59%	3.24%	2.96%
Economizer	4.54%	6.13%	5.91%	6.04%	6.12%	6.11%	5.90%
Evaporator	6.64%	3.99%	3.18%	3.06%	2.93%	2.79%	2.73%
Superheater	1.28%	0.87%	1.08%	1.19%	1.36%	1.56%	1.84%
Fluid-dynamic	6.26%	6.71%	9.12%	9.26%	9.34%	9.36%	9.31%
mecc-el	3.02%	3.24%	3.39%	3.42%	3.43%	3.42%	3.40%
Qlosses	1.28%	1.28%	1.28%	1.27%	1.26%	1.26%	1.26%
Others	0.30%	0.25%	0.25%	0.25%	0.26%	0.26%	0.27%

Table 9.13 – Second law losses breakdown for different mixtures

Conclusions and future works

In conclusion the use of mixture could be attractive for the exploitation of variable temperature heat sources because they are able to achieve higher efficiencies compare to pure fluid cycles. However, the design of each component has to be carefully evaluated in order to obtain also a LCOE reduction: the higher performances are obtained with more expensive heat exchangers but the turbine can be more compact even if it requires a higher stage number, highlighting once again that a techno-economic optimization is crucial in ORC power system design.

Future works should concern the study of different mixtures and experimental activities oriented to the evaluation of both thermodynamic and transport properties of new and promising mixtures.

9.3 Small direct solar power plants

A field of particular interest for ORCs is their use in rural and remote applications since in many areas around the world population doesn't have access to electricity. From IEA Energy Outlook 2011 [245] more than 1.317 billion of people live without electricity with all the consequences related to the limited developement of these regions and the possibility to increase the quality of life. Most of these contexts are located far from the big cities and art not connected to the national grid. Average rural electrification in sub-Saharan Africa is below 15% leaving more than 580 million people without the possibility to use a pump to extract water from the well, to stock vaccines or medicinal or conserve perishables. In these contexts it is possible to install stand-alone power systems also called RAPS (Remote Area Power Supply) connected to an off-the grid electricity system. These stand-alone grids are usually characterized by small utilities, like a water pump, an osmosis system for the water potabilization, a refrigerator for various purposes and a minimal domestic and public illumination. In most of the installed systems a diesel generator is used even if in several papers the integration between different renewable resources is investigated. The use of multiple generators is a common strategy in order to diversify the energy resources and to guarantee the grid stability.

	Population without electricity millions	Electrification rate %	Urban electrification rate %	Rural electrification rate %
Africa	587	41.8	68.8	25.0
North Africa	2	99.0	99.6	98.4
Sub-Saharan Africa	585	30.5	59.9	14.2
Developing Asia	675	81.0	94.0	73.2
China & East Asia	182	90.8	96.4	86.4
South Asia	493	68.5	89.5	59.9
Latin America	31	93.2	98.8	73.6
Middle East	21	89.0	98.5	71.8
Developing countries	1314	74.7	90.6	63.2
World*	1317	80.5	93.7	68.0

Table 9.14 – Electrification and access of energy for developing countries [245]

Some examples are focused on the integration of solar PV and wind energy [246], of PV, wind turbines, small scale hydropower and a diesel engine [247], PV, wind and diesel engine [248], PV and wind energy [249].

Solar energy is certainly one of the most suitable energy sources in those contexts characterized by a small power consumption and high values of irradiation all along the year. Both photovoltaic panels and solar thermal power technologies can be used: the first one allows achieving pretty good performances and it needs a low maintenance during the

operation, the reliability is high and main reasons of failure are related to physical damaging of the panel glass or malfunctioning of the inverters. Nevertheless, with the aim of not dissipating the excess of power in the central hours of the day an electrical storage is required. Lead-acid batteries can be used for this purpose: they are cheaper than other battery types but they are characterized by relevant losses in charge and discharge phases and a strong life reduction if the battery works at deep discharge operations [250; 251]. This is a critical issue in stand-alone micro grid since the electrical batteries are subject to frequent charge and discharge cycles especially if the PMS (Power Management System) is not able to act on the disconnection of low priority loads. Solar thermal power technology, on the other hand, has a more complicated plant layout; it requires a solar field (i) formed by an array of lineal solar collectors (parabolic troughs or Fresnel mirrors) or a point focus receiver, a HTF (Heat Transfer Fluid) loop (ii) and a power block system (iii) [252]. The availability of thermal power disconnected to the electrical power production allows designing a thermal storage which can be more economical and efficient than an electrical one. Different types of thermal storage systems are used in commercial plants combined with a solar field which is oversized[19] in order to face the transient effects of cloud passages and to guarantee a continuous production in hours after the sunset. The most common solution is a double tanks storage: the hot tank is filled with hot fluid during high insolation hours and it is discharged when the irradiation is not sufficient to produce the nominal rate of HTF at the nominal temperature. Other solutions are the single tank with thermocline which allows limiting the cost of fluid and foundations [253] and the phase change thermal storage where the latent heat of melting is exploited with the aim to contain both volumes and costs [254]. Finally a solution proposed especially for small systems consists in a tank filled by a solid medium which allows reducing the volume of heat transfer fluid in the system and the cost of the storage [118]. Power block in big commercial power plants is a steam water Rankine cycle since the power output ranges between 20 and 50 MW_{el} with maximum temperature of HTF of 390°C or 560°C if synthetic oils or molten salts are used.

The same concept can be applied in rural context and different companies are developing cheap parabolic trough collectors for this purpose. An example is the activity of STGinternational [88], a small start up company which is focused on the design of small ORCs for developing countries. Their technology is based on a low cost concentrating parabolic collector which is built with materials available on site, with the possibility to

[19] The oversizing of a solar field is commonly called Solar Multiple which represents the ratio between the actual field extension and the field extension required to provide the nominal thermal power in input to the power block.

involve the community interested by the project, to promote the transfer of technology and to form skilled operators on site. A goal that is not possible to achieve with photovoltaic technology since it requires advanced clean rooms and expensive equipment to manufacture the silicon cells. Heat is collected by the HTF, usually a glycol or an anti-freeze fluid used in automotive field or synthetic oil, which flows in the evacuated collector tubes. Hot fluid passes throughout a quartzite pebbled bed tank where heat is partially released. This solution allows reducing the amount of HTF required and thus the total cost since the thermal storage exploits the thermal inertia of the solid medium. The heat is eventually transferred from the HTF to the working fluid and it is used to drive an ORC. According to the temperature level 150-160°C and the target of these applications (3-100kW_{el}), ORC are the only suitable technology since the thermodynamic cycle and the component design can take advantage from the correct choice of the working fluid. The STGi team has been working on the development of this technology since 2004 and several prototypes have been constructed and installed in Cambridge, Massachusetts (USA); Bethel, Phamong (Lesotho), Matjotjo Village, Berea District (Lesotho), and St. Petersburg, Florida (USA).

STGi prototypes are based on a subcritical slightly superheated cycle working with R245fa, the expander is a scroll volumetric device derived from a compressor unit. However as already described in section 6.2.5 (Models comparison) they are developing in cooperation with university of Liege a new optimized scroll expander which allows increasing the plant efficiency of around five percentage points.

Despite the fact that all the solar plants installed so far are based on a binary single level subcritical cycles, possible advantages are represented by the capability of volumetric expanders to work with two phase fluids. With both screw and scroll devices it is possible to handle an expansion in presence of droplets of liquid without incurring in surface erosion because of the limited rotational speed and the low tip speed of these devices. In particular it is possible to expand the working fluid from a condition close to the saturated liquid throughout the two phase region allowing the design of triangular cycles. As already mentioned in Section 5.4 (Trilateral cycles) these cycles have a very low maximum temperature because of the limited volume ratio of volumetric devices, in addition since they cannot handle two phase fluid ad admission port, it is not possible to split the expansion in with a tandem configuration. A promising cycle is the flash-triangular cycle which uses two expanders in series: the first one expands the fluid from the saturated liquid condition while the second one expands the saturated vapor obtained by the flash stage. The main peculiarity of this cycle configuration consists in a heat introduction without phase transition which allows designing an advanced system characterized by the use of the working fluid in the solar field and a direct thermal

storage. This configuration reduces the cost of the system since the HTF loop and the heat exchanger between the HTF and the ORC are not required. In particular the PHE cost represents a relevant share of the total ORC power block cost because, for small size components, the scale economies are not exploited leading to a high specific cost for square meter. On the other hand the flash trilateral cycle shows a higher pump consumption since the working fluid flows directly into the solar collectors tubes which are characterized by a high pressure drops, and it requires two expanders and a more complicated plant layout with an higher weight of BOP cost.

Economic assumptions and methodology

A techno-economical comparison between the different cycle configurations is not trivial since it requires the definition of different parameters which can greatly affect the final solution like the solar field cost and the pressure drops in the solar collector loops. The analysis is carried out comparing the performances of several working fluids in both subcritical and flash trilateral cycle configurations. A sensitivity analysis is proposed varying the cost of the solar field and the pressure drops into the solar loops with the aim to obtain more robust results.

In Table 9.15 the main assumptions are reported, while all the other cycle parameters are reported in Table 8.2

Condenser type	ACC
Ambient air Temperature	30°C
Maximum temperature in solar collector	160°C
Collected thermal power, Q_{coll}	2 MW_{th}
Pressure drop in solar collector, bar	1.5-3
Specific cost of solar field c_{sf}, USD^{2013}/m^2	100-200
Reference DNI, W/m^2	800

Table 9.15 - Assumptions related to the condenser and the solar field common to all the investigated cases.

Unfortunately a very small literature is available about low temperature solar collectors and an estimation of their specific cost is not trivial. In a recent publication [255] the performances and the cost of different solar collectors for low enthalpy applications are compared by the authors highlighting the possibility to produce prototype with a specific cost around $170USD/m^2$ which is pretty different from large parabolic trough collectors for big concentrating solar plants [256] (~ $320USD/m^2$ with an estimation of 200 USD/m^2 in 2020). STGi claims a cost for the collectors around $80USD/m^2$. It is important to notice that big commercial collectors are based on a more advanced technology and are able to reach higher temperatures but they can conveniently exploit scale economies which

reduce notably their cost. On the other hand small, low temperature solar collectors use less expensive materials characterized by a lower reflectivity of the mirror and a higher emissivity of the coating but the limited number of units surely affect the specific cost of these components. Another crucial aspect is the efficiency of these devices which is affected by materials with lower performances, an effect which is partly balanced by a limitation of the heat dispersions thanks to the lower average temperature of the absorber tube. Experimental activities on low temperature parabolic collectors [255] highlight a maximum overall efficiency around 45% with a peak efficiency of 65% while Soponova collectors by Sophogy [257] have an average claimed efficiency equal to 58% (large parabolic trough collectors show higher efficiencies around 68% [252]). Finally an interesting publication on STGi collectors [258] highlights an efficiency slightly above 60% while in another report on the same technology [259] an averaged efficiency equal to 50% is reported. Here an nominal constant value for solar collectors efficiency (η_{coll}) equal to 60% is assumed, without taking into account the possible benefits of the flash trilateral cycle, which is characterized by a lower average temperature in the solar field and so a possibly higher thermal efficiency than the binary configuration.

The cost of the solar field is calculated by eq. 9.3.

$$C_{solar\ field} = c_{solar\ field}\ \frac{Q_{coll}}{\eta_{coll} DNI_{ref}} \qquad \text{eq. 9.3}$$

All the plants are optimized from a techno-economic point of view with the set of optimization variables as reported in Table 9.16. A selected number of 30 fluids is considered selecting them among pure linear and cyclic alkanes, refrigerant fluids and light siloxanes. Very high critical temperature fluids are excluded since they are the less suitable ones for the exploitation of low temperature heat sources, especially with volumetric expanders which are negatively affected by large volume ratios.

	One pressure level Techno-eco	Flash trilateral Techno-eco
T_{cond}	X	X
$T_{x,LP}$	X	X
$\Delta T_{sh,LP}$	X	-
$\Delta T_{pp,rec,LP}$	X	X
$T_{x,HP}$	-	X
$T_{out,HS}$	X	-
$\Delta T_{pp,cond}$	X	X
n	6	5

Table 9.16 - Optimized variables for the two investigated cycle configurations

For the single pressure level cycle, the optimal HTF lower temperature, namely the pinch point temperature difference in the PHE, is the result of the opposite effects between a lower cost of the PHE and a higher power consumption of the circulation pump. Since the maximum temperature in the solar field is fixed to 160°C and all the plants are compared at fixed solar field area, increasing the $\Delta T_{pp,PHE}$ leads to lower temperature increases in the solar collectors and to a higher mass flow rate of HTF. Considering a constant overall pressure drop in the solar collectors and in the headers of the solar field, the auxiliary consumption gets higher reducing the net power output of the system. On the other hand a higher pinch point temperature difference leads to a smaller PHE surface and a less expensive equipment. All the results are greatly affected by the components cost, in particular, for the investigated cases the correlation calibrated in Section 7.1 (Shell & tube heat exchangers) entails very expensive PHE according to the small heat transfer surfaces; other solutions can be adopted instead of S&T heat exchanger like brazed plate heat exchanger commonly used in smaller applications.

Single screw results

Results for single level subcritical cycles are proposed in Figure 9.30 in terms of plant specific cost for different class of fluids. A single screw expander is considered and is interesting to note that for alkanes, cycloalkanes and fluorinated fluids there is always an optimal fluid which has a critical temperature around 160°C[20] but relevant differences can be highlighted for lower and higher critical temperature fluids.

The results for propane, butane and nonane are reported in Table 9.17 while T-Q diagrams are displayed in Figure 9.31. With propane, the cycle is limited by the critical temperature and a high superheating is used in order to increase cycle efficiency, however the power production is relatively low because of the limited mean logarithmic temperature of heat introduction and the algorithm imposes a large ΔT_{pp} in the PHE in order to reduce the cost of this component. The plant cost is lower than in the other cases because of the smaller cost of the PHE and of the screw expander. Propane, due to its low critical temperature, shows a high pressure of condensation and small volume ratio are obtained in the expansion (~2.5) with a screw expander which can achieve really high efficiencies. In addition thanks to the high density of the discharged fluid the isentropic volume flow rate is small leading to a lower cost of the expander. For butane the lowest specific cost is achieved thanks to a better match between the hot stream and the working

[20] In the x-axis of the figure a reduce temperature is reported considering the reference temperature equal to 160°C which is the maximum temperature of the solar collectors.

fluid in the PHE. The evaporation temperature is higher than for propane since there is no limitation due to the proximity of critical point, the condensation temperature is slightly higher than the previous case because of the trade-off between a larger volume ratio and lower screw efficiency. The total absolute cost is higher but the larger power production leads to a reduction of specific cost. Finally nonane is considered as representative of a non-suitable fluid for this application. The high critical temperature involve very large volume flow rate at expander outlet and non-feasible volume ratios for condensation temperatures similar to the other fluids. For this fluid the expander is largely the most expensive component and the techno-economic optimization acts increasing the condensing temperature with the aim of reducing the cost (function of the volume flow rate) and increasing the screw expander efficiency (function of both size and volume ratio). The optimized volume ratio is slightly above 7, which corresponds to the point where the efficiency starts to be corrected by the off-design efficiency reduction factor. The optimized cycle has a very expensive PHE but more than 83% of the total power block cost is represented by the screw expander which has to handle a huge mass flow rate.

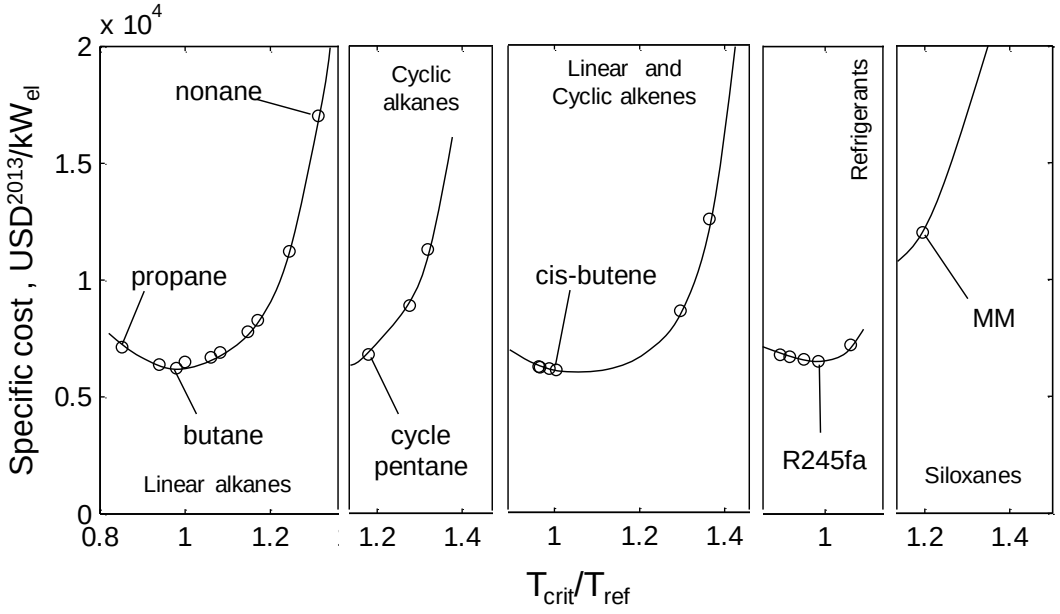

Figure 9.30 - Results for subcritical cycles with single screw expander

This example is important to underline two aspects related to the use of volumetric expanders which are not always taken into account:

- In thermodynamic optimization the use of a fixed efficiency can lead to misleading results since the important effects of the volume ratio and off-design effects beyond certain values are not considered. In most of the publications about the use of volumetric expanders usually a fixed efficiency is assumed with a maximum value of volume flow ratio depending on the device type. Only in one paper [258] the effect of size and volume ratio is considered for a 3 kW_{el} scroll expander for ORC.
- In the techno-economic optimization considering a fixed cost for the volumetric expander, or using a cost correlation dependent on the shaft power lead to optimized solution far to be reliable. In fact, considering the expanders working at their nominal rotational speed, increasing the volume flow rate the cost increases with a detrimental effect on the plant economics. In these cases, screw expanders can be operated at higher velocity but additional losses should be taken into account for higher friction losses in the machine and the mechanical losses of the gearbox or the electrical ones in the power electronics system.

	propane	butane	nonane
General results			
W_{net}, kW_{el}	184.38	228.14	163.80
plant efficiency	9.22%	11.41%	8.19%
Cost PB, $kUSD^{2013}$	686.6	767.0	4915.5
Cost TOT, $kUSD^{2013}$	1309.3	1413.8	3460.6
Costs PB, USD^{2013}/kW_{el}	3723.9	3362.0	21127.5
Costs TOT, USD^{2013}/kW_{el}	7100.8	6197.0	30009.5
$W_{pump\ SF}$, kW_{el}	8.59	12.70	16.95
Optimized parameters			
T_{cond}, °C	42.25	47.21	80.00
T_{eva}, °C	91.18	122.49	140.66
ΔT_{sh}	65.86	33.89	0.00
$\Delta T_{pp,rec}$	3.00	3.13	3.14
$T_{out,HTF}$, °C	120.97	133.57	140.17
$\Delta T_{pp,cond}$	4.00	6.26	10.00

	propane	butane	nonane
Power block cost breakdown			
Cond	29.06%	21.72%	3.43%
Des	7.09%	3.81%	0.59%
Rec	11.29%	8.68%	1.69%
Eco	-	12.85%	3.10%
Eva	15.92%	17.51%	7.43%
Sup	22.56%	15.74%	-
Screw	8.14%	15.22%	83.16%
Pump	3.46%	2.45%	0.29%
Others	2.49%	2.01%	0.32%
Screw expander			
η screw	83.23%	78.76%	72.42%
Vr	2.4966	4.9706	7.348
Vout, m^3/s	0.2426	0.52249	13.221
Cost,kUSD	55.89	116.74	2877.80

Table 9.17 - Results for the optimal subcritical cycles with propane, butane or nonane.

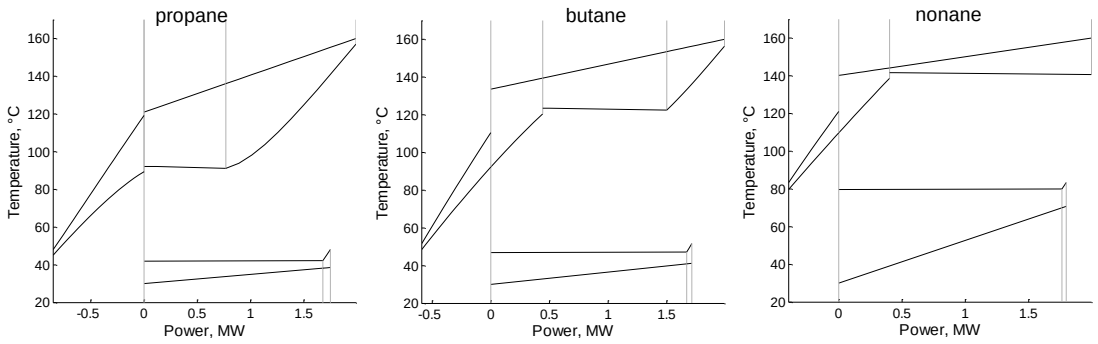

Figure 9.31 - T-s diagrams for propane, butane and nonane optimal subcritical cycles

A further improvement can be achieved for some low critical temperature fluids using a supercritical configuration. In the next sections both the configurations are considered and so the result displayed for a certain fluid is the minimum specific cost attainable with a subcritical or a supercritical cycle configuration.

It is finally interesting to note that R245fa fluid used from STGi international for a similar ($3kW_{el}$) application is the best fluid even in this case where a subcritical superheated single level cycle with a single screw expander is used.

The value of specific cost of the whole plant cannot be really validated because this is a niche application and studies on this topic do not consider techno-economic optimization of the system or they refer to plant sizes notably smaller or bigger. The specific cost of the power block is around 3300 USD^{2013}/kW_{el}, a value which is confirmed by a personal communication with a ORC producer which claims a cost close to 3000 $€/kW_{el}$ for a $130kW_{el}$ WHR unit receiving heat from a loop of pressurized water. The technology is different since it is based on a high speed centripetal turbine but the order of magnitude seems reliable.

Tandem screw

For some fluids, characterized by medium large volume ratios, the use of a two stage or tandem expansion can be profitable. This solution consists in two expanders in series, each one with a volume ratio equal to the square root of the global one with the possibility to notably increase the volumetric expander efficiency for those solutions characterized by large, but not extreme, volume ratios. The two expanders are connected in series and they elaborate a different volumetric flow rate. In the tandem screw compressor the two pair of helical rotors usually rotates at the same velocity and so they have different sizes, another option is to have a gearbox in order to limit the size of the

low pressure device. An efficiency increase around 11-13% is claimed by a two stage compressors producer [260].

It is important to notice that the same expansion handled with a tandem screw configuration is intrinsically more expensive since the low pressure expander cost is approximately the same of the single screw case and an additional cost has be considered for the high pressure expander. Nevertheless, if the adoption of a tandem expansion allow achieving a higher efficiency and exploiting a larger pressure drop, it might be profitable even from an economic point of view.

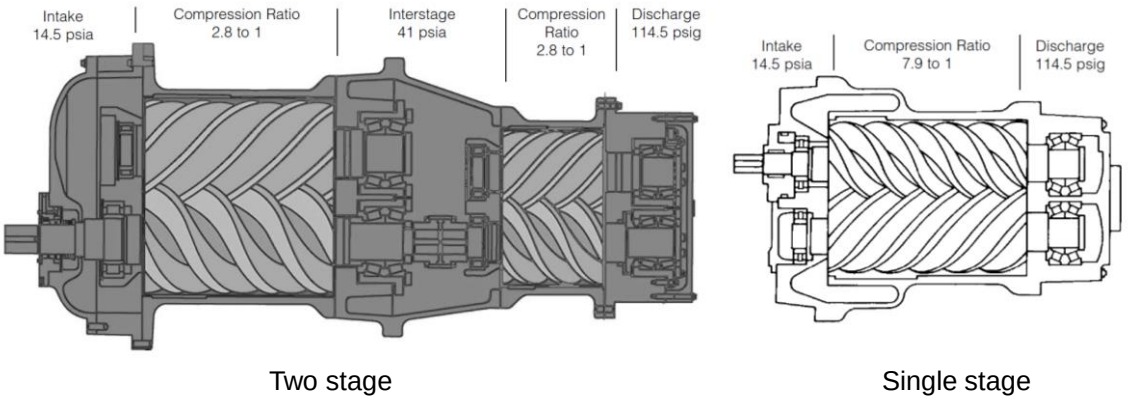

Figure 9.32 – Comparison between a commercial two stage air compressor (2.8+2.8) and single stage air compressor (7.9) produced by Sullair [260]

In Figure 9.33 the decrement of the specific cost is represented for all the investigated fluids: for linear alkanes, alkenes and refrigerants the attainable reduction of specific cost is relevant for fluids with critical temperatures between 140°C and 200°C. For low critical temperature fluids (e.g. propane), the use of a tandem expansion is not really profitable because the expansion is characterized by small volume ratio and so the advantages in terms of a higher power output are levelled off by the cost increase. For very high critical, a temperature fluids, a similar consideration can be done: the overall efficiency increases notably but also the high pressure expander cost increases significantly, with a detrimental effect on the specific cost of the plant.

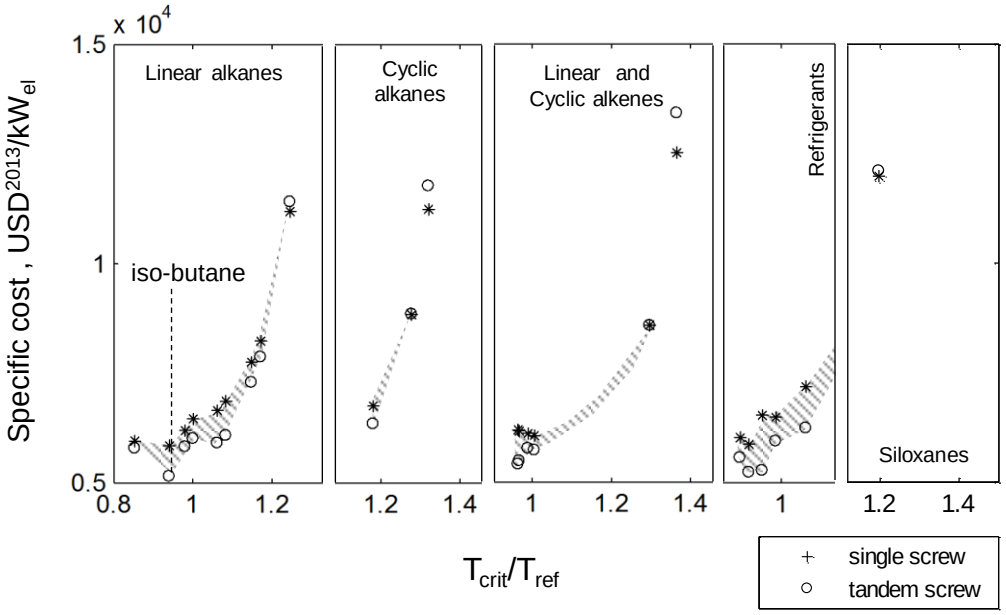

Figure 9.33 - Comparison between optimal solution attainable with a single screw or a tandem expansion. The shaded area highlights the decrement of plant specific cost.

A comparison between supercritical cycles with iso-butane is reported in Table 9.18. The first case is optimized using a single expander while the other one with a tandem expansion. The power output increases by more than 19% with the tandem configuration since the condensing temperature is reduced by 5°C and a higher enthalpy drop is available in expansion. The expander inlet condition is almost constant since the maximum temperature and pressure are constrained by the cost of the PHE. The overall volume ratio is increased from 6.4 to 7.3 but the overall efficiency is increased by 8.8 percentage points, partially confirming the over mentioned producer's data. The two screw expanders in series have the same volume ratio equal to 2.7 and they have an efficiency of 81.2% and 84.13% respectively for the high pressure and the low pressure device. The difference in performance is due to the larger size of the second expander, leading to smaller leakage losses. The cost of the power block increases, as well as the share of screw components on the total cost (from 13.9% to 19.2%). As a result, both the power block and the total plant specific costs decrease thanks to a higher power production. Finally it is interesting to note that the cost of the heat exchangers (PHE, recuperator and condenser) covers more than 70% of power block cost while screw expander share is around 14% for optimized solutions. This is not surprising since in this study the cost of commercial screw compressor is used, a component which is characterized by a huge number of units produced for several different applications which can take advantage from relevant scale economies the standardization of the production process.

	single	tandem
General results		
W_{net}, kW_{el}	203.48	244.65
plant efficeincy	10.17%	12.23%
Cost PB, $kUSD^{2013}$	595.34	648.79
Cost TOT, $kUSD^{2013}$	1190.61	1260.10
Costs PB, USD^{2013}/kW_{el}	2925.79	2651.92
Costs TOT, USD^{2013}/kW_{el}	5851.21	5150.61
Optimization parameters		
T_{cond}, °C	50.18	45.01
T_{eva}, °C	135.66	135.66
ΔT_{sh}	21.609	21.109
$\Delta T_{pp,rec}$	4.107	3.9076
$T_{out,HTF}$, °C	136.16	135.97
$\Delta T_{pp,cond}$	8.0853	5.8836

	Single	tandem
Prower block cost break down		
Cond	25.53%	26.60%
Des	5.96%	5.97%
Rec	10.03%	8.76%
PHE	37.85%	33.16%
Screw	13.89%	19.17%
Pump	4.23%	3.82%
Others	2.50%	2.51%
Screw expansder		
$\eta_{screw,eq}$	74.07%	82.85%
Vr	6.390	7.291
Vout, m^3/s	0.366	0.396
Cost,kUSD	82.70	124.40

Table 9.18 - Comparison between iso-butane supercritical cycles based on a single screw or a tandem screw expansion

Flash trilateral

Finally the flash-trilateral cycles are investigated: two screw expanders are used in series separated by a flash tank where the two phases are separated, the maximum temperature of the fluid is set to 160°C a value usually reached if the limit due to the proximity of the critical point is not activated. The flash trilateral cycles can be even more efficient than the single level cycles with tandem screw expander if the maximization of the power output is the goal of the study. However in this case, the techno-economic optimization leads to less efficient solutions. Capital cost for flash trilateral cycles is, in fact, lower than for binary cycles since they do not require the PHE which is the most expensive component (~35% of power block cost). In Figure 9.34 a comparison between single screw, tandem screw and flash-trilateral cycles is proposed and it is possible to note that the use of this latter cycle configuration allows achieving for many fluids a lower plant specific cost. For each series, the optimal fluid has a critical temperature higher than in the previous case because low critical temperature fluids can reach lower inlet temperatures at the high pressure screw intake with a limitation of cycle efficiency. Fluids with a critical temperature higher than the maximum achievable in the solar collectors can instead be freely optimized and they reach a lower overall specific cost. In Figure 9.35 the T-s and the T-Q diagrams for trans-butene are reported while a comparison between single screw, tandem screw and flash trilateral cycles with this fluid is reported in Table 9.19 and a focus on cost repartition reported in Figure 9.36. It can be noticed that the flash trilateral configuration allows achieving a notable specific cost reduction mainly because

the cheaper power block, while the net power output of the system is lower respect to both the single screw and the tandem screw configuration but it is due to cross effects related to the economic optimization. In the flash trilateral cycle the two screw expanders works with a similar volume ratio but the high pressure one has smaller rotor diameter than the low pressure one even if it expand the whole mass flow rate. For this reason it can reach a lower efficiency than the low pressure expander which is not affected by larger relative losses due size effect and the increase of leakage and friction losses (even if it works with a smaller volume ratio).

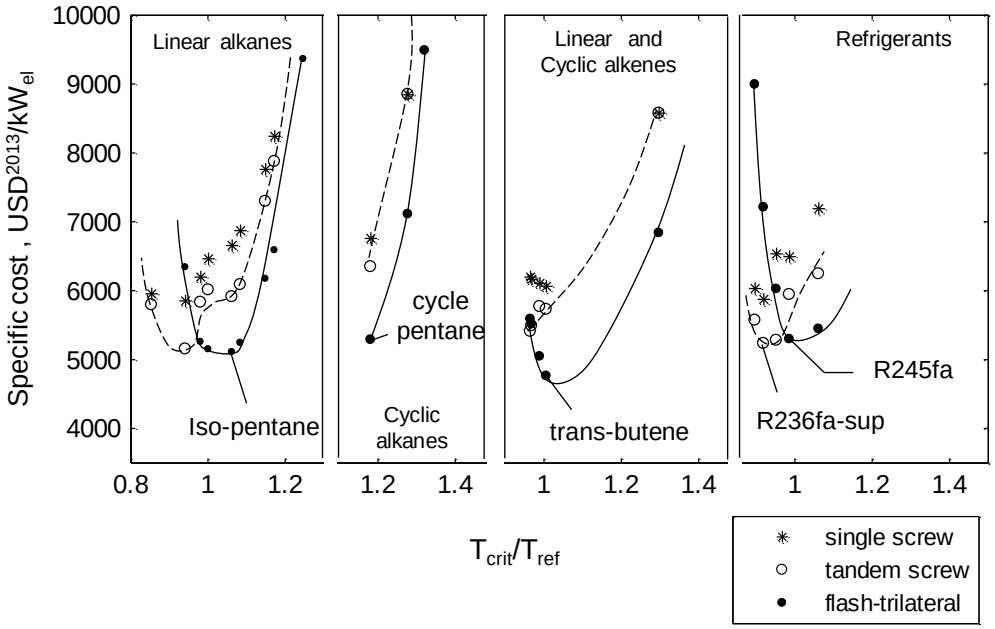

Figure 9.34 - Comparison between single screw binary cycles, tandem screw binary cycles and direct flash-trilateral systems

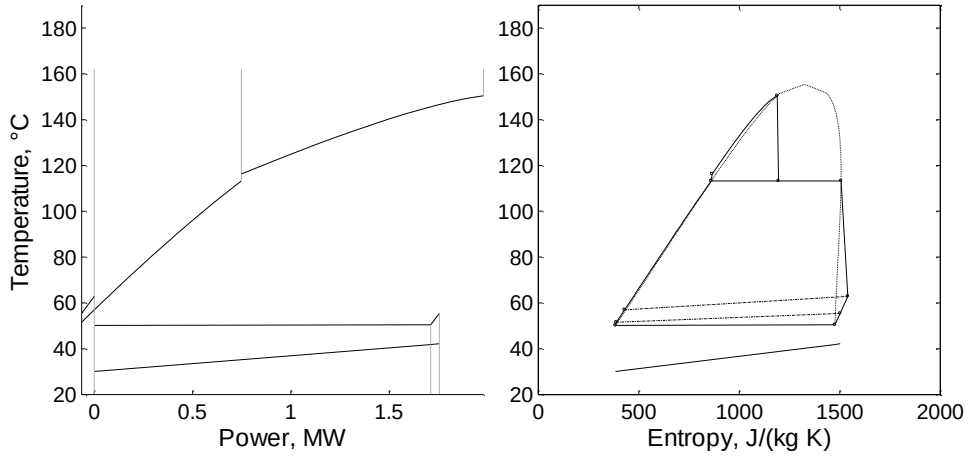

Figure 9.35 - T-Q and T-s diagrams for the optimal cycle with trans-butene

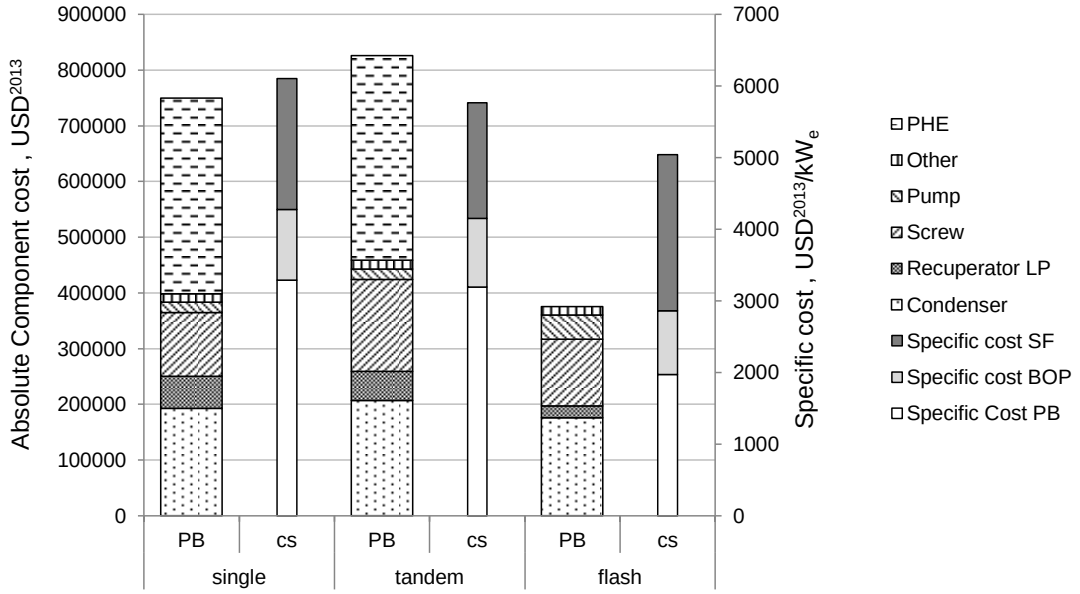

Figure 9.36 – Power plant cost breakdown (thicker bars) and specific plant cost (thinner bars) for single screw, tandem screw and flash trilateral cycles

Finally it is interesting to note that if the solar field cost increases the flash trilateral cycle is penalized since it can produce a lower power output and the specific cost related to the solar field is higher for this configuration than for the binary cycles.

	Single	Tandem	Flash
General and economic results			
Wnet plant, kW_{el}	227.77	258.56	190.61
plant efficiency	11.39%	12.93%	9.53%
Cost PB, $kUSD^{2013}$	749.66	826.29	375.82
Cost BOP, $kUSD^{2013}$	224.90	247.89	169.12
Cost SF, $kUSD^{2013}$		416.67	
Cost TOT, $kUSD^{2013}$	1391.22	1490.84	961.60
Specific Cost PB, USD^{2013}/kW_{el}	3291.35	3195.71	1971.67
Specific cost BOP, USD^{2013}/kW_{el}	987.41	958.71	887.25
Specific cost SF, USD^{2013}/kW_{el}	1829.36	1611.48	2185.98
Specific Cost TOT, USD^{2013}/kW_{el}	6.11	5.77	5.04

Expansion results					
		1stage	2 stage	LP	HP
η screw	78.86%	82.69%	85.28%	80.06%	77.24%
Vr	4.936	2.522	2.522	4.281	3.828
Vout	0.5146	0.2060	0.5210	0.4161	0.1052

Table 9.19 –Comparison between the optimized results for trans-butene with a single level-single screw binary cycle, with a tandem screw and for a flash trilateral cycle

Sensitivity analysis on solar field cost and collectors pressure drops

All the results achieved in the previous analysis are obviously affected by the specific cost of the solar field and the pressure drops in the tubes of the parabolic collectors. Increasing the pressure drops for direct flash trilateral cycles entails larger and more expensive pumping station with a higher consumption resulting in a lower turbine net power output. For binary cycles instead higher pressure drops in HTF loop leads to a lower minimum temperature of the oil, in order to reduce its mass flow rate and solar field pump consumption. Since the PHE is a relevant share of the total plant cost, the pinch point temperature difference in the evaporator cannot be strongly reduced leading to a slightly lower evaporation and condensation pressures in order to maintain a good thermodynamic cycle efficiency. These contrasting effects result in higher specific cost for all the three solutions with a higher penalization for single screw binary cycle and flash trilateral one. Assuming 3 bars of pressure drop an increase of specific plant cost equal to 3.60%, 3.47% and 3.57% is obtained for the three investigated cycles working with trans-butene. This variation compared to the gap between the specific costs in the previous case is not so relevant to modify the previous considerations. From a general point of view, higher fixed pressure drops penalize more the high critical temperature fluids since they work with low pressure differences between condensation and maximum pressure and so an absolute off-set has a stronger impact on final performances.

Specific solar field cost is instead a relevant share (around 30%-50% in the reference case) of the total plant cost and an increase of this parameter leads to more efficient optimal solutions since the economic optimization favors those solutions with higher power output. Results with a solar field cost twice than the reference case are reported in Figure 9.37 and they can be compared to those in Figure 9.34. The increase of average specific plant cost of the optimal solutions is close to 35% and the advantages in using flash trilateral cycles become negligible comparing the optimal solutions. For some classes of fluid the advantage is still relevant (cycle alkanes and alkenes) and the use of direct cycles allows reducing the total plant cost. On the other hand, if flammable fluids cannot be used, the optimal solutions in this case are supercritical recuperative cycles with a two stage expansion, but obviously the HTF should be non-flammable too.

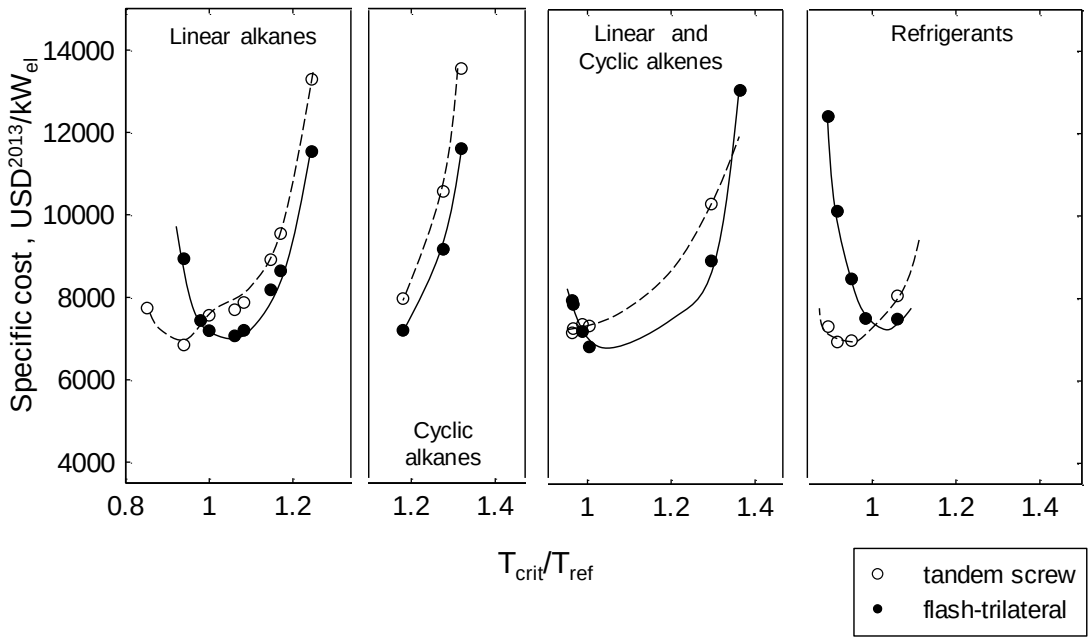

Figure 9.37 – Comparison between optimal binary cycle and optimal flash-trilateral cycle with a specific cost of solar field equal to 200 USD^{2013}/m^2

Conclusions and future works

A small solar thermal power plant coupled with a ORC is investigated. The system is based on low-cost and low-temperature parabolic collectors with a maximum temperature of 160°C and three different cycle configurations are analysed in order to determine which is the most suitable one to be installed in rural context. Some interesting results can be summarized:

- The use of well calibrated correlations for the efficiency and the cost of volumetric expander is crucial for thermodynamic and techno-economic optimizations. A fixed efficiency, even considering a limit on maximum volume ratio, is far from the reality and, for high critical temperature fluids, it pushes the optimal solution always toward the upper limit of volume ratio;
- The use of two stage tandem expansion can be really profitable, allowing an increase of power production and a reduction of specific cost for those fluids which can take advantage from the repartition of the expansion in two devices;
- The use of flash trilateral cycles is really interesting since it entails a lower power block cost and the possibility to perform a direct storage with the working fluid. This is an innovative concept and so far no experimental activities have been carried out since this niche market is oriented to conventional and low risk solutions

- A sensitivity analysis on the pressure drops in the solar collectors and on the specific cost of the solar fields has highlighted that:
  - An increase of pressure drop in solar collectors penalizes all the cycle configurations in a similar way. A higher specific cost increase is obtained for single screw and flash trilateral cycles but different assumptions on this parameter wouldn't affect the choice of the best combination of working fluid and cycle configuration;
  - For a higher cost of the solar field flash trilateral cycles are penalized due to their lower power output nevertheless they are still competitive even with a price of 200USD/m^2 of collector area or a 133 USD/m^2 and a solar multiple equal to 1.5.

Future works related to this technology should be focused on:

- A better description of the solar field with a model of solar collectors in order to link the thermal efficiency and the pressure drops to the HTF thermodynamic properties. Simplified and detailed models are available in the literature for the numerical characterization of parabolic trough technology [258; 261] and their implementation will probably advantage flash trilateral cycles where a lower mass flow rate flows into the solar field with a lower average temperature. A preliminary design of the solar field should be considered as well in order to account reliable pressure drops in the headers;
- A more deep bibliographic review of cost correlations for heat exchangers different from the S&T ones is required. Especially for smaller application the extrapolation with an exponential law to very small heat transfer surfaces would entail a non-realistic increase of heat exchanger specific cost. Other heat exchangers types, like plate fins or brazed plate heat exchangers, can be considered with the aim of reducing the power block cost;
- The off-design simulation of these plant configurations in order to highlight differences in efficiency and power production for one year of operation, in particular for plants without or with limited thermal energy storage.

9.1 WHR from Cement plants

Cement plants are energy intensive plants where low grade fuels are burned first to decompose limestone ($CaCO_3$) into Calcium Oxide and CO_2 at around 850°C and then to heat the primary feedstock (the raw meal) up to temperatures of 1400-1500°C. At these temperatures, clinkerization reactions are initiated and the clinker, a sintered mixture of Calcium Silicates, Calcium Alluminate and Calcium Aluminoferrite which represents the final product of cement plants, is formed. Waste heat in cement plants is available as hot air from clinker cooler and as hot flue gases from the raw meal preheater. These heat sources are both of relatively high quality, with maximum temperatures of the order of 300-390°C, and are hence suitable for heat recovery for power generation. The amount of heat can vary from few MW up to around 100 MW, depending on the size of the plant, on the efficiency of the process and on the humidity of the fuel and the raw limestone, hence requiring variable amounts of process heat for drying. Despite the strong interest in this field, the number of installations is still limited. In addition, a lack of scientific publications on this topic can currently be observed and specific studies for the definition the optimal combination of working fluid, cycle configuration and design parameters would be important.

Methodology and assumptions

If a large amount of heat is available at medium high temperature, ORCs have to compete with small steam water Rankine cycles. As already mentioned in Chapter 3 (ORC field) there is a large area for power output greater than 5 MW_{el} and temperature higher than 350°C, where the choice between a steam water cycle or an ORC is not univocal because both plants presents positive features and drawbacks. Water is an exceptional working fluid for power generation, it shows very high film heat transfer coefficients, it is cheap, it is neither corrosive nor toxic, nor flammable and the key components of the plant are fully optimized thanks to decades of improvements. On the other hand, it presents difficulties in the turbine design and manufacture for low power outputs because of the small volume flow rate and the small size of first stages which are negatively affected by a non-optimized rotational speed. Furthermore steam turbines require a large number of stages since the water, like any other light fluid, show huge enthalpy drop in expansion. Organic fluids instead allow designing a compact and cheap turbine but they usually require bigger heat exchangers and additional cost for the anti-firing system if a flammable fluid is used.

The aim of this study is to underline the main differences between steam Rankine cycles and ORCs for the exploitation of the hot gases released from a cement production facility. The heat source is modeled as a stream of hot gases with a maximum temperature of 385°C and a minimum temperature at the stack of 100°C. A parametric analysis is proposed for an available thermal power equal to 20, 50 and 100MW_{th}, involving plants with a power output which ranges between 4 and 30 MW_{el}. The mass flow rate of the flue gas is computed by assuming a constant heat capacity equal to 1.2 kJ/kgK. All the investigated solutions use a water cooled condenser where the coolant pump is characterized by an overall head equal to 80 m, comprehensive of the well depth and the pressure drops in the condenser and in the piping. For subcritical cycles a sub cooling temperature difference of 10°C is considered at the economizer outlet while all the other cycle parameters are reported in Table 8.2.

The comparison between the different fluids is performed by optimizing subcritical and supercritical cycles from a techno-economic point of view, with the aim of minimizing the specific cost of the plant. The choice of the objective function is justified by the fact that no variable cost are connected to the exploitation of waste heat which would be otherwise released to the environment. Finally, it is important to underline that, in all the investigated cycles, a direct heat transfer from the hot gases to the working fluid in realized in a HRSG[21] unit. This is not common in ORC WHR plants where usually a HTF loop is used between the power block and the heat source, allowing reducing the amount of working fluid and the presence of high pressure flammable fluids in the HRSG unit. However, the use of HTF results in a lower maximum temperature for the thermodynamic cycle because of the additional approach point temperature difference in the PHE.

Finally, it is important to underline that no fixed costs are directly associated to the exploitation of the heat source, differently from geothermal brines, where drilling expenses are accounted, or solar energy, where the solar field is required. In this case the hot stream is for free, but a fixed cost is hidden in the HRSG cost correlation which is formed by two terms: one dependent on the tube surface, the other one is function of the volume flow rate of hot gases.

Results

The model and the HRSG cost correlation are validated on a test case where water is used as working fluid in a large size application (100 MW_{th}). By observing the T-Q and the T-s

[21] The term HRSG defines the a vertical finned tube heat exchanger like those commonly used in combined cycles.

diagrams in Figure 9.40 it is possible to notice that the optimization algorithm acts increasing the condensation temperature in order to limit the liquid quality at turbine outlet and to contain the number of stages and the last stage diameter. The maximum temperature of the cycle is close to the maximum flue gas one and the evaporation temperature is set according to the wet expansion limit while exploiting the heat source with a good recovery efficiency. The pinch point temperature difference in the PHE is 9.1°C which is a reasonable value for this technology since steam cycles in combined plants are usually designed with a $\Delta T_{pp,PHE}$ equal to 8-10°C. The approach point temperature difference is instead slightly higher than values commonly used in big recovery steam cycles and the reason is related to both the turbine design and the necessity to efficiently cool down the hot gases. The specific cost of the plant is slightly lower than 2150 USD^{2013}/kW_{el}: a value compatible with the data from reference reported in Figure 7.19. This example gives a validation of the correlations of cost used for the HRSG unit and for multistage steam turbines. More details about the steam Rankine cycle are reported in Table 9.20 where a comparison with other promising solutions is provided.

The lower specific cost attainable with subcritical and supercritical single level cycles is reported in Figure 9.38 against the reduced temperature parameter referred to the maximum temperature of the flue gases.

The best plants are slightly supercritical but the difference in cost between them and the corresponding subcritical cycle is almost negligible for fluids with a critical temperature between 220°C and 290°C while large cost reductions are attainable for low critical temperature fluid while the opposite is true for high critical temperature fluids. A large number of fluids in a range of critical temperatures between 130°C and 320°C can reach low specific costs, in most of the cases with supercritical cycles, and these configurations are also characterized by a higher power production and a higher plant efficiency as reported in Figure 9.39. It is interesting to note that the reduction of specific cost for low critical temperature fluids is obtained by means of an increase of power production using supercritical cycles which can overcome the critical point reducing the temperature differences in the PHE. For high critical temperature fluids, instead, subcritical cycles are more efficient since in this case the transcritical transition entails a reduction of the recovery efficiency and the power production.

Three fluids look more suitable for this application, namely the benzene, the cyclo-pentane and the acetone in supercritical cycle configuration. All these fluids are flammable and so hazard issues has to be faced in order to guarantee the safety of the employers and to avoid the environmental contamination in case of leakage with an

increase of plant cost which might lead to exclude them from the list of the possible fluid candidates. Among low flammability fluids a pretty good performance can be achieved with a supercritical cycle operating with R236ea (a high critical temperature refrigerant) while the first non-flammable siloxane has a critical temperature definitely too high to be used in a power plant without cogeneration. The large size parameter at the last stage turbine entails a strong increase of both turbine and plant cost, the optimization algorithm increases the condensing temperature leading to a lower power production and a higher specific cost respect to other fluids with a lower critical temperature.

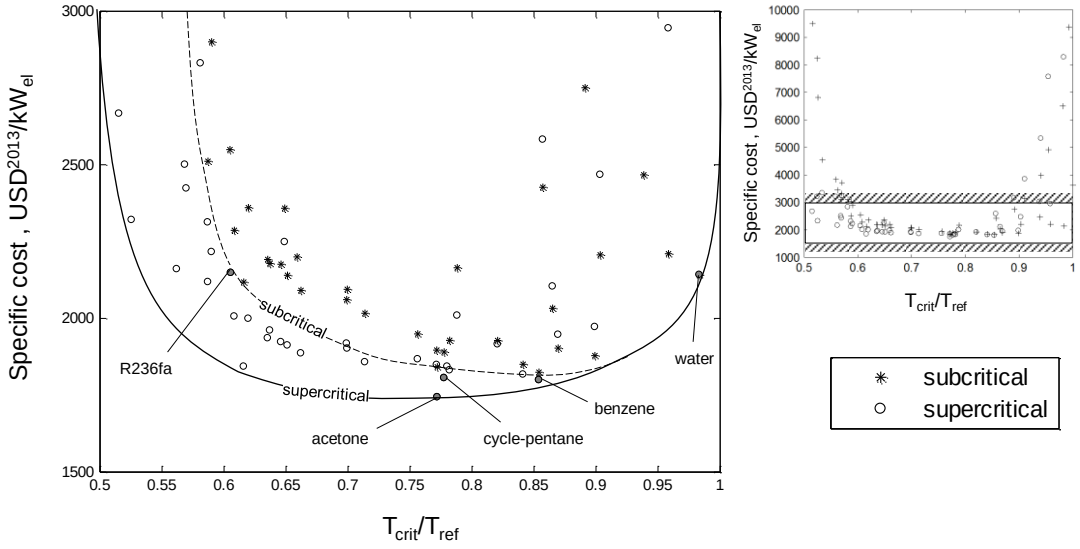

Figure 9.38 – Minimum specific cost attainable with single level subcritical and supercritical cycles. The bigger chart is a zoomed detail of the chart in the top right corner where all the solutions are represented. Grey markers represent the three solutions for a 100MW_{th} waste heat recovery application reported in Table 9.20

A lower specific cost might be attained with high critical temperature perflourinated fluids of the PP series. These fluids are characterized by long backbone chain of –(CF2)- units and thus they are non-flammable and stable up to high temperatures. Thanks to the high critical temperature, they can minimize the mean logarithmic temperature difference in the PHE, achieving higher performances. Nevertheless, their use is very limited even if some commercial plants are in operation [5]. The main limits in using these fluids are related to (i) their cost (which can be above 100 USD/kg) and (ii) to the lack in thermodynamic and reliable equation of states. Finally it is important to underline that R236fa is not the higher critical temperature refrigerant but others, like R245fa, have a lower thermal stability leading to a poor performance of the thermodynamic cycle and R365mcf is flammable because of its low F/H ratio. In Table 9.20 the main results for the five selected fluids are reported and a graphical comparison between the T-Q and T-s diagrams for water and acetone (the best fluid for this application) is shown in Figure 9.40.

	acetone		benzene		cycle-pentane		water		R236fa	
T_{rid}	0.772		0.8539		0.7775		0.9832		0.6048	
P_{rid}	1.0135		1.0129		1.0138		0.04		1.9126	
System efficiency										
cycle efficiency	23.82%		25.12%		24.46%		20.55%		20.06%	
plant efficiency	20.15%		20.84%		20.31%		17.22%		17.00%	
recovery efficiency	84.62%		82.97%		83.05%		83.79%		84.75%	
II law efficiency	47.28%		48.89%		47.66%		40.39%		39.87%	
General results										
Wnet plant, MW_{el}	20.154		20.841		20.315		17.217		16.996	
Cost TOT	35.146		37.505		36.686		36.876		36.451	
Specific Cost TOT, USD^{2013}/kW_{el}	1743.875		1799.598		1805.892		2141.829		2144.653	
HRSG % (no BOP)	63.72%		61.96%		60.83%		58.38%		58.67%	
Design parameters										
T_{cond}	45.80		43.63		39.27		51.50		37.31	
T_{eva} or T_x	235.95		289.87		239.57		176.21		144.15	
ΔT_{sh}	40.90		3.00		22.63		165.15		82.66	
$\Delta T_{pp,rec}$	2.58		2.50		2.21		-		1.66	
$T_{out,HS}$	143.82		148.54		148.30		146.21		143.47	
ΔT_{mlnPHE}	58.83		51.30		58.26		57.86		72.23	
Turbine results										
Turbine efficiency	86.64%		85.61%		86.01%		86.34%		88.65%	
Number of stages	3		4		4		9		3	
Rotational speed	6000		3000		3000		3000		3000	
Size parameter (min-max)	0.138	0.537	0.126	0.858	0.135	0.620	0.191	1.073	0.166	0.403
Specific speed (min-max)	0.052	0.189	0.036	0.176	0.036	0.134	0.026	0.221	0.062	0.140

Table 9.20 – Comparison between the three best fluids (acetone, cycle-pentane, benzene), water and R236fa for the exploitation of a 100MWth WHR application for cement industry

The three organic fluids can reach comparable specific costs and, even if they have a different shape of the Andrews curve (bell-shaped for acetone, overhanging for cycle-pentane and benzene), they have a molar mass and critical temperature which allows the best trade-off among cycle performances, turbine size and heat recovery efficiency. Water is instead characterized by a turbine with a higher number of stages (9 vs 3 or 4 for the organic fluids) and large size parameter of the last stage which result in a more expensive equipment. R236fa has a too low critical temperature which leads to the adoption of really high pressures and an increase of pump consumption. Finally, it can be noticed that for the optimal cycles operating with benzene, cycle-pentane, water and R236fa the turbine optimal rotational speed is 3000 RPM and the use of a gear box is not profitable. Acetone turbine is instead optimized with a rotational speed of 6000 RPM.

Two more aspects can be underline: (i) the HRSG unit is a relevant share (more than 60%) of the total equipment cost without BOP, which leads to prefer high efficiency solutions and (ii) the mean logarithmic temperature difference in the PHE is almost constant for all the cycles reported in Table 9.20 except for R236fa due to its lower critical temperature.

Finally, by observing the acetone optimal cycle in the T-s diagram in Figure 9.40, it is possible to note how it looks similar to a low temperature USC (Ultra Supercritical Cycle) steam cycle for power generation. This fact suggests, once again, that supercritical cycles are the most suitable ones for the exploitation of variable temperature heat sources and that for each thermal level a limited number of promising fluids can be selected.

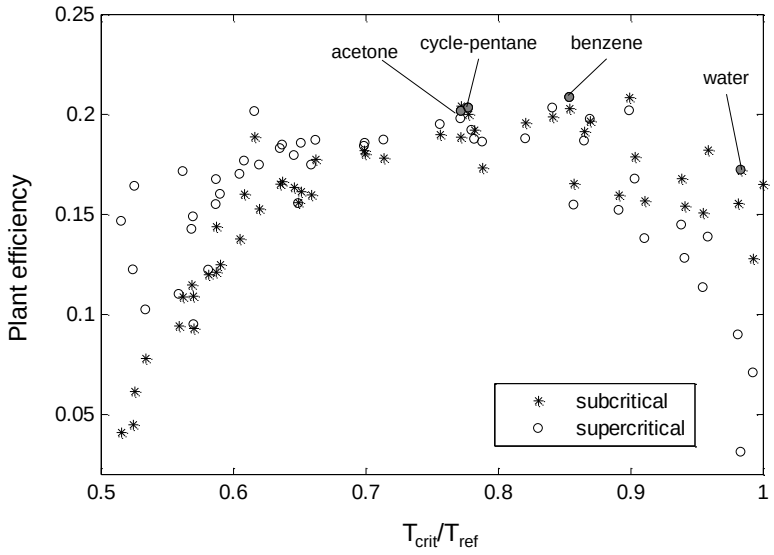

Figure 9.39 - Plant efficiency of single level subcritical and supercritical cycles optimized from a techno-economic point of view

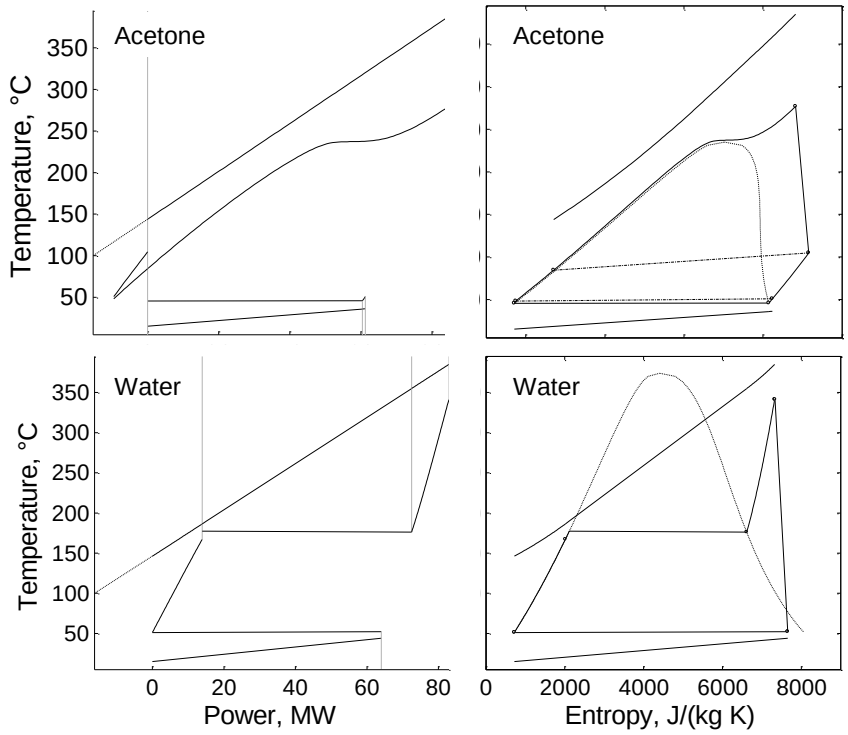

Figure 9.40 - T-Q and T-s diagrams for acetone and water at the optimal solutions.
Available thermal power=100 WM_{th}

Sensitivity analysis on available thermal power

Finally a sensitivity analysis varying the available thermal power is proposed in order to highlight the effects of components size on plant performances and on plant specific cost for water and organic fluids. Two comparisons are proposed: between water and acetone in Table 9.21 and between water and R236fa in Table 9.22.

Acetone remains the optimal fluid independently of the size of the plant, the specific cost is increased because of the non-proportional decrement of the power production and the capital cost. The same trend can be observed for steam Rankine cycles where specific cost around 3700 USD^{2013}/kW_{el} are obtained for power output of around 3.5 MW_{el}. The difference between the power production and the specific cost gets larger for low available thermal inputs in both absolute and relative values confirming that water is not a suitable fluid for low size applications. Increasing the available thermal power the gap is going to be reduced, but probably acetone in supercritical configuration will remain the optimal solution even for larger plants while water is the optimal fluid for higher temperature applications.

	20 MW_{th}		50 MW_{th}		100 MW_{th}	
	water	acetone	water	acetone	water	acetone
W_{net} plant, MW_{el}	3.410	4.485	8.554	10.736	17.217	20.154
Plant cost, USD^{2013}	12.688	11.813	22.462	21.600	36.876	35.146
Specific plant cost, USD^{2013}/kW_{el}	3720.95	2633.94	2625.87	2011.94	2141.83	1743.88
RPM	8000	10150	6000	6850	3000	6000
ΔW_{net}, MW_{el}	1.075		2.182		2.936	
ΔW_{net}, % (referred to acetone)	23.97%		20.32%		14.57%	
ΔCs, USD^{2013}/kW_{el}	-1087.008		-613.935		-397.954	
ΔCs, % (referred to acetone)	-41.27%		-30.51%		-22.82%	

Table 9.21 - Comparison between optimal plants with water and acetone for three different sizes.

The comparison between water and a suitable non-flammable working fluid suggests similar conclusions but for big applications water is more efficient and can reach a lower specific cost. For small plants, maintaining the same evaporation and condensation temperatures, the use of water entails a more challenging design of the turbine which is characterized by a small first stage size parameter and specific speeds of the first and the last stages, far to be optimized. The optimization algorithms acts reducing the evaporation temperature in order to increase the volume flow rate at turbine inlet achieving good turbine performances but penalizing the cycle efficiency. The pinch point temperature difference in the PHE reduces to 6.4°C (50 MW_{th}) and 5.3°C (20 MW_{th}) according to the fact that the relative fixed cost of the HRSG unit gets higher leading to a more efficient power plant in order to amortize the investment.

	20 MW_{th}		50 MW_{th}		100 MW_{th}	
	water	R236fa	water	R236fa	water	R236fa
W_{net} plant, MW_{el}	3.410	3.595	8.554	8.54636	17.217	16.996
Plant cost, USD^{2013}	12.688	11.465	22.462	15.976	36.876	36.451
Specific plant cost, USD^{2013}/kW_{el}	3720.95	3188.79	2625.87	2430.14	2141.83	2144.65
RPM	8000	7120	6000	5520	3000	3000
ΔW_{net}, MW_{el}	0.185		-0.008		-0.221	
ΔW_{net}, % (referred to R236fa)	5.16%		-0.09%		-1.30%	
ΔCs, USD^{2013}/kW_{el}	-532.164		-195.733		2.825	
ΔCs, % (referred to R236fa)	-16.69%		-8.05%		0.13%	

Table 9.22 - Comparison between optimal plants with water and R236fa for three different sizes.

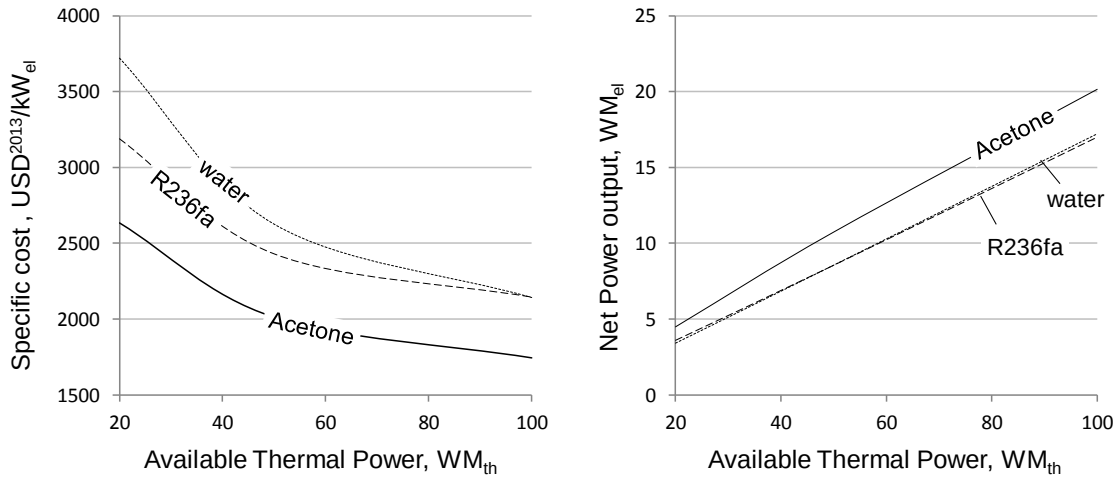

Figure 9.41 – Trend of specific cost and power production for acetone, water and R236fa varying the available thermal power

Conclusions and future works

The "grey zone" is investigated comparing the performance and the specific costs attainable with water in subcritical Rankine cycles and organic fluids. A cement industry is selected as reference case and three different sizes are investigated between 20 and 100 MW_{th}. A supercritical cycle with acetone is the best solution independently of the size of the plant but many other fluids in a relatively large range of critical temperatures can attain good performance with supercritical (low critical temperature fluids) and subcritical (high critical temperature fluids) cycles. For big size plants, water shows a specific cost approximately 23% higher than acetone but it is competitive with non-flammable organic fluids. For small plants, the difficulties related to turbine size lead to a higher penalization for water than for organic fluids, discouraging the use of steam Rankine cycles for available thermal output lower than 100 MW_{th} or net electrical power lower than 15 MW_{el}. Nevertheless, the use of ORC might be preferable even for bigger sizes if other aspects like the compactness of the turbine and the simplicity of operation are considered relevant factors in the selection of the technology. Finally, it is interesting to underline that usually ORCs are designed with a HTF loop between the hot gas and the working fluid leading to a higher cost of the ORC (because of the additional heat exchanger) and a lower efficiency (due to lower maximum temperature). In this case the steam Rankine cycle can be more competitive even at lower available thermal powers.

Future works will be focused on the investigation of different thermal levels of the heat source representative of others WHR applications like heat recovery from iron and steel industry. The use of two pressure levels cycles will be considered as well.

“That’s all folks!”

Porky Pig

10 Conclusions and future developments

Conclusions

This thesis work is focused on ORC power systems and, for a number of reasons, it contributes to enhance the knowledge about this technology. Various innovative aspects are analyzed with the aim of carrying out techno-economic optimizations which are rarely considered in the available scientific literature.

The core of the study is the definition of a general, comprehensive and innovative approach for the systematic optimization of ORC for any kind of applications. A software called ORCO (Organic Rankine Cycle Optimization) has been implemented in order to handle the complexity of the selected methodology. In fact, no commercial software is nowadays ready to perform this kind of analysis which requires a high flexibility in both cycle configuration selection and availability of working fluids plus reliable models for the estimation of key component performance and cost.

As a general conclusion, for any heat source and for any application, an optimal fluid, or at least a limited number of promising working fluids, can be selected on the basis of their critical temperature. The selection criteria changes from application to application, depending on the maximum temperature of the hot fluid, the plant size and the specific cost of the equipment. A preliminary analysis is always strongly encouraged in order to identify a limited number of suitable combinations of working fluid and cycle configuration. Nevertheless, this analysis has to be able to catch all the features which characterize a ORC power systems and the comparison between different solutions should be done only after their optimization. Assumptions commonly adopted, like a constant expansion isentropic efficiency, might lead to misleading results when different working fluids are used in similar conditions and when positive displacement expanders are adopted instead of axial flow turbines. On the other hand, the comparison of solutions, which are not fully optimized from a techno-economic point of view, leads to inaccurate conclusions.

The main innovative aspects of the proposed methodology can be summarized as:

- *Flexibility*: the proposed approach can be applied to any application since a large number of fluids can be used, several cycle configurations can be investigated and any solution can be optimized by a referenced algorithm acting on a relevant number of design parameters;

- *Reliability*: Refprop is used for the evaluation of working fluid properties ensuring the accuracy of the thermodynamic results. Furthermore, the expander component is studied in detail with the aim to link its performance to the characteristics of the fluid and to the cycle parameters. Do not consider this dependency often leads to misleading results considering plants which require unfeasible or extremely expensive components. The study has been focused on axial flow turbines and screw expanders and, for both of them, an innovative correlation of efficiency is proposed entailing the possibility, for the very first time, to consider the effects of number of stages, volume ratio and radial dimension on axial flow turbine performance and the effect of size and volume ratio for screw expanders. The overtaking of a fixed efficiency assumption is a great step forward and it allows achieving more realistic results.
- *Economic evaluation*: a cost correlation for each component of an ORC power system is proposed leading to the possibility to perform techno-economic optimizations. For most of the component, the bibliographic references are mixed together in order to define a general correlation. For the axial flow turbines and the HRSG unit, instead, a more complex procedure has been required due to the lack of direct information on these components. To the best of author knowledge no other examples in scientific literature are based on a similar approach with an equivalent level of detail

The methodology is hence validated on four very different test cases leading to interesting and general results which are reported in detail in Chapter 9 and briefly summarized below:

- Supercritical cycles can reach the highest efficiency and the lowest specific cost of electricity compared to other cycle configurations. They are the most suitable option for many different applications, especially when the heat source is characterized by a large temperature variation. The optimal working fluid is selected depending on the thermal level of the energy source but general considerations can be addressed reporting the results in terms of reduced temperature;
- The use of mixtures is extremely advantageous for biomass fired CHP plants, and more in general for those applications where the temperature glide in phase transition can be efficiently exploited in both evaporation and condensation. The higher cost of equipment is balanced by a larger power production leading to a lower LCOE;

- The use of volumetric expanders is interesting for small power application and the use of flash trilateral cycles is a promising solution for small direct thermal solar power plants in rural context;
- ORCs can compete with steam Rankine cycles in a large range of applications. For WHR from cement industry, various organic fluids can perform better than water leading to a reduction of the cost of electricity, even for large available thermal powers thanks to a better matching with the heat source and a more economical turbine.

Future developments

From the analysis of the obtained results many other features and aspects which would require more attention can be addressed. They should be object of future investigation and they will be implemented into the ORCO tool in order to realize an exhaustive methodology able to provide more detailed results.

- *Multi-objective optimization*: small changes in the methodology and the code are required to handle multi-objective optimization. The general approach could be applied to the optimization of automotive on-board applications or WHR ORC installed on ships since in these cases also the volume and the weight of the ORC are parameters to be carefully considered;
- *Heat exchangers design*: the integration of the code with simplified routines will allow achieving a higher level of detail removing some fixed assumptions at the basis of the present approach. Pressure drops and heat transfer coefficients won't be consider constant anymore and they will be linked to fluid properties leading to a differentiation between fluid having a similar thermodynamic behavior but different transport and physical properties. Main issues of this step are related to the large increase of the optimization variables and a problem which is intrinsically more difficult to be solved. Another problem concerns the availability of fluid properties: other database like Coolprop [262] can be integrated in ORCO tool in order to increase the number of available working fluids, to enhance the accuracy of the property estimation methods and to reduce the computational time;
- *Fluid cost*: in order to account for the fluid cost, information about the volume of the plant is required entailing a preliminary design of heat exchangers. Furthermore, a sufficient large database of cost for commercial fluids and for hazard protections and anti-fire systems is needed;

- *Expanders*: the review on positive displacement expanders should be extended to other devices, namely scroll and piston machines. The goal should be to realize semi-deterministic models for different devices with the aim of evaluating the performances of new expanders on the basis of the knowledge derived from numerical models calibrated on experimental activities. Radial inflow centripetal turbine should be considered as well;
- *New fields*: New fields of application can be investigated with the systematic methodology proposed in this thesis, like high temperature WHR and civil and domestic cogeneration;
- *Off-design*: This aspect is of particular interest for small solar systems without thermal energy storage and for automotive ORC. The introduction of the off-design simulation in the optimization of the plant will lead to the identification of those configurations able to guarantee better performances for one year, or one cycle, of operation and not only in nominal condition.

11 Nomenclature

Acronymis

BOP	Balance Of Plant
BS	Bottom Streams
CAC	Charge Air Cooler
CCVT	Closed Cycle Vapor Turbogenerator
CFC	Complete Flashing Cycle
CFC	Chloro Fluoro Carbons
CHP	Combined Heat and Power
COP	Coefficient of Performance
Cs	Specif Cost, USD/kW_{el}
DoF	Degree of Freedom
DSG	Direct Steam Generator
EGR	Exhaust Gas Recirculation
EoS	Equation of State
EPC	Engineering, Procurement and Construction
FC	Fluoro Carbons
GWP	Global Warming Potential index
HCFC	Hydro Chloro Fluoro Carbons
HFC	Hydro-Fluoro Carbons
HP	High Pressure
HRSG	Heat Recovery Steam Generator
HS	Heat Source
HTF	Heat Transfert Fluid
HVAC	Heating, Ventilation and Air Conditioning
ICE	Internal Combustion Engine
IRR	Internal Rate of Return
LB	Lower bound
LCOE	Levelized Cost of Electricity, USD/MWh or USD/kWh
LP	Low Pressure
MS	Medium Stream
NPV	Net Present Value
ODP	Ozone Depletion Potential index
OLS	Ordinary Least Square
ORC	Organic Rankine Cycles
ORCO	ORC Optimization tool
OTEC	Ocean Thermal Energy Conversion
PB	Power Block
PHE	Primary Heat Exchanger
R&D	Research and Development

RPM	Rotation Per Minute
S&T	Shell and Tube heat exchanger
SoS	Speed of Sound, m/s
TS	Top Stream
UB	Upper bound
UDC	User Defined Component
USD	United States Dollar
VLE	Vapor Liquid Equilibrium
WHR	Waste Heat Recovery

Nomenclature

A	Heat exchanger surface, m^2
C	cost, USD
Cp	constant pressure heat capacity, kJ/kgK
Cv	constant volume heat capacity, kJ/kgK
D	Diameter, m
h	specific enthalpy, kJ/kg or film transfer coefficient, W/m^2K
k	stage load coefficient
MM	Molar Mass
Ns	Stage Specific speed, rotation
p	pressure, bar
Q	Thermal Power, kW or MW
R	ideal gas constant, kJ/kmolK
rec/ no-rec	recuperative/ non recuperative cycle configuration
s	specific entropy, kJ/kgK
SA	Saturated or slightly superheated cycle
SH	Superheated cycle
SP	Stage size parameter, m
Sub	Subcritical cycle
Sup	Supercritical cycle
T	temperature, °C
u	fluid velocity in heat exchangers, m/s
U	global heat transfer coefficient, kW/(m2K)
V	volume flow rate, m^3/s
W	power, kW or MW
Z	Compressibility Factor
β	pressure ratio
ε	positive displacement device efficiency
η	efficiency
ν	specific volume, m^3/kg
π	positive displacement device volume ratio
ρ	Density, kg/m^3
σ	complexity index

Subscripts

0	reference condition for cost correlations
amb	ambient conditions
ap	approach point
c	upper Carnot temperature
ca	cooling air
cond	condensation (condition) or condenser (plant component)
crit	critical condition
cw	cooling water
des	desuperheating section of condenser (plant component)
eco	economizer (plant component)
el	electrical
eva	evaporation (conditions) or evaporator (plant component)
exp	expansion
geo	geothermal brine
ha	hot air from WHR
II	second law
in	inlet condition
is	isentropic process
l	lorentz (efficiency)
lim	limit in reinjection condition
loss	dispersion to the environment
m	mean stage diameter
mec	mecanical
mln	mean logaritmic
PHE	Primary Heat Exchanger
pp	pinch point
Pr. Lev.	Pressure Level (for subcritical cycles)
r	ratio
rec	recovery (efficiency) or regenerator (plant component)
ref	reference condition
reinj	reinjection conditions
sc	sub cooling
scroll-exp	scrool expander
sh	superheater (plant component)
SHE	superctical PHE
th	thermal
val	valve at turbine inlet (plant component)
wf	working fluid

12 References

1. **Astolfi, M., Romano, C.M., Bombarda, P., Macchi, E.** *Binary Orc Power Plants For The Exploitation Of Medium-Low Temperature Geothermal Sources – Part A Thermodynamic Optimization.* : Energy, 2014.

2. **Astolfi, M., Romano, M., Bombarda, P., Macchi, E.** *Binary Orc Power Plants For The Exploitation Of Medium-Low Temperature Geothermal Sources. Part B Techno-Economic Optimization.* s.l. : Energy, 2014.

3. **Astolfi, M., Lasala, S., Macchi, E.** *Comparison between the use of pure fluids and mixtures for the exploitation of variable temperature heat sources.* Rotterdam : 2st International Seminar in ORC power systems, 2013.

4. **Xodo, G. L., Spadacini, C., Astolfi, M., Macchi, E.** *Comparison Of Axial And Radial Outflow Turbines In A Medium-High Enthalpy Waste Heat Recovery Orc Application.* Rotterdam : s.n., 2013.

5. **Spadacini, C., Centemeri, L., Xodo, G. L., Astolfi, M.** *A new configuration for Organic Rankine Cycle power systems.* Delf : 1st International Seminar on ORC Power Systems, 2011.

6. **Macchi, E.** *The Choice Of Working Fluid: The Most Important Step For A Successful Organic Rankine Cycle (And An Efficient Turbine).* Rotterdam : 2nd International Seminar in ORC Power Systems, 2013.

7. —. *Design criteria for turbines operating with fluids having a low speed of sound.* Closed cycle gas turbines, lecture series 100, s.l. : Von Karman Institute for Fluid-dynamics, 1977.

8. **Chen, H., Goswami, D.T., Stefanakos, E.K.** *A review of thermodynamic cycles and working fluids for the conversion of low-grade heat.* : Renewable and Sustainable Energy Reviews, 2010. Vol. 14.

9. **Invernizzi, C., Iora, P., Silva, P.** *Bottoming micro-Rankine cycles for micro-gas turbines.* s.l. : Applied Thermal Engineering, 2007. pp. 100-110. Vol. 27.

10. **Dai, Y., Wang, J.,Gao, L.** *Parametric Optimization and Comparative Study of Organic Rankine Cycle (ORC) for Low Grade Waste Heat Recovery.* : Energy Conversion and Management, 2009. pp. 576–582. Vol. 50.

11. **Lakew, A., Bolland, O.** *Working fluids for low-temperature heat source.* : Applied Thermal Engineering, 2010. pp. 1262-1268. Vol. 30.

12. **Quoilin, S., Declaye, S., Tchanche, B.F., Lemort, V.** *Thermo-economic optimization of waste heat recovery Organic Rankine Cycles.* : Applied Thermal Engineering, 2011. pp. 2885-2893. Vol. 31.

13. **Drescher, U., Brüggemann, D.** *Fluid selection for the Organic Rankine Cycle (ORC) in biomass power and heat plants.* : Applied Thermal Engineering, 2007. Vol. 27.

14. **Tchanche, B. F., Lambrinos, G., Frangoudakis, A., Papadakis, G.** *Low-grade heat conversion into power using organic rankine cycles - A review of various applications.* : Renewable and Sustainable Energy Reviews, 2009. pp. 3963-397. Vol. 15.

15. **Rayegan, R., Tao, Y. X.,.** *A Procedure to Select Working Fluids for Solar Organic Rankine Cycles (ORCs).* s.l. : Renewable Energy, 2011. Vol. 36.

16. **Quoilin, S., Orosz, M., Hemond, H., Lemort, V.** *Performance and Design optimization of a low-cost solar organic Rankine cycle.* : Solar Energy, 2011. pp. 955-966. Vol. 85.

17. **Invernizzi, C., Bombarda, P.** *Thermodynamic Performance of Selected HCFs for Geothermal Applications.* s.l. : Energy, 1997. pp. 887-895. Vol. 22.

18. **Hettiarachchi, H.D.M., Golubovic, M., Worek, W.M., Ikegam,i Y.** *Optimum design criteria for an Organic Rankine cycle usig low-temperature geothermal heat sources.* s.l. : Energy, 2007. pp. 1698-1706. Vol. 32.

19. **Saleh, B., Koglbauer, G., Wendland, M., Fischer, J.** *Working fluids for low-temperature organic Rankine cycles.* : Applied Thermal Engineering, 2011. Vol. 31.

20. **Shengjun, Z., Huaixin, W., Tao, G.** *Performance comparison and parametric optimization of subcritical Organic Rankine Cycle (ORC) and transcritical power cycle system for low-temperature geothermal power generation.* : Applied Energy, 2011. Vol. 88.

21. **Guo, T., Wang, H.X.** *Fluids and parameters optimization for a novel cogeneration system driven by low-temperature geothermal sources.* s.l. : Energy, 2011. Vol. 36.

22. **Zhang, F. Z., Jiang, P. X.** *Thermodynamic analysis of a binary power cycle for different EGS geofluid temperatures.* : Applied Thermal Engineering, 2012. pp. 476-485. Vol. 48.

23. **Walraven, D., Laenen, B., D'haeseleer, W.** *Comparison of thermodynamic cycles for power production from low-temperature geothermal heat sources.* : Energy Conversion and Management, 2012.

24. **Astolfi, M., Xodo, L., Romano, M.C., Macchi, E.** *Technical and economical analysis of a solar–geothermal hybrid plant based on an Organic Rankine Cycle.* : Geothermics, 2011. Vol. 40.

25. **Karellas, S., Schuster, A.** *Supercritical Fluid Parameters in Organic Rankine Cycle Applications.* : Int. J. of Thermodynamics, 2008. Vol. 11.

26. **Guo, T., Wang, H., Zhang, S.** *Comparative analysis of natural and conventional working fluids for use in transcritical Rankine cycle using low-temperature geothermal source.* : International Journal of Energy Research, 2011. Vol. 35.

27. **Preißinger, M., Heberle, F., Brüggemann, D.** *Thermodynamic analysis of double-stage biomass fired organic rankine cycle for micro-cogeneration. International Journal of Energy Research.* : s.n., 2012. Vol. 36.

28. **Borsukiewicz, G. A., Nowak, W.** *Comparative analysis of natural and synthetic refrigerants in application to low temperature Clausius–Rankine cycle.* : Energy, 2007. Vol. 32.

29. **Chen, H., Goswami, D.Y., Rahman, M.M., Stefanakos, E.K.** *A supercritical Rankine cycle using zeotropic mixture working fluids for the conversion of low-grade heat into power.* : Energy, 2011. Vol. 36.

30. **Papadopoulos, A.I., Stijepovic, M.Z., Linke, P.** *On the Systematic Design and Selection of Optimal Working Fluids for Organic Rankine Cycles.* : Applied Thermal Engineering, 2010. Vol. 30.

31. **Biegler, L. T., Grossmann, I. E., Westerberg, A. W.,.** *Systematic Methods of Chemical Process Design.* : Prentice Hall, 1997.

32. **Hattiangadi, A.** *Working Fluid Design for Organic Rankine Cycle (ORC) Systems.* TUDelft. 2013. Thesis.

33. **Lampe, M., Stavrou, M., Gross, J., Bardow, A.** *Integrated Process And Working Fluid Optimization For Organic Rankine Cycle (Orc) Using Pc-Saft.* Rotterdam : 2nd Internationa Seminar on ORC Power Systems, 2013.

34. **Papadopoulos, A., Linke, C., Stijepovic, M., Seferlis, P., Voutetakis, S.** *Computer-Aided Design And Selection Of Optimum Working Fluids And Orc Systems For Power Generation From Low Enthalpy Heat Sources.* Delft : 1st Internationa Seminar in ORC power systems, 2011.

35. **Pierobon, L., Nguyen, T-V., Larsen, U., Haglind, F., Elmegaard, B.** *Multi-objective optimization of organic Rankine cycles for waste heat recovery: Application in an offshore platform.* : Energy, 2013. pp. 538-549. Vol. 58.

36. **Kuppan, T.** *Heat exchanger design handbook.* : Marcel Dekker Inc, 2000.

37. **Shah, R.K., Sekulic, D. P.** Chapter 17 - Heat exchangers. [book auth.] Hartnett J.P., Cho Y.I. Rohsenow W.M. *Handbook of Heat Transfer.* New York : McGraw-Hill, 1998.

38. **Schuster, A., Karellas, S., Aumann, R.** *Efficiency optimization potential in supercritical Organic Rankine Cycles.* : Energy, 2010. pp. 1033-1039. Vol. 35.

39. Modelica. [Online] www.modelica.org.

40. Dymola. [Online] www.dymola.com.

41. Thermo Power. [Online] www.thermopower.sourceforge.net.

42. AspenPlus. [Online] www.aspentech.org.

43. Thermoflex. [Online] www.thermoflex.com.

44. **Giostri, A., Binotti, M., Silva, P., Macchi, E., Manzolini, G.** *Comparison of two linear collectors in solar thermal plants: Parabolic trough versus Fresnel.* : Journal of Solar Energy Engineering, Transactions of the ASME, 2013. Vol. 135.

45. **The MathWorks, Inc.** *MATLAB version 8.1.0.604.* Natick : s.n., 2013.

46. **Gaia, M.** *30 Years of Organic Rankine Cycle Development.* Delft : 1st International seminar on ORC power systems, 2011.

47. Ormat. [Online] www.ormat.com.

48. Turboden. [Online] www.turboden.eu.

49. Exergy. [Online] www.exergy-orc.com.

50. ElectraTherm. [Online] electratherm.com.

51. Tri-O-Gen. [Online] www.triogen.nl.

52. TAS. [Online] www.tas.com.

53. Adoratec. [Online] www.adoratec.com.

54. Maxxtec. [Online] en.maxxtec.net.

55. GMK. [Online] www.gmk.info.

56. Atlas Copco. [Online] www.atlascopco.com.

57. Cryostar. [Online] www.cryostar.com.

58. **Calnetix.** [Online] www.calnetix.com.

59. Infinity Turbines. [Online] www.infinityturbine.com.

60. Verdicorp. [Online] www.verdicorp.com.

61. Durr. [Online] www.durr-cyplan.com.

62. Cogen. [Online] www.cogenmicro.com.

63. EnefTech. [Online] www.eneftech.com.

64. Flow Energy. [Online] www.flowenergy.uk.com.

65. **Saadatfar, B., Fakhrai, R., Fransson, T.** *Waste heat recovery Organic Rankine cycles in sustainable energy conversion: A state-of-the-art review.* : The Journal of MacroTrends in Energy and Sustainability, 2013. Vol. 1.

66. **Bonalumi, D., Astolfi, M., Roberto, R., Caldera, M., Romano, M. C., Turi, D. M., Silva, P., Giuffrida, A., Invernizzi, C., Macchi, E.** *High efficiency ORC for high temperature molten salt boiler for biomass applications.* Rotterdam : ASME-ORC, 2013.

67. **Bini R., Viscuso F.** *High efficiency (25%) ORC for power only generation mode in the range 1-3 MW: an already proven technology also available for partially cogenerative applications.* Delft : First international Seminar on ORC Power Systems, 2011.

68. **Báscones, E.** *Small scale biomass combustion plant for power generation: From waste wood to profit.* : European Biomass Conference and Exhibition Proceedings, 2011.

69. **De Ruyck, J., Bram, S., Delattin, F.** *Co-utilization of biomass and natural gas in combined cycles through primary steam reforming of the natural gas.* : Energy, 2007. Vol. 32.

70. **Rentizelas, A., Tatsiopoulos, I., Kakaras, E., Karellas, S.** *Comparative techno-economic analysis of ORC and gasification for bioenergy applications.* : Energy Convers Management, 2009.

71. **Obernberger, I., Thek., G.** *Combustion and gasificationof solid biomass for heat and power production in europe - state of the art- and relevant future developments.* Vilamoura Portugal : 8th European Conference on Industrial Furnaces and Boilers, 2008.

72. **Bombarda P., Macchi E.** *Optimum cycles for geothermal power plants.* Kyushu - Tohoku Japan : World Geothermal Congress., 2000.

73. **Campos Rodríguez, C.E., Escobar Palacio, J.C., Venturini, O.J., Lofrano Dotto, F.R., Gialluca, V.** *Exergetic and economic comparison of ORC and Kalina cycle for low*

temperature enhanced geothermal system in Brazil. : Applied Thermal Engineering, 2013. Vol. 52.

74. **Zhang, F.-Z., Jiang, P.-X.** *Thermodynamic analysis of a binary power cycle for different EGS geofluid temperatures.* : Applied Thermal Engineering, 2012. Vol. 48.

75. **Karellas, S. , Leontaritis, A.-D., Panousis, G., Bellos, E., Kakaras, E.** *Energetic and exergetic analysis of waste heat recovery systems in the cement industry.* : Energy, 2013. Vol. 58.

76. **Ari, V.** *Energetic and exergetic assessments of a cement rotary kiln system.* : Scientific Research Essays, 2011. Vol. 6.

77. **Amiri, A , Vaseghi, M.R.** *Waste heat recovery power generation systems for cement production process.* : Cement Industry Technical Conference (CIC) IEEE-IAS/PCA , 2013.

78. **Johansson, M.T., Soderstrom, M.** *Electricity generation from low-temperature industrial.* s.l. : Springer Science, 2013.

79. **Campana, F., Bianchi, M., Branchini, L., De Pascale, A., Peretto, A., Baresi, AF.** *ORC waste heat recovery in European energy intensive industries: Energy and GHG savings.* : Energy Convers Manag., 2013.

80. Ingeco. [Online] www.ingecoweb.com.

81. **Zhao, P., Wang, J., Gao, L., Dai, Y.** *Parametric analysis of a hybrid power system using organic Rankine cycle to recover waste heat from proton exchange membrane fuel cell.* : International Journal Hydrogen Energy, 2012. Vol. 37.

82. **Gao, X., Li, L., Zhao, Y., Shu, P.** *Research on a Scroll Expander Used for Recovering Work in a Fuel Cell.* s.l. : Internationa Lournal of Thermodynamics, 2004. Vol. 7.

83. **Al-sulaiman, FA., Dincer, I., Hamdullahpur, F.** *Energy analysis of a trigeneration plant based on solid oxide fuel cell and organic Rankine cycle.* : Intenational Journal Hydrogen Energy, 2010. Vol. 35.

84. **Rokni, M.** *Thermodynamic analysis of an integrated solid oxide fuel cell cycle with a rankine cycle.* : Energy Conversion Management, 2010. Vol. 51.

85. **Siemens, AG.** *Concentrated solar power technology for sustainable power generation.* Nuremberg, 2010.

86. **Hans, Muller-Steinhagen.** *Concentrating solar power: A review of the technology.* Stutgart, 2004.

87. **Giostri, A., Binotti, M., Astolfi, M., Silva, P., Macchi, E., Manzolini, G.** *Comparison of different solar plants based on parabolic trough technology.* s.l. : Solar Energy, 2012. Vol. 86.

88. STG International. [Online] www.stginternational.com.

89. **Casati, E., Galli, A., Colonna, P.** *Thermal energy storage for solar-powered organic Rankine cycle engines.* s.l. : Solar Energy, 2013. Vol. 96.

90. **Kane, M.** *Small hybrid solar power system.* s.l. : Energy, 2008. Vol. 28.

91. **Wang, X.D., Zhao, L., Wang, J.L., Zhang, W.Z., Zhao, X.Z., Wu, W.** *Performance evaluation of a low-temperature solar Rankine cycle system utilizing R245fa.* : Solar Energy, 2010.

92. **Wang, J., Wang, M., Zhao, P., Zhao, Y., Dai, Y.** *Thermodynamic analysis and optimization of a solar-driven regenerative organic Rankine cycle (ORC) based on flat-plate solar collectors.* : Applied Thermal Energy, 2013. Vol. 50.

93. **Jing, L., Gang, P., Jie, J.** *Optimization of low temperature solar thermal electric generation with Organic Rankine Cycle in different areas.* : Applied Energy, . Vol. 2010.

94. Whispergen. [Online] www.whispergen-europe.com.

95. Baxi. [Online] www.baxi.it.

96. **Teng, H., Regner, G., Cowland, C.** *Waste Heat Recovery from Heavy Duty Diesel Engines by Organic Rankine Cycle. Part I: Hybrid Energy Systems of Diesel and Rankine Engines.* : SAE Technical Papers, 2007.

97. **Delgado-Torres, A.M., García-Rodríguez, L.** *Comparison of solar technologies for driving a desalination system by means of an organic Rankine cycle.* s.l. : Desalination, 2007. Vol. 216.

98. **García-Rodríguez, L., Delgado-Torres, A. M.** *Solar-powered Rankine cycles for fresh water production.* s.l. : Desalination, 2007. Vol. 212.

99. **Bombarda, P., Invernizzi, C., Gaia, M.** *Performance analysis of OTEC plants with multilevel organic rankine cycle and solar hybridization.* : Journal of Engineering for Gas Turbines and Power, 2013. Vol. 135.

100. **Sun, F., Ikegami, Y., Ji, B., Arim, H.** *Optimization design and exergy analysis of organic rankine cycle in ocean thermal energy conversion.* : Applied Ocean Research, 2012. Vol. 35.

101. OTEC news. [Online] www.otecnews.org.

102. **Wikipedia.** *The Free Encyclopedia.* : Wikimedia Foundation, 2014.

103. **Agency, US. Environmental Protection.** *Ozone Layer Protection - Science.* : www.epa.gov, 2014.

104. Honeywell. [Online] www.honeywell.com.

105. **Invernizzi, C., Angelino, G.** *Experimental investigation on the thermal stability of some new zero ODP refrigerants.* : International Journal of Refrigeration, 2003. pp. 51-58. Vol. 26.

106. **Lemmon, E.W., Huber, M.L., McLinden, M.O.** *NIST Standard Reference Database 23: Reference Fluid Thermodynamic and Transport Properties-REFPROP: Version 9.1.* s.l. : National Institute of Standards and Technology, Standard Reference Data Program, 2013.

107. **Kouremenos, D. A., Antonopoulos, K. A.** *Isentropic exponents of real gases and application for the air at temperatures from 150 K to 450 K.* : Acta Mechanica, 1987. pp. 81-99. Vol. 65.

108. **Chang, K.C., Baik, Y.J., Lee, Y.S., Yoon, H.K., Kim, M.** *Power enhancement potential of a mixture transcritical cycle for a low-temperature geothermal power generation.* : Energy, 2012. Vol. 47.

109. **Brüggemann, D., Heberle, F., Preißinger, M.** *Zeotropic mixtures as working fluids in Organic Rankine Cycles for low-enthalpy geothermal resources.* : Renewable Energy, 2012. Vol. 37.

110. **Colonna, P., Angelino, G.** *Multicomponent Working Fluids For Organic Rankine Cycles (ORCs).* : Energy, 1998. Vol. 23.

111. **Bivens, D. B. and Yokozeki, A.** *Heat Transfer of Refrigerant Mixtures.* Purdue, 1992.

112. **Gu, J., Bart, H-J.** *Decrement Estimation of the Heat Transfer Coefficient in Mixture Boiling.* s.l. : The Canadian Journal Of Chemical Engineering, 1999. Vol. 77.

113. **Di Pippo, R.** *Ideal thermal efficiency for geothermal binary plants.* s.l. : Geothermics, 2007. pp. 276–285. Vol. 36.

114. **Astolfi, M., Bini, R., Macchi, E., Paci, M., Pietra, C., Rossi, N., Tizzanini, A.** *Testing Of A New Supercritical Orc Technology For Efficient Power Generation From Geothermal Low Temperature Resources.* Rotterdam : 2nd International Seminar in ORC power systems, 2013.

115. **Smith, I.K.,.** *Development of the trilateral flash cycle system Part 1 : fundamental considerations.* : Proceedings of the Institution of Mechanical Engineers Part A: Journal of Power and Energy, 1993.

116. **Smith, I.K.** *Development of the trilateral flash cycle system Part 2 : increasing power output with working fluid mixtures.* : Proceedings of the Institution of Mechanical Engineers, Part A: Journal of Power and Energy, 1194.

117. **Smith, I.K, Stosic, N., Kovacevic, A.** *An Improved System for Power Recovery from Higher Enthalpy Liquid-Dominated Fields.* s.l. : Proceedings World Geothermal Congress.

118. **Herrmann, U., Geyer, M., Kearney, D.** *Overview on Thermal Storage Systems.* s.l. : FLABEG Solar Int. GmbH, 2002. Workshop on Thermal Storage for Trough Power Systems.

119. **Smith, M.H.** *A simple correlation of turbine effciency.* : Journal of Royal Aeronautical Society, 1965. p. 467. Vol. 69.

120. **Baljè, O.E., Binsley, R.L.** *Axial turbine performace evaluation: part B - optimization with and without constraints.* : ASME Journal of Engineering for Power. pp. 349-360.

121. **Macchi, E., Perdichizzi, A.** *Efficiency prediction for axial flow turbines operating with non-conventional fluids.* s.l. : ASME, 1981.

122. **Lozza, G., Macchi, E., Perdichizzi, A.** *On the influence of the number of stages on the effciency of axial flow turbines.* : ASME, 1981. Vols. paper 82-GT-43.

123. **Craig, H.R.M., Cox, H.J.A.** *Performance estimation of axial flow turbines.* : Proceedings of the institution of mechanical engineers. pp. 407-423. Vol. 185 32/71.

124. **Kacker, S.C., Okapuu, U.** *A mean line prediction method for axial flow turbine performance prediction.* s.l. : ASME paper 81-GT-58, 1981.

125. **Traupel, M.H.** *Thermische Turbomaschinen.* 1977. ISBN 3-540-07939-4.

126. **Ainley, D.C., Mathieson, G.C.R.** *A method of performance estimation for axial-flow turbines.* : British Aeronautical Research Council, 1951. Vol. R&M 2974.

127. **Vavra, M.H.** *Axial flow turbines.* Brussels : Von Karman Institute for Fluid-dynamics, 1969. Vol. Lecture series 15.

128. **Deich, M.E., Filippov, G.A., Lazarev, L.Y.** *Atlas of axial turbine blade characteristics.* Moscow : Maschinostromie Publishing House, 1965.

129. **Lemmon, E.W., Huber, M.L., McLinden, M.O.** *NIST Standard Reference Database 23: Reference Fluid Thermodynamic and Transport Properties-REFPROP, Version 9.1* . National Institute of Standards and Technology, Standard Reference Data Program, Gaithersburg : 2013.

130. **Dixon, S. L., Eng., B.** *Fluid Mechanics, Thermodynamics of urbomachinery, Fifth Edition.* s.l. : Eselvier, 1998.

131. Gretl. [Online] ww.gretl.sourceforge.net/.

132. **Spadacini, C., Rizzi, D., Saccilotto, C., Salgarollo, S., Centemeri, L.** *The Radial Outflow Turbine Technology: Impact On The Cycle Thermodynamics And Machinery Fluid- And Rotordynamic Features.* Rotterdam : 2st International Seminar on ORC Power Systems, 2013.

133. **Pini, M., Persico, G., Casati, E., Dossena, V.** *Preliminary design of a centrifugal turbine for ORC applications.* Delft : 1st International Seminar on ORC power systems, 2011.

134. **Persico, G., Pini, M., Dossena, V., Gaetani, P.** *Aerodynamics of centrifugal turbine cascades.* Rotterdam : 2nd International Seminar in ORC Power Systems, 2013.

135. **Momoda, K.** *Measurement of the volumetric properties for Perfluoro-2-methylpentane in the range ot temperature 333 to 473K up to 5.7MPa.* : Berichte der Bunsengesellschaft für physikalische Chemie, 1984. pp. 1007-1010. Vol. 8.

136. **Kaneko, T., Hirayama, N.** *Study on Fundamental Performances of Helical Screw Expander.* s.l. : Bulletin of JSME, 1985. Vol. 28.

137. **Declaye, S., Quolin, V., Guillaume, L., Lemort, L.** *Experimental study on an open-drive scroll expander integrated into an ORC (Organic Rankine Cycle) system with R245fa as working fluid.* : Energy, 2013. pp. 173–183. Vol. 55.

138. **Ng, K.C., Bong, T.Y., Lim, T.B.** *A Thermodynamic model for the analysis of screw expander performance.* : Heat Reovery Systems & CHP, 1990. pp. 119-133. Vol. 10.

139. **Zanelli, R., Favrat, D.** *Experimental Investigation of a Hermetic Scroll Expander-Generator.* Purdue : International Compressor Engineering Conference, 1994.

140. **Kohsokabe, H., Koyama, M., Tojo, K., Matsunaga, M., Nakayama, S.** *Performance Characteristics of Scroll Expander for CO2 Refrigeration Cycles.* Purdue : International Compressor Engineering Conference, 2008.

141. **Wang, H., Peterson, R. B., Herron, T.** *Experimental performance of a compliant scroll expander for an organic Rankine cycle.* : s.n., 2009.

142. Atlas Copco. [Online] www.atlascopco.com.

143. Bitzer. [Online] www.bitzer.it.

144. Frascold. [Online] www.frascold.it.

145. Chicago Pneumatics. [Online] www.cp.com.

146. Sabre. [Online] www.sabre.com.

147. Man Compressors. [Online] www.mandieselturbo.com.

148. **Lemort, V., Guillaume, L., Legros, D., Declaye, S., Quoilin, S.** *A comparison of piston, screw and scroll expanders for small scale Rankine cycle systems.* : 3rd International Conference on Microgeneration and Related Technologies, 2013. http://hdl.handle.net/2268/147369.

149. **Orosz, S.M., Mueller, V.A., Dechesne, J.B., Hemond, F.H.** *Geometric Design of Scroll Expanders Optimized for Small Organic Rankine Cycles.* : Journal of Engineering for Gas Turbines and Power, 2013. Vol. 135.

150. **Platell, P.** *Displacement expanders for small scale cogeneration.* KTH. 1993. Thesis.

151. **Stosic, N., Smith, I. K., Kovacevic, A., Mujic, E.** *three decades of modern practice in screw compressors.* s.l. : Internationa Compressor Enineering conference, 2010.

152. **Quoilin, S., Declaye, S., Legros, A., Guillaume, L., Lemort, V.** *Working fluid selection and operating maps for Organic Rankine Cycle expansion machines.* Purdue : International Compressor Engineering Conference, 2012.

153. **Brummer, A.** Energy efficiency – waste heat utilization with screw expanders. *Pumps, Compressors and Process Components.* 2012.

154. **Clemente, S., Micheli, D., Reini, M., Taccani, R.,.** *Numerical Model and Performance Analysis of a Scroll Machine for ORC Applications.* s.l. : Proceedings of ECOS2010, 2010.

155. **Stoecker, W. F.** Chapter 5 - Screw compressors. *INDUSTRIAL REFRIGERATION HANDBOOK.* s.l. : McGraw Hill.

156. **Lemort, V., Teodorese, I.V., Lebrun, J.** *Experimental Study of the Integration of aScroll Expander into a Heat RecoveryRankine Cycle.* Purdue : 18th InternationalCompressor Engineering Conference, 2006.

157. **Peng, N., Deng, D., Xing, Z., Shu, P.** *New Rotor Profile and its Performance Prediction of Screw Compressors.* Purdue : International Compressor Engineering Conference, 1990.

158. **Hirai, T., Noda, S., Sagara, Y., Tsuzi, K.** *Performance Analysis of OIF Single Screw Compressor.* Purdue : International Compressor Engineering Conference, 1986.

159. **Kovacevic, A. Stocic, N., Mujic, E., Smith, K.I.** *CFD Integrated Design of Screw Compressors.* : Engineering Applications of Computational Fluid Mechanics, 2007. pp. 96-108. Vol. 1.

160. **Stosic, N., Hanjalic, K.** *Development and Optimization of Screw Machines with a Simulation Model, Part I: Profile Generation.* : ASME Transactions, Journal of Fluids Engineering, 1997. Vol. 119.

161. **Hanjalic, K., Stocic, N.** *Development and Optimization of Screw Machines With a Simulation Model—Part II: Thermodynamic Performance Simulation and Design Optimization.* s.l. : ASME Journal of Fluids Engineering, 1997. Vol. 119.

162. Heliex Power. [Online] www.heliexpower.com.

163. ORCnext. [Online] www.orcnext.be.

164. **Wang, Z., Zhang, Y. Sun, Y., Wei, L.** *Numerical simulation and experimental study on the performance of screw expander.* : ASHRAE transactions, 2010. Vol. 116.

165. **Wennema, J.** *Dry screw compressor performance and application range.*

166. Svenska Rotor Maskiner . [Online] www.opcon.se.

167. **Stosic, N., Hanjalic, K.** *General Method for Screw Compressor Profile Generation.* : International Compressor Engineering Conference, 1996.

168. **Singh, P. J., Onuschak, A. D.** *A Comprehensive, Computerized Method for Twin-Screw Rotor Profile Generation and Analysis.* Purdue : International Compressor Engineering Conference, 1984.

169. *Some Aspects of Estimating Geometric Characteristics of Screw Compressors.* **Buckney, D., Kovacevic, A., Mujic, E., Stosic, N.** Purdue, 2012. International Compressor Engineering Conference.

170. **Singh, P. J., Bowman, J. L.** *Calculation of Blow-Hole Area for Screw.* : International Compressor Engineering Conference, 1988.

171. **Tang, Y.** *Computer Aided design of twin screw compressors.* 1995. Thesis.

172. **Litvin, F.L.** *Theory of Gearing.* s.l. : NASA, 1989.

173. **Stocic, N.** *On gearing of helical screw compressor rotors.* s.l. : Institution of Mechanical Engineers, 1998.

174. **Litvin, F.L.** *An Analysis of Undercut Conditions and of Appearance of Contact Lines Envelope Conditions of Gears.* : ASME Journal of Mechanical Design, 1978. Vol. 100.

175. **Dunbar, M.K.** *Altering the volumetric expansion ratio of a Lysholm Helical Screw Expander.* , . Thesis.

176. **Sjoholm, L.** *Variable Volume-Ratio and Capacity Control in Twin-Screw Compressors.* Purdue : International Compressor Engineering Conference, 1986.

177. **Zaytsev, D., Ferreira, C.A.I.** *Aspects of Two-Phase Flow Screw Compressor Modelling Part II: Friction Between Rotors.* Purdue : s.n., 2000.

178. —. *Aspects of Two-Phase Flow Screw Compressor Modelling Part I: Leakage Flow and Rotor Tip Friction.* Purdue : s.n., 2000.

179. **Kudo, K., Giedt, W.H.m Park, I., Kumazawa, S.** *Analytical and Experimental Investigation of Two-Phase Flow Screw Expanders for Power Generation.* : ASME - Journal of Engineering for Gas Turbines and Power, 1988. Vol. 110.

180. **Smith, K.I., Stocic, N., Aldis, C.A.** *Lysholm Machines as Two-Phase Expanders.* Purdue : International Compressor Engineering Conference, 1994.

181. **Woodland, B.J., Braun, J.E., Groll, E.A., Horton, W.T.** *Experimental Testing of an Organic Rankine Cycle with Scroll-type Expander.* Purdue : s.n., 2012.

182. **Xiaojun, G., Liansheng, L., Yuanyang, Z., Pengcheng, S.** *Research on a Scroll Expander Used for Recovering Work in a Fuel Cell.* s.l. : International Journal of Thermodynamics, 2004. Vol. 7.

183. **Aoun, B., Clodic, D.F.** *Theoretical and Experimental Study of an Oil-Free Scroll Vapor Expander.* Purdue : InternationalCompressor Engineering Conference, 2008.

184. **Dickes, R., Orosz, M., Hemond, H.** *Non-Constant Wall Thickness Scroll Expander Investigation For A Micro Solar Orc Plant.* Rotterdam : 2nd International Seminar on ORC systems, 2013.

185. **Duprez, M.E., Dumont, E., Frere, M.** *Modelling of reciprocating and scroll compressors.* : International Journal of Refrigeration, 2007. pp. 873-886. Vol. 30.

186. **Quoilin, S., Orosz, M., Lemort, V.** *Modeling and experimental investigation of an Organic Rankine Cycle using scroll expander for small scale solar applications.* : EuroSun 2008, 1st International Congress on Heating, Cooling and Buildings, 2008.

187. **Stosic, N., Smith, I.K., Kovacevic, A.** *Screw Compressors: Mathematical Modeling and Performance.* Berlin : Springer Verlag, 2005. ISBN: 3-540-24275-9.

188. **Margolis, D. L.** *Analytical modeling of Helical Screw Turbines for Performance prediction.* : ASME, 1978. pp. 482-487. Vol. 100.

189. **Bluniera, B., Cirrincione, G., Herve, Y., Miraouia, A.** *A new analytical and dynamical model of a scroll compressor with experimental validation.* 2009. pp. 874-891. Vol. 32.

190. **Fujiwara, M., Kasuya, K., Matsunaga, T., Watanabe, W.** *Computer Modeling for Performance Analysis of Rotary Screw Compressor.* Purdue : International Compressor Engineering Conference, 1984.

191. **Singh, P., Schwartz, J.** *Exact Analytical Representation of Screw Compressor Rotor Geometry.* Purdue : International Compressor Engineering Conference, 1990. pp. 925-937.

192. **Gravesen, J., Henriksen, C.** *The Geometry of the Scroll Compressor.* : Society for Industrial and Applied Mathematics, 2001. pp. 113-126. Vol. 43.

193. **Boldvig, V., Villadsen, V.** *A Balanced View of Reciprocating and Screw Compressor Efficiencies.* Purdue, 1980.

194. **Sauls, J. R.** *Performance Characteristics of Fixed Volume Ratio Compressors.* Purdue : International Compressor Engineering Conference, 1982.

195. **Mayekawa Mfg Co Ltd.** *Screw type steam engine.* Tokyo : Internal report, 1984.

196. **Steidel, R. F. , Pankow, D., lkrger, R. E.** *Performance characteristics of the Lysholm engine as tested for geothermal power application.* : International Energy Conversion Engineering Conference (IECEC), 1981. pp. 1334-1340. Vol. 16.

197. **LU-VE.** *Dry and Spray catalogue.* : LU-VE Contardo, 2013.

198. **Green, D.W.** *Perry's chemical engineers' handbook, 7th edition.* : Mc-Graw Hill, 1997.

199. **Turton, R., Bailie, R. C., Whiting, W. B., Shaeiwitz, J. A., Bhattacharyya, D.** *Analysis, Synthesis, and Design of Chemical Processes, 4th edition.* s.l. : Prentice hall, 2012.

200. CAPCOST. [Online] http://www.capcost.ca/.

201. **Guthrie, K. M.** *Process plant Estimating evaluation and control.* Solana Beach : Craftsman Book Co., 1974.

202. —. *Data and Techniques for preliminary Capital Cost Estimating.* : Chemical Engineering, 1969. Vol. 24.

203. **Ulrich, G. D.** *A guide to chemical engineering process design and economics.* New York : John Wiley and Sons, 1984.

204. **Loth, H.P., Lysons, J., White, C. W.** *Process Equipment Cost Estimation - Final Report.* s.l. : Department of Energy- United States of America, 2002.

205. **TEMA.** *9th edition TEMA standars.* s.l. : TEMA, 2007.

206. **AA., VV.** *Gas Turbine World 2013 GTW Handbook.* : Pequot, 2013. Vol. 30.

207. **DOE/NETL.** *Cost and Performance Baseline for Fossil Energy Plants Volume 1: Bituminous Coal and Natural Gas to Electricity.* : Department of Energy, 2010.

208. **Kakac, S.** *Heat Exchangers Selection, Rating and Thermal Design, 2nd edition.* s.l. : CRC press, 2002.

209. —. *Boilers, Evaporators and Condensers.* : Wiley & Sons, 1991.

210. H&C Heat Transfer Solutions Inc. [Online] www.hcheattransfer.com.

211. **ESDU92013.** *Selection and Costing of heat exchangers.* : IHS, 1192.

212. **Span, R.** *Multiparameter Equation of State. An Accurate Source of Thermodynamic Property Data.* s.l. : Springer, 2000.

213. **Span, R., Wagner, W.** *Equation of State for Thecnical Applications I. Simultaneously Optimized Functional Forms for Nonpolar and Polar Fluids.* : International Journal of Thermophysics, 2003. Vol. 24.

214. —. *Equation of State for Thecnical Applications II. Results for Nonpolar Fluids.* : International Journal of Thermophysics, 2003. Vol. 24.

215. —. *Equation of State for Thecnical Applications III. Results for Polar Fluids.* : International Journal of Thermophysics, 2003. Vol. 24.

216. **Lemmon, E.W., Jacobsen, T.R.** *A New Functional Form and New Fitting Techniques for Equations of State with Application to Pentafluoroethane (HFC-125).* : Journal of Physical Reference Data, 2005. Vol. 34.

217. **Lemmon, W.E., Span, R.** *Short Fundamental Equations of State for 20 Industrial Fluids.* : Journal of Chemical Engineering Data, 2006. pp. 785-850. Vol. 51.

218. **Kunz, O., Klimeck, R., Wagner, W., Jaeschke, M.** *The GERG-2004 Wide-Range Equation of State for Natural Gases and Other Mixtures.* Düsseldorf : GERG Technical Monograph 15. Fortschr.-Ber. VDI, VDI-Verlag, 2007.

219. **Mehra, V.S., Thodos, G.** *Vapor-Liquid Equilibrium in the Ethane-n-Butane System.* s.l. : Journal of Chemical Engineering Data, 1965. Vol. 10.

220. **Ekiner, O. Thodos, G.** *Estimation of k-constants for binary aliphatic hydrocarbon mixtures: application to methane-free systems.* : The Canadian Journal of Chemical Engineering, 1965. Vol. 43.

221. **Dingrani, J.G., Thodos, G.** *Vapor-liquid equilibrium behavior of the ethane—n-butane—n-hexane system.* s.l. : Canadian Journal of Chemical Engineering, 1978. Vol. 56.

222. **Lhoták, V., Wichterle, I.** *Vapour-liquid equilibria in the ethane - propane - n-butane system at high pressures.* : Fluid Phase Equilibria, 1983. Vol. 12.

223. Dowtherm. *Synthetic oil thermo-physical properties.* [Online] www.dow.com.

224. **Dittman, G.L.** *Calculation of Brine Properties.* : Lawrence Livermore Laboratory, 1977.

225. **Lukosevicius, V.** *Thermal Energy Production from Geothermal Brine - Technological aspects and Energy Efficiency.* : UNU Geothermal Training Programme, 1993.

226. **NETL.** *Quality Guidelines for Energy System Studies. Cost Estimation Methodology for NETL Assessments of Power Plants Performance.* : U.S. Department of Energy, 2011.

227. **Wang, J., Yan, Z., Wang, M., Li, M., Dai, Y.** *Multi-objective optimization of an organic Rankine cycle (ORC) for low grade waste heat recovery using evolutionary algorithm.* : Energy Conversion and Management, 2013. Vol. 71.

228. **Gerber, L., Marechal, F.** *Environomic optimal configurations of geothermal energy conversion systems: Application to the future construction of Enhanced Geothermal Systems in Switzerland.* s.l. : Energy, 2012. pp. 908-923. Vol. 45.

229. **Martelli, E., Amaldi, E.** *PGS-COM, A Hybrid Method for Non-Smooth Black-box Constrained Optimization.* : Computers and Chemical Engineering, 2014.

230. **Torczon, V.** *On the Convergence of Pattern Search Algorithms.* : SIAM Journal on Optimization, 1997. Vol. 7.

231. **Lewis, R.M., Torczon, V.** *Pattern Search Algorithms for Bound Constrained Minimization.* s.l. : SIAM Journal on Optimization, 1999. Vol. 9.

232. **Lewis R. M., Torczon V.** *A Globally Convergent Augmented Lagrangian Pattern Search Algorithm for Optimization with General Constraints and Simple Bounds.* : SIAM Journal on Optimization, 2002. Vol. 12.

233. **Audet, C., Dennis, J. E.** *Analysis of Generalized Pattern Searches.* : . SIAM Journal on Optimization, 2003. Vol. 13.

234. **Council, EGEC-European Geothermal Energy.** *Financing Geothermal Technologies.* 2010.

235. **Bombarda, P.** *Estimating cost of the geothermal power technologies: main aspects and review.* Bruxelles, 2011.

236. **Guzman, J., Teja, A.S., Kay, W.B.** *Vapor-liquid equilibria in binary mixtures formed from hexamethyldisiloxane, toluene and ethanol.* s.l. : Fluid phase equilibria, 1981. Vol. 7.

237. **Kretschmer, C., Wiebe, R.** *Liquid-Vapor Equilibrium of Ethanol-Toluene Solutions.*

238. **Van Ness, H. C., Soczek, C. A., Peloquin, G. L., Machado, R. L.** s.l. : Journal of Chemical Engineering Data , 1967. Vol. 12.

239. **Duvia, A., Guercio, A., Rossi di Schio, C.** *Technical and economic aspects of Biomass fuelled CHP plants based on ORC turbogenerators feeding existing district heating networks.* s.l. : Turboden.

240. **Taljan, G., Verbič, G., Pantoš, M., Sakulin, M., Fickert, L.** *Optimal Sizing of Biomass-Fired Organic Rankine Cycle CHP System with Heat Storage.* s.l. : IEEE, 2011.

241. ForestFuels. [Online] www.forestfuels.co.uk.

242. **Krajnc, N., Jemec, T., Prislan, P.** *Monitoring Of Wood Fuel Prices In Slovenia, Austria, Italy, Croatia, Romania, Germany, Spain (Incl. Catalonia) And Ireland.* s.l. : Biomass Trade Center, 2013.

243. **Alves. M.S., Venturini, O.J., Palacio, J.C.E.** *Technical – Economical Evaluation Of 1Mwel Organic Rankine Cycle Using Eucalyptus Wood From Energy Forests In Brazil.* s.l. : WREF 2012, 2012.

244. **IRENA.** *RENEWABLE ENERGY TECHNOLOGIES: COST ANALYSIS SERIES. Biomass for Power Generation.* 2012. Vol. 1.

245. **IEA.** *Energy Outlook 2011.* 2011.

246. **Ranaboldo, M. , Lega, B.D., Ferrenbach, D.V., Ferrer-Martí, L., Moreno, R.P., García-Villoria, A.** *Renewable energy projects to electrify rural communities in Cape Verde.* s.l. : Applied Energy, 2014. Vol. 118.

247. **Sen, R. , Bhattacharyya, S.C.** *Off-grid electricity generation with renewable energy technologies inIndia: An application of HOMER.* s.l. : Renewable Energy , 2014. Vol. 62.

248. **Merei, G. , Berger, C., Sauer, D.U.** *Optimization of an off-grid hybrid PV-Wind-Diesel system with different battery technologies using genetic algorithm.* s.l. : Solar Energy , 2013. Vol. 97.

249. **Pradhan, N., Karki, N.R.** *Probabilistic reliability evaluation of off-grid small hybrid solar PV-wind power system for the rural electrification in Nepal.* s.l. : 2012 North American Power Symposium, NAPS 2012, 2012. Article number 6336317.

250. **Ruetschi, P.** *Aging mechanisms and service life of lead–acid batteries.* s.l. : Journal of Power Sources, 2004. Vol. 127.

251. **Bindner, H., Cronin, T., Lundsager, R., Manwell, J. F., Abdulwahid, U., Baring-Gould, I.** *Lifetime Modelling of Lead Acid Batteries.* : Riso National Laboratory, 2005.

252. **Giostri, A., Binotti, M., Silva, P., MacChi, E., Manzolini, G.** *Comparison of two linear collectors in solar thermal plants: Parabolic trough versus Fresnel.* s.l. : Journal of Solar Energy Engineering, Transactions of the ASME , 2013. Vol. 135.

253. **Flueckiger, S. M., Yang, Z., Garimella, S V.** *Design of Molten-Salt Thermocline Tanks for Solar Thermal Energy Storage.* : Heat Transfer Engineering, 2013. Vol. 34.

254. **Farid, M.M., Khudhair, A.M., Razack, S.A.K., Al-Hallaj, S.** *A review on phase change energy storage: materials and applications.* : Energy Conversion and Management, 2004. Vol. 45.

255. **Jaramillo, O.A., Venegas-Reyes, E., Aguilar, J.O., Castrejón-García, R., Sosa-Montemayor, F.** *Parabolic trough concentrators for low enthalpy processes.* : Renewable Energy, 2013. Vol. 60.

256. **Turchi, C., Mehos, M., Ho, C.K., Kolb, G.J.** *Current and Future Costs for Parabolic Trough and Power Tower Systems in the US Market.* s.l. : NREL, 2010. Presented at SolarPACES 2010.

257. Sopogy. [Online] www.sopogy.com.

258. **Quoilin, S., Orosz, M., Hemond, H., Lemort, V.** *Performance and design optimization of a low-cost solar organic Rankine cycle for remote power generation.* s.l. : Solar Energy, 2011.

259. **Orosz, M.S., Mueller, A., Quolin, S., Hemond, H.** *Small Scale Solar Orc System For Distributed Power.* s.l. : ORBI-Univerity of Liege, 20xx.

260. **Sullair.** *Two-Stage Rotary Screw - Tandem Series —TS-20 | TS-32 | TS-32S.* s.l. : Sullair.

261. **Forristall, R.** *Heat Transfer Analysis and Modeling of a Parabolic Trough Solar Receiver Implemented in Engineering Equation Solver.* : NREL-Technical Reports, 2003.

262. **Bell, I., Quoilin, S., Wronskiz, J., Lemort, V.** *CoolProp: An Open-Source Reference-Quality Thermophysical Property Library.* Rotterdam : 2nd International Seminar on ORC Power Systems, 2013.